UNIVERSITY OF KWAZULU-NATAL

THE SEPARATION OF HEXAFLUOROPROPYLENE AND HEXAFLUOROPROPYLENE OXIDE USING TOLUENE AND A NOVEL SOLVENT

2008

SHALENDRA CLINTON SUBRAMONEY

THE SEPARATION OF HEXAFLUOROPROPYLENE AND HEXAFLUOROPROPYLENE OXIDE USING TOLUENE AND A NOVEL SOLVENT

Shalendra Clinton Subramoney

A dissertation submitted in fulfillment of the academic requirements for the degree of Master of Science (MSc) in the School of Chemical Engineering at the University of KwaZulu-Natal, Durban

2008

ABSTRACT

PELCHEM, the chemical division of NECSA, produces the fluorocarbon hexafluoropropylene (HFP) on-site. In 2005 PELCHEM initiated research into the wet oxidation of HFP to produce the higher value fluorocarbon hexafluoropropylene oxide (HFPO). Although successful in the conversion of HFP to HFPO, the product stream contained both the product and the unreacted HFP. As a result, PELCHEM contracted the Thermodynamics Research Unit at the University of KwaZulu-Natal to investigate the separation of HFP and HFPO.

A solvent selection procedure was used to identify potential solvents and an initial list of two hundred and seven candidate solvents compiled. Utilising the UNIFAC group contribution method, the initial list was narrowed down to thirty solvents using the criterion of selectivity at infinite dilution. Through the comparison of specific solvent properties such as recoverability, safety, environmental factors and economic considerations, a final list of ten solvents was generated. The list of ten solvents was proposed to PELCHEM who identified four solvents for further studies. The work involving the two solvents, toluene and hexafluoroethane (R116), is presented in this dissertation. The solvent toluene has been previously used by the du Pont company for the separation of HFP and HFPO, while R116 is a novel solvent for this application. The solvent selection procedure was performed in collaboration with a member of the Thermodynamics Research Unit, and the work on the remaining two solvents is presented in the dissertation of (Nelson 2008).

Experimental binary high pressure vapour liquid equilibrium data were measured for the HFP + toluene, HFPO + toluene, R116 + HFP, and R116 + HFPO systems at two temperatures: 273.15 and 313.15 K. Pure component vapour pressure data for HFPO in the temperature range of 271.90 to 318.20 K were also measured. The HPVLE measurements were performed at the Thermodynamics Energy and Phase Equilibria laboratories at Ecoles des Mines de Paris using two experimental techniques and equipment. The binary systems involving toluene were measured on a static synthetic Pressure Volume Temperature apparatus equipped with a variable volume cell. The binary systems involving R116 were measured on a static analytic apparatus equipped with a Rapid On-line Sampler Injector. None of the systems measured for this project have been reported in the literature. The four binary systems and the pure component vapour pressure measurements thus constitute new data sets.

All experimental data were modelled via the direct method using the computer software Thermopack. Three model combinations were used to represent the data: the Peng-Robinson equation of state with the Wong-Sandler mixing rules, the Peng-Robinson equation of state with the Modified-Huron-Vidal first order mixing rules, and the Soave-Redlich-Kwong equation of state with the Wong-Sandler mixing rules. The Mathias-Copeman alpha function was used in conjunction with the equation of state models, and the

NRTL activity coefficient model was incorporated into the mixing rules. Due to time constraints, experimental data for the binary system HFP + HFPO were not measured. Data for this system was predicted at two temperatures, 273.15 and 313.15 K, via the PSRK-UNIFAC method. The critical line for the supercritical systems R116 + HFP and R116 + HFPO were calculated in Thermopack.

PELCHEM required a commercial grade HFPO product stream of purity greater than 99 % (mole), and a purified HFP product stream of purity greater than 95 % for the recycle and conversion of HFP into HFPO. Using the regressed experimental high pressure vapour liquid equilibrium data, two preliminary separation processes were designed in Aspen Plus to achieve these objectives. The first scheme involved toluene and utilised the process of extractive distillation with toluene introduced as a liquid solvent. The toluene bonded to the HFP and was removed as a bottoms product which allowed a purified HFPO stream to be recovered as a distillate. The second scheme involved R116 and utilised the process of gas stripping, with a liquid mixture of HFP and HFPO contacted with a gaseous stream of R116. The R116 removed the HFP from the liquid mixture, resulting in a purified HFPO stream. The toluene process resulted in an overall HFPO product recovery of 98.46 % and HFPO product purity of 99.88 % (mole). The R116 process resulted in an overall HFPO product recovery of 96.57 % and HFPO product purity of 99.71 %. For the component HFP, the toluene process resulted in an overall HFP product recovery of 99.42 % and product purity of 96.41 %. The R116 process resulted in an overall product recovery of 99.36 % and product purity of 93.45 %.

From a comparison of the preliminary design of the separation processes on the basis of patent issues, performance, and other miscellaneous factors, it was concluded that the R116 process compared favourably to the process involving the solvent toluene. The preliminary process designs were presented to PELCHEM in 2007, and pending further experimental work PELCHEM plans to patent the R116 separation process.

I, Shalendra Clinton Subramoney, declare that to the best of my knowledge, the work contained in this document is my own work, unless stated to the contrary in the text. This dissertation has not been submitted for degree purposes, in part or in whole, to any other university.

Shalendra Clinton Subramoney

As the candidate's supervisor, I, Prof. D. Ramjugernath, have approved this dissertation for submission.

Prof. D. Ramjugernath

As the candidate's supervisor, I, Dr. P. Naidoo, have approved this dissertation for submission.

Dr. P. Naidoo

ACKNOWLEDGEMENTS

In the compilation of this work, I have received considerable assistance from many sources. My deepest gratitude must be extended to the following people and/or organizations:

- I am indebted to my supervisors, Prof. D. Ramjugernath and Dr. P. Naidoo for the invaluable guidance, assistance and wisdom.
- I am indebted to Christophe Coquelet, Albert Chareton and the workshop staff at Ecoles des Mines de Paris for their help with the experimental measurements and thermodynamic modelling for this project.
- I acknowledge the National Research Foundation (NRF), the Nuclear Energy Corporation of South Africa (NECSA) and the University of KwaZulu-Natal Graduate Assistance for financial assistance during the course of this project.
- A tip of the cap to my colleagues in the Thermodynamics Research Unit and to Luke Watson, Adam Kubert and Thashree for their ideas, friendship and enthusiasm.

Finally, my heartfelt thanks to my wonderful family for their encouragement and support during my studies.

"There's a chair, and it's walking, it goes walking....."

Anonymous, 2004

CONTENTS

CHAPTER FOUR

CHAPTER FIVE

CHAPTER SIX

LIST OF FIGURES

CHAPTER ONE

CHAPTER TWO

CHAPTER THREE

CHAPTER FOUR

CHAPTER SIX

CHAPTER SEVEN

APPENDIX A

APPENDIX B

APPENDIX C

APPENDIX D

LIST OF TABLES

CHAPTER ONE

CHAPTER TWO

CHAPTER THREE

CHAPTER FOUR

CHAPTER FIVE

CHAPTER SIX

CHAPTER SEVEN

APPENDIX A

APPENDIX B

APPENDIX C

APPENDIX D

LIST OF PHOTOGRAPHS

NOMENCLATURE

Symbols

a	Equation of state energy parameter
a_{mn}	Binary interaction parameter for the UNIFAC model ((Fredenslund et al. 1977))
A	Molar Helmholtz free energy
b	Equation of state co-volume parameter
B	Second virial coefficient
f	Fugacity
G	Molar Gibbs free energy
H	Molar enthalpy
K	Equilibrium ratio or K-value
k_{ij}	Binary interaction parameter in a mixing rule
N	Number of data points
N_T	Total number of stages in a distillation column or stripping unit
N_F	Feed stage to a distillation column or stripping unit
N_{SF}	Solvent feed stage to an extractive distillation column or stripping unit
P	Pressure
Qk	van der Waals group surface area parameter for the UNIFAC model
R	Universal gas constant
R_k	van der Waals group volume paramter for the UNIFAC model
T	Temperature
V	Molar volume
x	Liquid phase mole fraction
y	Vapour phase mole fraction
Z	Compressibility factor

Greek Letters

α	Function in an equation of state
α	Non-randomness parameter in the NRTL ((Renon and Prausnitz 1968)) model
β	Selectivity
φ	Fugacity coefficient
γ	Activity coefficient
τ	Adjustable parameters in the NRTL equations
μ	Chemical potential

Subscripts and Superscripts

c	Critical property
calc	Calculated
exp	Experimental
i	Component identity
∞	Infinity
j	Component identity
k	Component identity
L	Liquid phase
R	Reduced property
sat	Property evaluated at the saturation pressure of the component
T	Total Property
V	Vapour phase

ABBREVIATIONS

AAE	Absolute Average Error
ASOG	Analytical solution of groups
CEOS	Cubic equation of state
CFC	Chlorofluorocarbon
COSMO	Conductor-like screening models
COSMO-RS	Conductor-like screening models for real solutions
DSV	Design/Spec/Vary function in Aspen
EOS	Equation(s) of state
FC	Fluorocarbon
GC	Gas chromatograph
HCFC	Hydrochlorofluorocarbon
HFC	Hydrofluorocarbon
HFP	Hexafluoropropylene
HFPO	Hexafluoropropylene oxide
HPVLE	High pressure vapour-liquid equilibria
HV	Huron-Vidal mixing rule
MC	Mathias-Copeman alpha function
MHV1	Modified Huron-Vidal first order mixing rule
NECSA	Nuclear Energy Corporation of South Africa
NRTL	Non-Random Two-Liquid activity coefficient model
ODP	Ozone depletion potential
PELCHEM	Pelindaba Chemicals
PR	Peng-Robinson equation of state
ROLSI	Rapid On-line Sampler Injector
RK	Redlich-Kwong equation of state
RR	Molar reflux ratio
SA	Static analytic
SRK	Soave-Redlich-Kwong equation of state
SS	Static synthetic
TEP	Thermodynamics Energy and Phase Equilibria
UNIFAC	UNIQUAC functional group activity coefficient model
UNIQUAC	Universal quasi-chemical activity coefficient model
vdW	van der Waals
VLE	Vapour-liquid equilibria
WS	Wong-Sandler mixing rules

CHAPTER ONE

1. INTRODUCTION

The Thermodynamics Research Unit at the University of KwaZulu-Natal has some 25 years of expertise in the field of high pressure thermodynamics and vapour liquid equilibrium measurements. This knowledge has served to earn the group a significant reputation in the thermodynamics field, which has been parlayed into working relationships with several major petrochemical, engineering and research institutes. This project, *The separation of hexafluoropropylene and hexafluoropropylene oxide using toluene and a novel solvent*, was initiated in early 2006 by Pelindaba Chemicals (PELCHEM), the chemical division of the Nuclear Energy Corporation of South Africa (NECSA). Owing to the prominent positioning of the research unit in the field of thermodynamics research, the group was contracted by PELCHEM to propose a separation scheme for a fluorocarbon mixture of hexafluoropropylene (HFP) and hexafluoropropylene oxide (HFPO).

1.1. PROJECT BACKGROUND

Fluorine chemistry as a separate branch of the chemical industry has been intensively developed from the middle of the 20th century. The fluorochemical industry has since become a pioneering technological juggernaut ((Maximov 1998)) facilitating technological progress in the aerospace, aircraft, micro-electronics and medical industry. The worldwide production of fluorine containing compounds was initially dominated by chlorofluorocarbons (CFCs) for use as refrigerants, in the manufacture of foam plastics, and as fire extinguishing agents. With the advent of the Montréal Protocol ((UN 1987)) for substances depleting the ozone layer, the production and consumption of CFCs has been stopped in developing countries since 1996. As a result, the demand for non-flammable, non-explosive and non-toxic refrigerants as a substitute for ozone depleting substances led to the rapid development of technologies for the production of the more ozone friendly hydrochlorofluorocarbons (HCFCs), hydrofluorocarbons (HFCs) and fluorocarbons (FCs).

In an industrial sense, the increased global demand for HCFCs can be considered temporary as the phase out of these less damaging substances is underway in accordance with the ongoing declarations of the Montréal Protocol. As a result, the demand for HFCs and FCs, the chemical family to which HFP and HFPO belong, has begun to dramatically increase on a global scale. According to the (Freedonia-Group 2007), growth prospects for fluorochemicals are being led by higher value specialty products such as fluoropolymers and specialty fluorine gasses, uses for which HFPO is well suited to. The continued advancement of manufacturing in a technological sense is generating widespread demand for the high performance capabilities of fluorochemicals such as HFPO, particularly in the electronics and motor

vehicle sectors. Prominent companies in the global fluorochemical industry include the du Pont de Nemours Company, Solvay, Daikin, Arkema, The Asahi Glass Company and 3M. In particular, du Pont, Asahi and Daikin, are major producers of HFP and HFPO worldwide.

At the Pelindaba site in Pretoria, PELCHEM manufactures a wide variety of high quality, advanced fluorochemicals and value added downstream products for the global fluorochemical industry ((PELCHEM 2007)). Along with the speciality inorganic and organic fluoride gasses and liquids produced from the onsite fluorine production facilities, PELCHEM manufactures organic fluorochemicals from tetrafluoroethylene (C_2F_4). Their portfolio of current high profile products includes calcium sulphate ($CaSO_4$), fluorine (F_2), fluoroboric acid (HBF_4), hydrofluoric acid (HF) and xenon difluoride (XeF_2).

HFP (C_3F_6) is produced as a by-product of the plasma reactors at the Pelindaba site. In 2005, PELCHEM, via their internal research laboratory, initiated the project of converting HFP into the higher value component HFPO (C_3F_6O), via the dry oxidation method with an unsupported catalyst utilising a method similar to that of (Huang et al. 2006). The method of dry oxidation was later abandoned by PELCHEM and research into the production of HFPO from HFP via the wet oxidation mechanism was undertaken. Due to confidentiality reasons, the details of the wet oxidation process have not been disclosed by PELCHEM.

The components HFP and HFPO have a wide variety of industrial uses, particularly HFPO, which is a high value speciality component in great demand. However, HFP is fast becoming increasingly important in both industrial and research activities, being used as an intermediate in chemical reactions ((Krespan 1986)), as a monomer in fluoropolymers ((Stolarska et al. 2007) and (Aravindan and Vickraman 2007)), in the semiconductor manufacturing industry for etching applications ((Bian et al. 2005)) and in the manufacture of HFPO ((Huang et al. 2006) and (Ikeda et al. 1990)).

HFPO is an important component in the production of high performance lubricating oils and heat resistant fluids ((Ohsaka and Tohzuka 1981)). It has been extensively utilised for the manufacture of high performance fluoropolymers such as O-rings and sealants ((Hirao et al. 2007)) and in the manufacture of elastomers ((Atkins 1973)). The use of HFPO in the manufacture of fluoropolymers is extremely important in an industrial and technological sense as fluoropolymers possess unique properties of high chemical and heat resistance as well as good insulation characteristics. Additionally, fluoropolymers are highly flexible in their operating conditions in that they are able to work at low operating temperatures while still preserving their elasticity, and at high operating temperatures of up to 673.15 K without any change in their properties ((Maximov 1998)). HFPO has also found prominent use in the manufacture of surfactants ((Darling 1982)) and ion exchange membranes ((Ikeda et al. 1990)). Fluorinated surfactants containing HFPO are applied to the surfaces of metals and liquids to form a film barrier to decrease surface energy, which results in a reduction of friction in machines and micro-scale mechanisms, typical examples being

high performance computer hard disk drives used for high priority data intensive server applications. The work of (Cho et al. 2006) demonstrated the use of HFPO for the plasma enhanced chemical vapour deposition of TiO_2 nanoparticles for the improvement of photocatalytic activity, with the patent of (Shibanuma et al. 2005) disclosing the invention of a process utilising HFPO for the manufacture of rigid polyurethane resin foams.

Table 1.1 indicates the typical market prices of commercial grade HFP and HFPO and other fluorochemical products produced by PELCHEM. The quoted prices listed in Table 1.1 were not obtained from PELCHEM but from the catalogue listing function of the research software SciFinder Scholar ((ACS 2007)), which contains a database of pure component prices from various industrial sources. The date of the quoted price for each component is indicated, as well as the commercial grade or purity of the product and the source. For ease of comparison, the costs of all the products have been converted into the units of Rands per kg.

	Source	Date	Purity [mole %]	Price [R•kg^{-1}]
HBF_4	Thermo Fisher Scientific	16/05/2007	50	588
HFP	Apollo Scientific	17/06/2007	99	6400
HFPO	Apollo Scientific	17/06/2007	97	13030
XeF_2	Synquest Fluorochemical	21/08/2007	99.5	26720

Table 1.1. Market prices for selected commercial grade fluorochemical products.

PELCHEM currently sells the fluorochemical products HBF_4 and XeF_2. With the research work undertaken in this project, PELCHEM plan to separate a stream of HFP and HFPO to produce commercial grade HFPO. From the table, the quoted price of HFPO per kg (97 % mole purity) is more than double that of HFP (99 % mole purity). This dramatic difference in product price indicates the rationale behind the conversion of HFP into the more lucrative commercial product HFPO. Relative to other selected fluorochemical products produced by PELCHEM in terms of price, HFPO (97 % mole purity) falls into the middle category of products, displaying a price of almost half that of the more expensive product XeF_2, and more than twenty one times greater than the least expensive product HBF_4. Although HFPO has a price per kg significantly lower than XeF_2, production and handling costs, as well as safety issues are significantly lower for HFPO (a non-toxic, non flammable gas) when compared to XeF_2.

PELCHEM requires a high purity HFPO stream, with a typical purity value of greater than 99 % HFPO (mole %) for their identified commercial grade product. Via their current experimental wet oxidation mechanism, PELCHEM produces a product stream in the molar ratio of 1:2 HFP to HFPO. The typical low conversion of HFP to HFPO, as discussed by (Huang et al. 2006) and (Ikeda et al. 1990), results in the

product stream containing the valuable HFPO product and the unreacted, less valuable HFP, which must be separated to produce the commercial grade HFPO. Due to the closeness in boiling points of the two components, 243.75 K and 245.75 K for HFP and HFPO respectively, they are difficult and rather impractical to separate via conventional distillation methods. Since 2001, PELCHEM and NECSA have developed a successful working relationship with the Thermodynamics Research Unit at the University of KwaZulu-Natal and contracted the research group to propose a separation scheme for the separation of HFP and HFPO. The mandate of the contract with PELCHEM was to investigate a separation scheme of a feed mixture of HFP and HFPO in a 1:2 molar ratio, with the following primary aims:

1. To produce a commercial grade HFPO stream (> 99 % purity by mole HFPO)

2. To produce a relatively pure HFP stream (> 95 % purity by mole HFP) for recycle and conversion into HFPO.

The contract with PELCHEM required the proposal, preliminary design and simulation of a separation process, including all the activities (solvent selection, experimental measurements and process design) involved therein. An overview of the project in its entirety and the work undertaken is presented via a flow diagram in Figure 1.1. A more detailed description of the research methodology employed throughout the course of this project is presented in subsequent chapters.

A literature review detailing various aspects pertinent to this project is presented in Chapter two. The solvent selection procedure utilised to identify suitable solvents to effect the separation of HFP and HFPO is presented in Chapter three. The solvent selection procedure was undertaken in conjunction with a member of the Thermodynamics Research Unit, W. M. Nelson, and the contribution of Nelson to the work presented in this dissertation is indicated accordingly. Experimental HPVLE measurements were performed via two experimental techniques, on two HPVLE apparatuses. Chapter four presents a description of the two HPVLE apparatus utilised for this project and describes the experimental procedure and techniques used for the measurements. The interpretation of the experimental HPVLE data via thermodynamic modeling and data regression is described in Chapter five along with a brief description of the thermodynamic models utilised. With the aid of the experimental and regressed HPVLE data, two separation processes were developed. The methodology and procedure behind the development and design of each unit operation, and thus the complete process, is presented in Chapter six and Appendix C. Chapter seven of this dissertation presents the results and relevant discussion of the work performed for this research project. The outcomes of the work undertaken are presented via the Conclusions in Chapter eight, while Chapter nine provides recommendations for future work that can be undertaken as an extension of the work performed for this project.

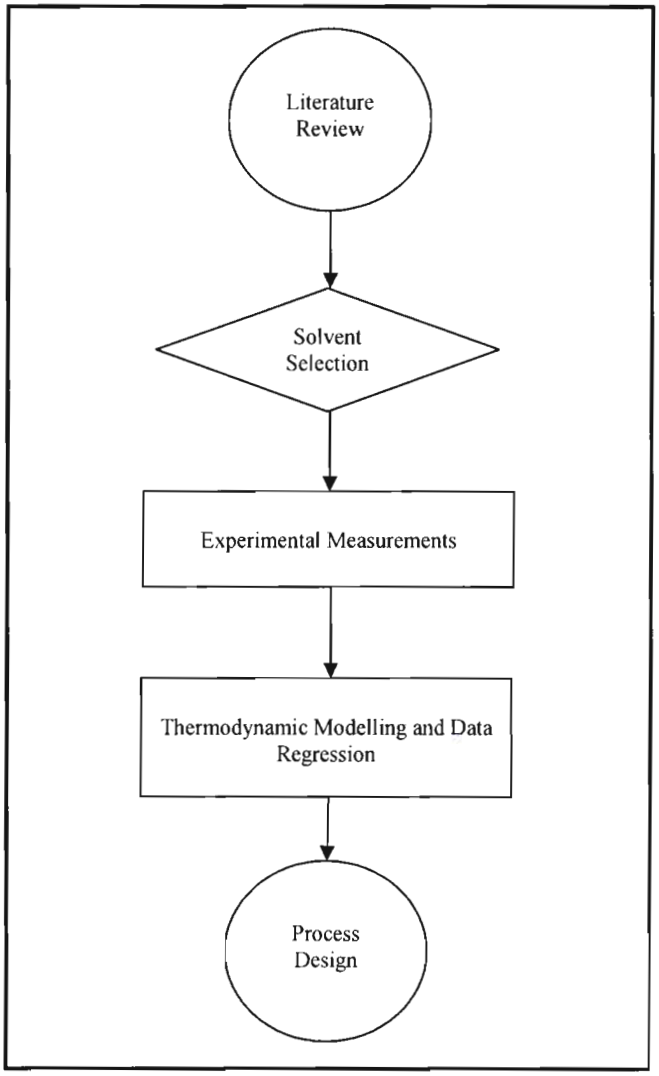

Figure 1.1. A flow diagram indicating the scope and methodology of the research project.

CHAPTER TWO

2. LITERATURE REVIEW

A comprehensive literature review into the separation of HFP and HFPO and associated topics was initiated in March 2006. During the course of this project, the literature review was revised and updated accordingly to reflect any significant changes in the direction of the research. The review involved the referencing of printed and on-line journal libraries and patent databases. Computer software such the research orientated software SciFinder Scholar ((ACS 2007)) and databases containing pure component and mixture properties, e.g. Component Plus ((ProSim 2001)) and the DDB or Dortmund Data Bank ((DDBST 2007)) were referenced.

2.1. PURE COMPONENT DATA

The key components involved in this project were hexafluoropropylene (HFP), hexafluoropropylene oxide (HFPO), toluene and hexafluoroethane (R116). A starting point for the literature review was to obtain pure component properties for the key components. At the onset of the research project only pure component properties for HFP and HFPO were reviewed. Once the solvents toluene and R116 were identified at a later stage via a solvent selection procedure, the pure component properties of these components were obtained.

The general pure component physical properties for HFP, HFPO, toluene and R116 are presented in Table 2.1. The properties for all components except HFPO were obtained from the Component Plus database. The component HFPO was not catalogued or defined in the Component Plus database and the pure component properties for this component were thus obtained from the DDB. The molecular formula, CAS index number for easy reference, molecular weight and normal boiling point are presented below.

Component	Formula	CAS Index Number	Molecular Weight [g•mol^{-1}]	Boiling Point [K]
HFP	C_3F_6	116-15-4	150.02	243.75
HFPO	C_3F_6O	428-59-1	166.02	245.75
Toluene	C_7H_8	108-88-3	92.14	383.78
R116	C_2F_6	76-16-4	138.01	194.95

Table 2.1. General pure component physical properties for HFP, toluene and R116 ((ProSim 2001)) and HFPO ((DDBST 2007)).

Table 2.2 presents the critical properties for the components HFP, HFPO, toluene and R116. The properties for all components except HFPO were obtained from the Component Plus database. The DDB only contained values for the critical temperature and critical volume for HFPO. Values for the critical pressure, P_c, accentric factor, ω, and critical compressibility, Z_c, have not been published and were thus not available.

Component	T_c [K]	P_c [Pa]	ω	Z_c	V_c [$cm^3 \cdot mol^{-1}$]
HFP	368.15	2900002	0.2046	0.254	268
HFPO	359.15	-	-	-	241
Toluene	591.72	4113795	0.2573	0.264	316
R 116	293.03	3041776	0.2291	0.277	224

Table 2.2. Critical properties for components HFP, toluene and R116 ((ProSim 2001)) and HFPO ((DDBST 2007)).

Figures 2.1 and 2.2 present the molecular structures of HFP and HFPO respectively, while Figures 2.3 and 2.4 present the molecular structures of toluene and R116. The molecular structures were obtained from the National Institute of Standards and Technology (NIST) website as a two dimensional molecular file which contained stored atomic coordinates, chemical bond and metadata information.

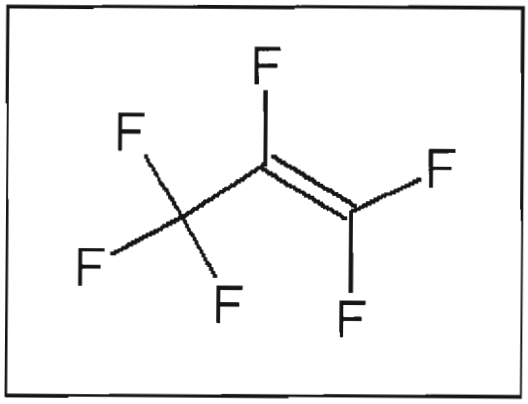

Figure 2.1. The molecular structure of HFP ((NIST 2007)).

HFP is a fluorocarbon species component containing three carbon atoms with no active hydrogen atoms. It is a multi-halogen olefin, with the double bond between the carbon 1 and carbon 2 atoms (according to the IUPAC naming system) and is highly electro-negative due to the six fluorine atoms.

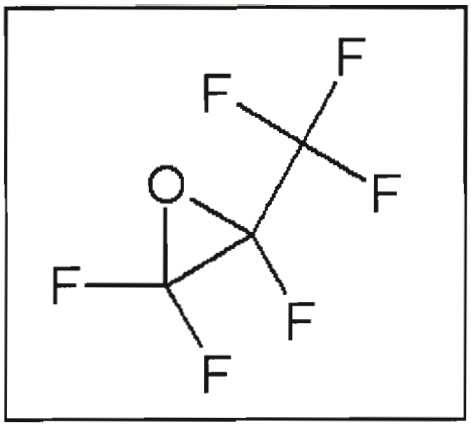

Figure 2.2. The molecular structure of HFPO ((NIST 2007a)).

HFPO is derived from HFP and contains three carbon atoms, six fluorine atoms and an oxygen atom. The oxygen atom contains an epoxide or oxirane structure which is a result of the oxidation of HFP, with the cyclic structure existing on the carbon 1 and carbon 2 atoms (according to the IUPAC naming convention).

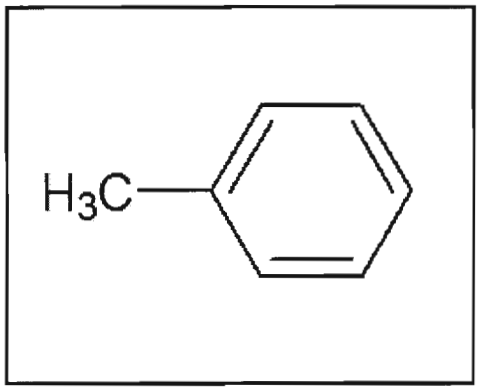

Figure 2.3. The molecular structure of toluene ((NIST 2007b)).

Toluene is a six membered aromatic ring. It displays similar chemical properties to benzene, but the presence of the methyl group increases the boiling point of the compound relative to benzene.

Hexafluoroethane, presented in Figure 2.4, is a fully substituted halogen compound. It is a fluorocarbon species component containing six fluorine atoms which imparts a high polarity.

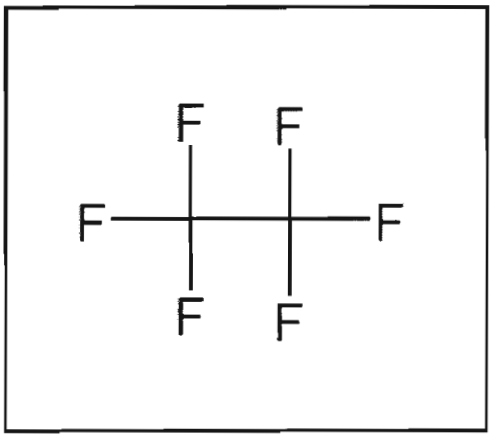

Figure 2.4. The molecular structure of R116 ((NIST 2007c)).

2.2. VAPOUR PRESSURE DATA

Only two sets of pure component vapour pressure data for HFP were identified in literature. Data for HFP in the temperature range of 256.45 to 293.23 K were found via the DDB in the work of (Li et al. 1996) and is presented graphically in Figure 2.5 and numerically in Table B.1, Appendix B.

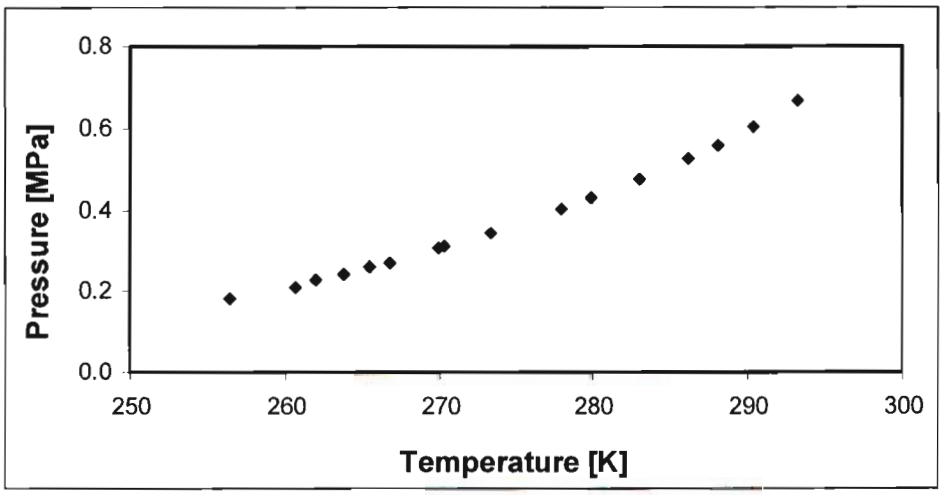

Figure 2.5. Pure component vapour pressure data for HFP in the temperature range 256.45 to 293.23 K ((Li et al. 1996)).

Pure component vapour pressure data for HFP in the temperature range of 272.30 to 312.30 K were measured in the work of (Nelson 2008) and is presented graphically in Figure 2.6 and numerically in Table B.2, Appendix B.

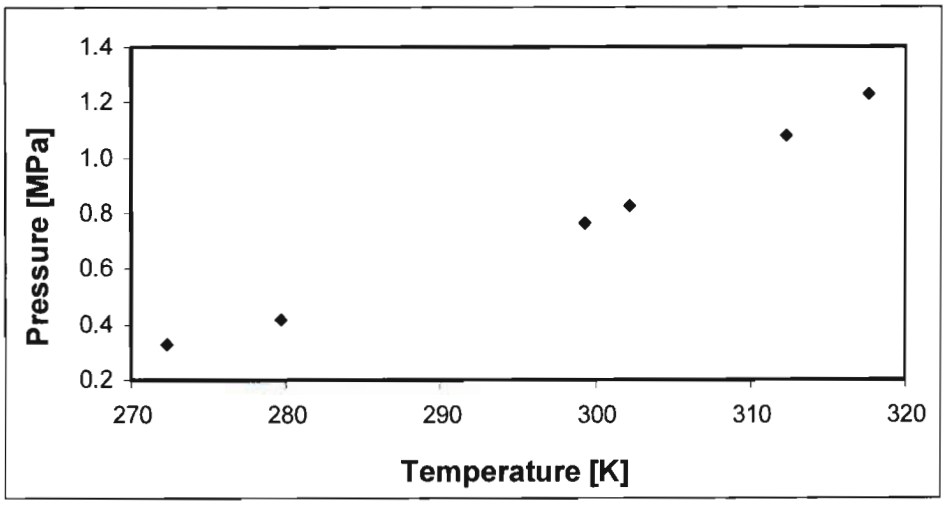

Figure 2.6. Pure component vapour pressure data for HFP in the temperature range 272.30 to 312.30 K ((Nelson 2008)).

The vapour pressure data presented in Figure 2.6 was measured on the static analytic apparatus of (Coquelet et al. 2003a) which was also utilised for the HPVLE measurements performed for this project.

No published pure component vapour pressure data for HFPO was found in literature. Numerous published sets of pure component vapour pressure data for toluene and R116 were identified via the DDB, however they are not presented in this dissertation.

2.3. VAPOUR LIQUID EQUILIBRIUM DATA

The primary aim of this research project was to propose a separation scheme to effect the separation of HFP and HFPO. The solvents determined suitable for this project via a solvent selection procedure were toluene and the refrigerant hexafluoroethane or R116. A prerequisite for the optimum design and operation of separation units and separation schemes is reliable data for fluid mixtures. The development of a separation scheme involving these components thus necessitated VLE data for the binary systems HFP + HFPO, HFP + toluene, HFPO + toluene, R116 + HFP and R116 + HFPO.

The literature review revealed that no published VLE data for the binary system HFP + HFPO exists. Due to the fact that HFP and HFPO are considered specialty chemicals, published data for any binary VLE

systems involving either HFP or HFPO are scarce. It was found that no published data for HFP or HFPO with either solvent toluene or solvent R116 existed.

For the component HFP, the literature review revealed that VLE data for HFP with only five components have been published. A summary of these five binary systems is presented in Table 2.3.

Set	System	Type	Conditions	Reference
1	R12 + HFP	Isobaric	0.275 MPa	(Whipple 1952)
2	R22 + HFP	Isobaric Isothermal	0.275 MPa 293.15 K	(Whipple 1952) (Maletskii and Kogan 1966)
3	R318 + HFP	Isobaric	0.986 MPa	(Chen et al. 1989)
4	R218 + HFP	Isothermal	273.15 K, 303.15 K	(Ho et al. 2004)
5	C_2ClF_3 + HFP	Isothermal	293.15 K	(Maletskii and Kogan 1966)

Table 2.3. A review of the published binary VLE involving the component HFP.

No published binary VLE data for the component HFPO were found in literature.

2.4. SEPARATION METHODS FOR HFP AND HFPO

Previous research in the field of separations involving mixtures of HFP and HFPO were found to be confined to companies developing commercial processes which have been patented, and in some cases implemented. Table 2.4 presents a review of the current state of separation processes involving HFP and HFPO.

The first major work in this field was performed by (Wiist 1967) for the du Pont Company, which involved the extractive distillation of a mixture of HFP and HFPO with a suitable solvent to produce a pure product stream of HFPO (99.5 % by mole). The solvents patented in this work included toluene, xylene, anisole, p-cymene, and mesitylene. For the work of (Wiist 1967), a batch distillation column with 23 theoretical stages was charged with a 120 g feed mixture comprised of 45 % HFP and 55 % HFPO (mass %), with the solvent xylene cooled to 243.15 K and introduced to the top of the column at a rate of 0.0015 $m^3 \cdot hr^{-1}$. The solvent selectively bonded with the HFP to lower the volatility which resulted in an overhead vapour stream of 99.5 % HFPO (mole %) and a pot vapour of 38.8 % HFPO (mole %). This work reported results with the solvents toluene and xylene utilising the same experimental set up and batch distillation procedure

for each solvent. Although experimental results with only two solvents are presented in this work, the five solvents disclosed were patented.

The work of (Oda et al. 1979) for the Asahi Glass Company reported a method of extractive distillation with solvent recycle to produce pure streams of 99.6 % HFPO and 97 % HFP (mole %). The solvents patented in this work included 1,2-dichloroethane, monochlorobenzene, di-isopropyl ether and trichloroethane (methyl chloroform). The schematic of the experimental setup of this work is presented in Figure 2.7.

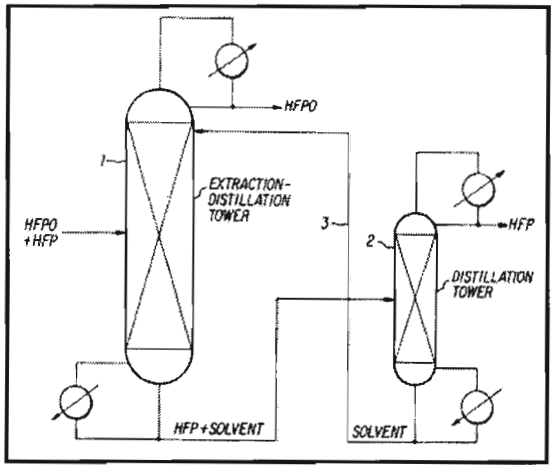

Figure 2.7. The extractive distillation scheme with solvent recycle as proposed by (Oda et al. 1979).

The extractive distillation scheme of Figure 2.7 consists of two columns. The first column, termed the 'extraction-distillation tower', is an Othmer type pressure equilibrium distillation apparatus with 20 equilibrium stages, fed with an equimolar mixture of HFP and HFPO at a rate of 150 $g \cdot hr^{-1}$. The solvent, 1,2-dichloroethane, was continuously fed at a rate of 300 $g \cdot hr^{-1}$ at the top of the column. The column was operated under a reflux ratio of 2.5 with a condenser temperature of 281.15 K and a bottoms temperature of 290.15 K. The bottom stream of the first column, rich in HFP, was fed to the second identical distillation tower. In the second tower, the HFP was separated from the solvent and removed as a distillate product with a relatively pure solvent bottoms product which was recycled to the top of the extraction distillation tower. With this experimental setup, (Oda et al. 1979) achieved a top product of 99.6 % HFPO (mole %) from the extraction distillation tower and a HFP stream of 97 % HFP (mole %) from the top stream of the second distillation tower.

(Sulzbach 1982), undertook the separation of a mixture of HFP and HFPO by bringing a gaseous feed stream of 89 % HFP (mass %) and 11 % HFPO (mass %) into contact with a cooled stream of liquid

Year	Patent Number	Assignee	Method	Solvent(s)	Reference
1967	US 3326780	E. I. du Pont de Nemours	Extractive Distillation	Toluene Xylene Anisole p-Cymene Mesitylene	(Wiist 1967)
1979	US 4134796	Asahi Glass Company Ltd.	Extractive Distillation	1,2-Dichloroethane Monochlorobenzene Di-isopropyl ether Trichloroethane	(Oda et al. 1979)
1982	US 4358348	Hoechst Aktiengesellschaft	Extractive Distillation	Methylene chloride	(Sulzbach 1982)
1997	JP 09020765	Asahi Glass Company Ltd.	Extractive Distillation	1,2-Dichlorofluoroethane Dichlorotrifluoroethane Dichloropentafluoropropane	(Ueno et al. 1997)
1997a	JP 9136882	Asahi Glass Company Ltd.	Distillation	-	(Ueno et al. 1997a)

Table 2.4. A review of the patented methods for the separation of HFP and HFPO.

methylene chloride via an extractive distillation tower. The gaseous stream at a rate of 7 $kg \cdot hr^{-1}$ was fed into a distillation column of diameter 100 mm and height 7 m, packed with Raschig rings of 10 mm diameter. The feed point for the gas was 3 m above the base of the column. The solvent methylene chloride was first cooled to 295.15 K and fed at a rate of 662 $kg \cdot hr^{-1}$ at the top of the column. The HFP was absorbed into the methylene chloride and removed from the bottom of the column and sent to a desorption column 3 m in length. The methylene chloride free vapour stream of the first distillation column contained 98.6 % HFPO (mass %) and 1.4 % HFP (mass %). In the desorption column, of same packing and diameter as the first distillation column, the mixture was heated to the boiling point and the HFP collected as a vapour stream of 99 % HFP (mass %) and 1 % by HFPO (mass %).

The work of (Ueno et al. 1997) was a continuation of the research of (Oda et al. 1979) for the Asahi Glass Company. Using an identical extractive distillation setup scheme with solvent recycle, several solvents with the general formula $C_nH_aCl_bF_c$, with the following constraints were patented: n being an integer with n = 2 to 6 with $a > 1$ and $a < n + 1$, $b > 1$ and $b < 2n$, $c > 1$ and $c < 2n$, with the final constraint $a + b + c = 2n + 2$. Examples of solvents which followed these constraints were several refrigerants and hydrogen containing halogenated hydrocarbons i.e. 1,2-dichlorofluoroethane (R141b), dichloropentafluoropropane (R225) and dichlorotrifluoroethane (R123). The extractive distillation scheme of (Oda et al. 1979) was run with several solvents identified by (Ueno et al. 1997) and compared with respect to the alteration of the relative volatility between HFP and HFPO.

Solvent	HFP [$kg \cdot hr^{-1}$]	HFPO [$kg \cdot hr^{-1}$]	Solvent [$kg \cdot hr^{-1}$]	Relative Volatility	Montreal Protocol
R141b	78	54	357	1.29	✓
R123	86	59	550	1.17	✓
R225ca	83	56	640	1.09	✓
R225cb	30	50	580	1.07	✓
CH_2Cl_2	55	49	297	1.78	x
$CHCl_3$	138	94	743	1.28	x
CCl_4	48	52	526	1.18	✓
CH_2ClCH_2Cl	84	57	309	1.91	x

Table 2.5. A review of the work of (Ueno et al. 1997) comparing the effect of different solvents on the relative volatility of HFP and HFPO.

Table 2.5 summarises the work of (Ueno et al. 1997) for an extraction distillation procedure utilising different solvents performed on the experimental setup of (Oda et al. 1979). The loading of the feed stream is indicated in the table, along with the mass flowrate of each solvent. The relative volatility is reported, indicating the difference in performance, and hence suitability, of each of the solvents in altering the relative volatility from a value of unity. The last column presented in Table 2.5 indicates the adherence of the chosen solvents to the Montréal Protocol ((UN 1987)). The solvents denoted with a '✓' indicates that

the substance is allowed under the Montréal Protocol, whereas a solvent denoted with an 'x' indicates that use of the solvent has been prohibited. The solvents used and thereafter patented in the work of (Ueno et al. 1997) included 1,2-dichlorofluoroethane (R141b), dichlorotrifluoroethane (R123) and dichloropentafluoropropane (R225ca).

(Ueno et al. 1997a) continued research into the separation of HFP and HFPO and patented a process involving the use of conventional distillation techniques to separate a mixture of HFP and HFPO under specific conditions. They decided to forego the typical method of extractive distillation with a solvent and performed distillation under stringent and well controlled conditions. The specific conditions employed by (Ueno et al. 1997a) were restricted to mixtures of HFP and HFPO in the mass ratio of 0.1:1 and at a column operating pressure of 0.49 MPa. It was found that by operating the distillation column under these restricted compositions and with a high theoretical stage count, it was possible to alter the relative volatility of the mixture to make it amenable to separation. A packed bubble cap column from the CHUBU Engineering company with 110 theoretical plates was utilised and was operated under the restricted conditions to produce an overhead stream of 99 % HFP (mole %) and a bottom stream of 98 % HFPO (mole %).

CHAPTER THREE

3. SOLVENT SELECTION PROCEDURE

To facilitate the separation of HFP and HFPO, (Wiist 1963) advocated the use of a third component, a solvent, to depress the volatility of HFP and increase the volatility of the remaining fluorocarbon HFPO, such that the mixture was separable by distillation. With five patented processes for the separation of HFP and HFPO examined and four processes utilising extractive distillation with a suitable solvent, the focal point for the proposal and design of this separation scheme thus became the identification of suitable solvents.

The work of (Seader et al. 1997) in the Enhanced Distillation section of Perry's Chemical Engineers' Handbook ((Perry and Green 1997)), demonstrated a solvent selection and screening approach divided into two primary steps, each with subsequent sub-stages. The first step focused on the identification of functional groups or chemical families that were likely to give favourable solvent/key component interactions. The second step identified and compared individual candidate solvents. The solvent selection procedure used for this research project followed the method of (Seader et al. 1997) and is summarized in Table 3.1, while Figure 3.1 describes the solvent selection procedure graphically in the form of a flow diagram.

Step 1	**Broad screening of solvents by functional group or chemical family**
1.1	*Homologous series and chemical nature:* Select candidate solvents from the high boiling homologous series of the key components.
1.2	*Robbins Chart and hydrogen bonding interactions:* Select candidate solvents from groups in the Robbins chart that tend to give positive or no deviations from Raoult's law for the key component desired in the distillate and negative or no deviations for the key component required in the bottoms.
1.3	*Polarity characteristic:* Select candidate solvents from chemical groups that tend to show a higher polarity than one key component or a lower polarity than the other key.
Step 2	**Identification of individual candidate solvents**
2.1	*Boiling point characteristics:* Select candidate solvents that boil at least 10 to 20 K above the key components to ensure that the solvent is relatively non volatile. The difference in boiling points ensures that the solvent will not form azeotropes with the other components.
2.2	*Selectivity at infinite dilution:* Evaluate and rank the candidate solvents according to the selectivity at infinite dilution (β^{∞}).
2.3	*Solvent properties:* Select most suitable solvent with regards to specific properties i.e. cost, availability, performance, safety and environmental factors.

Table 3.1. A summary of the two step solvent selection procedure of (Seader et al. 1997) utilised in this project.

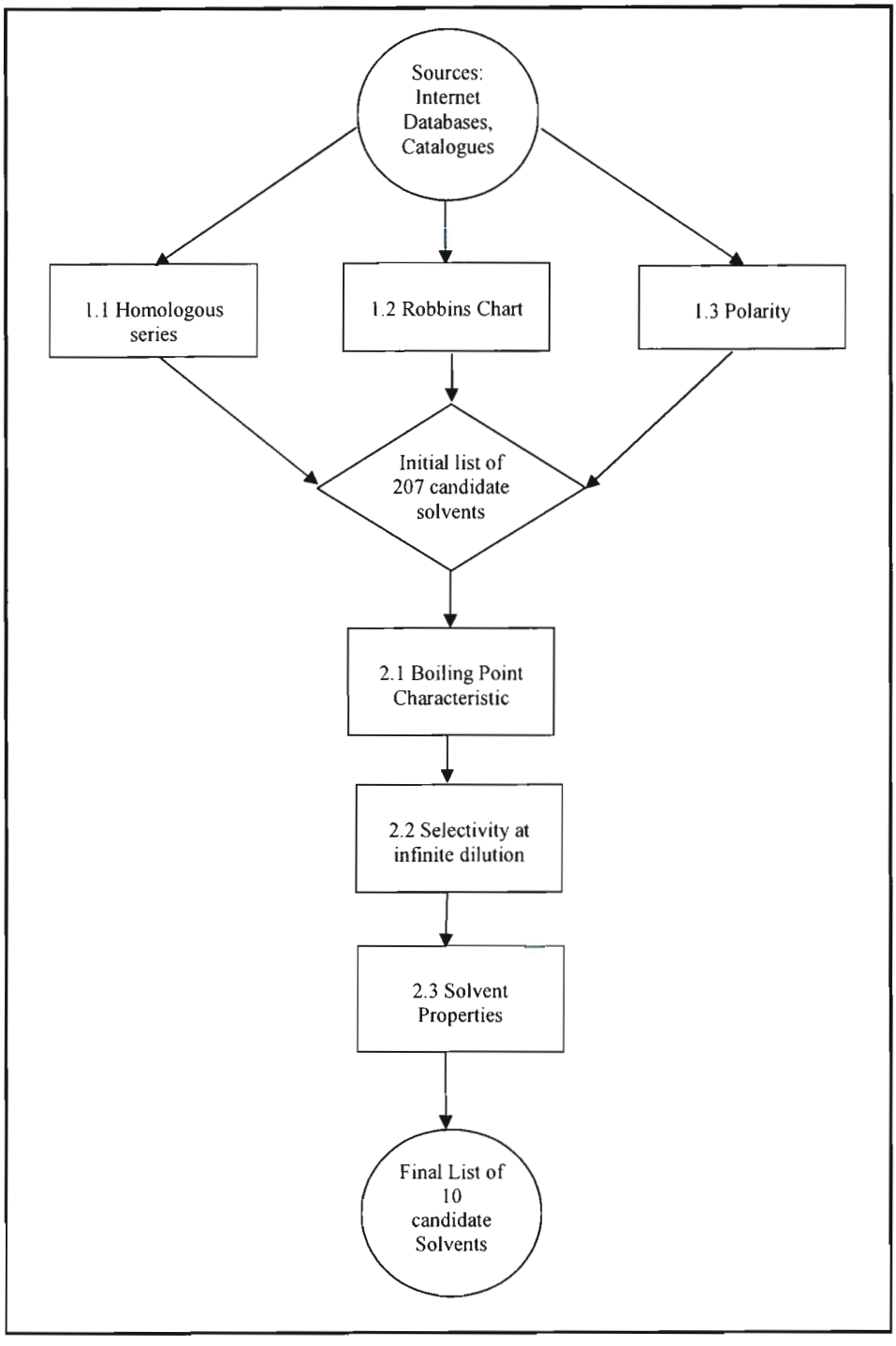

Figure 3.1. A flow diagram of the two step solvent selection procedure of (Seader et al. 1997).

Table 3.1 and Figure 3.1 summarise and illustrate the methodology behind the solvent selection process of (Seader et al. 1997). The two step procedure was systematically applied for the compilation of an initial list of two hundred and seven candidate solvents via step one, which upon further application of step two resulted in a shortlist of thirty solvents and a final list of ten solvents.

The solvent selection procedure is described in detail in the following section of this dissertation, however, only the methodology utilised for the solvent selection procedure is described. The rationale and individual choices made for each step in the procedure is presented in the discussion section of this dissertation.

3.1. BROAD SCREENING OF SOLVENTS BY FUNCTIONAL GROUP

The starting point of the solvent selection procedure lay in the compilation of a list of possible commercially available candidate solvents. Numerous sources were referenced in the compilation of the initial list of two hundred and seven solvents including several internet solvent databases such as (NCMS 2008), (Barton 2008) and (CARB 2008). The available catalogues of local chemical companies (Merck 2008) and (Sigma-Aldrich 2008), which distributes the Fluka Riedel-de-Haen brands, were consulted.

The initial list of two hundred and seven solvents is presented in Table A.1, Appendix A.

3.1.1. Homologous Series and Chemical Nature

The first identification of candidate solvents was made on the basis of the chemical nature and behaviour of the key components. The key components, HFP and HFPO are of the species fluorocarbons, i.e. fluorine containing hydrocarbons, and commercial solvents were identified that were homologous (display similar chemical characteristics i.e. boiling points, structure, bonding and other physical properties) in nature to the key components. Homologous solvents were thus identified from the various commercial solvent sources and short-listed on the initial candidate solvent list.

3.1.2. Robbins Chart and Hydrogen Bonding Interactions

Candidate solvents were further identified on the basis of hydrogen bonding interactions and the Robbins chart. Hydrogen bonding between a solvent and a solute, or in terms of a proton-donor and a proton acceptor, often plays an important role in affecting solubility and in the separation of various components, with hydrogen bonding and electron donor-acceptor interactions producing the strongest deviation from Raoult's law. Deviations from Raoult's law can be either positive ($\gamma_i > 1$), or negative ($\gamma_i < 1$). A negative deviation reduces the activity of a solute which can in some cases enhance the liquid-liquid partition ratio

but leads to the formation of maximum boiling azeotropes. Conversely, a positive deviation results in the formation of minimum boiling azeotropes. An indicator of solvent suitability was that the solvent should not form azeotropes with any of the key components in the mixture, hence it was desirable to choose a solvent which when added to the system, resulted in non-azeotropic easily separable mixtures.

In general, hydrogen bonding can be quite strong with the interaction increasing for more acidic donors and more basic acceptors. However, pK_a values are generally a poor guide to the relative strengths of compounds as hydrogen bonding donors or acceptors ((Rohrschneider 1973)). To overcome the use of pK_a values as an indication of hydrogen bonding interactions, (Barwick 1997) recommended the use of experimental data for hydrogen bonding compounds. The Robbins chart, Figure 3.2, is an empirical table of hydrogen bonding interactions between components which provided a qualitative guide to solvent selection. The chart categorises the solute and potential solvents into various classes based on chemical structure. To utilise the Robbins chart, the solute class must first be identified from the twelve available solute classes. With the solute class identified, one moves from left to right across Figure 3.2 to locate that solvent class which corresponds to a zero deviation from Raoult's Law. It must be noted that the solvents are segregated into the same twelve classes as the solutes on the Robbins chart. In this manner potential solvent classes for HFP and HFPO were identified and simultaneously certain solvent classes were excluded.

Solute class		Solvent class											
		1	2	3	4	5	6	7	8	9	10	11	12
	H donor groups												
1	Phenol	0	0	–	0	–	–	–	–	–	–	+	+
2	Acid, thiol	0	0	–	0	–	–	0	0	0	0	+	+
3	Alcohol, water	–	–	0	+	+	0	–	–	+	+	+	+
4	Active H on multihalogen paraffin	0	0	+	0	–	–	–	–	–	–	0	+
	H acceptor groups												
5	Ketone, amide with no H on N, sulfone, phosphine oxide	–	–	+	–	0	+	+	+	+	+	+	+
6	Tertiary amine	–	–	0	–	+	0	+	+	0	+	0	0
7	Secondary amine	–	0	–	–	+	+	0	0	0	0	0	+
8	Primary amine, ammonia, amide with 2H on N	–	0	–	–	+	+	0	0	+	+	+	+
9	Ether, oxide, sulfoxide	–	0	+	–	+	0	0	+	0	+	0	+
10	Ester, aldehyde, carbonate, phosphate, nitrate, nitrite, nitrile, intramolecular bonding, e.g., o-nitrophenol	–	0	+	–	+	+	0	+	+	0	+	+
11	Aromatic, olefin, halogen aromatic, multihalogen paraffin without active H, monohalogen paraffin	+	+	+	0	+	0	0	+	0	+	0	0
	Non-H-bonding groups												
12	Paraffin, carbon disulfide	+	+	+	+	+	0	+	+	+	+	0	0

Figure 3.2. The Robbins chart of organic group (hydrogen bonding) interactions for solvent selection ((Perry and Green 1997)).

3.1.3. Polarity Characteristics

Solutes and solvents can be broadly classified into polar (hydrophilic) and non-polar (lipophillic) classes. The polarity of a solvent determines in what type of compound it is able to dissolve and with what other solvents or liquid compounds it is miscible with. (Rohrschneider 1973) defined polarity as the relative ability of a molecule to engage in strong interactions with other polar molecules. However the relative polarity values for a solvent are not in themselves sufficient to predict the solubility of a given compound. (Barwick 1997) suggested that polarity considerations can be used to form an initial estimate of solvent solubility but specific molecular interactions (hydrogen bonding interactions via the Robbins chart) must also be considered, in conjunction with polarity, to refine this estimate of solubility. Polar solvents dissolve polar compounds best and non-polar solvents dissolve non-polar compounds best i.e. most solvents preferentially dissolve solutes of similar relative polarity. Fluorine is the most electronegative atom on the period table with a value of 3.98 on the Pauling scale. When bonded to a carbon atom, as in the compounds HFP and HFPO, the resulting compounds are primarily polar in nature. Further short listing of candidate solvents was thus done on the basis of choosing polar solvents over non polar alternatives. The determination of the polarity of the candidate solvents was performed in a qualitative manner via the identification of the molecular structure, attached functional groups or hetero-atom substituents and molecule chain length.

3.2. IDENTIFICATION OF INDIVIDUAL CANDIDATE SOLVENTS

Following the methodology outlined in step one of the solvent selection procedure, a list of two hundred and seven commercial solvents was compiled.

Step two of the solvent selection procedure was undertaken to refine the initial list to an intermediate list of thirty candidate solvents, which was consolidated into a final list of ten solvents and presented to PELCHEM and NECSA in August 2006. Step two of the solvent selection procedure is detailed in the following paragraphs. The list of the top thirty candidate solvents is presented in Table 7.2, while the list of the final ten solvents is presented in Table 7.3, Chapter seven of this dissertation.

3.2.1. Boiling Point Characteristic

(Lei et al. 2003) recommended that in general, a solvent should possess a much higher boiling point than the components to be separated in order to ensure the complete recovery of the solvent. The boiling points of each of the two hundred and seven individual candidate solvents from Table A.1, Appendix A, were identified via the Component Plus pure component database ((ProSim 2001)) and DDB ((DDBST 2007)),

and used as a basis to eliminate unsuitable solvents. It was desirable to obtain solvents which were relatively high boiling and non volatile components, to ensure that the formation of azeotropes with either HFP or HFPO did not occur. Solvents which displayed a 10 to 20 K boiling point difference either greater or less than the boiling points of HFP and HFPO were considered. This permitted the selection of both liquid and gases. Although only liquid solvents are suitable for an extractive distillation procedure, the selection of gases was allowed with the aim of using potential gases as supercritical solvents. Utilising the boiling point characteristic criteria, approximately twenty seven solvents were eliminated from the initial solvent list of two hundred and seven solvents. This resulted in a revised list of one hundred and eighty solvents which needed to be quantified and thus ranked according to a performance scale.

3.2.2. Selectivity at Infinite Dilution via UNIFAC

The performance of the identified solvents had to be evaluated and ranked such that the list of one hundred and eighty solvents could be consolidated to a more practical size. (Bastos et al. 1985) recommended the use of selectivity values, in conjunction with the activity coefficients at infinite dilution, for such an evaluation.

The concept of Selectivity

In an extractive distillation procedure, a high boiling solvent is added to a mixture to produce an alteration of the key components relative volatility. The ease of separation of a given mixture with key components *i* and *j* is given by the relative volatility:

$$\alpha_{ij} = \frac{y_i / x_i}{y_j / x_j} = \frac{\Phi_i^{sat} \Phi_j POY_i \gamma_i P_i^{sat}}{\Phi_j^{sat} \Phi_i POY_j \gamma_j P_j^{sat}} \qquad (3\text{-}1)$$

where the following definitions apply:

α	=	Relative volatility
γ	=	Activity coefficient
Φ	=	Fugacity coefficient in the vapour phase
Φ^{sat}	=	Fugacity coefficient at saturation
POY	=	Poynting correction factor
P^{sat}	=	Saturated vapour pressure

At low to moderate pressures, equation (3-1) simplifies to equation (3-2) as the fugacity coefficients and correction factors approximate to unity.

$$\alpha_{ij} = \frac{\gamma_i P_i^{sat}}{\gamma_j P_j^{sat}} \tag{3-2}$$

A solvent is introduced to a mixture to alter the relative volatility as far away from unity as possible. In the presence of a solvent, a new value of relative volatility is obtained, and equation (3-2) can be rewritten as (where the subscript S refers to the solvent):

$$\alpha_{ij} = \frac{\gamma^S{}_i P_{i,S}^{sat}}{\gamma^S{}_j P_{j,S}^{sat}} \tag{3-3}$$

As the ratio of the vapour pressures of the pure component is not normally significantly affected by changes in boiling point temperature at constant pressure due to the addition of the solvent, the solvent influence is usually quantified in terms of the selectivity, β, which is defined as the ratio of the activity coefficients of both key components in the presence of a solvent:

$$\beta = \frac{\gamma_i^S}{\gamma_j^S} \tag{3-4}$$

As the activity coefficients depend on phase composition and the role of the solvent tends to increase with an increase of its concentration, it is common practice to consider, at least in a preliminary step of solvent selection, the situation at infinite dilution. The selectivity at infinite dilution is defined as the ratio of the activity coefficients at infinite dilution of both components in the solvent.

$$\beta^{\infty} = \frac{\gamma_i^{\infty}}{\gamma_j^{\infty}} \tag{3-5}$$

Where γ_i^{∞} is the activity coefficient at infinite dilution for component i and γ_j^{∞} is the activity coefficient at infinite dilution for component j.

The selectivity model that was used for the calculations in this project is given by equation (3-6). It is defined as the value of the infinite dilution activity coefficient of HFPO in the solvent being evaluated, divided by the infinite dilution activity coefficient of HFP in the solvent being evaluated.

$$\beta^{\infty} = \frac{\gamma^{\infty}_{HFPO,S}}{\gamma^{\infty}_{HFP,S}} \tag{3-6}$$

The natural relative volatility of the HFP and HFPO mixture is such that in a conventional distillation column, the component HFP is removed as a distillate product with HFPO removed as a bottoms product. (Seader et al. 1997) states that the possibility that the expected relative volatility for a system may be reversed by the addition of a solvent, is entirely a function of the way the solvent interacts with and modifies the activity coefficients and thus the volatilities of the components in the mixture. In general, the addition of a solvent has a pronounced effect on the activity coefficient of a mixture. The solvent tends to lessen the non-idealities of the key component which exhibits similar liquid phase behaviour of the solvent, while enhancing the non-ideal behaviour of the dissimilar key component. The solvent and the similar key component thus form an ideal or nearly ideal liquid solution and exhibit little molecular interactions, while the solvent and the dissimilar key component demonstrate unfavourable molecular interactions which will cause the activity coefficient of this key to increase.

The natural relative volatility of the system is enhanced when the activity coefficient at infinite dilution of the lower boiling component, for this project HFP, is increased by the addition of the solvent. The increase of the activity coefficient of HFP indicates that the solvent preferentially dissolves HFPO forming an almost ideal liquid phase. In this case, the selectivity value at infinite dilution will decrease to a value less than unity and the lower boiling component HFP will be collected in the distillate according to the natural relative volatility of the system.

In order for the higher boiling component HFPO to be collected in the distillate, the addition of the solvent must increase the infinite dilution activity coefficient of the HFPO. This physically means that the solvent must preferentially bond with HFP and form an almost ideal liquid phase and thus increase the infinite dilution activity coefficient of HFPO in the mixture and thus the selectivity at infinite dilution to a value greater than unity.

According to the definition of selectivity used, the values of β^{∞} calculated thus signify the following, with HFP initially the more volatile component, i.e. the light key, while HFPO is initially the less volatile component, i.e. the heavy key:

Value	Physical Meaning
$\beta^{\infty} > 1$	Solvent preferentially bonds with HFP and increases the activity coefficient of HFPO such the mixture is amenable to separation and HFPO is removed in the distillate.
$\beta^{\infty} < 1$	Solvent preferentially bonds with HFPO and increases the activity coefficient of HFP such that the mixture is amenable to separation and HFP is removed in the distillate.

Table 3.2. Possible values of selectivity at infinite dilution.

In Table 3.2, the physical meanings of the calculated values of selectivity at infinite dilution are summarised. For systems which are difficult to separate via conventional means, the relative volatilities between the key components are unity or close to unity. According to the selectivity model used, if the calculated β^{∞} was greater than unity, then the solvent bonded with the HFP resulting a purified HFPO product stream. If the calculated β^{∞} was less than unity, then the solvent bonded with the HFPO resulting in a purified HFP stream.

For the evaluation of the selectivity at infinite dilution, values of the infinite dilution activity coefficient of HFP and HFPO in each of the candidate solvents were required. These values are typically found in thermo-physical property databanks such as the DDB, however, as revealed by the comprehensive literature review, published mixture and pure component data for HFPO is severely lacking. According to the excellent review of (Lei et al. 2003) there are four prominent methods to determine experimental infinite dilution activity coefficients and thus selectivity values: the direct method, the gas-liquid chromatography method, ebulliometry methods and inert gas stripping or gas chromatography methods. The most reliable values for the infinite dilution activity coefficient are obtained experimentally either by gas-liquid chromatography techniques or by ebulliometry. However, the measurement of phase equilibrium for multi-component systems (HFP, HFPO and each solvent) is generally time consuming and expensive, as demonstrated by (Gmehling 1999). As a result, a predictive thermodynamic model which would allow for the reliable prediction of the phase equilibrium behaviour of multi-component systems, in particular the infinite dilution activity coefficients as a function of temperature, pressure and composition was required.

The UNIFAC Group Contribution Method

For this research project, the original UNIFAC method of (Fredenslund et al. 1977) was utilised. The theory and concept behind the UNIFAC method is excellently presented in the work of (Fredenslund et al. 1977) and as such, only a summary of this method is presented in Section A.2, Appendix A. (Gmehling 2001) states that the general idea of a group contribution method is that a molecule consists of different functional groups and that the thermodynamic properties of a solution can thus be correlated in terms of these functional groups. The advantage of this method is that a very large number of mixtures can be

described by a relatively small number of functional groups. In the UNIFAC group contribution model, there are two types of functional groups:

1. Main Groups
2. Subgroups

Subgroups are the smallest building blocks which make up a molecule, while the main groups are used to group subgroups together. For example, the main group CH_2 contains the subgroups C, CH, CH_2 and CH_3. The reason for this distinction of groups is that although the subgroups have different volume and surface area parameters, the interaction parameters are the same for all subgroups within a particular main group.

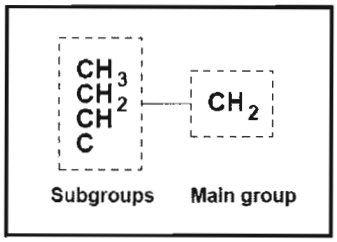

Figure 3.3. Schematic representation of the grouping of subgroups into main groups in UNIFAC.

To use the UNIFAC model, functional group assignment of the components involved must be carried out. The following examples illustrate the trivial group assignment for the components acetone and benzene.

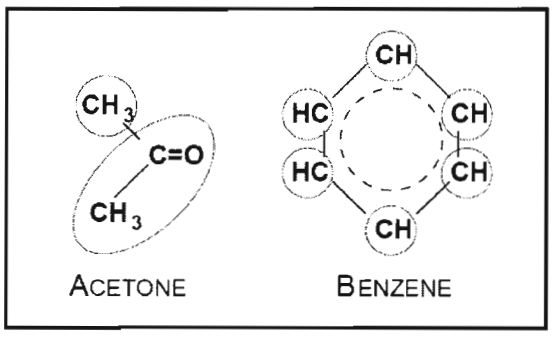

Figure 3.4. The division of components acetone and benzene into functional groups defined by the UNIFAC model.

There are three types of parameters needed for the UNIFAC model:

1. R_k = van der Waals group volume parameter
2. Q_k = van der Waals group surface area parameter
3. a_{mn} and a_{nm} = Group interaction parameter.

The group interaction parameters a_{mn} and a_{nm} are periodically published in journals for certain group interactions. These parameters are regressed from experimental binary VLE data, however the freely available published data ((Gmehling 1995), (Gmehling 2001) and (Bastos et al. 1985)) does not contain the latest revised interaction parameters for the UNIFAC model. The UNIFAC Consortium, which is a company consortium founded at the University of Oldenburg, periodically updates and revises the UNIFAC interaction parameters via VLE data obtained from the DDB ((Jakob 2008)). Access to these revised UNIFAC binary interaction parameters can only be obtained by joining the UNIFAC consortium. The Thermodynamics Research Unit at the University of KwaZulu-Natal became a member of the consortium in 2006 and the latest interaction parameters which were obtained via membership were used in this research project.

Selectivity Calculations and xlUNIFAC

The procedure used for the calculation of the infinite dilution activity coefficients and thus the resulting selectivity values, is outlined in Table 3.3.

Step	Description
1	Functional group assignment of HFP and HFPO
2	Functional group assignment of solvent to be evaluated
3	Evaluate infinite dilution activity coefficients at 273.15 and 323.15 K
4	Evaluate selectivity at infinite dilution

Table 3.3. Procedure for the evaluation of selectivity at infinite dilution.

The procedure outlined in Table 3.3 was undertaken for the one hundred and eighty solvents which remained on the candidate solvent list after the exclusion of solvents due to the boiling point characteristic criteria. Step 1 was performed once off and steps 2 to 4 were repeated for the selectivity calculations for each of the one hundred and eighty possible solvents. The repetitive calculations were undertaken in the computer software xlUNIFAC ((Randhol and Engelien 2000)), which is a Visual Basic based programme using the Microsoft Excel user interface. The functional group assignment for each of one hundred and eighty solvents were performed manually as the development of an algorithm to perform automatic functional group assignment or fragmentation for the identified diverse solvent classes was considered beyond the scope of this project.

The xlUNIFAC software was obtained as freeware under the GNU General Public License ((GNU 2007)), and as such allowed open ended modification of the software without the prior consent of the original coders. A brief description of the xlUNIFAC software is presented in Section A.3, Appendix A. The original version of xlUNIFAC (version 1) did not contain the necessary interaction parameters and functional groups that were needed for this project. Only forty seven primary functional groups were available in the original version and crucially, the chlorinated hydrocarbon and chlorofluorohydrocarbon groups were unavailable. The latest functional groups and corresponding interaction parameters purchased from the UNIFAC consortium were utilised and the program modified to incorporate the additional data. As a result, the modified version of xlUNIFAC which was used for this research project contained seventy two functional groups. Furthermore, the data purchased from the consortium contained updated interaction parameters for the forty seven groups in the original version of xlUNIFAC.

Each of the one hundred and eighty candidate solvents were broken up into their respective functional groups and input into the xlUNIFAC software. Problems were encountered with the functional group assignment for some of the solvent molecules due to a lack of binary interaction parameters for certain functional groups. The lack of data was the result of a lack of binary VLE data for systems involving certain functional groups. As a way to work around this problem, the functional group assignment for any affected molecules was performed in such a way as to minimise the effects of the missing interaction parameters.

Using the selectivity model defined in equation (3-6), in conjunction with UNIFAC model via the xlUNIFAC computer software, the selectivity at infinite dilution for HFP and HFPO in each of the one hundred and eighty solvents were evaluated. This evaluation allowed the ranking of the one hundred and eighty solvents, and from this list, the top thirty performing solvents were chosen.

The evaluation of the selectivity values at infinite dilution for each solvent was done in conjunction with (Nelson 2008), who evaluated the selectivity values at 273.15 and 323.15 K, via xlUNIFAC, for the following solvent classes: Chlorofluorocarbons, Esters, Glycol Ethers, Polyhydric Alcohols, the Methane series refrigerants and Amines. The selectivity values evaluated by (Nelson 2008) for the six solvent classes were used in conjunction with the selectivity values determined for the following five solvent classes for this research project: Alcohols, Hydrochlorofluorocarbons, Ethers, Ketones and the Ethane series refrigerants. In total, the selectivity values at 273.15 and 323.15 K for the one hundred and eighty solvents were determined and these values were used for this research project and in the work of (Nelson 2008).

The ranking of the top thirty solvents was done on the basis of identifying the best performing solvents with selectivity values far removed from unity, i.e. solvents with selectivity values far greater and far less than

one. The list of the one hundred and eighty solvents with calculated selectivity values at the two temperatures of evaluation, 273.15 and 323.15 K, is presented in Table A.3, Appendix A. The list of the top thirty solvents as well as the performance of the individual solvent classes is presented in Chapter seven, the results and discussion section of this dissertation.

3.2.3. Solvent properties

The list of thirty candidate solvents was produced by determining the best performing solvents with selectivity values far removed from unity from the list of one hundred and eighty solvents. This list of thirty was further narrowed down to a final list of ten solvents, on the basis of individual solvent properties.

(Barwick 1997) recommended the evaluation of the peripheral properties of solvents, i.e. properties which are of interest in a solvent selection procedure but do not directly affect the separation. Such properties included safety, economics, boiling point, density and viscosity. (Gani and Brignole 1983) stated that the primary solvent properties that should be taken into account include selectivity at infinite dilution, boiling point considerations, density and viscosity. The excellent work of (Seader et al. 1997) suggested that important solvent properties that should not be overlooked include selectivity, recoverability, solvent capacity and solvent solubility, while (Lei et al. 2003) concurred with the recommendations of (Barwick 1997) and (Seader et al. 1997) by stating that although relative volatility and therefore selectivity is the most important consideration, other criteria such as corrosion, price, availability and solvent recovery in terms of boiling point difference, should also be taken into account.

For this work, the following solvent properties for each of the solvents on the top thirty list were evaluated and used as a basis for the elimination of unsuitable candidates to obtain a final list of ten solvents:

1. *Recoverability:* The solvent should be easily separable from the distillation products to facilitate solvent recycling and should also be stable at the temperature of the distillation and extraction to prevent thermal degradation of the material. An indication of the degree of recoverability of the solvent with the solute was the difference in boiling points between the components. A large difference in boiling points indicates a good recoverability and vice versa, and this criteria was used to compare between the various solvents on the top thirty list

2. *Economic Considerations:* Desirable solvent properties were good availability and cost. Quotations for the various solvents on the top thirty list were obtained from the catalogue listing function of the SciFinder Scholar research software and compared. The degree of availability for the solvents was also quantified through the identification of the number of commercial sources available on the catalogue

listing function of the SciFinder Scholar research software, with each solvent accorded a rating of availability which was determined by the overall number of possible commercial sources

3. *Reactivity:* The chosen solvent should be inert or non reactive with respect to the key components and should not undergo decomposition or side reactions to form undesirable products. Material Safety and Data Sheets (MSDS) for each of the thirty solvents were referenced to ascertain the chemical compatibilities of each solvent and this criterion was used as a further basis of comparison among the thirty solvents on the list

4. *Safety and environmental:* Environmental considerations played an important role in the final stages of the solvent selection procedure. Several of the candidate solvents on the top thirty list were halogenated hydrocarbons containing fluorine and chlorine molecules. The use of such compounds is prohibited or restricted by the Montréal Protocol ((UN 1987)). The Montréal protocol on substances that deplete the ozone layer is an international treaty designed to protect the ozone layer by the phasing out of a number of substances believed to be responsible for ozone depletion. The treaty is structured around several groups of halogenated hydrocarbons that have been shown to play a role in ozone depletion. The ozone depletion potential (ODP) of the applicable solvents were used as a basis for comparison and selection of the final ten solvents. Additionally, health and safety aspects of each solvent were taken into consideration. The toxicity, via the LD_{50} values and flammability of each solvent was identified and taken into account.

Using the above solvent properties as individual criteria, the properties of the top thirty performing solvents were compared. On the basis of these comparisons, the list of thirty solvents was shortened to a final list of ten solvents which was presented to PELCHEM and NECSA in August 2006. This list of ten solvents can be found in the Chapter seven, Table 7.3 of this dissertation.

CHAPTER FOUR

4. EXPERIMENTAL MEASUREMENTS

(Gmehling 2001) states that for the synthesis, design and optimization of separation processes, reliable knowledge of the real phase equilibrium behavior of the system is necessary. The theories of phase equilibrium thermodynamics have provided a framework that allows for the interpolation and extrapolation of limited experimental data and to make reasonable predictions for systems that have not been previously investigated. However, in certain cases the behaviour of real, complex mixtures is far more complicated than the models available ((Naidoo 2004)). Therefore, the need for accurate experimental data is of paramount importance.

This project involved the preliminary design of a separation process for HFP and HFPO involving the aromatic solvent toluene and the refrigerant R116. The development of a separation scheme involving these components thus necessitated VLE data for the binary systems HFP + HFPO, HFP + toluene, HFPO + toluene, R116 + HFP and R116 + HFPO. A literature review revealed that no published data existed for any of these systems. It was thus necessary to experimentally determine the required sets of binary HPVLE data. The resulting experimental measurements were undertaken at the TEP laboratories headed by Professor Dominique Richon at Ecoles des Mines de Paris during a three month period in 2006. In addition to the binary HPVLE data sets, pure component vapour pressure data for HFPO were measured.

The two methods employed for the measurements were the static synthetic method and the static analytic method. (Richon 1996) states that for vapour-liquid equilibria, two methods exist for the classification of experimental methods and techniques.

The first classification is via the method in which equilibrium is obtained:

1. *Static methods:* In this method, a sufficient number of variables are fixed, generally the temperature, global composition, volume or pressure, and the system is allowed to attain equilibrium under stirring or agitation

2. *Dynamic methods:* In this method, at least one of the equilibrium phases is allowed to circulate, providing the necessary agitation to reach equilibrium.

The second method is according to the way in which composition is measured:

1. *Synthetic methods:* The global composition of the mixture to be studied is known *a priori*, typically by weighing, and experimental conditions are created in which the phase of known composition is brought to the bubble or dew point. An example of this method is given by (Meskel-Lesavre et al. 1981) and a feature of this technique is that no sampling of the equilibrium phases are necessary

2. *Analytical Methods:* (Coquelet et al. 2006) classifies the analytic method as a direct sampling technique, with the composition of the phases in equilibrium obtained by analysis after sampling. Gas chromatographic techniques are generally used for analysis of the sampled equilibrium phases.

4.1. MEASURED SYSTEMS

The binary data sets measured for this research project are indicated in Table 4.1:

Binary System	Component 1	Component 2	Method	Isotherm [K]
1	HFP	Toluene	SS	273.15, 313.15
2	HFPO	Toluene	SS	273.15, 313.15
3	HFP	R 116	SA	273.15, 313.15
4	HFPO	R 116	SA	273.15, 313.15

Table 4.1. A summary of the measured binary HPVLE data sets and conditions of measurement. SS = static synthetic method, SA = static analytic method.

For the systems involving the aromatic solvent toluene, the static synthetic method employing a variable volume cell for the experimental determination of the bubble point and saturated liquid molar volumes, was used. For the systems involving the refrigerant R116, the static analytic method employing a ROLSI sampler with chromatographic analysis, was utilised. The four binary systems were each measured at two isotherms as prescribed by PELCHEM viz. 273.15 and 313.15 K. The pure component vapour pressure for component HFPO was measured in the temperature range of 271.90 to 318.20 K. The four binary systems and the pure component vapour pressure data for HFPO have not previously been published and thus constitute new data.

4.2. CHEMICALS

A summary of the chemicals used for the experimental HPVLE measurements undertaken in this project is presented in Table 4.2.

Component	CAS Index Number	Supplier	Purity [mole %]
Hexafluoropropylene (R1216)	116-15-4	Interchim/Boc Edwards	99.5
Hexafluoropropylene oxide	428-59-1	Interchim/Boc Edwards	99
Toluene	108-88-3	Prolabo/Merck	99.9
Hexafluoroethane (R116)	76-16-4	Air Liquide	99.999

Table 4.2. A summary of the components, sources and associated chemical purities used in the HPVLE measurements.

The components HFP and HFPO were purchased in 500 g quantities from Interchim/Boc Edwards of Montlucon, France at purities of 99.5 HFP (mole %) and 99 % HFPO (mole %) respectively. Toluene, of Pestinorm or chromatography grade, was purchased from Prolabo/Merck, France in a 5 litre bottle at a certified minimum purity of 99.9 %. Hexafluoroethane (R116) was purchased in a 5 kg cylinder from Air Liquide of Richemont, France at a certified minimum purity of 99.999 %. All the chemicals used in the experimental measurements were degassed under vacuum before use to remove any impurities.

4.3. THE STATIC SYNTHETIC APPARATUS

The systems involving HFP, HFPO and the liquid solvent toluene were measured on the static synthetic apparatus of (Valtz et al. 1987) which utilized a variable volume cell for the determination of vapour-liquid equilibria (*P-x* data sets) and saturated liquid molar volumes. The apparatus of (Valtz et al. 1987) is a modification of the experimental setup of (Fontalba et al. 1984), which is further based on the novel variable volume equilibrium cell of (Meskel-Lesavre et al. 1981). The static synthetic apparatus has the ability to perform the simultaneous determination of vapour liquid equilibria and saturated liquid molar volumes at extreme operating conditions of up to 45 MPa and 433 K. The equipment was specifically designed for the study of hydrocarbon-carbon dioxide systems for the petroleum industry, and has since found extensive use in the TEP laboratories for the HPVLE measurements for refrigerant systems.

A review of measurements involving only refrigerants or aromatics measured on the static synthetic apparatus was undertaken and is presented in Table 4.3. The numerous refrigerant and aromatic systems measured on this apparatus indicated that the static synthetic equipment was well suited to these types of systems.

Reference	Systems	Temperature [K]
(Laugier et al. 1994)	R113 + C_2H_6O	298, 373
	R114 + C_2H_6O	298, 348, 372
(Laugier et al. 1994a)	C_4H_{10} + R113	363, 383, 403, 423
	C_5H_{12} + R114	363, 383, 403, 423
	C_6H_{14} + R114	362, 378, 393, 408
	C_6H_6 + R114	363, 383, 403, 423
(Richon et al. 1992)	N_2 + C_7H_8	313, 393, 473
	CO_2 + C_7H_8	313, 393, 473
	H_2S + C_7H_8	313, 393, 473
(Richon et al. 1992a)	CH_4 + C_7H_8	313, 393, 473
	C_2H_6 + C_7H_8	313, 393, 473
	C_3H_8 + C_7H_8	313, 393, 473
(Chareton et al. 1990)	R114 + FC75	398, 423
	R23 + R11	298, 348, 372
(Valtz et al. 1987)	R113 + R152A	298, 323, 348, 372
	R113 + R12	298, 323, 348, 372
(Galivel-Solastiouk et al. 1986)	C_3H_8 + CH_4O	313, 343, 373
(Guillevic et al. 1985)	H_2O+ NH_3	403, 453, 503
(Guillevic et al. 1983)	C_3H_8 + C_8H_{18}	427, 523
(Legret et al. 1982)	CH_4 + C_7H_8	313
(Meskel-Lesavre et al. 1982)	R113 + R11	298, 373
(Meskel-Lesavre et al. 1981)	C_2H_6 + $C_{12}H_{26}$	308, 338

Table 4.3. A review of binary HPVLE data involving refrigerants or aromatics measured on the static synthetic apparatus.

4.3.1. Equipment Description

A flow diagram detailing the experimental setup of the static synthetic apparatus is presented in Figure 4.1.

The components of the binary system to be studied are accurately weighed to determine the global composition of the mixture and then introduced separately into the equilibrium cell. The volume of the equilibrium cell (1) was varied through the use of a pressurizing device and associated pressurizing system. The cell and pressurizing device were kept at the constant temperature of the measurements in an air thermostat (7), while the pressure imparted by the pressurizing system was transmitted by a free moving piston which separated the inside of the equilibrium cell from the pressurizing liquid. The sealing between the binary mixtures that were studied and the pressurizing liquid was achieved through the use of the correct choice of polymer O-ring, which was placed into a groove that was machined around the piston. The correct type of polymer for the O-ring was chosen to prevent degradation of the seal by the components of the binary mixture. Degradation or failure of the O-ring led to the malfunctioning of the equipment as the pressurizing liquid would not be able to displace the piston. Table 4.4 lists the polymer O rings used on the equipment along with the name of the manufacturer and dimensions.

Part	Manufacturer	Polymer	Dimensions [mm]
Piston	Angst + Pfister	NBR Nitrile	25.07 x 2.62
Cell feeding line	Angst + Pfister	NBR Nitrile	4.2 x 1.9
Shaft	Victoria	FPM	4.9 x 1.9

Table 4.4. A summary of the types of O-ring used on static synthetic apparatus.

The NBR and FPM polymer O-rings were checked against the relevant chemical compatibility charts and found to be suitable for systems involving HFP and HFPO. For the piston and the cell feeding lines, the NBR Nitrile polymer O-ring was utilized. Nitrile is a copolymer of butadiene and acrylonitrile and has a good resistance to petroleum based oils and hydrocarbon fuels. It is suitable for low temperature applications, typically in the range of 238.15 to 393.15 K, and this coupled with the excellent resistance to petroleum products has made Nitrile the most widely used elastomer in the seal industry ((O-Ring-Info 2007a)). For the sealing on the shaft, the FPM polymer type O-ring was utilized. The FPM O-ring is a fluorocarbon rubber which has a wide range of chemical compatibility and is typically used in applications to resist harsh chemical attack ((O-Ring-Info 2007b)). The temperature range for the HPVLE measurements conducted for this research project was from 273.15 to 313.15 K which easily fell within the operating temperature limits for the two types of O-rings.

A cross sectional diagram of the equilibrium cell is presented in Figure 4.2. The cell, of maximum total volume V_T = 60 cm^3 as determined by the accurate calibration procedure described by (Meskel-Lesavre et al. 1981), was composed of a titanium alloy (AFNOR UTA6V). Cylindrical in shape, it contained the piston, 3 cm in diameter, which enveloped the embedded stirring attachment.

With reference to Figure 4.1, the system displacement transducer (2) acted under the pressure of the pressurising liquid to displace the piston and alter the volume of the equilibrium cell. The pressurising liquid, octane, was used as a pressure transmitter between the pressurizing device and a motorized high pressure volumetric pump (6). Inside the equilibrium cell, the binary vapour liquid equilibrium was maintained through vigorous magnetic stirring of the mixture by the stirrer attached to the movable piston. Rotating permanent magnets (8) were responsible for rotating the stirrer piston/stirrer attachment. A membrane pressure transducer (Bourdon Sedeme, 250 bar maximum) was fixed onto the cell for pressure measurements and at the bottom of the cell the translation of the piston was stopped by a specially designed stop screw.

The pressure in the cell is known as a function of the total volume of the cell, V_T, and the pressure transducer (12) was calibrated against a deadweight pressure tester, with the atmospheric pressure measured via a resonant sensor barometer. During the course of the experimental measurements, with the cell loaded with the binary system of interest and maintained at isothermal conditions, pressure as a function of V_T was obtained. The curve of P vs. V_T exhibits a discontinuity where the vapour phase disappears and this discontinuity corresponds to the bubble point of the mixture. Accurate values of the bubble pressure and saturated liquid phase molar volume can be simultaneously determined from the plot of P-V_T, and for different loadings of the equilibrium cell a P-x curve can be generated. At the bubble point, the liquid mole fraction is exactly the total mole fraction obtained by weighing of the individual components on the analytical balance.

The equilibrium cell was housed inside a climate controlled air bath or thermostat which was specially constructed by CLIMATS under the specifications of the TEP laboratory with a temperature range of operation from 233 to 433 K and a temperature regulation to within 0.1 K of set point. Two platinum resistance temperature probes (Pt-100) were located at different positions of the equilibrium cell and assembly, and the thermocouples are connected to a digital read out (FLUKE, model 2190A) with the two probes calculated against a 25 Ω reference platinum resistance thermometer. The 60 cm^3 cylindrical variable volume equilibrium cell is shown on Photograph 4.1. The location of the temperature probes, T1 and T2 are indicated on the image, along with the location of the pressure transducer and the feed line through which the cell is loaded and evacuated after use.

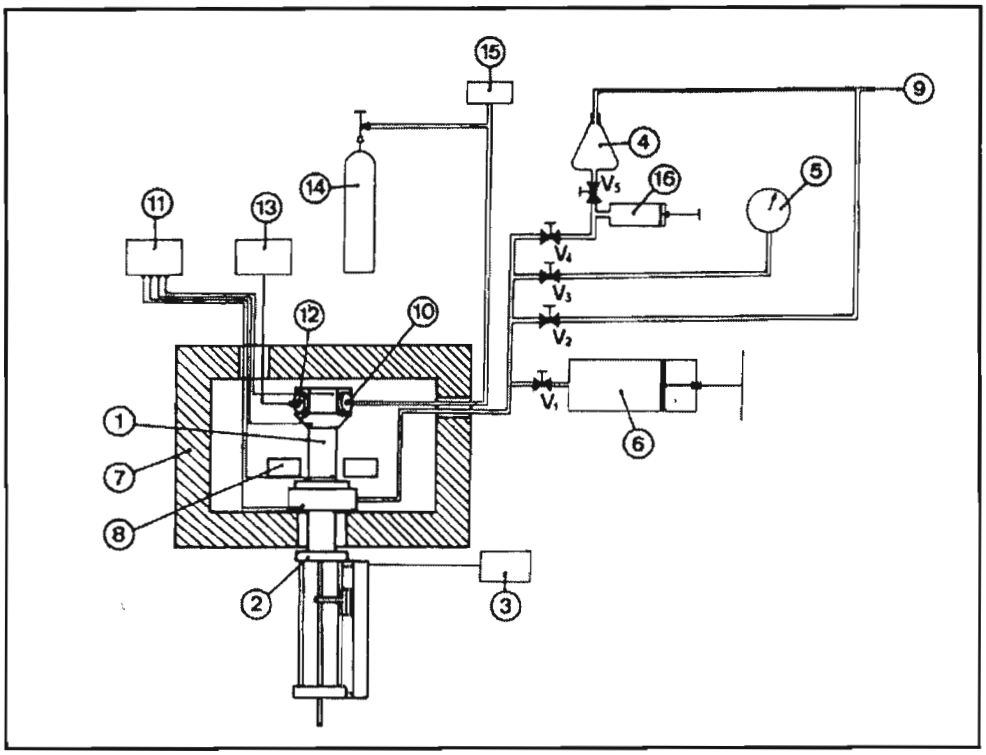

Figure 4.1. Flow diagram of the static synthetic apparatus.

Reproduced from (Valtz et al. 1987). 1: Equilibrium cell; 2: System Displacement transducer; 3: Displacement digital display; 4: Pressurising liquid degassing flask; 5: Manometer; 6: Motorised high pressure pump; 7: Air thermostat; 8: Rotating permanent magnets; 9: Fitting to vacuum pump; 10: Feed valve; 11: Temperature digital display; 12: Pressure transducer; 13: Pressure digital display; 14: Gas cylinder; 15: Heise digital manometer; 16: Manual pump.

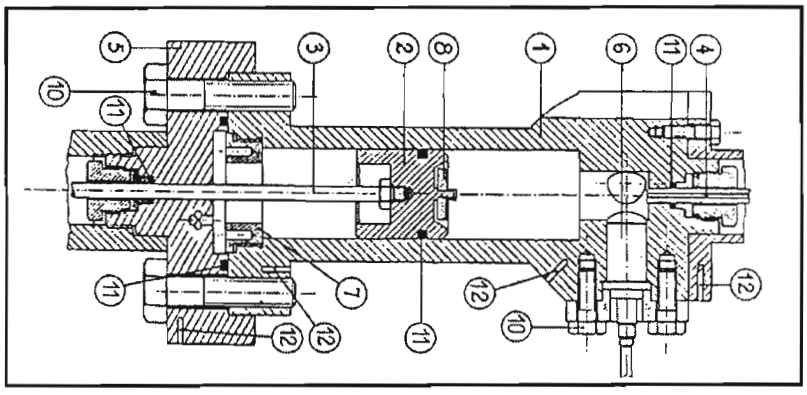

Figure 4.2. A cross section of the variable volume equilibrium cell.

Reproduced from (Fontalba et al. 1984). 1: Cell body, 2: Piston, 3: Piston measuring device, 4: Thermistor probe, 5: Pressurising assembly, 6: Membrane pressure transducer, 7: Stop screw, 8:Magnetic rod, 9: Seat of the loading valve, 10: Bolt, 11: O ring, 12: Thermocouple well.

Photograph 4.2 provides a pictorial overview of the static synthetic apparatus and equipment not visible in the flow diagram of Figure 4.1. The digital read out and displays for the temperature probes, pressure transducer and piston displacement unit are indicated, as well as the piston displacement control unit and vacuum pump. Table 4.5 lists the major ancillary equipment of the static synthetic apparatus, along with manufacture names and model numbers.

Equipment	Brand	Model
Piston displacement display	Heidenhain	PGM 246 180 10
Temperature probe (Pt-100) display	Fluke	2190A
Pressure transducer	Bourdon Sedeme, 250 bar	TF01A
Pressure transducer display	MeasureX	Beta-M 105628
Vacuum pump	Trivac	D2.5E, T121111212
Analytical balance	Mettler Toledo	H315
Electrical balance	Ohaus	GT41000 V

Table 4.5. Equipment listing for the static synthetic apparatus.

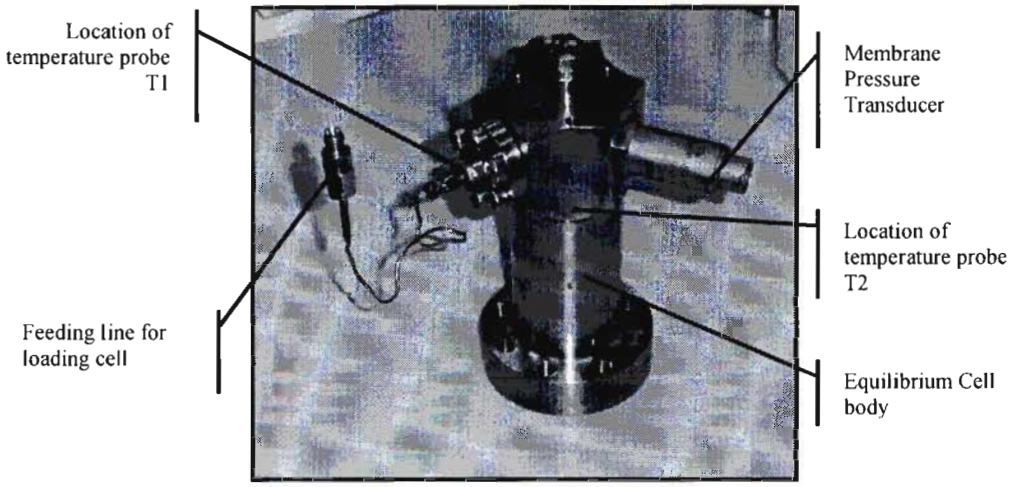

Photograph 4.1. The variable volume equilibrium cell.

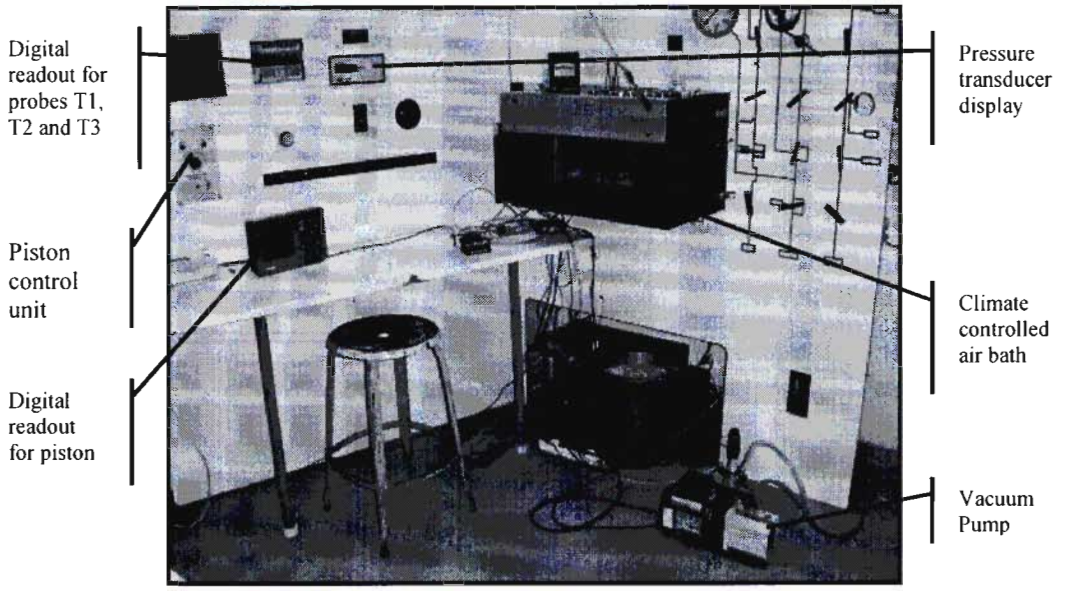

Photograph 4.2. The static synthetic apparatus.

4.3.2. Experimental procedure

Before the HPVLE measurements were initiated, components of the static analytic apparatus were calibrated. Calibration refers to the process of determining the relationship between the output or response of a measuring instrument and a measurement standard, and is necessary to ensure that the recorded variables, temperature or pressure, are indicative or a true reflection of the actual measurements and not due to equipment bias.

4.3.2.1. Pressure transducer calibration procedure

The calibrations for the pressure transducer located on the variable volume equilibrium cell were performed against a measurement standard, the dead weight pressure tester (Desgranges et Huot, model: 5202 S CP, 2-40 Mpa range). A dead weight tester works on the principle that an incoming pressurising force is counterbalanced by a dead weight on the testing unit. When this force is balanced, the actual pressure of the system is simply a measure of the dead weight load placed on the testing unit. The pressurizing medium, air, was connected from the air cylinder to the inlet port on the deadweight tester. The outlet port of the tester was connected to the inlet line of the equilibrium cell, so that the same pressure flowed though both the tester and the transducer. A data acquisition unit with a digital display (Hewlett Packard 34420A) was connected to the pressure transducer on the equilibrium cell. The air cylinder was initially opened to a low pressure, approximately 2 bar, with the dead weight tester under the default initialising load of 2 bar. With the air flowing from the cylinder through the equilibrium cell via the dead weight tester, the pressure

transducer on the cell emitted a pressure reading on the digital display. The pressure reading on the display is termed the 'Measured Pressure', while the pressure obtained from the deadweight tester or pressure standard is termed the 'Actual Pressure'. The actual pressure value of the tester was obtained by manually adjusting the incoming air flow on the cylinder via a regulator, to balance the weight load on the deadweight tester. Once the load was balanced with the air flow and the system was in equilibrium, the actual or 'true' pressure reading was obtained from the weight of the load on the dead weight tester and the measured pressure values are obtained from the digital display readout of the pressure transducer on the cell. Subsequent weight loads in the form of metal discs were added to the dead weight tester, and the air flow and thus pressure to the system increased from 2 bar to a maximum of 70 bar, and from 70 bar down to 2 bar, to investigate the effects of hysteris. At different weight loads of the system the actual pressure and measured pressure values were recorded and the resulting correlation or relationship determined.

4.3.2.2. Temperature probe calibration procedure

The two Pt-100 temperature probes designated T1 and T2, were calibrated against a 25 Ω reference platinum probe (TINSLEY Precision Instrument type 5187) which was certified by the Laboratoire National d'Essais (LNE Paris) according to the International Temperature Scale (ITS-90) protocol ((BIPM 2008)). Data acquisition for the temperature probes as well as the reference probe was performed on a computer linked to a data acquisition unit (Hewlett Packard 34420A). The temperature calibration consisted of immersing the two Pt-100 probes T1 and T2 as well as the reference probe in a liquid bath unit (Lauda, Ultra Kryomat), which utilised a ramping function for automatic incremental adjustment of the temperature. For the calibration procedure, the bath was filled with three liquids, depending on the temperature range of the calibrations. For the low temperature calibrations, in the temperature range of 233.15 to 273.15 K, the liquid bath was filled with ethanol, while in the low to medium temperature range, 273.15 to 353.15 K, the liquid bath was filled with water. In the high temperature range, 303.15 to 353.15 K, the liquid bath was filled with specialised heating oil supplied by DowTherm. The calibration procedure consisted of ramping the temperature from 273.15 to 323.15 K in increments of 0.005 K and logging the actual and measured temperatures. In this manner the relationship between actual temperature reading of the reference probe, and the measured temperature values of the three Pt-100 probes were obtained.

4.3.2.3. Vapour-Liquid equilibrium measurements

The experimental procedure followed for binary HPVLE measurements on the static synthetic apparatus was similar to that of (Valtz et al. 1987). The systems measured on this apparatus were HFP + toluene and HFPO + toluene at the 273.15 and 313.15 K isotherms, with the same experimental procedure employed for both systems.

The procedure consisted of three major steps, the filling of the cell, the set up of the cell in the air bath apparatus and the equilibrium measurements.

The equilibrium cell was first removed from the air bath and ancillary housings, cleaned with ethanol, evacuated and then weighed. The cell was light enough (1.8 kg) to allow the use of an accurate analytical balance. During the handling of the equilibrium cell, cottons gloves were worn at all times to prevent the formation of condensation on the cell which could potentially alter the accurate weighing procedure. After weighing the empty cell the heavy or less volatile component (toluene) was loaded into the equilibrium cell. The toluene was injected via a plastic syringe, under a fume hood, directly into the loading line of the equilibrium cell. The cell was then degassed (under vacuum) and first weighed on the electronic balance and then accurately weighed on the analytic balance, to precisely determine the amount of component added. For the addition of the lighter component HFP and in subsequent measurements HFPO, the cylinder was heated to create a temperature gradient and thus force the HFP or HFPO into the equilibrium cell. After the addition of the light component, the cell was once again weighed using the same precautions and procedure as before, and the overall or global composition of the mixture calculated. The uncertainties on the liquid mole fraction (Δx) due to the weighing procedure are calculated and tabulated with the experimental VLE data.

The equilibrium cell was then assembled in its housing and placed into the regulated air bath and allowed to reach thermal equilibrium. The attainment of thermal equilibrium took approximately three hours due the large volume of the air bath and the thickness of the metal of the equilibrium cell and ancillary support structures which were in contact with the cell.

The air bath set point was set to the temperature of the measurements, either 273.15 or 313.15 K and thermal equilibrium was assumed when the temperature probes T1 and T2 gave equivalent equilibrium temperature values within their uncertainty values (determined by the temperature calibration procedure) for at least ten minutes. The attainment of thermal equilibrium took approximately three hours. Once the system had reached thermal equilibrium, the pressurising liquid octane was loaded into the pressurising circuit and the measurements started. The pressure of the octane was increased in the pressurising circuit by means of the motorised high pressure hydraulic pump, up until the pressure existing in the equilibrium cell. The volume of the equilibrium cell was then modified by changing the position of the piston inside the cell in varying increments of 1 mm to 40 mm. At different variations of the piston displacement, the associated pressure reading was recorded. The piston displacement was increased until the binary mixture was brought to the bubble point. At the bubble point of the mixture, the pressure reading of the cell increased dramatically when compared to the variation in piston displacement. The volume of cell, via the displacement of the piston, was initially increased to bring the system to a point beyond the bubble point,

4.4. THE STATIC ANALYTIC APPARATUS

The systems involving the components HFP, HFPO and the solvent R116 were measured on the static analytic apparatus of (Coquelet et al. 2003a), which utilised a fixed volume equilibrium cell and the ROLSI for vapour and liquid equilibrium sample handling and chromatographic analysis. The static analytic apparatus has been used extensively in the TEP laboratories for HPVLE measurements. A review of previous measurements involving only refrigerants performed on the static analytic apparatus fitted with the ROLSI was undertaken and is presented in Table 4.6.

Reference	Systems	Temperature [K]
(Coquelet et al. 2005)	R32 + DME	283, 298, 313, 328, 343, 353, 363
(Valtz et al. 2005)	R134a + DME	293, 303, 323, 343, 358
(Valtz et al. 2004)	$CO_2 + H_2O$	278, 288, 298, 308, 318
(Valtz et al. 2004a)	SO_2 + R227ea	288, 303, 323, 343, 363, 374, 376, 383, 393, 403
(Mohammadi et al. 2004)	$C_2H_6 + H_2O$	278, 283, 288, 293, 298, 303
(Rivollet et al. 2004)	CO_2 + R32	283, 293, 303, 305, 313, 323, 333, 343
(Valtz et al. 2003)	CO_2 + R227ea	276, 293, 303, 305, 313, 333, 367
(Coquelet et al. 2003a)	R32 + C_3H_8	278, 294, 303, 313, 343
(Coquelet et al. 2003b)	R32 + R227ea	283, 303, 323, 343
(Laugier and Richon 1997)	$CO_2 + C_6H_{12}O$	433, 453
	CO_2 + C6$H_{10}O$	433, 473

Table 4.6. A review of binary HPVLE data involving refrigerants measured on the static analytic apparatus of (Coquelet et al. 2003a) fitted with the ROLSI.

4.4.1. Equipment Description

A flow diagram detailing the experimental setup of the static analytic apparatus is presented in Figure 4.3.

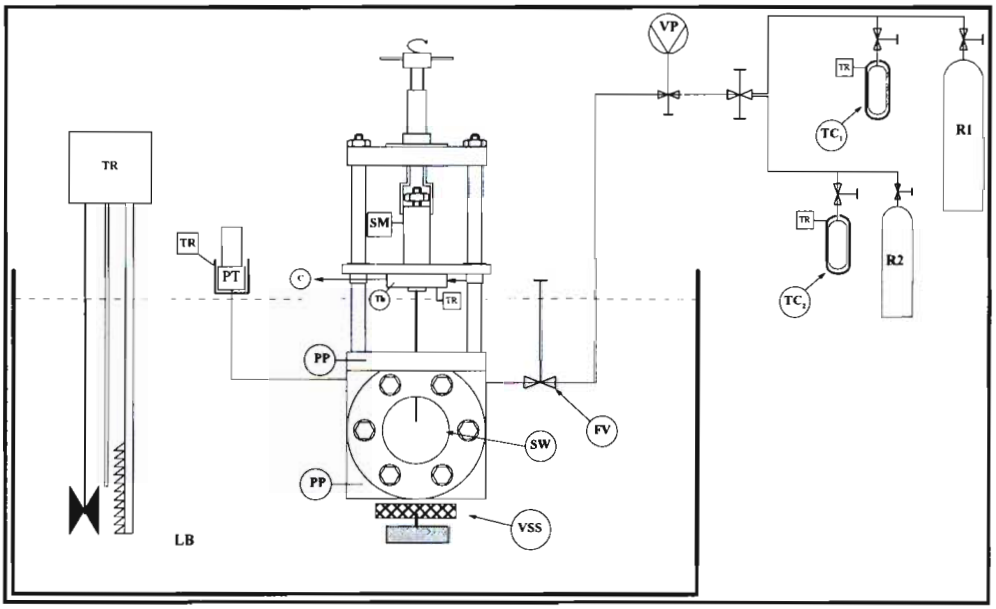

Figure 4.3. The flow diagram of the static synthetic apparatus.

Reproduced from (Valtz et al. 2005). C: Carrier Gas; EC: Equilibrium Cell; FV: Feeding Valve; LB: Liquid Bath; PP: Platinum Probe; PT: Pressure Transducer; R1: Refrigerant 1 Cylinder; R2: Refrigerant 2 Cylinder; SM: Sampler Monitoring; SW: Sapphire window; TC_1 and TC_2 Thermal Compressors; Th: Thermocouple; TR: Temperature Regulator; VSS: Variable Speed Stirring; VP: Vacuum Pump.

The constant volume equilibrium cell (EC) is submerged in a liquid bath (LB) which is either filled with water or ethanol depending on the temperature of the measurement. The liquid bath was self regulated and was able to maintain a temperature to within 0.05 K from set point. The cell was constructed of a titanium alloy and had a maximum internal volume of 50 cm^3. A sapphire window was installed on the front of the cell to allow visual observation of the binary mixture under study, with the feeding valve (FV) located on the right of cell to allow loading and evacuation of the cell contents. Internal stirring of the binary mixture under study was achieved through the magnetic stirrers inside the cell, with the revolving magnets located on the base of the unit. The revolving magnets were controlled by a stirrer apparatus (VVS) which allowed variable speed stirring to ensure that sufficient agitation of the equilibrium cell was achieved, or conversely, that vigorous stirring did not disrupt the equilibrium measurements.

The cylinders R1 and R2 in Figure 4.3 represent the components of the binary systems to be measured, with R1 denoting hexafluoroethane (R116) and R2 denoting either HFP (R1216) or HFPO. Thermal

compressors, TC1 and TC2 allowed for loading of the equilibrium cell under pressures greater than available bottle pressures of the components. Equilibrium temperature measurements were achieved through the use of two platinum resistance temperature probes (PP) which were located inside wells drilled directly into the body of the equilibrium cell at different levels as indicated in Figure 4.3. Pressure measurements were obtained via two pressure transducers (PT) of the type Druck (model PTX611) which were maintained at a constant temperature (at a temperature approximately 20 K higher than the highest temperature of the measurements) by an air-thermostat controlled by a PID regulator (WEST instrument, model 6100). The two pressure transducers were utilised to allow accurate pressure measurements in the high and low pressure range, with the first transducer designated 'P301' operable in the region of 0 to 6 bar and the second transducer designated 'P302' which had an upper operating limit of 60 bar. The temperature probes and pressure transducers were connected to a data acquisition unit (HP 34970A), which was connected to a personal computer via a RS-232 interface which allowed for real time monitoring and recording of temperatures and pressures during each isothermal run.

Sample monitoring (SM) was performed through the use of the movable pneumatic ROLSI, as described by (Guilbot et al. 2000), which could be manually positioned via a screw type handle for either liquid or vapour phase sample analysis. The ROLSI was operated by pneumatic activation of the capillary column which could instantaneously withdraw a liquid or vapour sample, depending on the position of the sampler, up the capillary and into the body of the ROLSI. The ROLSI was able to withdraw multiple samples of equal volume in a period of time defined by the user. For this project the sample time was set to 15 s, which led to four samples being withdrawn per minute The same carrier gas (C) that was utilised by the gas chromatograph entered across the ROLSI chambers and swept away the withdrawn sample to the gas chromatograph (VARIAN, CP-3800). A thermal conductivity detector was used with a Poropack N 80/100 Mesh column, with the chromatograph connected to a data acquisition system for logging and analysis of GC data. Photograph 4.3 provides a pictorial overview of the static analytic apparatus and equipment not visible in the flow diagram Figure 4.3. Photograph 4.4 provides an overview of the fixed volume equilibrium cell of the static analytic apparatus, detailing the stirring assembly for the magnetic internal stirrer, the location of the ROLSI and ROLSI heating plates as well as the heated sample carrier line to the gas chromatograph.

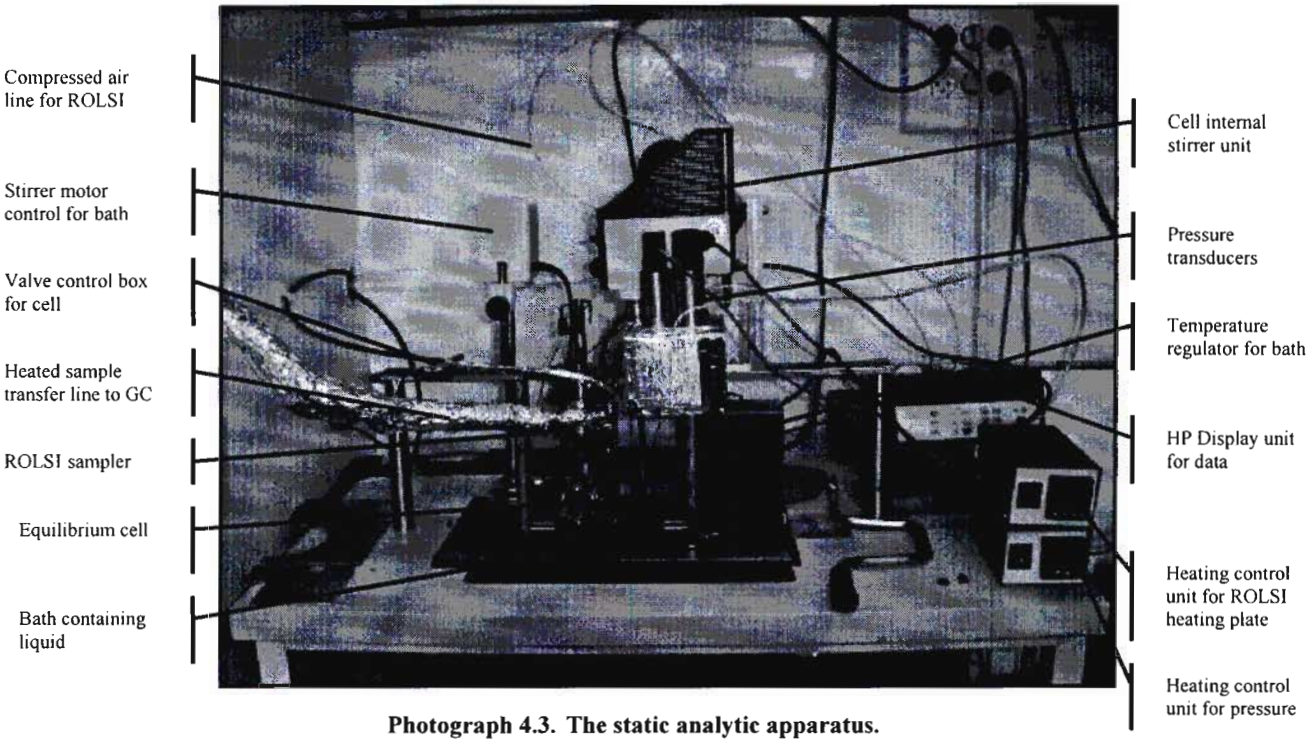

Photograph 4.3. The static analytic apparatus.

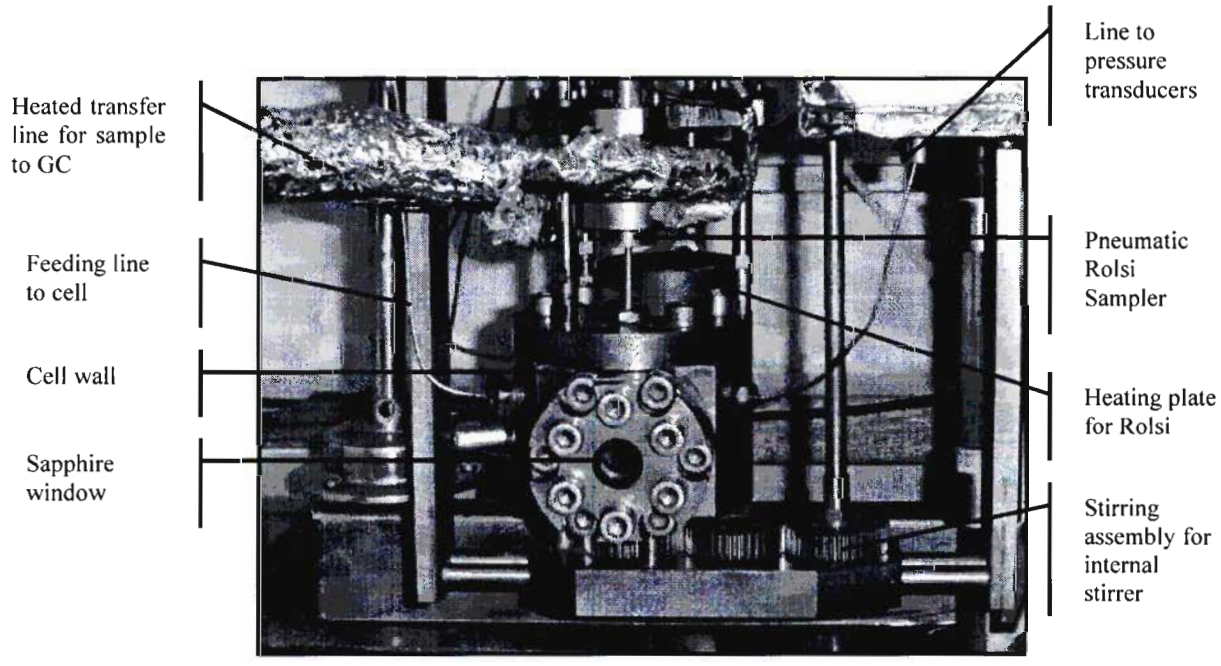

Photograph 4.4. The fixed volume equilibrium cell of the static analytic apparatus.

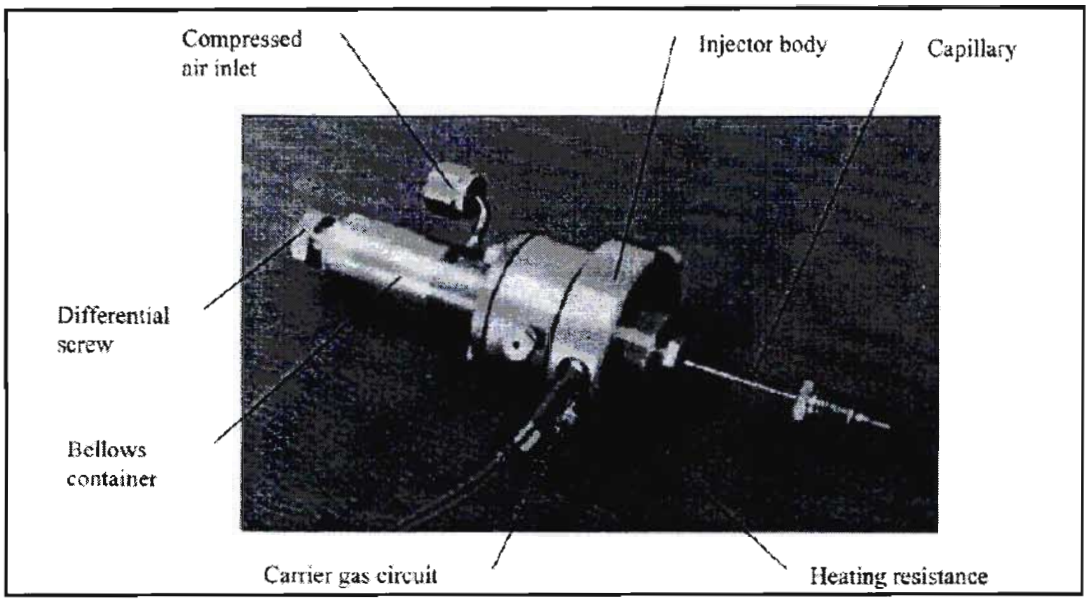

Photograph 4.5. The movable pneumatic ROLSI sampler. From (Guilbot et al. 2000).

Photograph 4.5 provides an overview of the movable pneumatic ROLSI. The ROLSI sampler is a compact piece of equipment without any dead volume which was constructed with a stainless steel body. All other parts of the ROLSI in contact with sample were constructed from titanium or hastelloy which ensured that the ROLSI was able to operate under harsh or corrosive conditions, and conditions of high temperature and pressure. It was connected to the equilibrium cell through a Monel capillary of 0.1 mm inner diameter and length 150 mm and the capillary length was extended through the use of a titanium micro needle. The carrier gas which swept the liquid or vapour sample to the gas chromatograph, entered at the carrier gas inlet as indicated in the photograph. The ROLSI sampler was insulated and heated independently from the equilibrium cell via heating resistance to allow vaporisation of a liquid sample in the gas circuit of the gas chromatograph, which ensured quicker chromatographic analysis. A significant feature of the ROLSI was the ability to alter to sample size volume electronically from several hundredths to several mg of sample, and to take repeated and reproducible samples in a short period of time with great accuracy and reliability. The automated nature of the ROLSI sampler, reliability, reproducible results and the ability to operate under conditions of high pressure ensured that the ROLSI was well suited to the HPVLE measurements undertaken in this research project.

The equipment listing for the major ancillary items on the static analytic apparatus is presented in Table 4.7, along with the manufacturer name and model numbers.

Equipment	Brand	Model
Data acquisition unit	Hewlett Packard	34970A
ROLSI heating control unit	West	6100
Cell stirrer	Bioblock Scientific	94403
Stirrer control unit	Heidolph	EP5
Bath temperature regulator	Chauffauge	33194
Gas chromatograph	Varian	CP-3800

Table 4.7. Equipment listing for the static analytic apparatus.

4.4.2. Experimental Procedure

4.4.2.1. Pressure transducer and temperature probe calibration

The two Pt-100 platinum resistance temperature probes were calibrated according to the procedure used for the temperature probes of the static synthetic method. Similarly, the high pressure range and low pressure range transducers were calibrated in the manner described for the static synthetic apparatus.

4.4.2.2. Gas chromatograph calibration

The calibration of the gas chromatograph required calibration of the thermal conductivity detector (TCD). The direct injection method similar to that of (Naidoo 2004) was utilized, which involved injecting known volumes of each pure component into the GC, to generate a plot of GC peak area (A) versus number of moles (n). The components HFP, HFPO and R116, which are gases at room temperature, were withdrawn directly from the regulator on each gas cylinder. This was achieved by attaching a tube connection with a septum attached to one end of the regulator, with the pressure on the regulator for each component being set to a constant value which was maintained for each gas withdrawal. Three syringes of volume 50 µl, 250 µl and 500 µl, manufactured by Hamilton, were used for the calibration. For the component HFPO, nine different volumes were injected into the GC: 10 µl, 20 µl, 30 µl, 40 µl, 50 µl, 100 µl, 150 µl, 200 µl and 250 µl with each volume injected five times to ascertain the reproducibility of the injections. For the component HFP, five different volumes: 50 µl, 100 µl, 150 µl, 200 µl and 250 µl were injected five times each, while for component R116, eight different volumes: 50 µl , 100 µl, 150 µl, 200 µl, 250 µl, 300 µl, 400 µl and 500 µl, were injected five times for each volume. At each injection, the ambient temperature and ambient pressure were recorded and the volume of gas injected was converted into moles using the rearranged form of the ideal gas equation of state:

$$n = \frac{PV}{RT} \tag{4-1}$$

Where the following definitions apply:

V	=	Volume of the injected sample [cm^3]
T	=	Temperature of the syringe [K]
R	=	Universal gas constant [$cm^3 \cdot MPa \cdot K^{-1} \cdot mol^{-1}$]
P	=	Ambient pressure [MPa].

In this manner, it was possible to generate a curve of number of moles (n) versus GC peak area (A) and through data regression, the relationship between peak area and number of moles in the form of a second order polynomial obtained:

$$n = x_1 A^2 + x_2 A + x_3 \tag{4-2}$$

Where the following definitions apply:

n	=	Number of moles [mol]
A	=	GC peak area
x_1, x_2, x_3	=	Coefficients obtained through data regression.

Table 4.8 presents the calibration and analytical conditions for the gas chromatograph that was used for quantitative sample analysis. For data logging for the Varian chromatograph, the BORWIN computer software, version 1.5, from Le Fontanil, France was used under license.

Item	Specification
Model	Varian CP-3800
Column	Poropack Q packed column
Column length [m]	3
Column width [inch]	0.125
Column mesh	80/100
Oven temperature [K]	423.15
Injector model	1041
Injector temperature [K]	393.15
TCD temperature [K]	423.15
TCD range	0.5
Carrier gas	He
Carrier gas flow [$ml \cdot min^{-1}$]	26
Reference gas	He
Reference gas flow [$ml \cdot min^{-1}$]	29

Table 4.8. Calibration and analytical conditions for the gas chromatograph.

4.4.2.3. Vapour-Liquid equilibrium measurements

The experimental procedure undertaken for binary HPVLE measurements on the static analytic apparatus was similar to that of (Coquelet et al. 2003b). The systems measured on this apparatus were R116 + HFP and R116 + HFPO at the 273.15 and 313.15 K isotherms, with the same experimental procedure employed for both systems. Additionally, the pure component vapour pressures for component HFPO were measured on the static analytic apparatus.

A typical measurement on the static analytic apparatus began with the initialisation of the GC. The flow of the carrier gas, He, was first set to 26 ml•min^{-1} and the reference gas flow to 29 ml•min^{-1}. A bubble flow meter was used to verify the flow of the carrier gas in the system, and once this was accomplished, the TCD was switched on. The equilibrium cell was removed from the liquid bath to allow easier loading of the cell. The bath temperature regulator was then set to the temperature of the measurements, either 273.15 or 313.15 K.

Before loading of the equilibrium cell, the cell and all lines were put under vacuum to evacuate the cell of any components. The less volatile component of each binary mixture was first loaded into the equilibrium cell via the feeding valve (FV), either HFP or HFPO which are both less volatile than R116. The HFPO or HFP cylinder was connected onto the feeding line of the cell, and with the pressure transducers operational, the regulator on the cylinder and the feeding valve both opened to allow the lighter component, either the HFP or HFPO, to enter the equilibrium cell. While the heavier component loaded into the cell, observations of the liquid level of the cell via the sapphire window and the pressure of the cell via the transducers were made. For all measurements, the equilibrium cell was filled to approximately 1/10th (5 cm^3) of the total cell volume with the heavier component. When the cell was loaded to the desired volume, all lines to the cell were closed via valves and the cylinder of the less volatile component removed. The equilibrium cell was then submerged into the liquid to allow the system to reach thermal equilibrium.

For the HPVLE measurements at 313.15 K, the liquid bath was filled with water, for the measurements at 273.15 K, the bath was filled with ethanol which, when compared to water, allowed the lower temperatures to be maintained. Thermal equilibrium of the system was assumed when the temperature probes gave equivalent equilibrium temperature values within their temperature uncertainty for at least ten minutes. The attainment of thermal equilibrium took approximately two hours. When the system reached equilibrium, the pure component vapour pressure measurements were taken. The temperature of system was varied, the system allowed to reach equilibrium, and the corresponding vapour pressure recorded. In this manner, the pure component vapour pressure curve for component HFPO was recorded in the temperature range of 271.90 to 318.20 K. The pure component vapour pressure measurements for HFPO were completed and the system was subsequently allowed to reach the equilibrium temperature for the measurement of the binary HPLVE data. The cylinder of the lighter component, R116, was attached to the feeding line and loaded into

the equilibrium cell to the desired pressure of the measurement. After the R116 was loaded, the feeding line valve was closed, the stirring mechanism for cell activated and the cell allowed to reach equilibrium.

Equilibrium was assumed when the total pressure of the system remained unchanged, within the pressure uncertainty values (as determined by the calibration of the pressure transducers), for a period of ten minutes under efficient stirring. Once the system was in equilibrium, the ROLSI was purged via the ROLSI control box, and the interval of sampling and number of samples input. For each data point on the *P-x* and *P-y* curve, a minimum of four equilibrium samples were taken. In general, multiple samples of each composition were taken until good reproducibility of the samples was obtained, with good reproducibility defined as mole fractions at the same composition differing by at most 0.02 %. The equilibrium liquid phase was sampled first with the ROLSI positioned in the liquid phase at a sufficient depth and the sampling initiated on the ROLSI control unit. When the liquid phase samples were complete, the ROLSI was positioned via the adjustable screw type lever to sample the vapour phase, in a manner analogous to the liquid phase sampling. During the course of the sampling, careful observation of the liquid level in the cell was made via the sapphire window. If the liquid level in the cell was too high due to the condensation of the vapour phase in the liquid, then the equilibrium cell was vented. The system was then loaded with the more volatile component, allowed to reach equilibrium and the measurements continued. With the sampling for a particular composition complete, the ROLSI unit was deactivated via the control box, and the R116 introduced to the system to the next desired pressure, and the system allowed to reach equilibrium. The sampling of the vapour and liquid phases at the new composition were performed identically for all compositions. The R116 was introduced in a step by step manner leading to successive equilibrium mixtures of increasing overall lighter component compositions. Each introduction of the lighter component corresponded to a single point on the two phase envelopes (liquid and vapour), which allowed a full range of P-x-y data to be measured for all the binary systems.

The results of the calibration procedure for the pressure transducer and temperature probes, and the full set of *P-x-y* data including the multiple vapour and liquid samples and standard deviations, are presented in Sections B.1 and B.4, Appendix B. The final *P-x-y* data for the binary systems R116 + HFP, R116 + HFPO and the pure component HFPO vapour pressure measurements are presented in Chapter seven.

CHAPTER FIVE

5. THERMODYNAMIC MODELLING AND DATA REGRESSION

In 1987, the Montréal Protocol prohibited the worldwide use and production of CFCs which resulted in the proposal of FCs and HFCs for use as alternative refrigerants and industrial reagents. The fluorocarbons HFP and HFPO thus require accurate experimental thermodynamic data to better understand and utilise these components. However, the existence of experimental HPVLE data is a necessary but not sufficient condition to accomplish this objective. (Coquelet and Richon 2007) suggested that accurate experimental data *and* predictive techniques, via thermodynamic modelling of the high pressure systems, are a prerequisite to better understand the behaviour and performance of systems and processes involving refrigerants. (Muhlbauer and Raal 1995) stated that the thermodynamic interpretation and modelling of HPVLE data is a much more difficult task than for the low pressure case. This is compounded by the fact that the measurement of HPVLE data is both more expensive and complex than for the low pressure scenario ((Ramjugernath 2000)), which makes the correct theoretical interpretation of the HPVLE data of paramount importance. In general, rigorous thermodynamic modelling and interpretation of experimental data allows for the interpolation and extrapolation of data to new conditions where data is non-existent and for the proper correlation of phase behaviour from the minimum amount of experimental data.

5.1. THEORY

A description of fundamental thermodynamic relationships and the elementary treatment of phase equilibrium are not presented in this dissertation. The fundamentals and the various relationships required to describe the equilibrium condition can be found in (Smith et al. 2001). A brief overview of the direct method, the equations of state utilised, the mixing rules and activity coefficient model are presented in this section.

Only the thermodynamic models utilised for the data regression of the experimentally obtained data are presented and discussed in this chapter. A brief description of the predictive thermodynamic models utilised for this work is presented in Appendix A.

The thermodynamic approach of phase equilibria is based on the concept of chemical potential, which can cause substances to react chemically or to be transferred from one phase to another. (Smith et al. 2001) states that multiple phases at the same T and P are in equilibrium when the chemical potential (μ) of each constituent species is the same in all phases. However, the chemical potential is an awkward quantity, so it is desirable to express the chemical potential in terms of some auxiliary function that might be more easily

identified with physical reality ((Naidoo 2004)). As a result, the concept of fugacity is utilised, which is a physically more meaningful quantity that is generally applied in the solution of phase equilibria. Fugacity, *f*, is defined with the units of pressure ((Smith et al. 2001)) and refers to a 'corrected pressure'. These corrections are due to non-idealities between a substance's chemical potential at the state of interest and at a standard state. In general, for vapour liquid equilibrium to be satisfied there must exist an equality of the fugacity for a species *i* in both the vapour and liquid phases.

Two methods exist for the thermodynamic modelling and interpretation of binary isothermal HPVLE data: the combined and the direct methods. According to (Muhlbauer and Raal 1995), HPVLE was initially modelled by the combined method, which was an extension of low pressure correlation techniques at the time. In the combined method, activity and fugacity coefficients are used to describe the liquid and vapour non-idealities respectively, which requires an activity coefficient model and an equation of state (EOS) model. The activity coefficient, γ_i, represents the non-ideality correction of the liquid phase and is dependant on composition, temperature and pressure. A shortcoming of the combined method is that it only permits excellent representation of the liquid and vapour phases of complex systems in low to medium pressure ranges and has problems describing supercritical components and the high pressure critical region. To overcome the shortcomings of the combined method, the direct method was developed.

In the direct method, the evaluation of both the vapour and liquid phase fugacity coefficients is required, which can both be evaluated via a single equation of state. The direct method was utilised for all the data regression and thermodynamic modelling performed in this research project. The computer software Thermopack ((Coquelet and Baba-Ahmed 2002)) was used to undertake all regression calculations and the models and methodology used to interpret and model the HPVLE data are detailed in this chapter. The results of the data regression and modelling are presented in the Chapter seven.

The Direct Method

In the direct method, the fugacity coefficient for the liquid and vapour phase in an equilibrium mixture are described by:

$$\hat{f}_i^L = x_i \hat{\phi}_i^L = \hat{f}_i^V = y_i \hat{\phi}_i^V \tag{5-1}$$

The equilibrium ratio, *K* is defined as:

$$K_i = \frac{y_i}{x_i} = \frac{\hat{\phi}_i^L}{\hat{\phi}_i^V} \tag{5-2}$$

The effect of temperature, pressure and composition on the liquid and vapour phase fugacity can be determined by the effect these variables have on the fugacity coefficient.

$$\hat{\phi}_i^L = \phi(T, P, x_i, ..., x_n) \tag{5-3}$$

$$\hat{\phi}_i^V = \phi(T, P, y_i, ..., y_n) \tag{5-4}$$

Fugacity coefficients obtained from volumetric data can be calculated using the following equations:

$$\ln \hat{\phi}_i = \frac{1}{RT} \int_0^P \left[\left(\frac{\partial V}{\partial n_i} \right)_{(T,P,n_j)} - \frac{RT}{P} \right] dP \tag{5-5}$$

and

$$\ln \hat{\phi}_i = \frac{1}{RT} \int_V^\infty \left[\left(\frac{\partial P}{\partial n_i} \right)_{(T,V,n_j)} - \frac{RT}{V} \right] dV - \ln \left[\frac{PV}{RT} \right] \tag{5-6}$$

Equation (5-5) is used when the volumetric data are presented in volume explicit form and equation (5-6) represents the more common case when volumetric data are expressed in the pressure explicit form. The fugacity coefficients are calculated using an equation of state (EOS). One or two binary interaction parameters are included in the EOS parameters to describe the interactions between the species in the mixtures.

(Muhlbauer and Raal 1995) list the difficulties that are generally associated with the application of the direct method, as follows:

1. Selection of the most appropriate EOS to describe the liquid and vapour phase non-idealities is the first problem since several hundred EOS have been developed. The chosen EOS must be flexible enough to fully describe a pure substance's PVT behaviour for both phases within the temperature, pressure and concentration ranges required

2. Selection of an appropriate mixing rule is required to describe the phase behaviour of mixtures from the pure component form of an EOS. Empirical mixing rules, which are derived using theoretical assumptions, are generally not satisfactory since they tend to be system specific and in some cases parameters need to be included to account for inaccurately calculated cross terms or the high non-ideality of the system

3. Locating the appropriate roots for the liquid and vapour molar densities is another problem when higher than cubic order EOS are used

4. At conditions close to the critical point, the computational techniques for the calculation of the dew and bubble points are unreliable and exhibit difficulty when converging to a final solution.

Equations of State

Two methods exist for the determination of the thermodynamic properties of pure fluids and fluid mixtures: (a) experimental measurements or (b) an equation of state model. EOS methods provide one of the most effective and common techniques used in engineering practice for modelling phase equilibria. EOS refers to the mathematical relation between volume, pressure, temperature and composition.

Numerous EOS have been developed and can be categorised as follows ((Muhlbauer and Raal 1995)):

1. Family of virial EOS
2. EOS in the corresponding states format
3. van der Waals family of cubic EOS
4. EOS derived from statistical thermodynamics and based on lattice models, perturbation theory or integral equation theory
5. EOS derived from fitting computer simulation data

For this research project, the EOS utilised were categorised as the van der Waals family of cubic EOS and as such, these types of EOS will be briefly explained in the following sections.

van der Waals family of cubic EOS

These cubic EOS are semi-empirical in nature. Semi-empirical methods are practical methods since they are derived from a theoretically based functional form of the EOS and consist of few parameters as adjustable quantities to experimental data. The van der Waals type EOS are derived for pure fluids but can be extended to mixtures by making simplifying assumptions. The key assumption is the one fluid theory of mixtures. This theory proposes that the configuration properties of the mixture are the same as those of a hypothetical pure fluid and the characteristics of this hypothetical pure fluid, which are expressed by constants in an EOS, are some composition dependant average of the pure components in the mixture. These composition dependant EOS constants are obtained using mixing rules that are mostly empirical.

Using the one fluid theory and an EOS, the pressure explicit form is:

$$P = F[V, T, a(z), b(z), ...] \tag{5-7}$$

Where V is the molar volume of the mixture and *a(z)* and *b(z)* designate constants *a* and *b* as functions of the mole fraction *z*. The number of these constants is arbitrary but generally most EOS limit these constants to two or three to keep experimental data requirements low. These constants are frequently defined in terms of critical temperature, critical pressure and the accentric factor.

The formulation of a general empirical cubic EOS is based on the combination of a repulsion and an attraction term:

$$P = P_{attraction} + P_{repulsion} \tag{5-8}$$

The repulsion term is given in terms of the van der Waals hard sphere equation:

$$P_{repulsion} = \frac{RT}{V - b} \tag{5-9}$$

where the constant *b* is related to the size of the hard sphere. The attraction term is usually expressed in the following general form:

$$P_{attraction} = \frac{a}{g(V)} \tag{5-10}$$

The constant *a* refers to the intermolecular attraction force and *g(V)* is a function of the molar volume. The choice of *g(V)* determines the accuracy to which the EOS reproduces the critical compressibility factor of a fluid. Combining equations (6-9) and (6-10), the traditional van der Waals family cubic EOS can be expressed in the following form:

$$P = \frac{RT}{V - b} - \frac{a}{g(V)} \tag{5-11}$$

The simplest equations that are capable of representing both the vapour and liquid states are cubic in volume and are hence termed cubic equations of state. They are used extensively in representing phase behaviour and there is a trade-off between the ease of use in computation and flexibility in describing wide-ranging phase behaviour.

van der Waals (vdW) EOS

The most famous cubic equation of state is the van der Waals EOS which was developed in 1873:

$$P = \frac{RT}{V-b} - \frac{a}{V^2} \tag{5-12}$$

where

$$a = \frac{27R^2T_c^2}{64P_c} \tag{5-13}$$

and

$$b = \frac{RT_c}{8P_c} \tag{5-14}$$

The parameter a is a measure of the attractive force between the molecules and the parameter b refers to the co-volume or excluded volume i.e. the part of the molar volume that is not available to the molecule as it is occupied by other molecules. These parameters are calculated using the critical properties of the fluid.

The van der Waals EOS, equation (5-12), was the first EOS to give qualitative descriptions of both the vapour and liquid phase equilibria and phase transitions. However, for critical properties and phase equilibria calculations, this representation is not quantitavely accurate. The vdW EOS predicts Z_c as 0.375 for all fluids, while the real value varies from 0.24 to 0.29 for various hydrocarbons and this range is wider for non hydrocarbons ((Ramjugernath 2000)).

More accurate EOS models have been proposed and the popular models used in this research project are presented and discussed in terms of the modifications of the attraction terms of the basic van der Waals model.

Redlich-Kwong (RK) EOS

A significant variation of the van der Waals EOS was made by (Redlich and Kwong 1949). The expression included a temperature dependence and different volume dependence in the attraction term:

$$P = \frac{RT}{V-b} - \frac{a}{T^{0.5}[V(V+b)]} \tag{5-15}$$

where

$$a = 0.4278 \frac{R^2 T_c^{2.5}}{P_c} \tag{5-16}$$

and

$$b = 0.08664 \frac{RT_c}{P_c} \tag{5-17}$$

The RK EOS gives an improved critical compressibility of Z_c = 0.333, as well as better second virial coefficients when compared to the vdW EOS. However, it is still not accurate for vapour pressures and liquid densities. The RK EOS is generally successful for ideal systems and for simple fluids for which the accentric factor equals zero i.e. Ar, Kr and Xe. For complex compounds with accentric factors not equal to zero, the RK EOS was proved to be inaccurate by (Abbott 1979).

Soave-Redlich-Kwong (SRK) EOS

The most important modification of the vdW EOS involving the temperature dependency of the attraction term was proposed by (Soave 1972) for his modification of the RK EOS. An α parameter which included the temperature and accentric factor was introduced into the attraction term which subsequently improved the vapour pressure predictions for light hydrocarbons. This notable improvement led to the cubic EOS becoming an important tool for the prediction of phase equilibria at moderate and high pressures for non-polar fluids. The SRK EOS is given by:

$$P = \frac{RT}{V-b} - \frac{a(T)}{V(V+b)} \tag{5-18}$$

where the temperature dependence is given by:

$$a(T) = a(T_c)\alpha(T) \tag{5-19}$$

$$a(T_c) = 0.42748\frac{(RT_c)^2}{P_c} \tag{5-20}$$

For normal fluids, $\alpha(T)$ is given by:

$$\alpha(T) = \left[1 + \kappa\left(1 - \sqrt{\frac{T}{T_c}}\right)\right]^2 \tag{5-21}$$

where

$$\kappa = 0.480 + 1.574\omega - 0.176\omega^2 \tag{5-22}$$

The co-volume parameter b is given by:

$$b = 0.08664\frac{RT_C}{P_C} \tag{5-23}$$

The SRK EOS has proved successful in calculating more accurate vapour pressures of several hydrocarbons, as well as correlating phase behaviour of multicomponent systems consisting of non-polar and slightly polar fluids, however, it was found by (Peng and Robinson 1976) that the SRK EOS produced slightly higher liquid phase specific volume predictions than literature values.

Peng-Robinson (PR) EOS

(Peng and Robinson 1976) proposed a further modification of the SRK equation by including a different volume dependence and temperature dependence of α. This expression produced slightly improved liquid volumes where Z_c = 0.307 and gave increased accuracy for the vapour pressure predictions for hydrocarbons in the six to ten carbon number range. The PR EOS is given by the following equation:

$$P = \frac{RT}{V-b} - \frac{a(T)}{V(V+b)+b(V-b)} \tag{5-24}$$

where the temperature dependence is given by:

$$a(T) = a(T_c)\alpha(T) \tag{5-25}$$

$$a(T_c) = 0.457235\frac{(RT_c)^2}{P_c} \tag{5-26}$$

$$\alpha(T) = \left[1+\kappa\left(1-\sqrt{\frac{T}{T_c}}\right)\right]^2 \tag{5-27}$$

where

$$\kappa = 0.37464 + 1.54226\omega - 0.26992\omega^2 \tag{5-22}$$

The co-volume parameter b is given by:

$$b = 0.077796\frac{RT_c}{P_c} \tag{5-23}$$

The SRK and PR EOS are the two most widely used EOS in industry. They are popular due to the fact that they require minimal input information (only critical properties and accentric parameters for the generalised parameters), exhibit low computational time and produce good phase equilibrium predictions for hydrocarbon systems. Their primary disadvantages include inaccurate prediction of liquid densities,

inaccurate generalised parameters for non-hydrocarbons and less than satisfactory prediction of the phase behaviour of long chained molecules. Further important deficiencies in these two models are the inaccurate predictions of vapour pressures below ten torr and inaccurate predictions in the critical region.

Mathias-Copeman (MC) α function

Shortcomings of the SRK and PR EOS were the inability to predict accurately vapour pressures and inaccurate predictions in the critical region. (Mathias and Copeman 1983) proposed an extension of the PR EOS for complex mixtures to better predict vapour pressures and to allow the PR EOS the flexibility to describe complex mixture behaviour. The modification of the alpha function for the calculation of the attractive term as proposed by (Mathias and Copeman 1983) is given by (for $T < T_c$):

$$\alpha = \left[1 + c_1\left(1 - \sqrt{\frac{T}{T_c}}\right) + c_2\left(1 - \sqrt{\frac{T}{T_c}}\right)^2 + c_3\left(1 - \sqrt{\frac{T}{T_c}}\right)^3\right]^2 \tag{5-24}$$

The original alpha function for the PR and SRK EOS is obtained when $c_2 = c_3 = 0$. The additional parameters were added to correlate the vapour pressures of highly polar substances, such as water and methanol, as inaccurate pure component vapour pressure representation artificially distorts the analysis of mixture effects ((Mathias and Copeman 1983)). The modification of the cubic EOS via the MC alpha function is justified for compounds presenting polarity and high molecular weight. It has been demonstrated by (Chiavone-Filho et al. 2001) that representation of the vapour pressure is significantly improved and that good vapour pressure representation of pure components reflects directly on the prediction of mixtures.

The extension of cubic EOS to mixtures

The single most important benefit regarding the use of a cubic EOS involves the extension of the pure component models to mixtures for phase equilibrium calculations. All that is required to extend the EOS to use for mixtures is to specify how *a(T)* and *b* depend on composition i.e. mixing rules are required to describe this dependence. One of the simplest methods is to apply the classical one fluid mixing rules proposed by van der Waals for the vdW EOS. The one fluid theory of mixtures assumes that the equation of state for the mixture is the same as that for a hypothetical pure fluid whose characteristic constants *a(T)* and *b* depend on composition. The vdW mixing rules provide a good correlation for mixtures of hydrocarbons, hydrocarbons with organic gasses, non-polar and slightly polar components only if the components are of similar size. A weakness of the one fluid theory lies in the application to mixtures of relatively moderate solution non-ideality.

For the use of a cubic EOS for mixtures exhibiting greater complexity and at higher densities than the vdW one fluid theory, a different approach of the extension of the cubic EOS was proposed. The main deficiency of the vdW theory was the inability to accurately predict the liquid phase non-ideality. The excess Gibbs energy models (or activity coefficient models) have shown good representation in correlating low pressure data ((Muhlbauer and Raal 1995)). Consequently, models have been developed in which the liquid phase non-idealities (described accurately using an excess Gibbs free energy model) is combined with an EOS approach (to calculate the fugacity coefficients of both the liquid and vapour phases).

The Huron-Vidal (HV) and the Modified-Huron-Vidal first order (MHV1) mixing rules

Systems exhibiting complex behaviour were traditionally described using activity coefficient models instead of a cubic EOS. (Huron and Vidal 1979) were the first to combine an EOS with an excess Gibbs free energy equation to model highly non-ideal systems. They obtained a general equation relating the excess Gibbs free energy to the pure component and mixture fugacity coefficients as shown:

$$G^E = RT[\ln\phi - \sum_{i=1}^{n} x_i \ln\phi_i] \tag{5-25}$$

where the expressions for the fugacity coefficients rely solely on the equation of state used which is the same for ϕ and ϕ_i. In order to relate G^E to the mixing rules, a necessary condition was to assume that the excess Gibbs free energy is independent of pressure, an assumption which was later proved incorrect by (Sandler and Orbey 1998). As a result, the excess free energy and an equation of state are related at infinite pressure using the following expression:

$$G^E = A^E + PV^E \tag{5-26}$$

where A represents the Helmholtz energy. The equation for G^E was given by (Huron and Vidal 1979) as:

$$G^E_\infty = \Lambda\left[\frac{a_m}{b_m} - \sum_{i=1}^{n} z_i \frac{a_i}{b_i}\right] \tag{5-27}$$

Where Λ is a numerical constant which depends on the EOS utilised, m denotes a mixture and z the composition. From equation (5-27) the HV mixing rule was thus proposed as:

$$a_m = b_m\left[\sum_{i=1}^{n} z_i \frac{a_i}{b_i} - \frac{G_\infty^E}{\Lambda}\right] \tag{5-28}$$

At infinite pressure, the excess Gibbs energy obtained from an EOS is the same as the excess Gibbs energy calculated from an activity coefficient model:

$$G_{EOS}^E(T, P \to \infty, x_i) = G_\gamma^E(T, P \to \infty, x_i) \tag{5-29}$$

Therefore the mixing parameter a_m can be easily obtained from the following expression:

$$a_m = b_m\left[\sum_{i=1}^{n} z_i \frac{a_i}{b_i} - \frac{G_\gamma^E(T, P \to \infty, x_i)}{\Lambda}\right] \tag{5-30}$$

with b_m given by:-

$$b_m = \sum_{i=1}^{n} x_i b_i \tag{5-31}$$

Even though the HV mixing rules presented above have successfully correlated data for a variety of highly non-ideal systems, (Sandler and Orbey 1998) demonstrated that the HV mixing rules contain a collection of theoretical and computational difficulties:

1. Inaccurate representations for non-polar hydrocarbon mixtures. This created a problem for multicomponent mixtures containing polar and non-polar components since all species are represented using the same mixing rule.

2. The second virial coefficient boundary condition is not satisfied at the low density limit which does not lead to satisfactory predictions for reproducing high pressure data. Virial coefficients are related to the forces between molecules, while the second virial coefficient represents the interactions between two molecules. Generally the virial equation and the second virial coefficient are used for low or moderate densities ((Naidoo 2004)).

3. Pressure effects were not taken into account when using the excess Gibbs energy function as the G^E value at low pressures is different at infinite pressures.

Many attempts have been made in literature to correct the inconsistencies of using the excess Gibbs energy model at infinite pressure as suggested in the HV mixing rules.

(Mollerup 1986) modified equation (5-28) by evaluating the mixture parameter a_m directly from the zero pressure excess free energy expression, as well as maintaining that the excess volume was zero. The Modified-Huron-Vidal first order (MHV1) mixing rules by (Michelsen 1990) were based on the ideas of (Mollerup 1986). Using a zero pressure reference and the SRK EOS, the proposed parameter for a_m was:

$$a_m = \sum_{i=1}^{n} z_i \alpha_{ii} + \frac{1}{q_1}\left[\sum_{i=1}^{n} z_i \ln(\frac{b_m}{b_{ii}}) + \frac{G_\gamma^E(T, P \to \infty, x_i)}{RT}\right] \tag{5-32}$$

where

$$\alpha_m = \frac{a_m}{b_m RT}$$

$$b_m = \sum_{i=1}^{n} z_i b_{ii}$$

$$\alpha_{ii} = \frac{a_{ii}}{b_{ii} RT} \tag{5-33}$$

The recommended values for the term q_1 for the SRK and PR EOS are 0.593 and 0.530 respectively.

The Wong-Sandler (WS) mixing rules

The most promising mixing rule development was that of (Wong and Sandler 1992b). These mixing rules adequately addressed the shortcomings of HV based mixing rules in that it satisfied the second virial coefficient boundary condition at the low density limit and was consistent with experimental data at the high density limit. The WS mixing rules also brought about other improvements. It is a density independent mixing rule and allows parameter tables for G^E models to be applied to allow for extrapolation over large ranges of temperature and pressure ((Wong et al. 1992a)). It also provided the simplest method of extending the UNIFAC group contribution method or other low pressure predictive methods to higher temperatures and pressures.

The WS mixing rules are based on the following observations:

1. The second virial coefficient boundary condition is a sufficient but not necessary condition. Constraints were thus brought on by the vdW one fluid mixing rule on the functions a and b to satisfy the expression:

$$B(x_i,T) = \sum\sum x_i x_j B_{ij}(T)$$

$$= \sum\sum x_i x_j (b_{ij} - \frac{a_{ij}}{RT})$$

$$= b_m - \frac{a_m}{RT} \qquad (5\text{-}34)$$

The last equality was used as one of the restrictions on the EOS a and b parameters. Incorporating a combining rule, the expression is:

$$\left(b - \frac{a}{RT}\right)_{ij} = \frac{1}{2}\left[\left(b_{ii} - \frac{a_{ii}}{RT}\right) + \left(b_{jj} - \frac{a_{jj}}{RT}\right)\right](1 - k_{ij}) \qquad (5\text{-}35)$$

where k_{ij} is the binary interaction parameter.

2. In contrast to the HV mixing rule, the WS mixing rule utilised the excess Helmholtz free energy (A^E) at infinite pressure to develop the mixing rule. The primary advantage was that it was not necessary to assume $V^E = 0$ and for a liquid, A^E is not as strongly dependant on pressure as G^E. (Wong and Sandler 1992b) were thus able to show that at low pressures the excess Gibbs free energy was equal to the excess Helmholtz energy at infinite pressure, and were thus able to show that an activity coefficient model could be used to describe the Helmholtz free energy derived from an EOS.

For a vdW type cubic EOS, (Wong and Sandler 1992b) showed that the Helmholtz free energy at infinite pressure is given by:

$$A_\infty^E = \Lambda\left[\frac{a_m}{b_m} - \sum_{i=1}^{n} z_i \frac{a_i}{b_i}\right] \qquad (5\text{-}36)$$

where Λ is a numerical constant which depends on the EOS utilised.

The relationship between the mixture parameters a_m and b_m was determined by (Wong and Sandler 1992b) as the following:

$$a_m = b_m\left[\sum_{i=1}^{n} z_i \frac{a_i}{b_i} + \frac{G_\gamma^E(T, lowP, x_i)}{\Lambda}\right] \tag{5-37}$$

In order to satisfy the boundary condition of a quadratic composition dependence of the second order virial coefficient, (Wong and Sandler 1992b) thus set:

$$b_m = \frac{\sum\sum z_i z_j (b - \frac{a}{RT})_{ij}}{1 - \sum_{i=1}^{n} z_i \frac{a_i}{b_i} - \frac{G_\gamma^E(T, lowP, x_i)}{\Lambda}} \tag{5-38}$$

The WS mixing rules have produced excellent correlations of vapour-liquid, liquid-liquid and vapour-liquid-liquid equilibria (Wong et al. 1992a). It has the ability to accurately describe the phase behaviour of both simple and complex systems consisting of diverse binary and ternary mixtures. This mixing rule combined with an appropriate cubic EOS can be used for a wide range of highly non-ideal systems that were previously only described by an activity coefficient model. Additionally, (Sandler and Orbey 1998) demonstrated that this mixing rule is capable of extrapolating and predicting data over a wide range of temperatures and pressures.

Activity coefficient models

For the extension of the cubic EOS to mixtures, mixing rules incorporating an excess Gibbs free energy model were utilised. An activity coefficient represents the non-ideality correction of the liquid phase and is dependant on its composition, temperature and pressure. The liquid phase activity coefficient can be determined by relating the activity coefficient to the molar excess Gibbs free energy. In general, G^E/RT is a function of T, P and composition and the quantity $\ln \gamma_i$ obeys the summability relationship:

$$\frac{G^E}{RT} = \sum x_i \ln \gamma_i \tag{5-39}$$

The quantity $\ln \gamma_i$ can be related to the variables from the Gibbs Duhem equation and the use of constant pressure activity coefficients for isothermal conditions results in the following relationship:

$$\sum x_i d \ln \gamma_i = 0 \tag{5-40}$$

Equation (5-40) is a differential equation and the integrated form of this equation relates γ_1 to γ_2 for which there exists several semi-empirical models.

For a binary mixture, the activity coefficients can be calculated from an expression of G^E using the following expressions:

$$\ln \gamma_1 = \frac{G^E}{RT} + x_2 \frac{d\left(\frac{G^E}{RT}\right)}{dx_1} \tag{5-41}$$

$$\ln \gamma_2 = \frac{G^E}{RT} - x_1 \frac{d\left(\frac{G^E}{RT}\right)}{dx_1} \tag{5-42}$$

For liquids at low to moderate pressures, G^E/RT is a weak function of pressure and thus the pressure dependence is often neglected. Numerous functional forms for the excess Gibbs energy have been proposed over the years and these equations can be expressed with respect to liquid mole fractions, volume fractions and molecular surface fractions. When the molecules involved differ greatly in size or chemical nature, the forms are expressed in terms of volume fractions and molecular surface fractions. The correlations for the excess Gibbs energy are mostly empirical in nature and some examples include the Margules equation, the van Laar equation, the Wilson equation, the T-K Wilson equation and the NRTL model. For this research project, the activity coefficient model utilised was the NRTL model, and as such, only this model is presented in this section.

The NRTL activity coefficient model

The concept of local composition was utilised by (Renon and Prausnitz 1968) for the derivation of the NRTL equation. This equation, unlike the Wilson equation (Wilson 1964) is applicable to partially miscible, as well as completely miscible systems. The NRTL equation for the excess Gibbs energy is:

$$\frac{G^E}{RT} = x_1 x_2 \left[\frac{\tau_{21} G_{21}}{x_1 + G_{21} x_2} + \left[\frac{\tau_{12} G_{12}}{x_2 + G_{12} x_1} \right] \right] \tag{5-43}$$

where the following definitions apply:

$$\tau_{ji} = \frac{g_{ji} - g_{ii}}{RT} = \frac{\Delta g_{ji}}{RT} \tag{5-44}$$

$$G_{ji} = \exp(-\alpha_{ji}\tau_{ji}) \tag{5-45}$$

where g_{ji} is an energy parameter for interaction between components j and i, and Δg_{12}, Δg_{21} and α_{ij} are adjustable parameters. The energy parameters characterising the molecular interactions Δg_{12} and Δg_{21} are considered to be independent of temperature over narrow temperature ranges. Over a wider range these parameters can be linear functions of temperature.

The parameter α_{ij} refers to the non-randomness of the mixture. When α_{ij} is set to zero then the equations reduce to the Margules two-suffix model ((Smith et al. 2001)). The parameter $\alpha_{12} = \alpha_{21}$ and α_{12} can vary from 0.2 to 0.7 depending on the components involved. When experimental data is scarce, α_{12} can be set to an arbitrary value and it is generally set to 0.3 for polar systems ((Renon and Prausnitz 1968)).

The activity coefficient expressions for the NRTL model were derived as:

$$\ln\gamma_1 = x_2^2\left[\tau_{21}\left(\frac{G_{21}}{x_1 + G_{21}x_2}\right)^2 + \frac{\tau_{12}G_{12}}{(G_{12}x_1 + x_2)^2}\right] \tag{5-46}$$

$$\ln\gamma_2 = x_1^2\left[\tau_{12}\left(\frac{G_{12}}{x_2 + G_{12}x_2}\right)^2 + \frac{\tau_{21}G_{21}}{(G_{21}x_2 + x_1)^2}\right] \tag{5-47}$$

For moderately non-ideal systems the NRTL equation offers no advantages over simpler equations such as the Margules and van Laar equations ((Ramjugernath 2000)). The real advantage of the NRTL model lies in the simultaneous description of VLE and heats of mixing, and for the accurate description of strongly non-ideal mixtures in particular partially miscible systems.

5.2. DATA REGRESSION AND MODELLING

Popular thermodynamic models, well suited to the systems of interest, were used to interpret and model the experimental data that were measured for this research project. The reduction of the measured data via the software Thermopack involved the determination of the optimal parameters for each thermodynamic model utilised via the direct method. For the systems involving R116, the system temperature and pressure were used to generate estimates of the vapour and liquid mole fractions using the chosen thermodynamic models. The calculated liquid and vapour mole fractions were then compared to the experimental values and the difference between these values were minimised by solving for the optimal parameter solutions of each of the thermodynamic models. For the regression of the systems involving toluene, the direct method calculations undertaken in Thermopack involved the use of the temperature and liquid mole fractions and the generation of pressure and vapour compositions. The calculated pressure values were compared to the experimental values and the difference between these values was minimised by solving for the optimal model parameters of each thermodynamic model. For all the data regression, the least squares estimation method of (Marquardt 1963) for non-linear parameters was used to obtain the optimised parameters.

The binary HPVLE data for the systems HFP + toluene, HFPO + toluene, R116 + HFP and R116 + HFPO, were regressed and modelled via three possible model combinations, which are defined in Table 5.1. The pure component vapour pressure data for HFPO were regressed and modelled via two EOS, also defined in Table 5.1.

Data	EOS	α function	Mixing Rule	G^E model
HFPO vapour pressure	PR	MC	-	-
	SRK	MC	-	-
Binary HPVLE data	PR	MC	WS	NRTL
	PR	MC	MHV1	NRTL
	SRK	MC	WS	NRTL

Table 5.1. A summary of the thermodynamic models used in the interpretation of binary HPLVE data for this project.

Key:

PR = Peng-Robinson EOS ((Peng and Robinson 1976))
SRK = Soave modification of the Redlich-Kwong EOS ((Soave 1972))
MC = Mathias-Copeman alpha function ((Mathias and Copeman 1983))
WS = Wong-Sandler mixing rules ((Wong and Sandler 1992a))
MHV1 = Modified Huron-Vidal mixing rules ((Michelsen 1990))
NRTL = Non Random Two Liquid γi model ((Renon and Prausnitz 1968)).

The pure component vapour pressure data for HFPO were modelled by two EOS, the PR EOS and the SRK EOS, with the use of the MC alpha function for both EOS to allow better representation of the pure component vapour pressures. Three combinations of models were used to represent the binary HPVLE data, the PR EOS with WS mixing rules, the PR EOS with the MHV1 mixing rules and the SRK EOS with the WS mixing rules. The MC alpha function and the NRTL activity coefficient model were used for each of the three model combinations, with the non randomness parameter of the NRTL model, α_{12}, set equal to 0.3 as per convention for polar systems.

For the data regression for the pure component vapour pressures of HFPO, the regressed parameters that were determined in the MC alpha function correlation are usually termed c_1, c_2 and c_3 ((Mathias and Copeman 1983)), however, for ease of reference, these parameters are referred to as MC1, MC2 and MC3 in this dissertation.

For easy reference, a summary of the equations of the thermodynamic models used for the regression and modelling of the HPVLE data is presented from Table 5.2 through Table 5.5:

Equation	Description	Reference
$P = \frac{RT}{V-b} - \frac{a(T)}{V(V+b)+b(V-b)}$	Peng-Robinson EOS	(Peng and Robinson 1976)
$P = \frac{RT}{V-b} - \frac{a(T)}{V(V+b)}$	Soave-Redlich-Kwong EOS	(Soave 1972)

Table 5.2. A summary of the EOS used in thermodynamic modelling of the HPVLE data.

Equation	Condition	Reference
$\alpha = \left[1 + c_1\left(1 - \sqrt{\frac{T}{T_c}}\right) + c_2\left(1 - \sqrt{\frac{T}{T_c}}\right)^2 + c_3\left(1 - \sqrt{\frac{T}{T_c}}\right)^3\right]^2$	$T < T_c$	(Mathias and Copeman 1983)
$\alpha = \left[1 + c_1\left(1 - \sqrt{\frac{T}{T_c}}\right)\right]^2$	$T > T_c$	(Mathias and Copeman 1983)

Table 5.3. A summary of the MC alpha function.

Equation	Description	Reference
$b_m = \frac{\sum\sum z_i z_j (b - \frac{a}{RT})_{ij}}{1 - \sum_{i=1}^{n} z_i \frac{a_i}{b_i} - \frac{G_\gamma^E(T, lowP, x_i)}{\Lambda}}$	Wong-Sandler Mixing Rules	(Wong and Sandler 1992b)
$\left(b - \frac{a}{RT}\right)_{ij} = \frac{1}{2}\left[\left(b_{ii} - \frac{a_{ii}}{RT}\right) + \left(b_{jj} - \frac{a_{jj}}{RT}\right)\right](1 - k_{ij})$		
$a_m = \sum_{i=1}^{n} z_i \alpha_{ii} + \frac{1}{q_1}\left[\sum_{i=1}^{n} z_i \ln(\frac{b_m}{b_{ii}}) + \frac{G_\gamma^E(T, P \to \infty, x_i)}{RT}\right]$	Modified Huron-Vidal First order mixing rules	(Michelsen 1990)
$b_m = \sum_{i=1}^{n} z_i b_{ii}$		
With q_1= -0.593 for SRK EOS, and q_1= -0.53 for PR EOS		

Table 5.4. A summary of the mixing rules used in thermodynamic modelling of the HPVLE data.

Equation	Description	Reference
$\ln \gamma_1 = x_2^2\left[\tau_{21}\left(\frac{G_{21}}{x_1 + G_{21}x_2}\right)^2 + \frac{\tau_{12}G_{12}}{(G_{12}x_1 + x_2)^2}\right]$	NRTL activity coefficient Model	(Renon and Prausnitz 1968)
$\ln \gamma_2 = x_1^2\left[\tau_{12}\left(\frac{G_{12}}{x_2 + G_{12}x_2}\right)^2 + \frac{\tau_{21}G_{21}}{(G_{21}x_2 + x_1)^2}\right]$		
$\tau_{ji} = \frac{g_{ji} - g_{ii}}{RT} = \frac{\Delta g_{ji}}{RT}$, $G_{ji} = \exp(-\alpha_{ji}\tau_{ji})$		

Table 5.5. A summary of the NRTL activity coefficient model.

The optimal parameters for the models were obtained in Thermopack by minimizing the sum of the squares of the errors between the calculated and the experimental values of one of more equilibrium properties. Depending on the variables used in the regression procedure, two such functions were used in the Thermopack software for the data regression. The objective function utilised for the systems R116 + HFP and R116 + HFPO was a flash adjustment, in which the temperature and pressure are given, and the systems adjusted according to the vapour and liquid mole fractions, x and y, according to equation (5-48):

$$F = \frac{100}{N}\left[\sum\left(\frac{x_{\exp} - x_{calc}}{x_{\exp}}\right)^2 + \sum\left(\frac{y_{\exp} - y_{calc}}{y_{\exp}}\right)^2\right] \qquad (5\text{-}48)$$

where the following definitions apply:

F	=	Objective function to be minimized
calc	=	Calculated quantities
exp	=	Experimental quantities.

For the systems HFP + toluene and HFPO + toluene, a bubble point adjustment on pressure was utilized, in which the liquid phase compositions are known and the vapour phase compositions are unknown. This is represented by equation (5-49):

$$F = \frac{100}{N}\left[\sum\left(\frac{P_{\exp} - P_{calc}}{P_{\exp}}\right)^2\right] \tag{5-49}$$

For the experimental HPVLE data, the parameters that were solved for using the least squares regression model were as follows:

For pure component calculations:

1. Parameters for the Mathias-Copeman alpha function for the PR and SRK EOS
    - MC1, MC2 and MC3

The pure component parameters, MC1, MC2 and MC3 for both the PR and SRK EOS were evaluated through Thermopack by a least squares regression of the experimental pure component vapour pressure data for component HFPO. The inputs required for the Thermopack calculation procedure were the temperature and pure component critical properties: the critical temperature, critical pressure and accentric factor and initial estimates of the MC alpha parameters. The saturated pressure at each temperature were calculated using either the PR or SRK EOS and the difference between the calculated experimental and calculated pressures minimised and new MC alpha function parameters obtained, with the procedure repeated until an optimal solution was found.

For mixtures:

1. Binary interaction parameter for the mixing rules:
    - k_{ij} in the WS mixing rules.

2. Parameters for the G^E activity coefficient models:
    - τ_{ij} and τ_{ij} in the NRTL model.

In general, the input data required for the reduction of the experimental binary HPVLE included pure component properties such as critical temperatures and pressures, accentric factors, alpha function correlation parameters (specific to the EOS utilised), system temperature and liquid compositions of the measured data and initial estimates for both the mixing rule binary interaction parameters and NRTL activity coefficient model parameters.

At the 313.15 K isotherm, the binary systems R116 + HFP and R116 + HFPO enter the supercritical region. The calculation of the critical point of each binary mixture and the critical line was undertaken in the Thermopack software. Thermopack utilises the works of (Stockfleth and Dohrn 1998) for the calculation of the critical line. This is based on the works of (Heidemann and Khalil 1980) and (Michelsen and Heidemann 1981) which assumed that the stability criterion for an isothermal variation can be explained with a minimum of molar Helmholtz energy. (Michelsen and Heidemann 1981) stated that the critical point corresponds to the limit of stability and developed an algorithm for the calculation of the critical point with a van der Waals type EOS. (Stockfleth and Dohrn 1998) improved on the works of (Heidemann and Khalil 1980) and (Michelsen and Heidemann 1981) by developing a newer generalised algorithm, and this algorithm from the work of (Stockfleth and Dohrn 1998) was utilised in Thermopack to calculate the critical line for the supercritical systems R116 + HFP and R116 + HFPO at 313.15 K.

The physical properties of the pure components that were required for the theoretical treatment of the experimental HPVLE data were obtained from the Component Plus databank ((ProSim 2001)), the Dortmund DDB ((DDBST 2007)), data regression and calculation. The MC parameters for HFPO were determined from the data regression of the experimental pure component vapour pressures which were measured for this research project. The MC parameters for the component HFP were obtained from the experimental pure component vapour pressure measurements for HFP by (Nelson 2008). The critical pressure of HFPO, which was unavailable in literature, was obtained using the regressed PR and MC model parameters to predict the vapour pressure curve for HFPO up until the critical temperature. The MC parameters for the components Toluene and R116 were obtained from the Component Plus database, while the critical properties for R116 and Toluene were obtained from the DDB.

To quantify the fit of a model to the experimental pressure and equilibrium vapour and liquid compositions, the absolute average error in terms of the pressure, and liquid and vapour compositions was computed. Equation (5-50) defines the percentage absolute average error for pressure, vapour and liquid mole fractions:

$$AAE-U(\%)=\frac{\left(\sum_{i=1}^{N}\left|\frac{U_i^{calc}-U_i^{\exp}}{U_i^{\exp}}\right|*100\right)}{N} \tag{5-50}$$

The BIAS of the measurements were calculated for the pressure, liquid and vapour phase mole fractions. The BIAS is given by:

$$BIAS-U(\%)=\frac{\left(\sum_{i=1}^{N}\left(\frac{U_i^{calc}-U_i^{\exp}}{U_i^{\exp}}\right)*100\right)}{N} \tag{5-51}$$

where N represents the number of data points and U represents P, x or y. The BIAS value, expressed as a percentage, can have either a positive or negative value, however, the better the fit of the data, the closer this value is to zero. The difference between the BIAS and the AAE, is that in the BIAS, positive and negative errors tend to cancel each other which makes the prediction look better than it actually is. The absolute average error can only have a positive value because of the absolute value function. It is a better indicator of the fit of the experimental and modelled data than the BIAS. A small BIAS and a large AAE value usually indicate a systematic deviation between the experimental data and the predicted data.

All of the data regression and modelling were undertaken in the computer software Thermopack. A description of this software, as well as examples of the pure and multi-component data regression procedures utilised for this project, are presented in Section C-1, Appendix C of this dissertation. The results of the data regression and correlation of the experimental data is presented in Chapter seven.

CHAPTER SIX

6. PROCESS DESIGN

(Luyben 2006) states that there are three steps in developing a successful process design. The first is 'Conceptual design', in which approximate and historical (previous) methods are used to develop a preliminary flowsheet. The second step is 'Preliminary Design' in which rigorous simulation methods are used to evaluate the steady state and dynamic performance of the proposed flowsheet. The final step is the 'Detailed Design' in which the hardware is specified in great detail, with specifics such as valve sizes, heat exchanger areas, types of distillation trays and reflux piping.

The primary purpose of the research project was to propose a preliminary separation scheme for the separation of the fluorinated hydrocarbons HFP and HFPO. Following the methodology of (Luyben 2006), the conceptual design was performed from the analysis of previous methods for the separation of HFP and HFPO. The literature review revealed that primarily, methods for the separation of HFP and HFPO involved the addition of a third component, a solvent, to alter the relative volatilities of the key components to make the system amenable to separation. On this basis, the solvent selection procedure, outlined in Chapter three, identified two solvents which were used in this research, the liquid toluene and the gas hexafluoroethane (R116).

Two processes for the separation of HFP and HFPO were designed for this research project and they are designated by the following:

- The Toluene separation process
- The R116 separation process.

For the solvent toluene, which is patented in the work of (Wiist 1967), the preliminary design for an extractive distillation procedure, analogous to the work of (Ueno et al. 1997), was undertaken. For the solvent R116, which is a gas at room temperature, the process of supercritical fluid extraction technology was initially proposed and preliminary design undertaken. However, initial results utilising supercritical R116 indicated that significant separation between HFP and HFPO was not possible due to the similarities between the liquid phase equilibrium compositions as the system approached the critical region. The preliminary design for a gas stripping process utilising R116 as the gaseous solvent was undertaken, with a literature survey revealing that R116 has not been patented as a solvent for the separation of HFP and HFPO. The literature survey also revealed that the process of stripping with a gaseous solvent has not previously been used to effect such a separation.

For this research, only the conceptual and steady state preliminary design for the two separation processes were undertaken. The complete preliminary design for the processes involving the solvents toluene and R116 were undertaken in the process engineering suite Aspen Plus ((AspenTech 2004)). Only the key separation units, i.e. the distillation columns and stripping units were designed, with no preliminary sizing of equipment, such as column sizing and heat exchanger surface areas, undertaken. A set methodology for the general design of distillation columns in Aspen was adapted and modified from the work of (Luyben 2006) and used to design the extractive distillation column, distillation columns and stripping towers in the preliminary separation processes. The set methodology was used in the design of each unit in a systematic manner to allow the comparison of the two separation schemes with respect to energy usage, solvent considerations and efficiency.

The general design procedure for the two separation schemes, involving the methodology and techniques employed, are presented in this chapter. The detailed process design for each unit in the toluene separation process is presented in Section D.2, Appendix D. The detailed design of the R116 process can be inferred from the toluene process and is thus not presented in this dissertation.

6.1. ENHANCED DISTILLATION AND SEPARATION TECHNIQUES

(Seader et al. 1997) states that in distillation operations, separations result from differences in vapour and liquid phase compositions which in turn result from the partial vaporisation of a liquid mixture or the partial condensation of a vapour mixture. As a result, the vapour phase becomes enriched with the lighter more volatile component thus causing the liquid phase to be depleted of the same component. Under certain conditions, due to the physical characteristics of the key components to be separated, the change in the composition between the equilibrium vapour and liquid phases is so small that a large number of successive partial vaporisations and condensations (i.e. equilibrium stages) are required to achieve a desired separation. Alternatively, the equilibrium vapour and liquid phases may have identical compositions, due to the formation of an azeotrope and separation via simple or conventional distillation is not feasible. Enhanced distillation and separation techniques have been developed for close boiling or low relative volatility systems exhibiting azeotropic behaviour (Seader and Henley 1998). In general, these enhanced techniques are based on the same differences in the vapour and liquid equilibrium compositions as ordinary distillation, but require an additional mechanism to modify the vapour-liquid behaviour of the key components. The enhanced techniques can be broadly classified according to their effect on the thermodynamic relationship between the vapour and liquid compositions:

1. *Azeotropic distillation and pressure swing distillation:* These enhanced methods cause or exploit azeotropic formation or behavior, through the use of an entrainer, to alter the boiling characteristics and separability of the mixture

2. *Extractive distillation and salt distillation:* These enhanced methods involve the addition of a solvent to modify the liquid phase behaviour to alter the relative volatility of the key components in the mixture

3. *Reactive distillation:* Enhanced methods that use a chemical reaction to modify the composition of the mixture, or methods that use existing vapour-liquid differences between reaction products and reactants to enhance the performance of a reaction.

For the research undertaken and presented in this dissertation, the enhanced techniques employed, extractive distillation and stripping with a gaseous solvent, involved the addition of a solvent or a stripping agent to effect the separation of the key components. A brief discussion on the general process of extractive distillation and gas stripping follows.

6.1.1. Extractive Distillation

(Seader et al. 1997) in the handbook of (Perry and Green 1997) define extractive distillation as a partial vaporisation process in the presence of a miscible, high boiling, non volatile mass separating agent (the solvent), which is added to the feed mixture to alter the relative volatilities of the key components without the formation of any additional azeotropes. Extractive distillation has been extensively used in the petrochemical and chemical processing industries for the separation of close boiling, azeotropic systems when simple single feed or conventional distillation procedures is either too expensive or impossible.

Figure 6.1 illustrates the general scheme for an extractive distillation procedure for the separation of a binary mixture of A and B. C1 represents the extractive distillation column and C2 the solvent recovery column, with A and B representing either close boiling components with a low relative volatility or a minimum boiling azeotropic mixture. Extractive distillation operations usually occur in typical distillation apparatus, i.e. trayed columns with condensers and reboilers. The solvent is generally introduced into column C1 at a high concentration at a stage below the condenser, but above the primary feed stage. The solvent is chosen to be non-volatile so as to remain at relatively high concentrations in the liquid phase in the sections below the feed stages. As a result of the action of the solvent, one of the components, A, which is not necessarily the more volatile component of the original feed mixture, can be withdrawn as an essentially pure distillate stream from column C1. The bottoms product of C1, consisting of component B and the solvent is then sent to the solvent recovery column C2. The distillate from the C2 is pure component B, and the bottoms product which is high in purity with respect to the solvent, is recycled back to the extractive column.

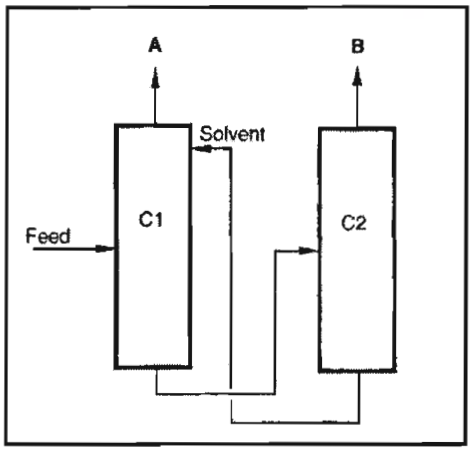

Figure 6.1. Typical extractive distillation procedure for a feed of components A and B. The solvent is selective to component B. ((Perry and Green 1997)).

6.1.2. Gas Stripping

In the process of inert gas stripping, a liquid mixture containing the key components to be separated is contacted with a gaseous stream to selectively dissolve one or more components by mass transfer from the liquid to the gas. The component transferred to the gas is termed the solute, and the gas stream the solvent or absorbent. Gas stripping is analogous to the process of gas absorption, where a gas mixture is contacted with a liquid, the solvent, to selectively dissolve one or more components by mass transfer from the gas to the liquid.

The process of gas stripping which usually occurs in packed columns or trayed towers termed strippers, is represented in Figure 6.2. The liquid stream, L_{in}, enters at the top the trayed column containing the binary mixture to be separated. The gaseous solvent steam, G_{in}, enters at the bottom of the column consisting of primarily the solvent. Due to density differences, the gas stream moves up the column and the liquid stream moves downwards, contacting the gaseous stream, and in this manner selectively transferring the solute from the liquid stream to the gaseous stream. The liquid stream minus the solute, L_{out}, leaves at the bottom of the column. The gas stream rich in the solute, G_{out}, leaves at the top of the stripping unit and is sent for further processing to remove the solute from the solvent for solvent recycle.

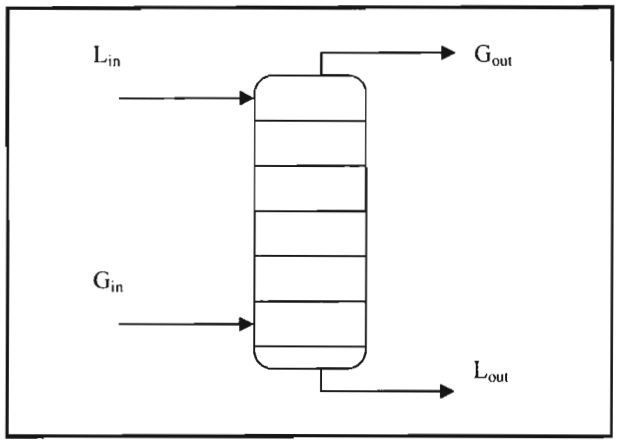

Figure 6.2. Typical gas stripping procedure for a trayed stripping unit with the liquid feed and gaseous solvent entering in countercurrent flow ((Seader and Henley 1998)).

6.2. PROCESS DESIGN PROCEDURE

The separation processes involving the solvents toluene and R116 were designed and simulated on the process engineering suite Aspen Plus. A modified design methodology adapted from the work of (Luyben 2006) was utilized for the preliminary process design, and along with a general overview of the process design procedure, is presented in the following sections. Appendix C presents a description of the process simulation in the Aspen engineering suite, including a description of the component definition, importing of the regressed data into Aspen and property method selection. A detailed description of the design procedure for each unit of the toluene separation process, including the closing of the recycle loop is also presented in Appendix D.

6.2.1. Feed Stream Conditions and Required Product Purities

The feed composition ranges for the stream entering the toluene and R116 separation processes were specified by PELCHEM and are presented in Table 6.1:

Composition	Minimum [mole %]	Maximum [mole %]
HFP	5	35
HFPO	25	65
CO_2	15	35
Toluene	0	2

Table 6.1. Feed composition ranges for the HFP and HFPO feed stream to be separated.

PELCHEM obtained the above estimated values for the feed compositions based on their preliminary experimental work utilising the wet oxidation route for the conversion of HFP to HFPO. For the design of the toluene and R116 separations processes, a worst case scenario was utilised and the following feed stream conditions used for the simulations.

	Mole Fraction
HFP	0.21
HFPO	0.42
CO_2	0.35
Toluene	0.02

Table 6.2. Feed conditions for Toluene and R116 processes.

The feed compositions presented in Table 6.2 were obtained by assuming a worst case scenario, i.e. the maximum amount of impurities of toluene and CO_2 in the feed stream. The ratio HFPO to HFP was set to a 2:1 molar ratio. Further specifications defined by PELCHEM related to the feed stream flow rate, desired product purities, and allowable impurities:

1. Estimated feed rate of process stream for separation: 5 $kg \cdot hr^{-1}$
2. Desired HFP purity: 95 [mole %]
3. Desired HFPO purity: 99.9 [mole %]
4. HFP impurities: Not important as HFP stream will be utilized as recycle stream to process
5. HFPO impurities: HFP, R116 and CO_2 tolerated; toluene not tolerated.

6.2.2. Design Methodology

Although the use of toluene as an extractive distillation solvent has been patented by the du Pont company ((Wiist 1967)), the toluene procedure designed during the course of this research project only utilized the patented solvent and not the extraction scheme or flowsheet of the du Pont process. There can be no set method for the design of a separation scheme for systems with different solvents, however, the same logic was applied for both the preliminary process designs. Both the toluene and R116 processes have been designed from the 'ground up' utilising a set methodology such that there could be a basis of comparison between the two processes, which would enable PELCHEM to effectively compare and the contrast the separation schemes.

The designs undertaken for the toluene and R116 processes are of a preliminary nature, as per the contract defined by PELCHEM. As such, only the steady state design of the extractive distillation column, distillation columns, stripping units and closing of the solvent recycle loop were undertaken for this project. Dynamic simulation, control schemes and equipment sizing were not performed which resulted in the omission of pumps and control valves from the preliminary process design. All columns and strippers were designed using the 'RadFrac' model in Aspen. The RadFrac model is a rigorous model for simulating all types of multistage vapour-liquid fractionation operations. Unit operations that RadFrac is capable of simulating include ordinary distillation, absorption, stripping, reboiled stripping, extractive distillation and azeotropic distillation columns.

6.2.2.1. General Distillation Column

For the general design of a distillation column, the following general procedure was utilised. The procedure is for the design of a distillation column for the separation of a binary mixture without the addition of a solvent and was utilized for the design of the solvent recovery and purification columns. The column parameters that need to be specified for the RadFrac model are total number of stages N_T, feed stage location N_F, condenser type (either total or partial-vapour depending on the desired condition of the distillate), distillate rate, molar reflux ratio and column pressure. The generalized procedure is as follows:

1. *Set the distillate rate of the column to be the flow rate of the light key component (more volatile component) in the feed.* The distillate rate of the RadFrac model was set to be the flow rate of the light key component in the feed on the basis that the light key or more volatile component is removed at the top of a distillation column via the distillate

2. *Set the operating pressure of the column to the vapour pressure of the light key component at 325.25 K.* The specification of the operating pressure of the column was generally set to the vapour pressure of the light key component in the distillate at 325.15 K. This value was set such that in the preliminary stages of the design, cooling water could be used in the column condenser, as it is an inexpensive alternative to compared to refrigeration. In a worst case scenario, cooling water is available at 305.15 K. According to (Luyben 2006), a reasonable temperature difference for heat transfer in the condenser is approximately 20 K, which will set the reflux drum temperature of the column at approximately 325.15 K. As the pressure down a distillation column typically decreases, the reflux drum pressure thus sets the column pressure. After the simulation with the initial specifications is completed, the reflux drum or stage one temperature is monitored. If the reflux temperature is lower than 325.15 K, then the operating pressure of the column was increased to try and obtain the desired reflux temperature

3. *Estimate the molar reflux ratio.* The molar reflux ratio (RR) for the column was initially estimated, with (Luyben 2006) recommending a high reflux ratio, typically a RR of 20 for a system where the separation is difficult, and a molar RR of 2 for systems where the separation is neither difficult or easy

4. *Estimate the initial total number of stages (N_T) and set the feed stage (N_F) to be initially half the number of stages.* The total number of stages, N_T, was typically set to an initial value of ten for all the columns in the simulation processes and the feed stage location N_F, set to half the N_T value. The simulation was run with these default values and if the simulation process was not working correctly the value of N_T and then N_F adjusted. The setting of initial values for RR, N_T and N_F is somewhat arbitrary as the 'Design/Spec/Vary' function is later utilized to obtain more realistic values

5. *Perform a sensitivity analysis to determine a revised estimate of N_T.* The next step of the design procedure was to perform a sensitivity analysis on the total number of stages. In Aspen, the sensitivity analysis function allowed the variation of an input parameter (between certain specified user limits while holding all other input variables constant), to determine the effect of the variation of the input variable on specific monitored variables. The total number of stages was varied and the effect on the recovery and purity of either the light key component in the distillate or heavy key in the bottom stream monitored (depending on which stream contained the high value or important component). Through the sensitivity analysis a revised value of N_T was set by choosing that value which resulted in a high value of recovery and purity for the component of interest, with the value of N_F unchanged at this point

6. *Utilise the 'Design/Spec/Vary' (DSV) function to obtain a revised estimate of the molar reflux ratio.* To obtain a revised value of the molar RR, the DSV function of Aspen was utilized. For the DSV function, a desired value of some controlled variable is specified and a variable to be manipulated is also specified. When the simulation is initiated, Aspen attempts to adjust the manipulated variable in such a way that the specified value of the controlled variable is achieved. For the design of a column, the controlled variable was generally set to be the value of an impurity in either the distillate or bottoms stream and the manipulated variable the molar RR. In such a manner the molar RR was continually adjusted by Aspen until the desired product purities were achieved, providing the desired value was physically possible.

7. *Utilise the DSV function to determine the optimum feed stage which minimises reboiler heat input for a specified value of N_T.* The optimum feed stage for the distillation was determined using the DSV function. In most distillation columns, a significant operating expense is the reboiler energy consumption and the optimum feed stage was defined as that feed stage which minimized the reboiler heat input. The DSV function was used to hold product purity constant and the feed tray location and the reflux ratio varied. All other input variables including N_T were unchanged and effect of feed stage location on the reboiler heat input evaluated. The feed stage location which resulted in the minimum amount of required reboiler heat input was chosen as the optimum feed stage and used for the further design of the column.

8. *With the optimum location of feed stage, use the ratio of N_F/N_T to vary N_T and find the minimum number of stages (N_{MIN}) for the column.* The optimum value of N_F was determined with respect to required reboiler heat for the value of N_T determined by sensitivity analysis. Using this ratio of N_F/N_T it is possible to determine the minimum number of required stages for the separation. The minimum number of stages, N_{MIN}, was that number of stages which caused the molar RR to tend to ∞, or rather caused the value of the RR to become appreciably large. Using a DSV function to hold the desired product purities of the column constant, the total number of stages of the column was varied (with the feed stage varying according to the ratio of N_F/N_T) and the reflux ratio of the column monitored.

9. *Use N_{MIN} to determine a revised estimate of N_T.* For the preliminary design of the separation process, the widely used heuristic (as recommended by (Luyben 2006)) of setting the total number of trays in the column to twice that of the minimum number of trays was utilized. In this manner, the value N_{MIN} determined in step 8 was used to provide a revised estimate of N_T, by multiplying N_{MIN} by two and adding two extra stages for the reboiler and condenser if a partial condenser was utilised, or a single extra stage if a total condenser was utilised.

6.2.2.2. Extractive Distillation Column

The design procedure for the extractive distillation columns in the toluene separation process is similar to the methodology outlined above. An additional variable that needs to be defined is the location of the feed stage for the solvent. Initially, the extractive column was designed without a feed stream of solvent to process, i.e. only the feed stream consisting primarily of HFP and HFPO entered the extractive column. The molar RR, optimum feed tray location, N_{MIN} and final revised value of N_T were obtained through the use of the sensitivity analysis and DSV function as for a conventional distillation column and once completed, the solvent stream was added to the column. The effect of the solvent was to selectively bond with the HFP to allow removal of the HFP from the bottoms stream, thus causing the initially heavy key or less volatile component HFPO to be removed from the distillate. The solvent stream of pure toluene was initially added in a 1:1 molar ratio with HFPO, i.e. the amount of toluene in the solvent was equal to the amount of HFPO in the feed, as recommended by (Oda et al. 1979). The solvent stream feed stage was added at an arbitrary location higher than that of the optimum feed tray location for the HFP and HFPO stream. The simulation was run and the effect of the addition of toluene on the separation of HFP and HFPO noted. A sensitivity analysis was run by varying the solvent toluene flow rate and noting the effect on the purity and recovery of HFPO in the distillate. That solvent flow rate which resulted in the highest purity HFPO distillate product was utilized for the remaining design. A further sensitivity analysis was run by varying the location of the solvent feed stage (with the upper limit being the condenser and the lower limit the feed stage location for the HFP and HFPO mixture) and noting the effect on HFPO product purity and recovery.

6.2.2.3. Stripping Unit

The stripping unit utilised in the Aspen simulation utilises the RadFrac model and was designed in a manner analogous to that of the general distillation column. The location of the feed trays for the incoming liquid stream containing the HFP and HFPO and the solvent stream containing R116, are fixed at the top and the bottom of the column respectively. The initial feed rate of solvent to the process was set to a molar ratio of 6:1 of R116 to component HFPO as recommended by (Sulzbach 1982). The variables that were defined for the RadFrac stripping model included the distillate rate, number of stages and column operating pressure.

1. *Specification of the column operating pressure and* N_T. The column operating pressure for all the strippers were set to one atmosphere, with the total number of stages initially set to the arbitrary value of ten. This value was adjusted if the initial Aspen simulation process produced errors

2. *Specification of the distillate rate.* The action of the gaseous solvent R116 was to selectively remove the HFP from the liquid stream entering the stripper, resulting in an exit liquid stream rich in HFPO and an exit gaseous stream rich in solvent and HFP. The distillate rate, which in the case of the stripper referred to the flow rate of the gaseous stream containing the solvent and the stripped solute leaving the top of the column, was initially set to be the total amount of solvent entering the column plus the total amount of HFP in the feed liquid stream

3. *Perform a sensitivity analysis on the solvent flow rate.* The solvent flow rate to the process was varied, and the distillate rate, which depends on the solvent flowrate, was changed accordingly. At different values of the solvent flow rate and distillate rate, the purity and recovery of HFPO was observed and the solvent flowrate which resulted in the optimum values of purity and recovery of HFPO was utilised

4. *Perform a sensitivity analysis to determine a revised estimate of* N_T. A sensitivity analysis, in a method analogous to that for the design of a general distillation column was performed. The number of stages was varied and the monitored variables included the purity and recovery of HFPO in the exiting liquid stream, and as such a revised estimate of N_T, which corresponded to optimum values of purity and recovery, was obtained

5. *Perform a sensitivity analysis to determine a revised estimate of the distillate rate.* A sensitivity analysis was run by varying the distillate rate whilst holding the solvent feed flowrate constant, and noting the effect on HFPO purity and recovery in the exiting liquid stream to obtain a revised estimate of the distillate rate.

6.2.2.4. Closing the Recycle Loop

The component HFP selectively bonded to the solvents toluene and R116 in the respective separation processes. Each process featured solvent recovery columns where the solvents were separated from the HFP and any other products resulting in highly pure toluene and R116 solvent streams. In order to decrease the fresh solvent overhead, the solvents were recycled, in the case of toluene back to the extractive distillation column and in the case of the R116 back to the first stripping unit. The following methodology was used for the closing of the recycle loop in both the toluene and R116 processes:

1. *Split the recovered solvent stream into a 'Purge' and 'Recycle' stream.* The solvent stream that was separated from the HFP and other impurities was split into two streams, a purge stream and a recycle stream, with the recycle loop initially open (i.e. the recycle stream was not connected to the extractive column or stripping unit). The division of the recovered solvent stream between the purge and recycle streams was determined by the split fraction which was the fraction of the recovered solvent flowrate that went to the purge stream, i.e. a split fraction of one signified that the entire recovered solvent stream left through the purge stream with no recovered solvent flowing through the recycle stream.

2. *Initially set the split fraction to one.* The split fraction was initially set to one and the recycle loop closed. The simulation was then initiated and checked for simulation or FORTRAN errors.

3. *Decrease split fraction in order to recycle solvent and in a step wise manner decrease fresh solvent feed by amount of solvent recycled.* With the recycle loop closed and no FORTRAN errors encountered, the split fraction was decreased by a small amount (in a step of 0.05) to allow some of the solvent to be recycled, with the fresh solvent flow rate initially left unchanged. The simulation was run and the monitored variables include the HFPO product purity and overall HFPO recovery. If the recovery and purity were within specifications, the fresh solvent flow rate was first decreased by approximately half of the amount of the solvent recycled to the extractive distillation column or stripper. The simulation was run and if the recovery and purity of HFPO were satisfactory, the fresh solvent flow rate was then decreased by an amount equal to the amount of solvent recycled and the purity and recovery of the HFPO monitored.

4. *Continue in a step wise manner decreasing split fraction and fresh solvent feed rate.* The split fraction of the recovered solvent stream was once again decreased in an increment of 0.05 and the procedure in step three repeated. The HFPO product purity and recovery were constantly monitored and steps three and four were constantly repeated (i.e. decreasing the split fraction and fresh solvent feed rate and increasing the amount of solvent recycled) until the desired product specifications for HFPO could not be fulfilled, at which point the final value of the fresh solvent feed became the initial solvent feed to the process. A quick check on the conservation of mass was performed by checking if the fresh solvent feed rate equated to the amount of solvent leaving in the purge stream and in the HFP product stream.

CHAPTER SEVEN

7. RESULTS AND DISCUSSION

7.1. GENERAL CONSIDERATIONS

HFP (R1216) and HFPO are of the chemical species fluorinated hydrocarbons or fluorocarbons. Fluorocarbons contain carbon-fluorine bonds and the relatively low reactivity and high polarity of these bonds impart unique characteristics to this class of compound ((EFCTC 2008)). A typical example of the unique characteristics imparted by the nature of the atoms and bonding, is demonstrated for the compound hexafluoroacetone which is an isomer of HFPO. Hexafluoroacetone is the 'fluoro' analogue of acetone, which has a normal boiling point of 246.15 K as compared to a normal boiling point of 329.15 K for acetone itself. This difference illustrates the effect of replacing a C-H bond with a C-F bond which results in relatively low boiling points as well as low reactivity and increased stability for fluorocarbon systems.

In general, for the evaluation of a separation method for a particular system, an important consideration is the normal boiling points of the individual components. With a boiling point difference of 2 K for HFP and HFPO, and thus associated similarities between the pure component vapour pressures, it was considered impractical and uneconomical to separate this system via conventional distillation methods. Research of prior methods for the separation of a binary mixture of HFP and HFPO revealed that five separation technologies have been patented. Four of the patents utilised the process of extractive distillation with a liquid solvent. The fifth patent, which featured the work of (Ueno et al. 1997a), utilised the process of conventional distillation to separate HFP and HFPO. The common theme of the previous methods for the separation of HFP and HFPO indicated that the addition of third component, a solvent, was required to alter the phase behaviour of the HFP and HFPO to effect such a separation. Although the work of (Ueno et al. 1997a) utilised conventional distillation, the proposed patent was restricted to feed mixtures of HFP and HFPO in a mass ratio of 0.1:1 and with a high theoretical stage count. The restriction on the composition of the feed mixture imposed by the conventional distillation process made this method unattractive as PELCHEM required a general, non restrictive separation process for feed mixtures of varying compositions, with a typical feed mixture in the molar ratio of 1:2 HFP to HFPO.

7.2. SOLVENT SELECTION PROCEDURE

To determine suitable solvents for a separation scheme, a rigorous solvent selection procedure involving the UNIFAC ((Fredenslund et al. 1977)) group contribution method was utilised. The solvent selection procedure is discussed in detail in Chapter three of this dissertation.

The first step of the solvent selection procedure lay in the compilation of list of possible commercially available candidate solvents for the separation of HFP and HFPO. For the screening of solvents, identification was first made on the basis of candidates displaying a similar structure or chemical nature to the fluorocarbons HFP and HFPO (step 1.1 of the solvent selection procedure). Solvents homologous to fluorocarbons included the chlorocarbons species, in which a chlorine molecule replaced the fluorine molecule on the fluorocarbon analogue. Further compounds homologous to HFP and HFPO were several refrigerants, as HFP (R1216), and to a lesser extent HFPO, are used as refrigerants in industrial applications. For compounds displaying a similar structure to that of HFPO, solvents which contained the ethylene or epoxide (oxirane) structures, typical examples of which were alkyl ethers of ethylene glycol, were identified. The carbon-fluorine bond in the fluorocarbon molecules altered the chemical nature of the compound by increasing the polarity of the compound as a whole. This was due to the fact that certain heteroatom substituents, typically oxygen, sulphur, nitrogen, chlorine and fluorine molecules, created an uneven sharing of electrons which led to the formation of a dipole moment which increased the polarity of the compound as a whole ((Barwick 1997)). However it must be noted that while individual bonds in a molecule might be polarised due to electro-negativities of the atoms involved, the overall dipole moment of a molecule can still be zero due to the fact that individual dipole moments are vector quantities and their algebraic sum can be zero due to symmetry effects. Broad solvent classes which contained suitable substituents were identified as possible candidate solvents. Solvent classes that worked with chlorinated systems, typical examples of which where aromatics and alcohols, were identified on the basis that they would interact to a similar extent with the fluorinated systems.

Further solvent identification was undertaken through the use of the Robbins chart (step 1.2 of the solvent selection procedure). According to the Robbins chart, presented in Figure 3.2, HFP and HFPO were both considered class 11 solutes since they are multi-halogen components without active hydrogen molecules. Solvent classes which were compatible with class 11 solutes and did not produce a deviation from Raoult's Law included the following:

1. *Class 4 solvents:* Ketone, Sulfone, Phosphine Oxide compounds
2. *Class 6 solvents:* Tertiary Amines
3. *Class 7 solvents:* Secondary Amines
4. *Class 9 solvents:* Ether, Oxide, Sulfoxide compounds

5. *Class 11 solvents:* Aromatic, Olefin, Halogen Aromatic, Multi-Halogen Paraffin without active Hydrogen, Mono-Halogen Paraffin compounds
6. *Class 12 solvents:* Paraffin, carbon disulfide.

The high polarity of HFP and HFPO, in conjunction with the generally held convention that 'like substances dissolve like substances', led to the identification of solvents based on polarity considerations (step 1.3 of the solvent selection procedure). The determination of the polarity of the solvents was performed in a qualitative manner via the identification of the molecular structure, attached functional groups, heteroatom substituents and chain length. Quantitative measurements of polarity were possible, as demonstrated by (Rohrschneider 1973) and (Barwick 1997) for the Rohrschneider-Snyder solvent classification scheme and the Hildebrand polarity scale, however the sheer number of solvents that were evaluated for the candidate solvent list made this impractical and beyond the scope of this project. As discussed previously, the type of heteroatom substituent greatly influenced the polarity of a solvent, which reinforced the selection of solvent classes which displayed oxygen, sulphur, nitrogen, chlorine and fluorine substituents. (Gani and Brignole 1983) suggested that although aromatic compounds are generally polar in nature due to the benzene ring (double bonds, hyper-conjugation and the pi-electron cloud which led to the formation of a dipole moment), the nature of the substituent group attached to the ring greatly affected the property of the compound as a whole. Aromatic compounds which contained chlorine substituents which increased the polarity of the molecules, for example Chlorobenzene and 1,2-Dichlorobenzene, were identified. Alcohol solvents which contained the hydroxyl group (OH), consisted of the non-polar alkyl group and the polar OH group. As the alkyl group of the alcohol increased in size it became a more significant fraction of the alcohol and the compound as a whole became less polar in nature. Linear alcohol solvents with four carbon atoms or less were thus identified. The polarity of alcohol class solvents also depended on the structure of the alkyl group. Alcohols with branched or conjugated (double or triple bond) alkyl groups are more polar than the analogous straight chained alcohol. A typical example was the case of tert-butyl alcohol which was more polar than n-butyl alcohol. A similar situation existed for the compound class ether and other compounds which contained the carbonyl group. The oxygen molecule of an ether compound contributed to the polarity of the molecule and conjugation and branching of any attached alkyl groups served to increase the polarity of the molecule as a whole. Branched ethers containing double or tripe bonds, with typical examples being glycol ethers and bulky ethers, were identified as potential solvents. A further group of compounds which exhibited polar characteristics were the low molecular weight amines. The polar characteristics were due to the tendency of the nitrogen molecule to form hydrogen bonds, as a result, this class of solvents was identified for further study.

The initial candidate list of two hundred and seven solvents obtained via step one of the solvent selection procedure is presented in Table A.1, Appendix A.

Step 2 of the solvent selection procedure was the identification of individual solvents from the initial list of two hundred and seven solvents. The identification of the individual solvents began with the evaluation of the boiling point characteristic of the solvents (step 2.1 of the solvent selection procedure). Due to the low boiling characteristics of HFP and HFPO, 243.75 and 245.75 K respectively, several solvents were suitable for use as the average candidate solvent boiling points were above 273.15 K. A notable exception was the refrigerant solvent class, which typically displayed normal boiling values of below 263.15 K. In total, it was found that thirty one solvents on the initial list displayed boiling points less than 273.15 K. The initial list of solvents was shortened to one hundred and eighty candidate solvents, with twenty seven solvents discarded due to the proximity of the boiling point. Solvents excluded via this method included certain ethyl and methyl amines, halogenated hydrocarbons such as dichlorotrifluoromethane, which displayed a boiling point of 243.45 K, and certain methane and ethane refrigerants which displayed normal boiling values below 253.15, typical examples of which were the compounds chloropentafluoroethane, tetrafluroethane and difluoromethane.

The performance of the one hundred and eighty candidate solvents were ranked through the evaluation of the selectivity at infinite dilution (step 2.3 of the solvent selection procedure). The selectivity model used is derived in Chapter three and presented in equation (3-6), with the possible values of selectivity and their physical meanings presented in Table 3.2. To evaluate the selectivity at infinite dilution, the UNIFAC group contribution method via the computer software xlUNIFAC ((Randhol and Engelien 2000)) was utilised.

For this research, a predictive model which lent itself well to reliable, flexible calculations with low computational time and accurate descriptions of the real phase behavior of mixtures was of paramount importance. Numerous predictive models are available in literature: PSRK UNIFAC ((Holderbaum and Gmehling 1991)), COSMO ((Klamt and Schuuurmann 1993)), COSMO RS (Klamt, COSMO*logic*), ASOG ((Kojima and Tochigi 1979)), UNIFAC, Modified UNIFAC Dortmund ((Weidlich and Gmehling 1987)) and Modified Unifac Lyngby ((Larsen et al. 1987)). In the field of group contribution methods, UNIFAC and Modified UNIFAC (Dortmund) have become very popular due to the wide range of applicability, ease of use and the constant periodical updating of interaction parameters via the UNIFAC consortium ((Gmehling 1999)). The primary difference between the Modified UNIFAC (Dortmund) model and the original UNIFAC model, was that the modified model took into account the temperature dependencies of the binary interaction parameters, which since the conception of the modified model, allowed for a more reliable description of the phase equilibrium behavior over a wider temperature and concentration range than the original UNIFAC model ((Gmehling 2001)). However, the original UNIFAC method allowed the accurate prediction of the VLE behavior for mixtures in a temperature range of 270 to 400 K ((Gmehling 1995)). For this project, the selectivity values for HFP and HFPO in each of the one hundred and eighty solvents were evaluated in a temperature range of 273.15 to 323.15 K, which was within the operating

limits of the original UNIFAC model. Additionally, updated model parameters for the UNIFAC model were purchased from the UNIFAC Consortium in July 2006 and utilised for this work. The functional group assignment for HFP, HFPO and each of the 180 solvents were undertaken for the calculations.

For the functional group assignment of the key components HFP and HFPO for the UNIFAC model, Dr. Antje Jakob, a scientific co-worker at the UNIFAC consortium was consulted in May 2006. From personal communication via electronic mail, Dr. Jakob stated that for the UNIFAC group contribution method "*...the calculation of molecules like HFP and HFPO are non-trivial.*", and through this consultation with Dr. Jakob the functional group assignment of HFP, and at a later stage HFPO, were proposed.

For the fragmentation or functional group assignment of HFP, UNIFAC main group 40, the 'CF_2' group, was utilised. This main group contained the following sub groups:

1. Sub-group 74 = CF_3
2. Sub-group 75 = CF_2
3. Sub-group 76 = CF.

For the fragmentation or functional group assignment of HFPO, UNIFAC main group 52, the '*Epoxy*' group, was utilised. This main group contained the following sub groups:

1. Sub-group 110 = H_2COCH
2. Sub-group 111 = H_2COC
3. Sub-group 112 = HCOCH
4. Sub-group 113 = COCH
5. Sub-group 114 = H_2COCH_2

The functional group assignment for the key components, HFP and HFPO are as follows:

1. HFP : 1 x CF_3 group, 1 x CF_2 group and 1 x CF group
2. HFPO : 1 x CF_3 group, 3 x CF group and 1 x COCH group.

For the fragmentation of HFP used for this research, the double bond between the central carbon atom and the CF_2 molecule could not be taken into account with the available sub-groups. For the fragmentation of component HFPO, no single fluorine atoms were available in the UNIFAC (or Modified UNIFAC) sub-groups. To work around this problem, three single CF molecules, represented by sub-group 76 were utilised instead.

The selectivity at infinite dilution for the one hundred and eighty solvents were evaluated at two temperatures via the xlUNIFAC software described in Section A.3, Appendix A. The list of calculated selectivity values for each component at the two temperatures of evaluation, 273.15 and 323.15 K are presented in Table A.3, Appendix A. Table 7.1 presents a summary of the calculated selectivity values at infinite dilution values for the various solvent classes at 273.15 K. From Table A.3, Appendix A, a list of the top thirty performing solvents was generated. The list of the top 30 solvents, in ascending order according to selectivity, is presented in Table 7.2.

From Tables 7.1 and 7.2, for selectivity values less than unity, the best performing solvent class were the ethers, in particular ethylene glycol diethyl ether which produced a selectivity value of 0.59. The worst performing solvent classes for selectivity values less than unity were the amine, ester and alcohols classes. The polyhydric alcohols, which were alcohols which contained at least two hydroxyl groups performed better than the conventional alcohols due to the increased polarity imparted by the additional OH group. In the glycol ether and ether categories, propylene glycol and di-ethyl ether produced selectivity values of 0.77 and 0.66 respectively. For selectivity values greater than unity, the best performing solvent classes were the aromatic hydrocarbons which produced a maximum selectivity value of 4.65 for the compound hydroquinone and the isomers resorcinol and catechol. The chlorinated hydrocarbons and chlorofluorohydrocarbons exhibited good values of selectivity at infinite dilution, in particular the ethane series refrigerants dichlorofluoroethane (1.46), dichlorotrifluoroethane (1.42) and trichloroethane (1.65). The chlorinated aromatic compounds chlorobenzene and dichlorobenzene produced selectivity values of 1.59 and 1.48 respectively, which were the highest aromatic selectivity values, excluding hydroquinone and the isomers.

Solvent Class	β_i^∞ Minimum	β_i^∞ Maximum
Alcohols	0.70	1.16
Aromatic Hydrocarbons	1.10	4.65
Esters	0.79	1.02
Ethers	0.59	0.89
Glycol Ethers	0.69	0.89
Ketones	0.68	1.12
Polyhydric alcohols	0.59	0.81
Chlorinated hydrocarbons	1.50	2.50
Fluorinated hydrocarbons	0.71	2.30
Chlorofluorohydrocarbons	0.72	1.42
Amines	0.70	0.90

Table 7.1. A summary of minimum and maximum selectivity at infinite dilution values for the various solvent classes at 273.15 K.

Solvent	β_i^∞
Ethylene Glycol diethyl ether	0.59
Ethylene glycol	0.63
1,3-Butanediol	0.64
Di-Isopropyl Ether	0.66
Diethylene Glycol	0.74
Propylene Glycol	0.77
Dichlorodifluoroethane	1.19
Bromodichlorofluoromethane	1.19
Trichlorofluoromethane	1.21
Trichlorofluoroethane	1.22
Dichlorodifluoromethane	1.29
Hexafluoroethane	1.30
Dichloromethane	1.32
Toluene	1.35
Carbon Dioxide	1.35
Dichlorofluoromethane	1.38
Chlorodifluoromethane	1.38
Benzene	1.40
Dichlorotrifluoroethane	1.42
1,1,1-Trichlorotrifluoroethane	1.46
Dichlorofluoroethane	1.46
Chlorobenzene	1.48
1,2-Dichlorobenzene	1.59
Pentachlorofluoroethane	1.63
1, 1, 1, 2-Tetrachloro-2, 2-Difluoroethane	1.65
Trichloroethane	1.66
Pentachloroethane	2.01
Hexachloroethane	2.30
Trichloromethane	2.59
Hydroquinone	4.65

Table 7.2. A summary of the top 30 performing solvents according to selectivity at infinite dilution at 273.15 K.

The list of the top thirty solvents determined from infinite dilution separation factors, Table 7.2, was narrowed to a final list of ten solvents (step 2.3 of the solvent selection procedure) which was presented to PELCHEM in August 2006. To shortlist the final ten solvents, the criteria utilised were individual solvent properties as described in Chapter three.

Environmental acceptability played an important role in the selection of the final ten solvents. Several of the candidate solvents on the top thirty list were halogenated hydrocarbons, in some cases consisting of chlorine as well as fluorine containing molecules. The use of such compounds has been scientifically proven to affect the environment, in particular the ozone layer and as such there are laws and guidelines

which govern the consumption of halogenated hydrocarbons. The most notable of such laws was the Montréal Protocol ((UN 1987)) which governed the use of ozone depleting substances and provided recommendations for the phasing out and eventual non-use of these harmful substances. Solvents for the final list of ten for proposal to PELCHEM were thus chosen with the aim of adhering to the guidelines set down by the Montréal Protocol. Certain solvents which produced a high selectivity at infinite dilution, most notably tetrachloro-difluoroethane (R112), 1,1,1-trichloroethane (R140) and trichloromethane or chloroform (R20), with selectivity values of 1.65, 1.66 and 2.59 respectively, were not considered as suitable solvents for the system due their harmful nature and restriction in terms of the Montreal Protocol. Further compounds on the top thirty list which were banned under the jurisdiction of the protocol were the solvents pentachlorofluoroethane (R111), trichloroflouromethane (R11), bromochlorodifluoromethane (R12B1) and dichlorodifluoromethane (R12). These solvents were thus excluded from the solvent selection procedure despite having good selectivity values.

The ozone depletion potential (ODP) for each of the refrigerants in the top thirty list were examined. The ODP is the ratio of calculated ozone column change for each mass unit of a gas emitted into the atmosphere relative to the calculated depletion for the reference gas trichlorofluoromethane (R11), for which the ODP value is set as unity ((UNEP 2001)). ODP values for refrigerants under unity were considered acceptable and as such a comparison between the ODP of the various refrigerants on the top thirty list was made. The remaining environmentally acceptable refrigerants on the list with ODP values less than unity were hexafluoroethane (R116), trichlorofluoroethane (R131), dichlorofluoromethane (R21), chlorodifluoromethane (R22), dichlorotrifluoroethane (R123), dichlorofluoroethane (R141b) and pentachloroethane (R120) and hexachloroethane (R110), which exhibited ODP values of significantly less than unity. Chlorinated solvents such as chlorobenzene, 1,2-dichlorobenzene and dichloromethane (R30) contain chlorine constituents which do not promote green chemistry. Although not illegal, the use of certain chlorine containing substances is being phased out of industrial usage due to environmental considerations. However, it was found that these particular solvents are considered less harmful than most chlorocarbons or chlorine containing compounds, and additionally produced good selectivity values at infinite dilution. Chlorofluorocarbons and bromine containing compounds (halons) were overlooked due to their high ozone depletion potential, particularly bromine containing refrigerants which are exceptionally harmful to ozone molecules. Fluorinated hydrocarbon solvents were considered for the top ten list as they were a suitable replacement for chlorofluorocarbons since their ozone depletion potential is not as great as CFCs or other substances banned under the Montréal Protocol.

Non chlorine containing solvents were examined, in particular the aromatics hydroquinone and toluene. Although aromatic compounds have associated carcinogenic effects, the favourable values of selectivity produced warranted further investigation, with comparatively high values of 4.65 and 1.35 for hydroquinone and toluene respectively. The ether class solvents, di-isopropyl ether and ethylene glycol

diethyl ether showed promise as potential solvents as they were relatively non-toxic compounds and produced acceptable values of selectivity at infinite dilution of 0.66 and 0.59 respectively. Carbon dioxide, which was intended for use in a supercritical extraction process, produced a selectivity value of 1.35.

Health and safety aspects were taken into consideration for the solvent selection procedure. In an ideal case, the chosen solvent should exhibit non-toxic properties and should be non-flammable with minimal adverse health effects. The LD_{50} values for each of the solvents were examined where possible, as well as the safety rating, which referred to both flammability and toxicity. For the halogenated hydrocarbon solvents, fluorocarbons are in general, lower in toxicity than the corresponding chlorinated or brominated hydrocarbons. This lower toxicity was associated with the greater stability of the C-F bond. Thus the fluorocarbons on the top thirty list were given preference over chlorinated and brominated counterparts. The flash points and safety ratings of the various candidate solvents were examined to give an indication of flammability and the material safety and data sheets obtained to acquire the necessary health and safety information. Compounds were divided into three groups based on their flammability tendencies. Class one compounds were non flammable and showed no flame propagation at ambient conditions at any concentration. Class 2 compounds were moderately flammable while Class 3 compounds were highly flammable. Halogenated hydrocarbon mixtures, including refrigerants, fell into the Class 1 category, while hydrocarbon mixtures generally fell into the Class 3 category. Most of the refrigerants on the top thirty list were non flammable. Components which were found to be flammable were the ethers and aromatics, in particular diethyl ether and toluene.

The material safety and data sheets of the top 30 solvents were examined to determine the stability and reactivity of the solvents. Desirable properties for the solvents included chemical stability, limited reactivity and non-toxic decomposition products, with the chosen solvent inert with respect to either HFP or HFPO. For the chlorobenzene compounds, 1,2-dichlorobenzene and chlorobenzene, the component 1,2-dichlorobenzene produced the higher selectivity value of 1.59 as compared to 1.48 for chlorobenzene. However, it was found via the material safety and data sheet that 1,2-dichlorbenzene is incompatible with halogenated hydrocarbons as they react violently to give off heat in an exothermic process. Chlorobenzene did not interact with halogenated hydrocarbons in such a manner and as such was preferred over 1,2-dichlorobenzene.

Cost and availability factors were taken into account. Average costs of the components on the top thirty list were obtained through use of the catalogue listing function of the research software SciFinder Scholar ((ACS 2007)). Through the use of the program, average costs of the potential solvents were obtained from the on-line catalogues of international chemical companies. The catalogue prices were obtained in July 2006 and converted into the South African currency (1 U.S. $ = 7.0688 ZAR, 1 G.B. £ = 12.8234 ZAR as at July 2006). The prices that were obtained were not taken as indicative of precise market prices, but were

used rather as an indication of the price range for a particular component. It was generally difficult to compare solvents on the basis of economics as the price of each component varied with quantity. As a result, prices for each individual solvent were converted to the standardised units of 'R' per 1 'litre' of product. To quantify the availability of a particular solvent, a rating scheme was devised. The availability was quantified through the number of commercial sources found via the catalogue listing function of the research software SciFinder and accorded a rating. If a solvent was researched in SciFinder and 40 different companies carried the product, then the availability was afforded a rating of 'Good'. If more than 60 commercial sources were found for a product, the availability rating was deemed 'Very Good' and if more than 100 sources were found for a product, then the availability rating was afforded a rating of 'Excellent'. Solvents with 10 or less sources were deemed 'Poor' with respect to availability, whilst 'Moderate' availability solvents had between 10 and 40 sources.

From the examination of the individual solvents properties, the list of top 30 solvents based on selectivity values was short-listed into a final list of 10 solvents. The final list of solvents is presented in Table 7.3:

CAS Index No.	Solvent	Formula
124-38-9	Carbon dioxide	CO_2
76-16-4	Hexafluoroethane (R 116)	C_2F_6
306-83-2	2,2-Dichloro-1,1,1-trifluoroethane (R 123)	$CHCl_2CF_3$
1717-00-6	1,1-Dichloro-1-fluoroethane (R 141b)	CH_2CCl_2F
27639	Dichloromethane	CH_2Cl_2
111-43-3	di-Isopropyl ether	$C_6H_{14}O$
108-88-3	Toluene	$C_6H_5CH_3$
629-14-1	Ethylene glycol diethyl ether	$C_2H_5OCH_2CH_2OC_2H_5$
108-90-7	Chlorobenzene	C_6H_5Cl
108-46-3	Hydroquinone	$C_6H_4(OH)_2$

Table 7.3. The final list of 10 candidate solvents determined by the solvent selection procedure.

Table 7.4 presents a summary of the individual solvent properties that were examined for the final list of 10 solvents, in ascending order according to boiling point. The price per litre of each component was obtained from SciFinder scholar and was correct as at 31 July 2006. The selectivity values at infinite dilution at 273.15 K are presented, as well as the recoverability of the substances which is quantified as the boiling point difference between the solvent and the less volatile component, either HFP or HFPO.

The final 10 solvents determined by the rigorous solvent selection procedure contained four refrigerants, hexafluoroethane (R116), dichlorotrifluoroethane (R123), dichlorofluoroethane (R141b) and the 'old' refrigerant CO_2. The chlorinated solvents on the list were chlorobenzene and the commonly used laboratory solvent dichloromethane. Two ethers made the final list of ten solvents, ethylene glycol diethyl ether and di-isopropyl ether, with the aromatic compounds toluene and hydroquinone completing the list. From Table

7.4, only two solvents on the final list of 10 exhibited selectivity values less than unity, ethylene glycol diethyl ether and di-isopropyl ether, with the remaining solvents, as per the definition of selectivity utilised for this project, bonding preferentially to component HFP. From the analysis of the selectivity values in Table 7.4, all components exhibited values far removed from unity, which is indicative of the suitability of each solvent for the separation of a stream of HFP and HFPO. All the solvents show excellent recoverability values well above the 10 to 20 K limit imposed by the solvent selection procedure. The reactivity, safety and availability data are additionally presented in the table with all components exhibiting '*Good*' or higher availability, which indicated that greater than 40 commercial sources were available for each solvent. Of the ten proposed solvents determined by the rigorous solvent selection procedure, 5 of the solvents were previously patented. The solvent toluene was patented in the work of (Wiist 1967) for the du Pont Company, with solvents R123 and R141b patented by (Ueno et al. 1997) for the Asahi Glass Company. A further patent of the Asahi company, in the work of (Oda et al. 1979) included the solvents cholorobenzene and di-isopropyl ether.

The list of ten proposed solvents was presented to PELCHEM in August 2006. From the ten solvents, PELCHEM chose four solvents for further investigation into the separation of a stream of HFP and HFPO. From the four solvents prescribed by PELCHEM, two solvents were utilised for this research project, the solvents toluene and hexafluoroethane (R116) and the work thereon is presented in this dissertation. Further work undertaken on the remaining two solvents chosen by PELCHEM can be found in the work of (Nelson 2008).

PELCHEM selected a patented solvent, toluene, and a novel untested solvent R116 such that two separation schemes could be proposed, simulated and compared via the Aspen Engineering Suite. The separation of HFP and HFPO via extractive distillation utilising toluene has been performed extensively by the du Pont Company, however to bypass the royalty fees associated with patented technologies, PELCHEM needed to determine firstly if it was possible to develop a novel process with an untested solvent, and secondly, if the new technology compared favorably with the existing separation methods. The process developed around the solvent toluene was to be used as a 'yardstick' against which to measure the performance and feasibility of the novel process developed around the untested solvent R116. The decision to utilise the solvent R116 was additionally made on the basis that PELCHEM produced R116 onsite at Pelindaba, and as such a fresh solvent feedstock was readily available, which made the choice of R116 as a solvent economically logical.

Solvent	Selectivity $\beta i\infty$	Recoverability [K]	Cost [R•L^{-1}]	Reactivity	Availability	Safety
Carbon dioxide	1.35	49.10	105	Generally stable. May decompose with electrical discharge.	Excellent	Non flammable. Non toxic
Hexafluoroethane	1.30	50.80	2340	Generally stable. May decompose to toxic, corrosive products.	Good	Non flammable. Non toxic
2,2-Dichloro-1,1,1-trifluoroethane	1.42	56.40	1820	Stable. May decompose to HF, HCl, CO, CO_2.	Good	Non flammable. Non toxic
1,1-Dichloro-1-fluoroethane	1.46	61.45	21260	Stable. May decompose to HF, HCl, CO, CO_2.	Good	Non flammable. Non toxic
Dichloromethane	1.32	69.40	237	Reactive with strong acids and alkali metals. Decomposes to HCl and phosgene.	Very Good	Non flammable. Harmful
di-Isopropyl ether	0.66	119.40	166	Reactive with aldehydes, amides, acids. May decompose to peroxides.	Very Good	Flammable. Non Toxic
Toluene	1.35	140.00	267	Reactive with strong oxidising agents, strong acids, heat. No decomposition products.	Very Good	Highly flammable. Harmful
Ethylene glycol diethyl ether	0.59	149.40	1242	Reactive with oxygen and strong oxidising agents. Decomposes to peroxides.	Very Good	Flammable. Harmful
Chlorobenzene	1.48	161.40	414	Reactive with oxidising agents, DMSO, sodium. May decompose to HCl upon heating.	Very Good	Flammable. Harmful
Hydroquinone	4.65	310.40	854	Reactive with strong oxidising agents, bases, amines. No decomposition products.	Good	Non flammable. Harmful

Table 7.4. A summary of the individual solvent properties for the final 10 solvents as determined by the solvent selection procedure.

7.3. EXPERIMENTAL MEASUREMENTS

VLE data for the binary system HFP + HFPO were required for this project. This data could not be experimentally determined due to time constraints and lack of sufficient quantities of HFP and HFPO. The HFP and HFPO were each purchased in 500 g quantities. Preference were given to the binary systems involving HFP, HFPO, Toluene and R116 and measurements involving these systems were undertaken first. The measurements were performed over a three month period, from October to December 2006, at the TEP laboratory at Fontainebleau, France, and the measurements for the toluene and R116 binaries were completed by the end of December. The measurements of these systems consumed the majority of the available HFP and HFPO and it was not feasible to order more quantities of HFP and HFPO owing to the delivery time of these components which was approximately 2 to 3 weeks. The data for the binary systems HFP + HFPO at 273.15 and 313.15 K were predicted via Thermopack utilising the PSRK UNIFAC ((Holderbaum and Gmehling 1991)) method in conjunction with the SRK EOS ((Soave 1972)) and the Mathias-Copeman alpha function ((Mathias and Copeman 1983)). The data for the HFP + HFPO systems was predicted with the assistance of C. Coquelet of Ecoles des Mines de Paris, the programmer of the Thermopack software. In lieu of measured data the predicted data was considered acceptable for further use in this project as the components HFP and HFPO exhibited similar boiling points, and the system has a low relative volatility close to one. The data predicted by the PSRK UNIFAC method thus provided a sufficient description of this system for the purposes of this project. The predicted data for the systems HFP + HFPO are presented in Section 7.4.

The binary systems that were measured for this project involved HFP, HFPO and the identified solvents toluene and R116. In total, four binary systems at two isotherms were measured, resulting in eight data sets. A summary of the binary HPVLE data sets measured is presented in Table 4.1. None of the binary data sets have been published in literature and as such no comparison could be made with literature data. Pure component vapour pressure data for the component HFPO were measured and presented in this section. No previous published pure component vapour pressure measurements for HFPO have been found in literature.

In vapour-liquid equilibrium measurements, the properties that are typically measured are temperature, pressure and phase compositions. It is thus crucial that proper calibration procedures are undertaken for these properties. The results of the calibrations for the pressure transducers, temperature sensors and gas chromatograph are presented in this section.

7.3.1. Chemicals

The chemicals utilised for the HPVLE measurements are listed in Table 4.2, along with the source and relevant purities. All the chemicals utilised in the experimental measurements were degassed under vacuum before use to remove any impurities.

7.3.2. Accuracy of the measured properties

The primary properties that were measured during the course of the HPVLE measurements were temperature, pressure and composition. To ensure accurate measurements the measuring equipment were calibrated beforehand. The measurements were undertaken on two types of equipment viz. a static synthetic *P-V-T* apparatus and a static analytic apparatus. The equipment were calibrated independently and the results presented.

7.3.2.1. Temperature

The calibration method for the temperature sensors for the static synthetic *P-V-T* apparatus and static analytic apparatus are identical, and is presented in Chapter four.

For the static synthetic *P-V-T* apparatus, temperature measurements were obtained via two Pt-100 resistor probes. The probes, designated T1 and T2 were calibrated against a reference 25 Ω platinum probe which was certified according to the ITS 1990 Protocol ((BIPM 2008)). The calibration data was fitted using a first order polynomial expression and the deviations between the reference pressure and the calculated pressures evaluated. Taking into account the uncertainties due to calibration, the resulting uncertainty on the temperature measurements was estimated to less than ± 0.06 K for probe T1 and less than ± 0.08 K for probe T2 for the static synthetic PVT apparatus. The uncertainty due to the calibration procedure is presented graphically in Appendix B, Figure B.1 for probe T1, and in Figure B.2 for probe T2.

For the static analytic apparatus, the temperature sensor calibration procedure estimated the uncertainty on the temperature measurements for probes T306 and T307 to be less than ± 0.04 K. The uncertainty due to the calibration procedure is presented graphically in Appendix B, Figure B.5 for probe T306, and in Figure B.6 for probe T307.

7.3.2.2. Pressure

The calibration method for the pressure transducers for the static synthetic *P-V-T* apparatus and static analytic apparatus are identical, and is presented in Chapter four of this dissertation.

For the static synthetic *P-V-T* apparatus, pressure measurements were obtained via a Bourdon Sedeme pressure transducer (250 bar maximum pressure). The calibration of the pressure transducer was performed against a dead weight pressure tester with atmospheric pressure measured via a resonant sensor barometer. The pressure transducer was calibrated at the two temperatures of the measurements, 273.15 and 313.15 K, with the calibration data fitted using a second order polynomial expression and the deviations between the reference pressure and the calculated pressures evaluated. Taking into account the uncertainties due to calibration, the resulting uncertainty on the pressure measurements was estimated to less than ± 0.005 MPa at 273.15 K and less than ± 0.004 MPa at 313.15 K. The uncertainty due to the calibration procedure is presented graphically in Appendix B, Figure B.3 for 273.15 K, and in Figure B.4 for 313.15 K.

For the static analytic apparatus, the transducers were manufactured by Druck (PTX611). The pressure transducer calibrations estimated the uncertainty on the pressure measurements for transducers P301 (6 bar maximum pressure) and P302 (60 bar maximum pressure) to be less than ± 0.0003 MPa and ± 0.0004 MPa respectively. The uncertainty due to the calibration procedure is presented graphically in Appendix B, Figure B.7 for P301, and in Figure B.8 for P302.

7.3.2.3. Composition

For the static synthetic *P-V-T* apparatus, vapour-liquid equilibrium phase sampling was not necessary as the global composition of the mixture was determined beforehand via an accurate weighing procedure on an analytical Mettler scale. The accuracy of the weighing procedure and the resulting liquid composition uncertainties are given by the following equation:

$$\Delta x_1 = x_1\left[\frac{\Delta m_1}{m_1} + \frac{\Delta m\left(\frac{1}{M_1} + \frac{1}{M_2}\right)}{\frac{m_1}{M_1} + \frac{m_2}{M_2}}\right] \qquad (7\text{-}1)$$

Where the following definitions apply:

x_1 = Liquid mole fraction of component 1

Δm = $\Delta m_1 = \Delta m_2$ = Uncertainty due to measurement of mass on Mettler scale (g)

m_1 = Mass of component 1 (g)

m_2 = Mass of component 2 (g)

M_1 = Molar mass of component 1 ($kg \cdot kmol^{-1}$)

M_2 = Molar mass of component 2 ($kg \cdot kmol^{-1}$).

The uncertainty of the global composition measurements on the analytical Mettler balance was certified as 1×10^{-6} kg by Mettler Switzerland.

The uncertainty values for measurements on the static synthetic apparatus are presented in Table 7.5:

X_{HFP}	Uncertainty $\|\Delta x\|$
0.0854	0.0004
0.2050	0.0004
0.3909	0.0004
0.7040	0.0006
X_{HFPO}	Uncertainty $\|\Delta x\|$
0.1615	0.0005
0.1765	0.0005
0.2771	0.0004
0.3722	0.0005
0.7306	0.0006

Table 7.5. Uncertainty values for HFP and HFPO composition measurements on the static synthetic apparatus.

Form Table 7.5, the maximum mole fraction uncertainty for the liquid mole fraction measurements for both HFP and HFPO is ± 0.0006, while the minimum uncertainty is ± 0.0004. These low uncertainty values are indicative of the accuracy of the weighing procedure and resulting HPVLE measurements.

For the static analytic apparatus vapour and liquid equilibrium phase compositions were determined by GC analysis. The GC calibration procedure is discussed in Chapter four. The direct injection method was utilised with the calibration and analytical conditions for the calibration procedure presented in Table 4.8. Table 7.6 presents a summary of the uncertainties or maximum errors for composition measurements for the components HFP, HFPO and R116.

Component	Uncertainty [%]
HFP	1.0
HFPO	0.9
116	0.7

Table 7.6. Uncertainty values for HFP, HFPO and R116 composition measurements on the static analytic apparatus.

The calibration data was fitted using a second order polynomial expression and the deviations between the reference and the calculated values determined and the resulting uncertainty values presented in Table 7.6. The uncertainty value represents the maximum errors for composition measurements via the GC analysis, with the minimum uncertainty being 0.7 % for the volatile component R116, with uncertainties of 1.0 and 0.9 % for the non-volatile components HFP and HFPO respectively. The GC calibration curve for HFP, HFPO and R116 are presented in Figures 7.1 to 7.5 for the different calibration volumes. The calibration factors for the second order polynomial expression obtained through regression of the data points is also given.

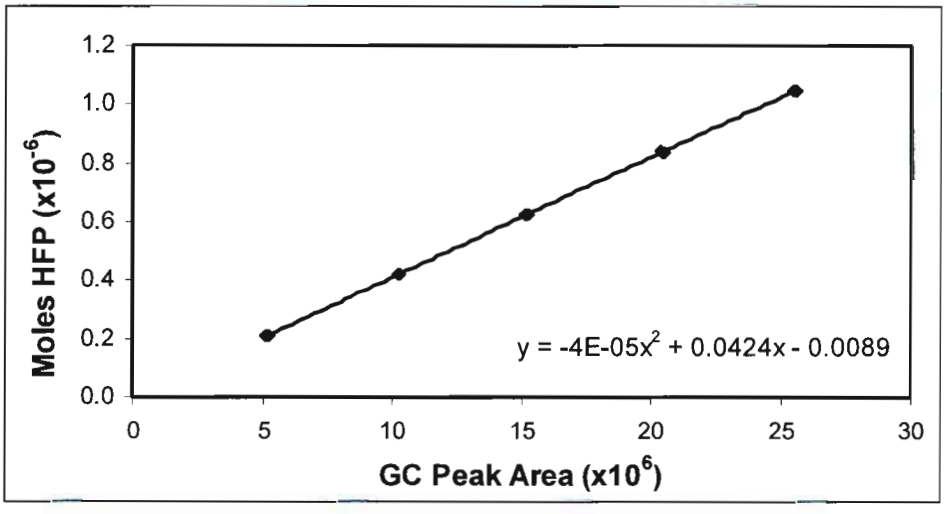

Figure 7.1. GC calibration curve for HFP for the 0 to 250 µl volume range.

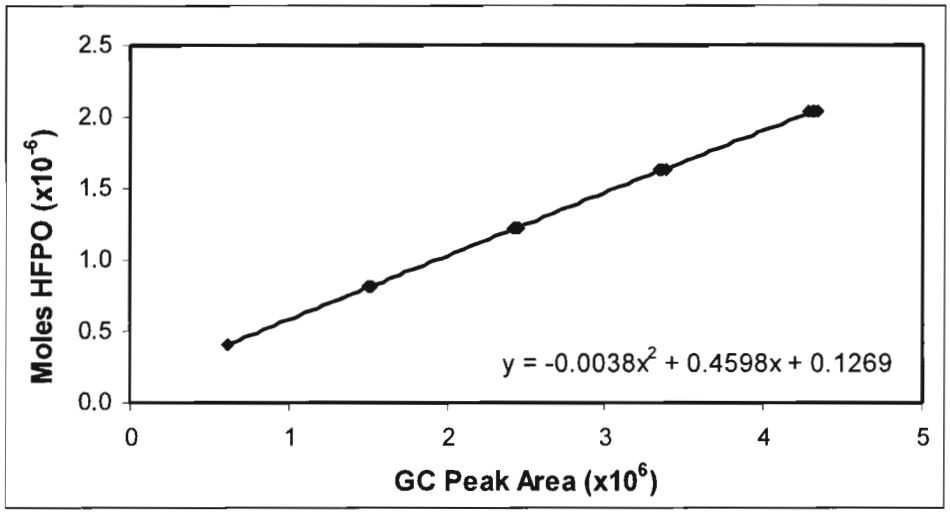

Figure 7.2. GC calibration curve for HFPO for the 0 to 50 µl volume range.

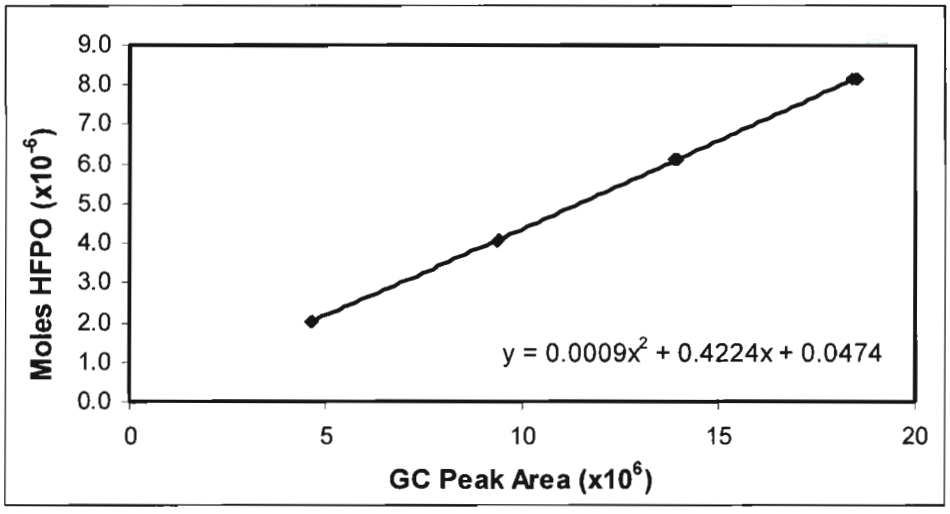

Figure 7.3. GC calibration curve for HFPO for the 0 to 250 µl volume range.

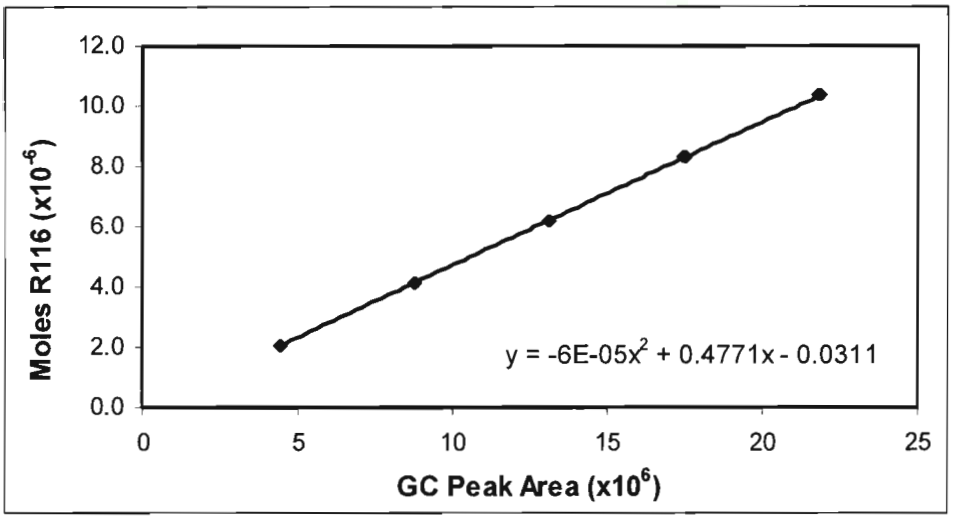

Figure 7.4. GC calibration curve for R116 for the 0 to 250 µl volume range.

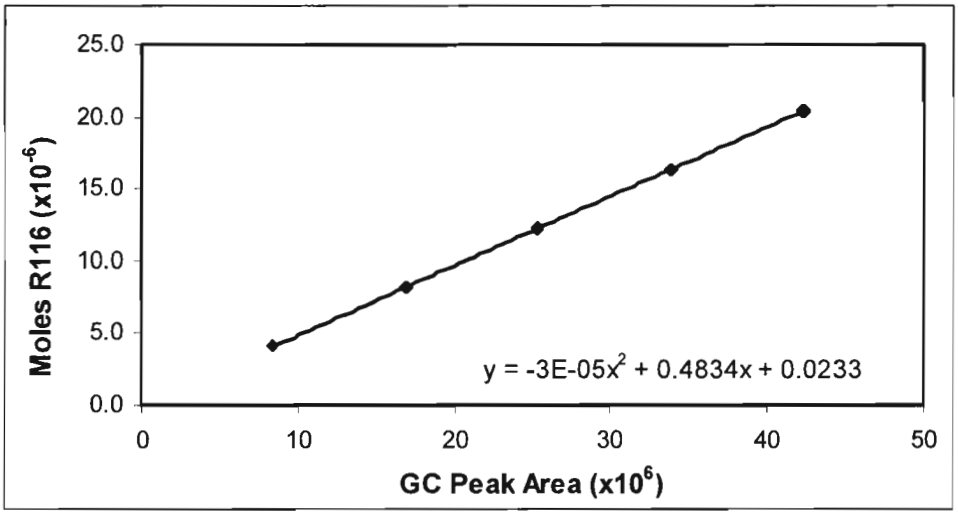

Figure 7.5. GC calibration curve for R116 for the 0 to 500 µl volume range.

7.3.3. Pure component vapour pressure measurements

Table 7.7 presents the experimentally determined pure component vapour pressure data for HFPO measured on the static analytic apparatus. Figure 7.6 is a graphical representation of this data. No published pure vapour pressure data for HFPO existed and as such no comparison could be made.

Temperature [K]	Pressure [MPa]
271.88	0.3022
295.53	0.6499
300.47	0.7456
303.11	0.7985
306.50	0.8747
310.48	0.9701
312.64	1.0249
318.16	1.1753

Table 7.7. Measured pure component vapour pressure data for HFPO.

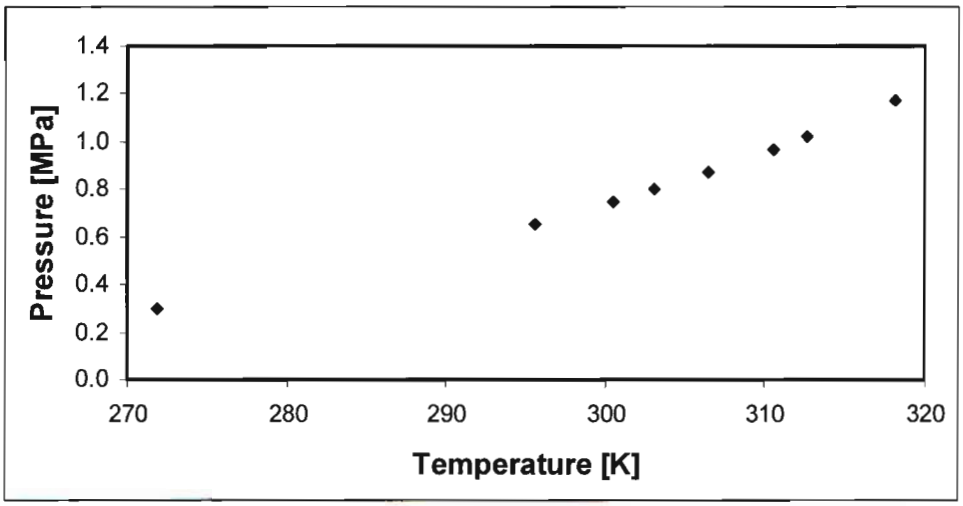

Figure 7.6. Measured pure component vapour pressure data for HFPO.

7.3.4. Vapour-liquid equilibrium measurements

For the binary systems involving HFP, HFPO and toluene, the measurements were undertaken on the static synthetic apparatus. This involved loading the equilibrium with a mixture of known composition and recording pressure versus volumes values for a particular isotherm. This experimental method only allowed the determination of the saturated liquid (*P-x*) curve, with the saturated vapour curve (*P-y*) obtained through thermodynamic modeling of the system. The graphs of pressure versus volume were plotted and the location of the break point or discontinuity on the graph determined. The break point on the graph corresponded to the saturated bubble pressure for that particular cell loading or mole fraction. The cell was loaded at different compositions and the break point was evaluated to determine a single point on the *P-x* curve for that particular system. In this manner a complete *P-x* curve was generated. Presented in this section are the final *P-x* data that resulted from the *P-V* data measurements on the static synthetic apparatus. The recorded pressure versus volume data for each isotherm and loading of the equilibrium cell, for the binary systems HFP + toluene and HFPO + toluene at the 273.15 and 313.15 K isotherms are presented in Section B.3, Appendix B of this dissertation.

A limited amount of HFP and HFPO were available for the experimental measurements due to the expensive nature of these specialty components. Consequently, only four interior data points for the binary system HFP + toluene at 272.15 and 273.15 K were measured. For the system HFPO + toluene at 313.15 K, five interior data points were measured with four interior data points measured for this system at 273.15 K. This was due to the fact that during the measurement at 272.13 K for the mole fraction of HFPO of 0.1615, degradation of the O-ring around the cell piston occurred and the pressuring liquid octane mixed with the binary mixture which caused the results of the ongoing run to be invalidated.

For the binary systems involving the components HFP, HFPO and R116, the measurements were performed on the static analytic apparatus with equilibrium liquid and phase sampling achieved through the use of the movable pneumatic ROLSI. For each point on the *P-x* or *P-y* curve, a minimum of four samples of the equilibrated liquid or vapour phases were taken and analysed via the on-line GC. The four most representative samples were utilised to determine the average value of composition for that particular data point. Only the final *P-x-y* data for each system is presented in this section, along with the standard deviation for each data point. The complete data which includes the four vapour or liquid sample compositions for each data point, along with the standard deviation of the four measurements and the average value of the vapour or liquid composition is presented in Section B.4, Appendix B.

No literature data exists for any of the binary systems presented in this section and as such no comparison between literature data and experimental data was possible.

7.3.4.1. HFP + Toluene: 273.15 K isotherm

Pressure [MPa]	Liquid Composition
0.087	0.0854
0.166	0.2050
0.190	0.3909
0.186	0.7040

Table 7.8. Measured P-x data for the system HFP + Toluene at 273.15 K.

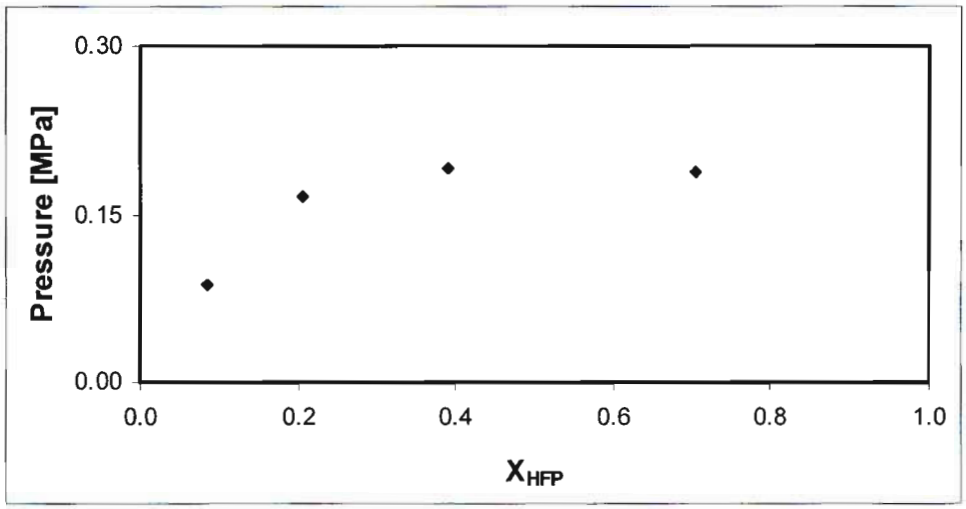

Figure 7.7. Measured P-x data for the system HFP + Toluene at 273.15 K.

7.3.4.2. HFP + Toluene: 313.15 K isotherm

Pressure [MPa]	Liquid Composition
0.349	0.0854
0.622	0.205
0.747	0.3909
0.790	0.704

Table 7.9. Measured P-x data for the system HFP + Toluene at 313.15 K.

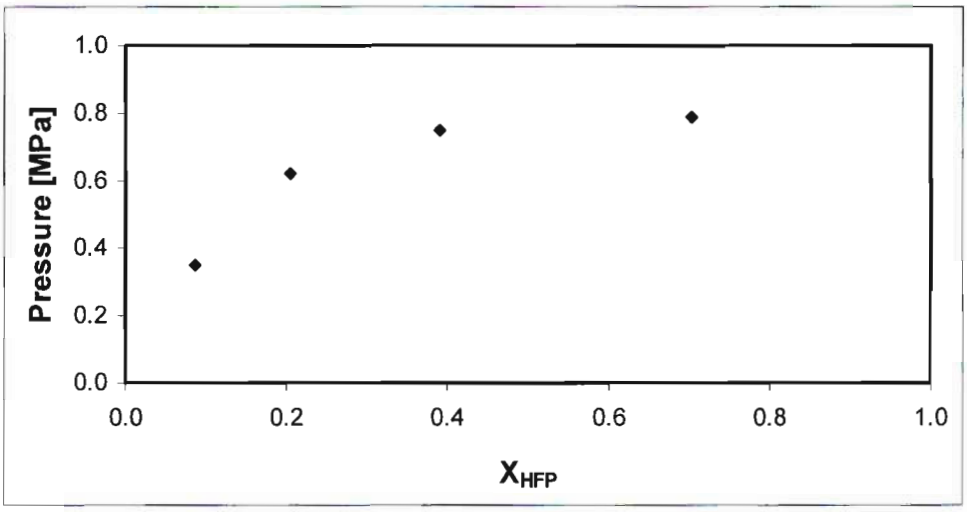

Figure 7.8. Measured P-x data for the system HFP + Toluene at 313.15 K.

7.3.4.3. HFPO + Toluene: 273.15 K isotherm

Pressure [MPa]	Liquid Composition
0.193	0.1765
0.197	0.2771
0.205	0.3722
0.201	0.7306

Table 7.10. Measured P-x data for the system HFPO + Toluene at 273.15 K.

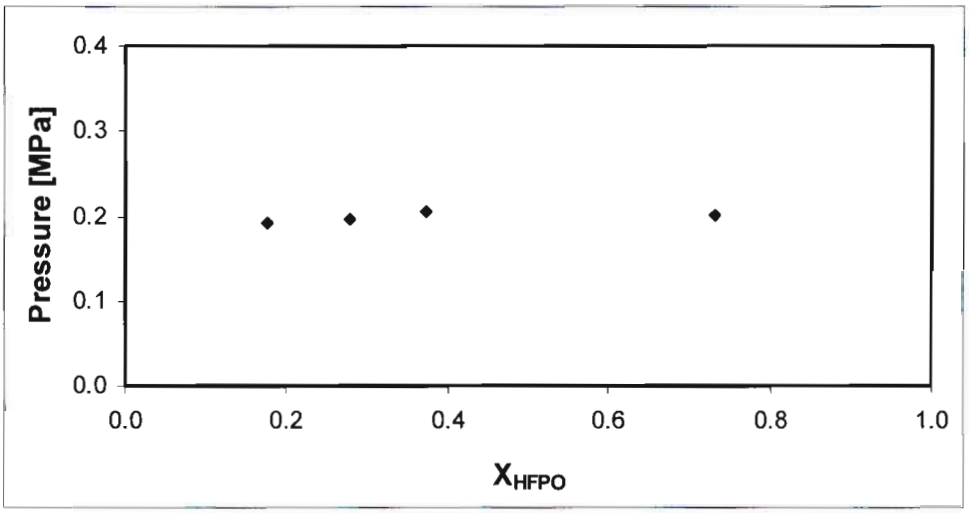

Figure 7.9. Measured P-x data for the system HFPO + Toluene at 273.15 K.

7.3.4.4. HFPO + Toluene: 313.15 K isotherm

Pressure [MPa]	Liquid Composition
0.797	0.1615
0.813	0.1765
0.816	0.2771
0.829	0.3722
0.809	0.7306

Table 7.11. Measured P-x data for the system HFPO + Toluene at 313.15 K.

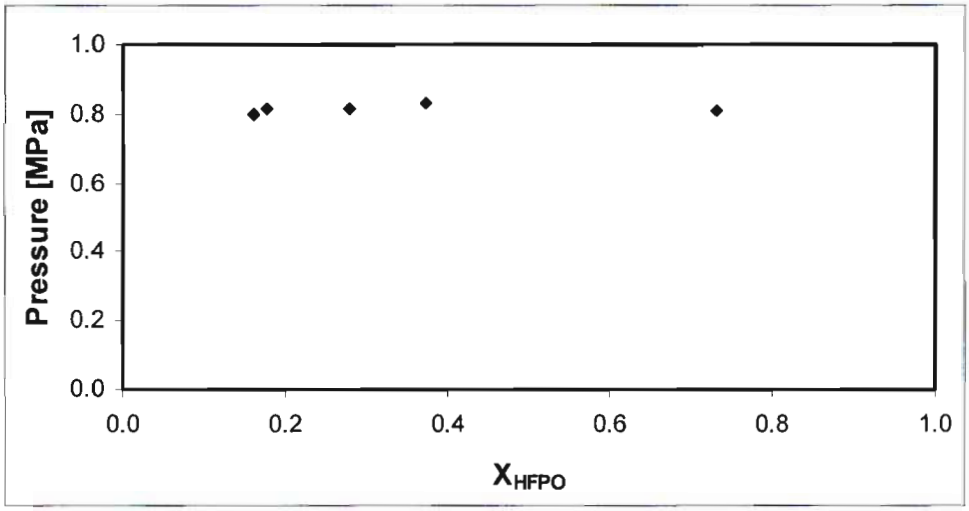

Figure 7.10. Measured P-x data for the system HFPO + Toluene at 313.15 K.

7.3.4.5. R116 + HFP: 273.15 K isotherm

The measured *P-x-y* data for the system R116 + HFP at 273.15 K are presented in Table 7.12. For a single data point, four samples each of the equilibrium vapour and liquid phases were obtained to determine measurement accuracy and reproducibility. Only the standard deviation of the measurements and the average values for liquid and vapour mole fractions are presented in Table 7.12 and Figure 7.11, with the complete data presented in Section B.4, Appendix B.

Pressure [Mpa]	Standard Deviation σX_{R116}	Liquid Composition X_{R116}	Standard Deviation σY_{R116}	Vapour Composition Y_{R116}
0.5057	0.0008	0.1154	0.0006	0.3714
0.6935	0.0029	0.2463	0.0012	0.5790
1.0133	0.0030	0.4612	0.0010	0.7564
1.1863	0.0010	0.5884	0.0003	0.8243
1.4180	0.0004	0.7457	0.0011	0.8939
1.5402	0.0003	0.8218	0.0007	0.9253

Table 7.12. Measured P-x-y data for the system R116 + HFP at 273.15 K.

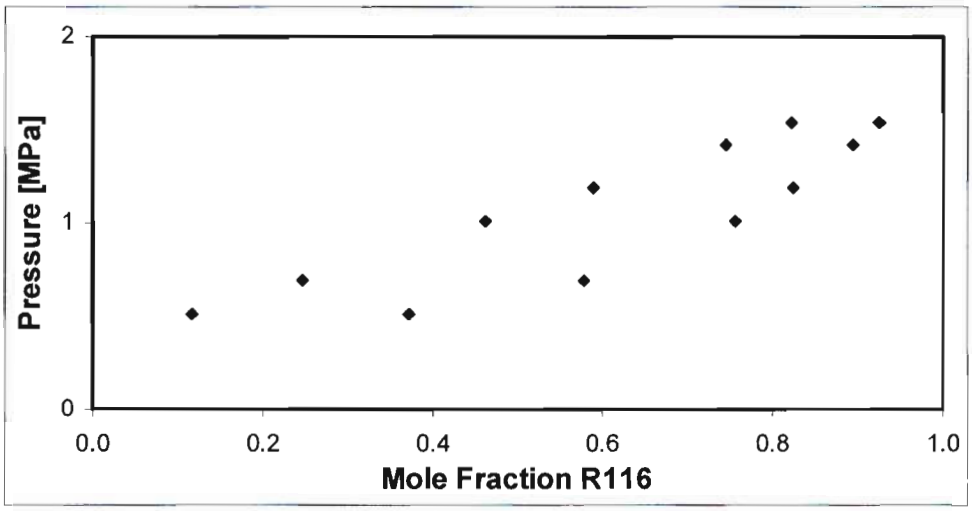

Figure 7.11. Measured P-x-y data for the system R116 + HFP at 273.15 K.

7.3.4.6. R116 + HFP: 313.15 K isotherm

Pressure [Mpa]	Standard Deviation σX_{R116}	Liquid Composition X_{R116}	Standard Deviation σY_{R116}	Vapour Composition Y_{R116}
1.6760	0.0003	0.1454	0.0253	0.2537
2.0493	0.0006	0.2652	0.0020	0.4262
2.6021	0.0003	0.4367	0.0016	0.5667
2.9621	0.0002	0.5425	0.0005	0.6490
3.2983	0.0003	0.6437	0.0003	0.6864

Table 7.13. Measured P-x-y data for the system R116 + HFP at 313.15 K.

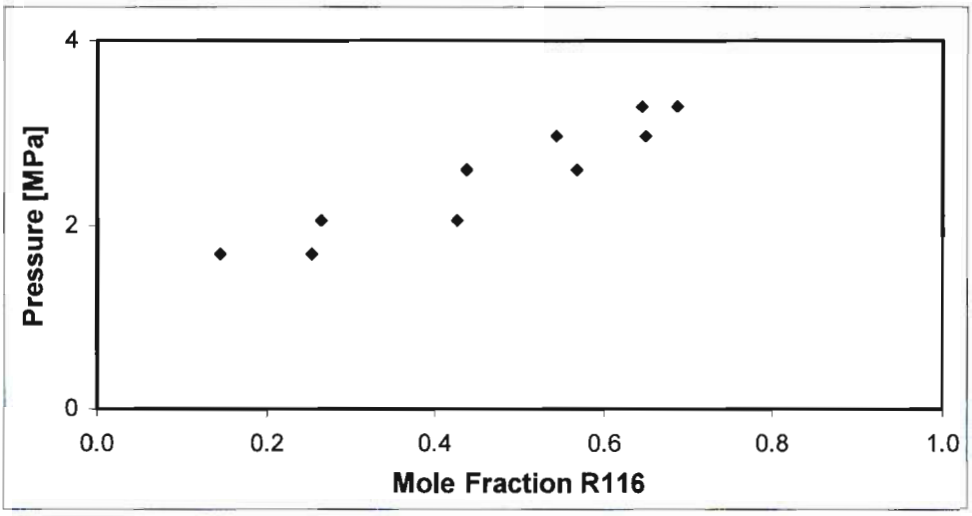

Figure 7.12. Measured P-x-y data for the system R116 + HFP at 313.15 K.

7.3.4.7. R116 + HFPO: 273.15 K isotherm

Pressure [Mpa]	Standard Deviation σX_{R116}	Liquid Composition X_{R116}	Standard Deviation σY_{R116}	Vapour Composition Y_{R116}
0.5314	0.0020	0.1562	0.0042	0.4516
0.7725	0.0020	0.3267	0.0004	0.6600
1.0371	0.0015	0.5111	0.0003	0.7878
1.1772	0.0005	0.6036	0.0010	0.8365
1.4015	0.0011	0.7422	0.0006	0.8987
1.6293	0.0009	0.8768	0.0012	0.9526

Table 7.14. Measured P-x-y data for the system R116 + HFPO at 273.15 K.

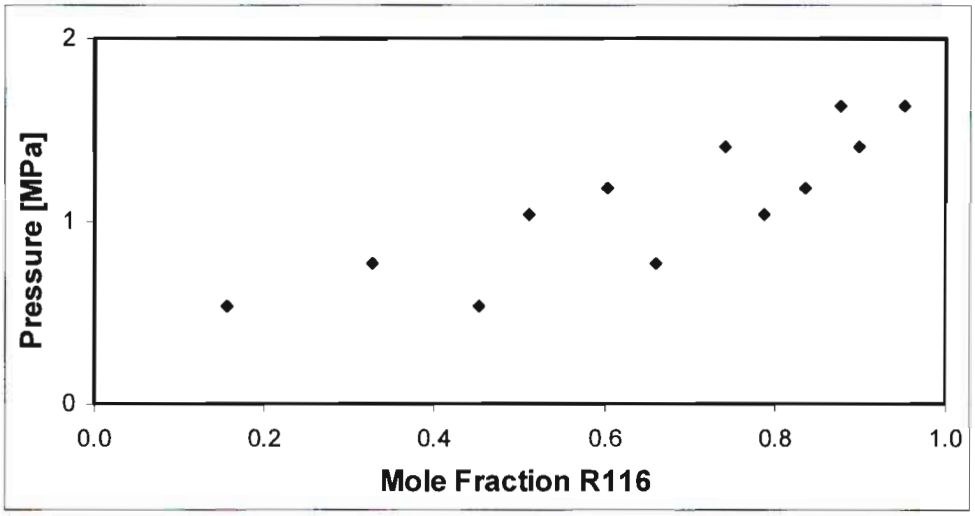

Figure 7.13. Measured P-x-y data for the system R116 + HFPO at 273.15 K.

7.3.4.8. R116 + HFPO: 313.15 K isotherm

The measured *P-x-y* data for the system R116 + HFPO at 273.15 K are presented in Table 7.15. The system reached the supercritical state for pressures greater than 3.3 MPa. Sampling of the equilibrium vapour phase for the equilibrium pressure of 3.3986 MPa was not possible as the system had reached the supercritical state and only a single liquid phase was present.

Pressure [Mpa]	Standard Deviation σX_{R116}	Liquid Composition X_{R116}	Standard Deviation σY_{R116}	Vapour Composition Y_{R116}
1.6560	0.0005	0.1654	0.0036	0.2421
1.9984	0.0001	0.2690	0.0005	0.4452
2.5419	0.0011	0.4312	0.0006	0.5859
3.0224	0.0001	0.5696	0.0003	0.6580
3.3986	0.0006	0.6645	-	-

Table 7.15. Measured P-x-y data for the system R116 + HFPO at 313.15 K.

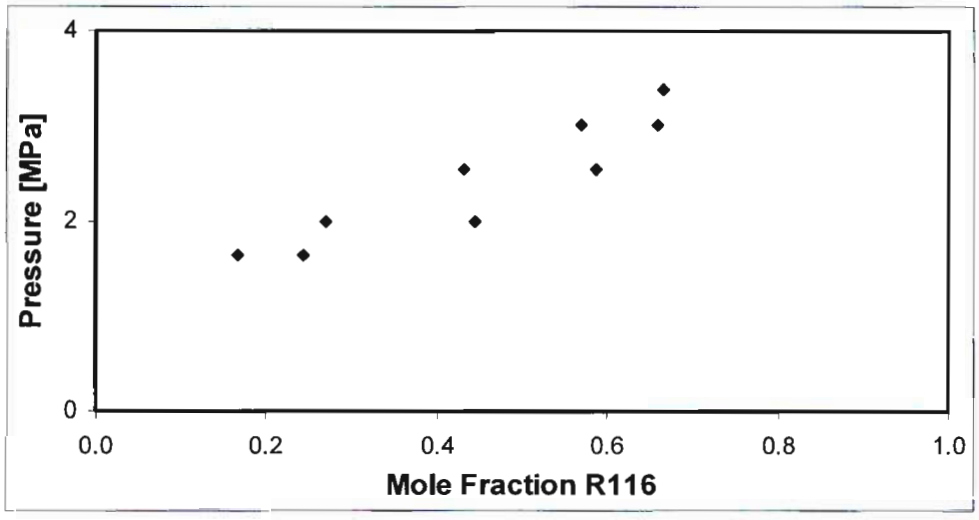

Figure 7.14. Measured P-x-y data for the system R116 + HFPO at 313.15 K.

7.4. THERMODYNAMIC MODELLING AND DATA REGRESSION

Due to the costly and demanding nature of HPVLE measurements, it is essential that experimental data be properly modeled and interpreted. The methods and procedures adopted in this project for the interpretation and modeling of the experimentally determined HPVLE binary systems are discussed in Chapter five. In this section the results of the regression and modeling are presented and discussed.

The modelling of the measured HPVLE data for the systems HFP + toluene, HFPO + toluene, R116 + HFP, R116 + HFPO, and for the HFPO pure component vapour pressures, were performed on the computer software Thermopack ((Coquelet and Baba-Ahmed 2002)). The software Thermopack was utilised as it was specifically coded for the regression and modeling of HPVLE data involving refrigerant systems. Use was made of the direct method for the data regression and modeling, with three model sets, which featured two EOS models, two mixing rules and a single activity coefficient model. For the regression of the pure component vapour pressure data for HFPO two equation of state (EOS) models were utilised. A summary of the thermodynamic models and combinations used for this project is presented in Table 5.1.

As reported by (Ramjugernath 2000) and (Muhlbauer and Raal 1995), the direct method of data reduction is preferred by a vast majority for HPVLE data. The direct method utilises a single EOS to describe both the vapour and liquid phases. Cubic EOS were used in this project as a result of their simplicity, accuracy and ease of use, with the roots of a cubic EOS easily determined when compared to higher order EOS. The systems involved in this project were highly non-ideal systems involving fluorinated hydrocarbons. The EOS models utilised in this project were the Peng-Robinson ((Peng and Robinson 1976)) and Soave-Redlich-Kwong EOS ((Soave 1972)).

The use of the Mathias-Copeman (MC) alpha function was employed for both the EOS. The MC alpha function enabled a more accurate prediction of the vapour pressures of highly polar substances, and this was important as according to (Mathias and Copeman 1983) inaccurate pure component vapour pressure representation could artificially distort the excess Helmholtz free energy and interfere with the analysis of mixture effects. To extend the use of the EOS to mixtures, the MHV1 (Modified-Huron-Vidal first order) and the WS (Wong-Sandler) mixing rules were utilised.

In collaboration with the mixing rules, the activity coefficient model utilised was the NRTL ((Renon and Prausnitz 1968)) activity coefficient model. The theory behind the EOS model, mixing rules and activity coefficient model is presented in Chapter five along with a summary of the model sets and relevant equations utilised for the thermodynamic data regression and modelling.

The data regression involved fitting parameters for each of the models, with the parameters determined by least squares regression of the experimental data. The objective function utilised for the regression of the HPVLE data for the systems involving R116, HFP and HFPO is given by equation (5-48). The objective function utilised for the systems involving toluene, HFP and HFPO is given by equation (5-49). Depending on the EOS and mixing rules used, one to three parameters were fitted for the model sets. In the NRTL Gibbs excess free energy model, two adjustable parameters were utilised, $\tau_{1,2}$ and $\tau_{2,1}$ with the third parameter ($\alpha_{1,2}$) set equal to 0.3 for all the computations. For the model set utilising the PR EOS and the WS mixing rules, three parameters in total were fitted viz. $k_{1,2}$ (the mixing rule interaction parameter) and $\tau_{1,2}$ and $\tau_{2,1}$ the NRTL model parameters. For the PR EOS and the MHV1 mixing rules, only two parameters were fitted i.e. $\tau_{1,2}$ and $\tau_{2,1}$. For the model set utilising the SRK EOS and WS mixing rules, three parameters were fitted viz. $k_{1,2}$ and $\tau_{1,2}$ and $\tau_{2,1}$. It must be borne in mind that only two isotherms were measured for each binary system, it was thus not possible to effectively compare the temperature dependency of the binary interaction parameters for each of the three model combinations, as with only two data points a linear relationship results. As such, discussion of the binary interaction parameters is limited.

Measurements were undertaken in the critical region for the systems R116 + HFP and R116 + HFPO. The critical regions for these systems were calculated via Thermopack utilising the method of (Stockfleth and Dohrn 1998). The calculations for the critical lines were performed with the assistance of C. Coquelet of Ecoles des Mines de Paris, the programmer of the Thermopack computer software. Due to time constraints and lack of sufficient quantities of HFP and HFPO, the HPVLE data for the binary system HFP + HFPO were predicted in Thermopack utilising the PSRK UNIFAC method ((Holderbaum and Gmehling 1991)).

To quantify the fit of a particular model to the experimental data, the absolute average error (AAE) in terms of pressure, vapour or liquid composition were computed according to equation (5-50). Additionally, the BIAS of the measurements, given by equation (5-51) was also calculated.

Once the fitted parameters were obtained, each system was modelled in Thermopack to determine the entire *P-x-y* diagram. The experimental data measured for this project was then compared to the correlated data using the direct method with the appropriate EOS and mixing rules.

The results of the data regression i.e. the fitted parameters, along with the calculated AAE and BIAS values are presented in the following sections. The entire *P-x-y* diagram for each system predicted by the various model sets is also presented.

7.4.1. Pure component vapour pressure measurements

The measured pure component vapour pressure data for HFPO were fitted to the PR and SRK EOS utilising the Mathias-Copeman alpha function. The experimental vapour pressure data and the data predicted by the PR EOS and the SRK EOS are presented numerically in Table 7.16. This data is also presented graphically in Figure 7.15. The deviation (ΔP) between the calculated pressure (P_{calc}) and the experimental pressure (P_{exp}) are presented in Table 7.16. Table 7.17 presents the fitted Mathias-Copeman parameters, MC1, MC2 and MC3 for the two EOS.

P_{exp} [MPa]	T_{exp} [K]	P_{calc}: PR [MPa]	ΔP: PR [MPa]	P_{calc}: SRK [MPa]	ΔP: SRK [MPa]
0.3022	271.87	0.3023	0.0001	0.3023	0.0001
0.6499	295.53	0.6480	-0.0019	0.6481	-0.0019
0.7456	300.47	0.7458	0.0001	0.7458	0.0002
0.7985	303.10	0.8004	0.0019	0.8004	0.0019
0.8747	306.50	0.8760	0.0012	0.8759	0.0012
0.9701	310.48	0.9710	0.0009	0.9710	0.0009
1.0249	312.63	1.0237	-0.0012	1.0237	-0.0012
1.1753	318.15	1.1740	-0.0013	1.1739	-0.0014

Table 7.16. Results for the modeling of the HFPO pure component vapour pressure data.

EOS	MC1	MC2	MC3
PR	0.825	0.292	-2.757
SRK	0.928	-1.638	9.585

Table 7.17. Fitted Mathias-Copeman parameters for the PR and SRK EOS.

From Table 7.16 and Figure 7.15, both the PR and SRK EOS fit the experimental data well. According to the ΔP values, which represents the difference between the calculated and experimental values, there is little discrepancy between experimental and modelled data.

Overall, the PR EOS with the MC alpha function correlates the experimental pure component vapour pressure data better than the SRK EOS with lower ΔP values for the 300.47 and 318.15 K data points.

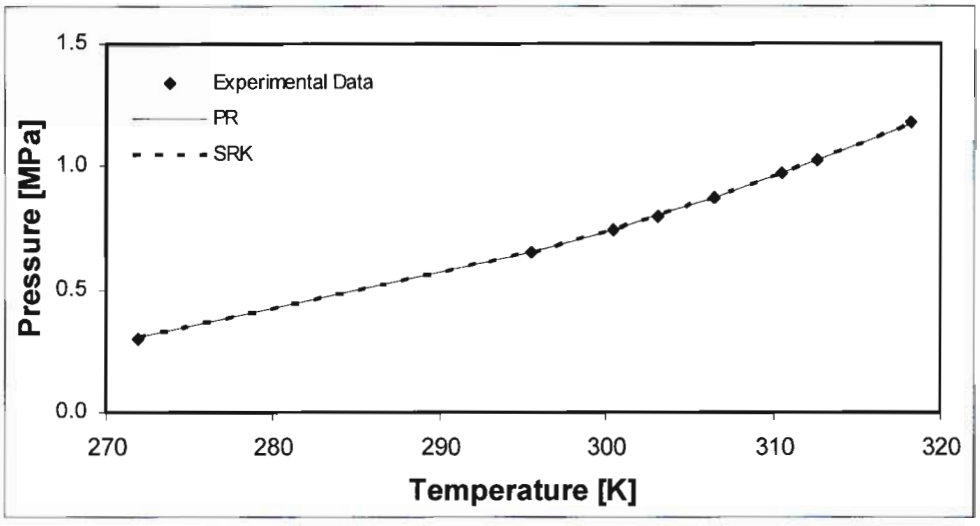

Figure 7.15. Results for the modelling of the HFPO pure component vapour pressure data.

7.4.2. HFP + HFPO

Data for the binary system HFP + HFPO were not determined experimentally. The VLE data for this binary system was predicted utilising the regressed MC/SRK parameters in conjunction with the SRK EOS and PSRK UNIFAC model. For the group assignment for HFP and HFPO in the PSRK UNIFAC model, subgroups 70, 74, 75, 76 and 141 were utilised. The predicted data for the 273.15 K isotherm is presented graphically in Figure 7.16. The predicted data for the 313.15 K isotherm is presented graphically in Figure 7.17. The predicted data was fitted to the three model combinations used for this research project, the PR-WS, PR-MHV1 and SRK-WS model sets, all utilising the MC alpha function and NRTL activity coefficient model. The parameters determined by the fitting of the predicted data are presented in Table 7.18.

Model	T [K]	$k_{1,2}$	$\tau_{1,2}$ [J•mol^{-1}]	$\tau_{2,1}$ [J•mol^{-1}]
PR-WS	273.15	0.0912	-1163.70	1035.60
	313.15	0.0877	-1225.30	1056.20
PR-MHV1	273.15	-	669.71	-398.09
	313.15	-	736.95	-431.22
SRK-WS	273.15	-1.2434	6440.30	3787.20
	313.15	-1.0037	6632.60	4080.70

Table 7.18. Fitted parameters for the system HFP + HFPO at 273.15 and 313.15 K.

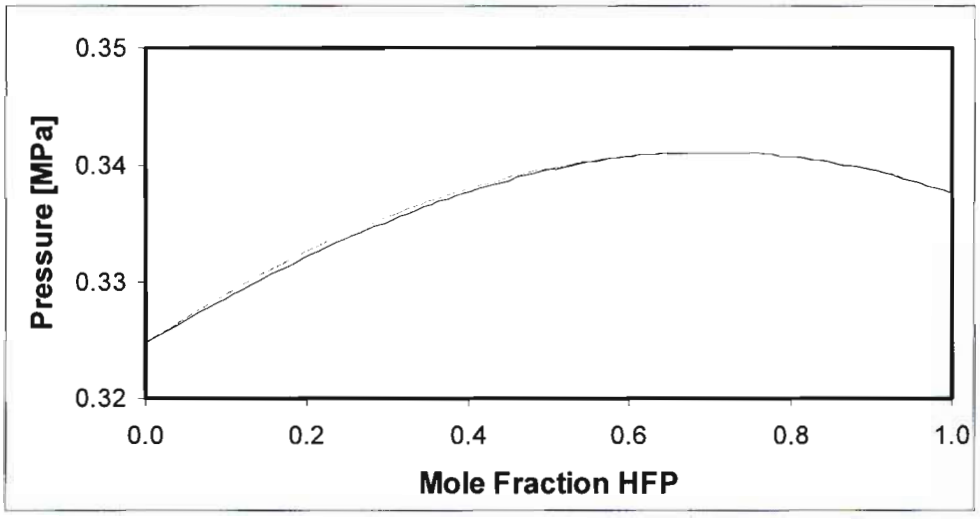

Figure 7.16. Results for the binary system HFP + HFPO at 273.15 K predicted via the SRK EOS and PSRK UNIFAC method.

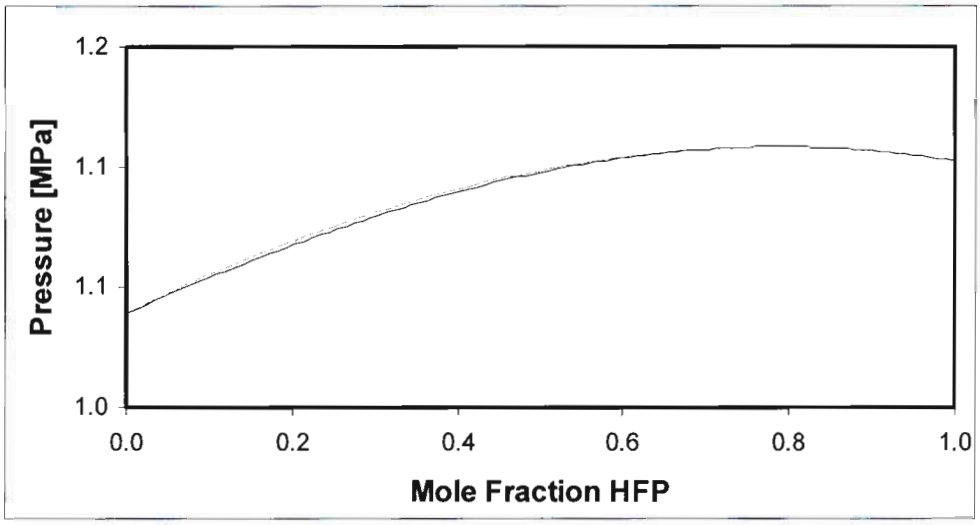

Figure 7.17. Results for the binary system HFP + HFPO at 313.15 K predicted via the SRK EOS and PSRK UNIFAC method.

7.4.3. HFP + Toluene

Table 7.19 summarises the fitted interaction parameters viz. $k_{1,2}$, $\tau_{1,2}$ and $\tau_{2,1}$, for the PR-WS, PR-MHV1 and SRK-WS models for the binary system HFP + toluene. Table 7.20 summarises the absolute average errors and BIAS values for the system pressure for the three model sets. Figures 7.18 and 7.19 provide a graphical comparison between the experimental data and data predicted by the three thermodynamic model sets utilised.

Model	T [K]	$k_{1,2}$	$\tau_{1,2}$ [J•mol^{-1}]	$\tau_{2,1}$ [J•mol^{-1}]
PR-WS	273.15	-0.7720	5850.00	4150.00
	313.15	-0.2561	7224.00	2961.10
PR-MHV1	273.15	-	-836.97	4456.30
	313.15	-	1228.80	3224.80
SRK-WS	273.15	-0.7627	5948.80	4081.80
	313.15	-0.2510	7444.20	2896.10

Table 7.19. Fitted parameters for the system HFP + Toluene at 273.15 and 313.15 K.

The NRTL binary interaction parameters for the PR-WS model, $\tau_{1,2}$ and $\tau_{2,1}$, both decrease as the temperature increases. For an increase in temperature for the PR-MHV1 model, the $\tau_{1,2}$ parameter increases while the while the $\tau_{2,1}$ parameter decreases. Similarly for the SRK-WS model, the $\tau_{1,2}$ parameter increases while the while the $\tau_{2,1}$ parameter decreases. The $\tau_{1,2}$ parameter at 273.15 K for the PR-MHV1 model represents the only negative interaction parameter for this system.

	273.15 K		313.15 K	
Model	AAE-P [%]	BIAS-P [%]	AAE-P [%]	BIAS-P [%]
PR-WS	5.06	0.49	0.90	0.17
PR-MHV1	6.67	3.03	3.08	1.27
SRK-WS	5.13	0.51	1.06	0.21

Table 7.20. Absolute average errors and BIAS values for the system HFP + Toluene at 273.15 and 313.15 K.

From Table 7.20 it was found that at the 273.15 K isotherm the PR-MHV1 set modelled the system the worst, with the highest absolute average error value for pressure of 6.67 % and high BIAS value of 3.03 % which indicated that the PR-MHV1 model systematically overestimated the vapour pressures for the system. This was clearly evident for the data point corresponding to a mole fraction of 0.704 HFP where the PR-MHV1 model set failed to accurately represent the data point. In general, all three model

combinations failed to accurately represent the data point at 0.7040 HFP at 273.15 K. The PR-WS and SRK-WS model sets both modelled the system similarly at 273.15 K, with the PR-WS model performing the best with the lowest AAE-P of 5.06 % and lowest BIAS value of 0.49 %. The relatively low BIAS value for the pressure of 0.49 % indicated that the PR-WS model set only slightly overestimated the experimental data.

At the 313.15 K isotherm, the observations are the same. The PR-MHV1 model produced the highest AAE-P value of 3.08 % and thus performed the worst. At a mole fraction of 0.7040 HFP the PR-MHV1 model set once again failed to accurately represent the data point, while the PR-WS and SRK-WS model sets correlated the data adequately at this composition. The degree to which the PR-MHV1 model set failed to represent the experimental data at high concentrations of HFP for both the 273.15 and 313.15 K isotherm indicated the possibility of a problem with the MHV1 mixing rules. Additionally, the $\tau_{1,2}$ parameter at 273.15 K for the PR-MHV1 model represented the only negative interaction parameter obtained for the system HFP + toluene. The SRK-WS model was the second best performing model set, with the PR-WS model producing the lowest AAE-P and BIAS values of 0.90 % and 0.17 % respectively.

From the analysis of the data, the three model combinations correlate the experimental data adequately. In general the modelling of the system at the 313.15 K isotherm produced better results than at the lower isotherm of 273.15 K. Figure 7.18 and 7.19 presents the graphical correlation between the modelled data and the experimental data. It must be borne in mind that the for the binary systems HFP + toluene at 273.15 and 313.15 K, the data was measured on the static synthetic apparatus which only allowed the determination of *P-x* data for the system. The corresponding P-y data and hence a full range of P-x-y data was determined through the modelling of the systems via a bubble pressure calculation in Thermopack utilising the direct method.

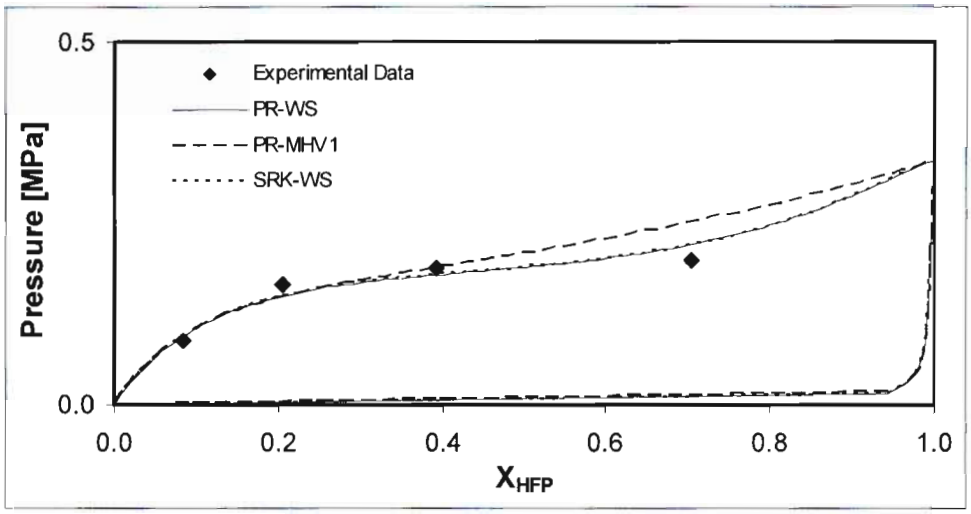

Figure 7.18. Comparison between the predicted and experimental data for the system HFP + Toluene at 273.15 K.

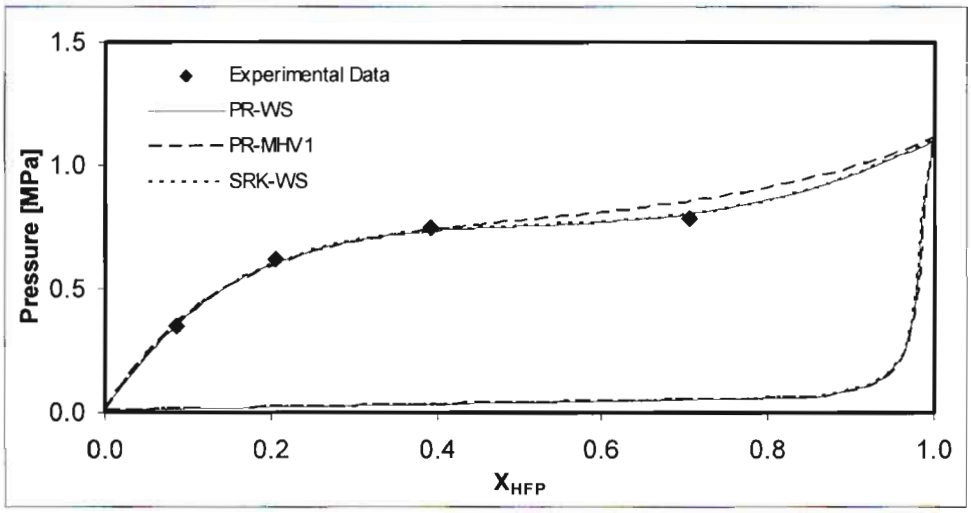

Figure 7.19. Comparison between the predicted and experimental data for the system HFP + Toluene at 313.15 K.

7.4.4. HFPO + Toluene

Table 7.21 summarises the fitted interaction parameters viz. $k_{1,2}$, $\tau_{1,2}$ and $\tau_{2,1}$, for the PR-WS, PR-MHV1 and SRK-WS models for the binary system HFPO + toluene. Table 7.22 summarises the absolute average errors and BIAS values for the system pressure for the three model sets. Figures 7.20 and 7.21 provide a graphical comparison between the experimental data and data predicted by the three thermodynamic model sets utilised.

Model	T [K]	$k_{1,2}$	$\tau_{1,2}$ [J•mol^{-1}]	$\tau_{2,1}$ [J•mol^{-1}]
PR-WS	273.15	-0.5087	5299.60	5924.00
	313.15	0.0644	3656.50	5013.30
PR-MHV1	273.15	-	133.39	6136.50
	313.15	-	2068.60	5194.70
SRK-WS	273.15	-0.3873	5411.60	5579.00
	313.15	0.0750	4505.50	4992.30

Table 7.21. Fitted parameters for the system HFPO + Toluene at 273.15 and 313.15 K.

The NRTL binary interaction parameters for the PR-WS model, $\tau_{1,2}$ and $\tau_{2,1}$, both decrease as the temperature increases. For an increase in temperature for the PR-MHV1 model, the $\tau_{1,2}$ parameter increases while the $\tau_{2,1}$ parameter decreases. The behaviour of the interaction parameters for the PR-WS and PR-MHV1 models mirrors the behaviour of the interaction parameters for the system HFP + toluene. For the SRK-WS model, both the $\tau_{1,2}$ and $\tau_{2,1}$ parameters decrease as the temperature increases, which is in contrast to the behaviour of this model set for the system HFP + toluene.

	273.15 K		313.15 K	
Model	AAE-P [%]	BIAS-P [%]	AAE-P [%]	BIAS-P [%]
PR-WS	1.01	0.54	0.70	0.01
PR-MHV1	3.39	0.84	0.72	0.01
SRK-WS	5.07	-1.64	2.92	1.18

Table 7.22. Absolute average errors and BIAS values for the system HFPO + Toluene at 273.15 and 313.15 K.

The SRK-WS and PR-MHV1 model sets did not model the system HFPO + toluene accurately at 273.15 K. From Table 7.22, at the 273.15 K isotherm, the SRK-WS set modelled the system the worst with the highest absolute average error value for pressure of 5.07 % and high BIAS value of -1.64 %. This was followed by the PR-MHV1 model which produced a relatively high AAE value of 3.39 % and a BIAS

value of 0.84 % for the system pressure. From Figure 7.20, the SRK-WS model systematically under-estimates the vapour pressure for the system throughout the entire HFPO composition range, this was also evident by the negative BIAS value of -1.64 %. The PR-MHV1 model set over estimated the vapour pressures for the system yet it provided a slightly better fit of the data than the SRK-WS model set. The PR-WS model performed the best for this isotherm with the lowest AAE-P of 1.01 % and lowest BIAS value of 0.54 %.

At the 313.15 K isotherm, presented graphically in Figure 7.21, the observations are the same. The SRK-WS model produced the highest AAE-P value of 2.92 % and thus performed the worst. The PR-MHV1 model was the second best performing model set, with the PR-WS model producing the lowest AAE-P and BIAS values of 0.70 % and 0.01 % respectively. A possible reason for the SRK-WS model set performing the worst in this system was the addition of the oxygen molecule in the component HFPO. The oxygen atom would act to increase the polarity of the system and thus the non-ideality of the system. The PR EOS was initially developed to handle the weaknesses of the SRK EOS which included the unsatisfactory handling of polar fluids, as a result, the model sets featuring the PR EOS performed better for this system that the SRK model set. In general the modelling of this system produced better results for the 313.15 K isotherm than at the lower temperature of 273.15 K. The only model set which adequately modeled the experimental data at 273.15 K was the PR-WS model, which also provided excellent correlation of the experimental data at the 313.15 K isotherm. This was also true for the modelling of the binary system HFP + toluene, where the thermodynamic models provided a better fit for the data at the higher isotherm of 313.15 K, with the PR-WS model set performing the best.

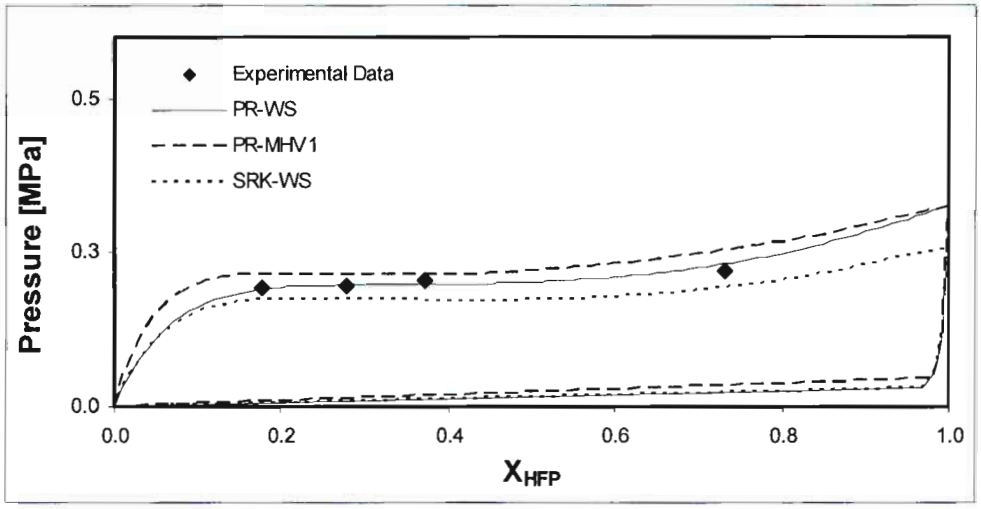

Figure 7.20. Comparison between the predicted and experimental data for the system HFPO + Toluene at 273.15 K.

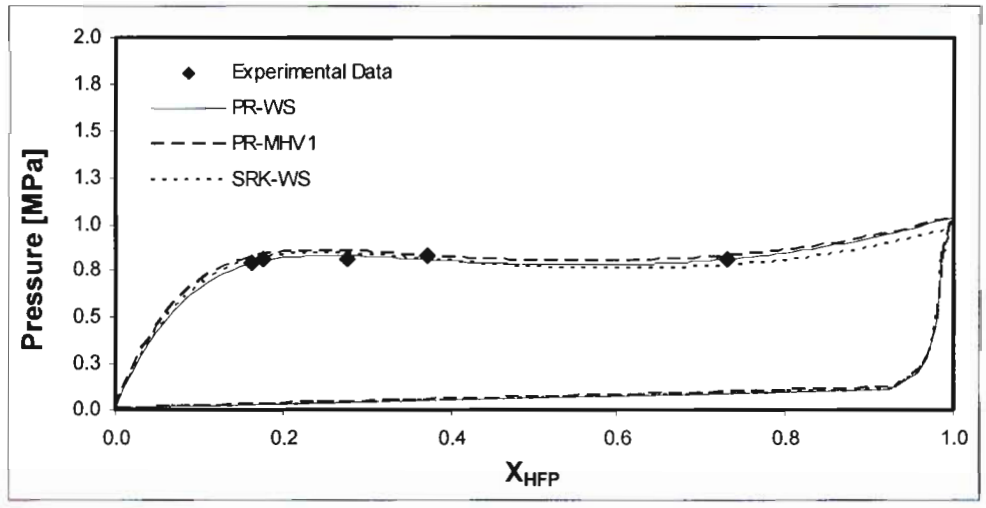

Figure 7.21. Comparison between the predicted and experimental data for the system HFPO + Toluene at 313.15 K.

7.4.5. R116 + HFP

Table 7.23 summarises the fitted interaction parameters viz. $k_{1,2}$, $\tau_{1,2}$ and $\tau_{2,1}$, for the PR-WS, PR-MHV1 and SRK-WS models for the binary system R116 + HFP. Table 7.24 summarises the absolute average errors and BIAS values for vapour and liquid compositions. Figures 7.22 and 7.23 provide a graphical comparison between the experimental data and data predicted by the three thermodynamic model sets utilised for the different temperatures of the measurements, 273.15 and 313.15 K respectively.

Model	T [K]	$k_{1,2}$	$\tau_{1,2}$ [J•mol^{-1}]	$\tau_{2,1}$ [J•mol^{-1}]
PR-WS	273.15	-0.0027	1451.90	-548.42
	313.15	0.1444	-2295.30	3509.20
PR-MHV1	273.15	-	-529.93	729.38
	313.15	-	2071.10	-1238.20
SRK-WS	273.15	-0.0168	2105.10	-882.39
	313.15	0.1413	306.94	-0.000723

Table 7.23. Fitted parameters for the system R116 + HFP at 273.15 and 313.15 K.

For the PR-WS model, the parameter $\tau_{1,2}$ decreases dramatically as the temperature increases, while the parameter $\tau_{2,1}$ increases with an increase in temperature. For an increase in temperature for the PR-MHV1 model, the $\tau_{1,2}$ parameter increases while the $\tau_{2,1}$ parameter decreases. For the SRK-WS model, both the NRTL parameters decrease. The value of the $\tau_{2,1}$ parameter at 313.15 K for the SRK-WS model seems odd in that differs greatly in magnitude than the 273.15 K parameter. This system was modelled multiple times with the SRK-WS model at 313.15 K, however there was no appreciable difference in the regressed NRTL parameters.

	273.15 K				313.15 K			
Model	AAE-X [%]	AAE-Y [%]	BIAS-X [%]	BIAS-Y [%]	AAE-X [%]	AAE-Y [%]	BIAS-X [%]	BIAS-Y [%]
PR-WS	1.37	0.80	0.90	-0.66	1.66	2.86	-0.24	2.67
PR-MHV1	1.05	0.77	-0.12	-0.40	2.15	3.56	-0.73	1.41
SRK-WS	1.30	0.75	0.84	-0.61	1.82	3.47	-0.27	3.27

Table 7.24. Absolute average errors and BIAS values for the system R116 + HFP at 273.15 and 313.15 K.

For the measurements undertaken at 273.15 K, the three model combinations correlated the data similarly, as indicated in Table 7.24 and Figure 7.22. For the liquid compositions at 273.15 K the PR-MHV1 model

set performed the best with the lowest AAE-X value of 1.05 % and a BIAS-X value of -0.12 % which indicated that the model under-estimated the liquid compositions. The second best performing model at 273.15 K was the SRK-WS model set which produced an AAE-X value of 1.30 %, while the PR-WS model set produced the highest AAE-X value of 1.37 %. For the vapour compositions at 273.15 K, similar behaviour was observed with the lowest AAE-Y value of 0.77 % produced by the PR-MHV1 model set, with an associated BIAS-Y value of -0.40 %. The SRK-WS model set produced the second best AAE-Y value of 0.75 % and the PR-WS model set produced the highest AAE-Y value of 0.80 %.

The system R116 + HFP reached the supercritical state for pressures greater than 3.13 MPa. From Table 7.24 for the modeling of the liquid phase, the model which performed the best was the PR-WS model which produced the lowest AAE-X value of 1.66 %. The model which performed the second best was the SRK-WS model set which produced an AAE-X value of 1.82 %. The model set which performed the worst was the PR-MHV1 model set which produced the highest AAE-X value of 2.15 %. The model set which produced the highest BIAS-X value of -0.73 % was the PR-MHV1 model, which indicated that the model consistently under-predicted the liquid compositions at the 313.15 K isotherm. In general, all three model sets produced negative values of the BIAS for the liquid composition, which is evident from Figure 7.23. For the modelling of the vapour phase, similar behaviour of the various models was observed. The best performing model set was the PR-WS model which produced the lowest AAE-Y value of 2.86 % with an associated BIAS-Y value of 2.67 %. The second best performing model was the SRK-WS model which produced an AAE-Y value of 3.47 %, while the PR-MHV1 model combination produced the highest AAE-Y value of 3.56 %. In general, the modelling of the liquid phase produced better results than the vapour phase, with lower absolute errors for all the model sets in the liquid phase than the vapour phase. For the 313.15 K isotherm, the PR-WS model set correlated the data the best. This was expected as the PR EOS and the WS mixing rules have been used successfully in literature for the modelling of supercritical systems. The model which correlated the supercritical system the worst was the PR-MHV1 model, which contained the MHV1 mixing rules which has been noted in literature to have difficulties in the modelling of supercritical components.

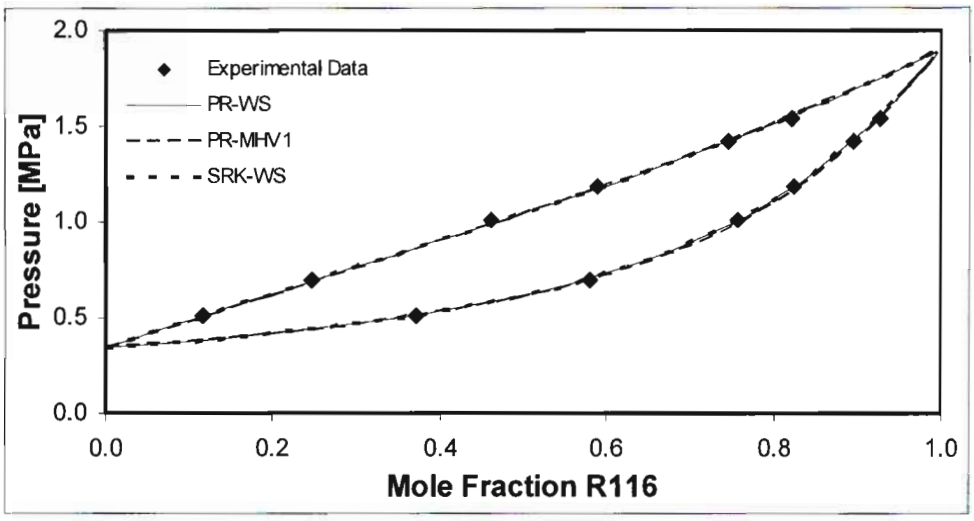

Figure 7.22. Comparison between the predicted and experimental data for the system R116 + HFP at 273.15 K.

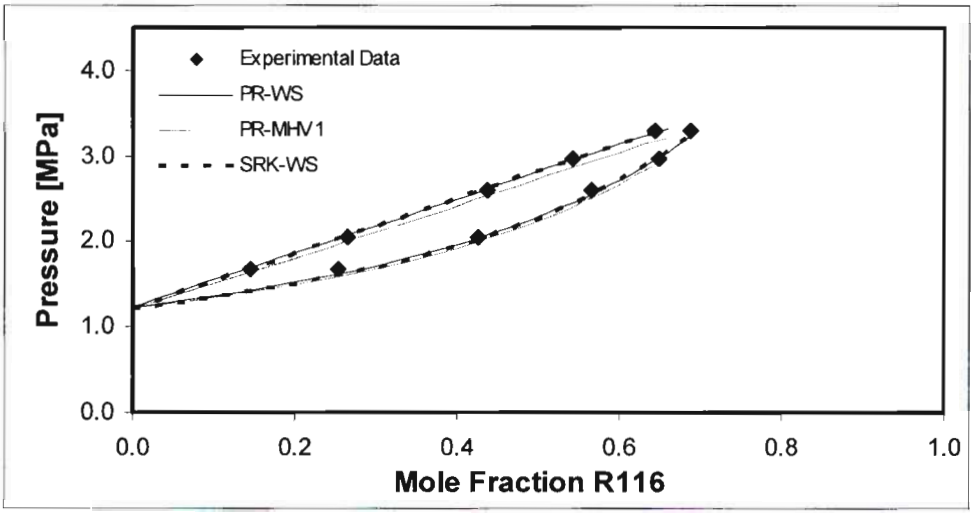

Figure 7.23. Comparison between the predicted and experimental data for the system R116 + HFP at 313.15 K.

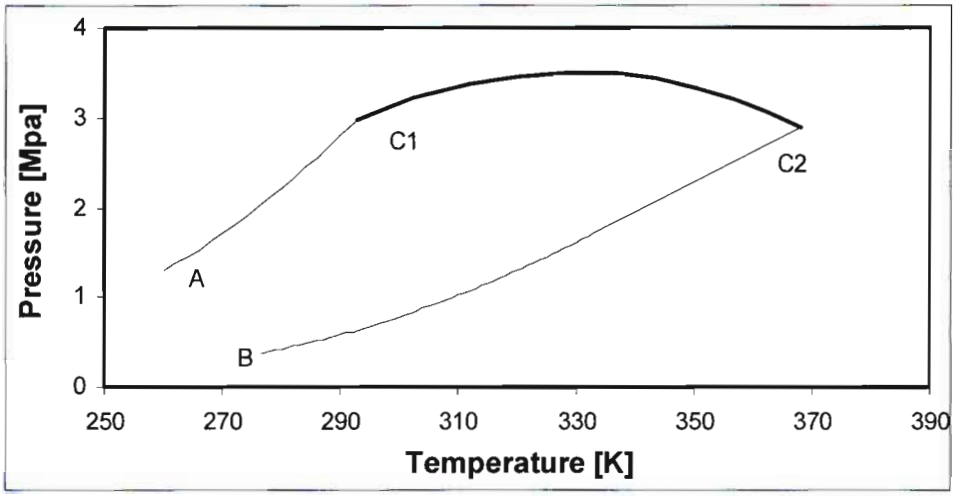

Figure 7.24. Plot of pressure versus temperature and critical pressure curve for the system R116 + HFP binary system.

Figure 7.24 is a plot of the pressure versus temperature, and features the critical pressure curve for the system R116 + HFP. Curve A-C1 represents the pure component vapour pressure curve for R116, while curve B-C2 represents the pure component vapour pressure curve for HFP. Curve C1-C2 represents the critical pressure temperature curve calculated using the PR EOS via Thermopack from the work of (Stockfleth and Dohrn 1998).

7.4.6. R116 + HFPO

Table 7.25 summarises the fitted interaction parameters viz. $k_{1,2}$, $\tau_{1,2}$ and $\tau_{2,1}$, for the PR-WS, PR-MHV1 and SRK-WS models for the binary system R116 + HFPO. Table 7.26 summarises the absolute average errors and BIAS values for vapour and liquid compositions for the binary system R116 + HFPO. Figures 7.25 and 7.26 provide a graphical comparison between the experimental data and data predicted by the three thermodynamic model sets utilised for the different temperatures of the measurements, 273.15 and 313.15 K respectively.

Model	T [K]	$k_{1,2}$	$\tau_{1,2}$ [J•mol^{-1}]	$\tau_{2,1}$ [J•mol^{-1}]
PR-WS	273.15	-0.0377	3179.60	-1721.90
	313.15	0.0677	6631.60	-3000.30
PR-MHV1	273.15	-	529.32	-551.38
	313.15	-	3712.60	-2259.80
SRK-WS	273.15	0.0509	-721.73	292.64
	313.15	0.1067	1350.80	-1289.60

Table 7.25. Fitted parameters for the system R116 + HFPO at 273.15 and 313.15 K.

For the PR-WS model, the parameter $\tau_{1,2}$ increases as the temperature increases, while the parameter $\tau_{2,1}$ decreases with an increase in temperature. The behaviour of the interaction parameters for the PR-WS model is in contrast to the behaviour for the system R116 + HFP. For an increase in temperature for the PR-MHV1 model, the $\tau_{1,2}$ parameter increases while the while the $\tau_{2,1}$ parameter decreases, which mirrors the behaviour of these model parameters for the system R116 + HFP. For the SRK-WS model, the $\tau_{1,2}$ parameters increases, while the $\tau_{2,1}$ parameter decreases.

	273.15 K				313.15 K			
Model	AAE-X [%]	AAE-Y [%]	BIAS-X [%]	BIAS-Y [%]	AAE-X [%]	AAE-Y [%]	BIAS-X [%]	BIAS-Y [%]
PR-WS	0.67	0.81	-0.12	0.64	1.33	4.08	-1.27	4.06
PR-MHV1	0.92	0.94	0.72	0.32	1.66	4.27	-1.10	4.07
SRK-WS	1.29	2.66	0.59	2.26	4.12	6.13	-3.32	4.63

Table 7.26. Absolute average errors and BIAS values for the system R116 + HFPO at 273.15 and 313.15 K.

For the measurements undertaken at 273.15 K, the three model combinations correlated the data similarly, as indicated in Table 7.26 and Figure 7.25. For the liquid compositions at 273.15 K the PR-WS model set performed the best with the lowest AAE-X value of 0.67 % and a BIAS-X value of -0.12 % which

indicated that the model under-estimated the values of x and y as evident on the graph. The second best performing model at 273.15 K was the PR-MHV1 model set which produced an AAE-X value of 0.92 %, while the SRK-WS model set produced the highest AAE-X value of 1.29 %. For the vapour compositions at 273.15 K, similar behaviour was observed with the lowest AAE-Y value of 0.81 % produced by the PR-WS model set, with an associated BIAS-Y value of 0.64 %. The PR-MHV1 model set produced the second best AAE-Y value of 0.94 % and the SRK-WS model set failed to accurately model the HFP rich vapour region and produced the highest AAE-Y value of 2.66 %. All three models produced positive values of BIAS which resulted in a systematic over-predicting of the vapour compositions particularly for the SRK-WS model in the HFP rich region.

The system R116 + HFPO reached the supercritical state for pressures greater than 3.32 MPa. The PR-WS model set provided the best description of the vapour and liquid compositions over the entire composition range. From Table 7.26 for the modeling of the liquid phase, the model which performed the best was the PR-WS model which produced the lowest AAE-X value of 1.33 %. The model which performed the second best was the SRK-WS model set which produced an AAE-X value of 1.66 %. The model set which performed the worst was the SRK-WS model set which produced the highest AAE-X value of 4.12 %. The model set which produced the lowest BIAS-X value of -1.10 % was the PR-MHV1 model. For the modelling of the vapour phase, similar performance of the various models was observed. However, the only model which accurately described the vapour phase was the PR-WS model set. The best performing model set was the PR-WS model which produced the lowest AAE-Y value of 4.08 % with an associated BIAS-Y value of 4.06 %. The second best performing model was the PR-MHV1 model which produced an AAE-Y value of 4.27%, while the SRK-WS model combination produced the highest AAE-Y value of 6.13 %. In general, the modelling of the liquid phase produced better results than the vapour phase, with lower absolute errors for all the model sets in the liquid phase then the vapour phase. The 313.15 K isotherm is presented in Figure 7.26. The PR-WS model adequately predicted the critical region, while both the PR-MHV1 and SRK-WS models over predicted the critical region.

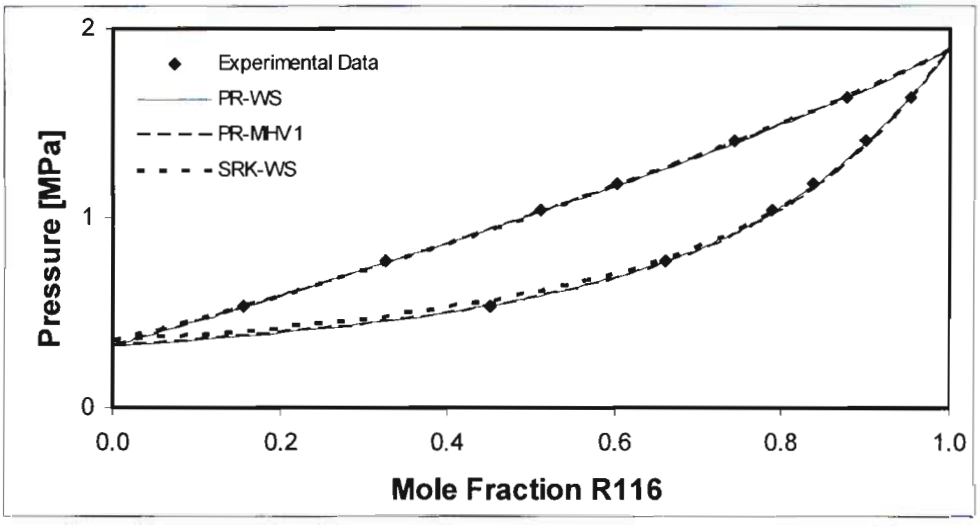

Figure 7.25. Comparison between the predicted and experimental data for the system R116 + HFPO at 273.15 K.

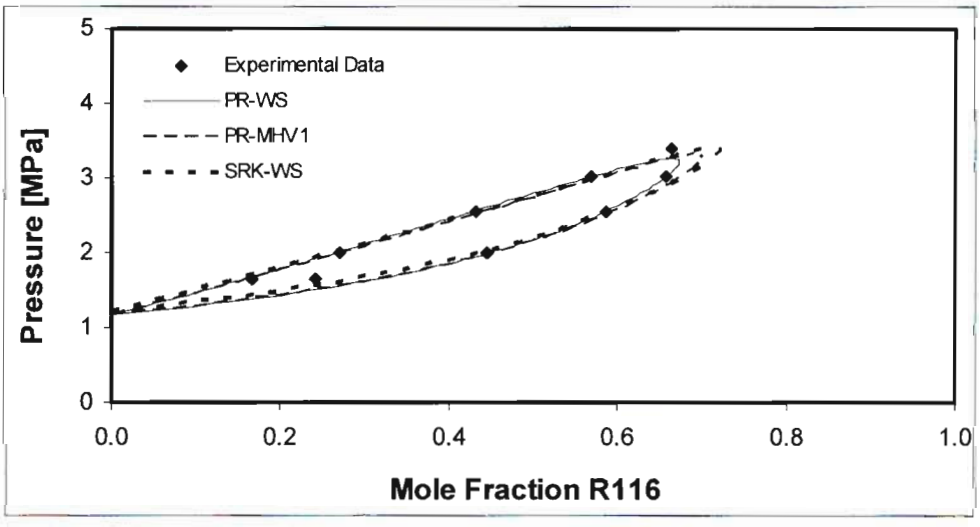

Figure 7.26. Comparison between the predicted and experimental data for the system R116 + HFPO at 313.15 K.

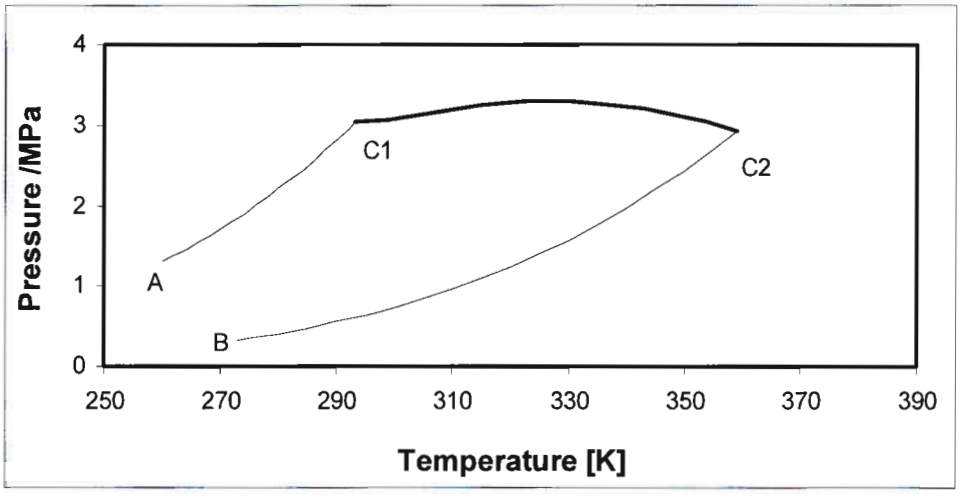

Figure 7.27. Plot of pressure versus temperature and critical pressure curve for the system R116 + HFPO binary system.

Figure 7.27 is a plot of the pressure versus temperature, and features the critical pressure curve for the system R116 + HFPO. Curve A-C1 represents the pure component vapour pressure curve for R116, while curve B-C2 represents the pure component vapour pressure curve for HFPO. Curve C1-C2 represents the critical pressure temperature curve calculated using the PR EOS via Thermopack from the work of (Stockfleth and Dohrn 1998).

7.5. PROCESS DESIGN

The primary outcome of this research project was to propose a preliminary separation scheme for the separation of the fluorinated hydrocarbons HFP and HFPO. To effect the separation of HFP and HFPO, two solvents were determined via a solvent selection procedure, as detailed in Chapter three of this dissertation, the liquid toluene and the gaseous component R116. Two separation processes were designed around the solvents and are designated by the following:

1. *The Toluene separation process:* An extractive distillation process analogous to the work of (Ueno et al. 1997) utilising the liquid toluene as the extractive solvent

2. *The R116 separation process:* A separation process involving the use of three gas stripping units with intermediate solvent recovery columns utilising the solvent R116 as the gaseous stripping agent.

The separation schemes were designed in the Aspen Engineering Process Suite utilising Aspen Plus version 2004.1 ((AspenTech 2004)). Aspen is a versatile process simulation software package that is used extensively by prominent engineering companies such as SASOL, BP and SHELL, to name a few. The availability and flexibility of Aspen in terms of customizable thermodynamic model sets and customizable unit operations facilitated the use of the software for this research project.

The solvent toluene was previously patented for use as an extractive distillation solvent in the work of (Wiist 1967), while the solvent R116 has not been patented for the use as a solvent for the separation of HFP and HFPO. PELCHEM desired the preliminary design of separation processes around a patented and as yet non-patented solvent, such that comparisons could be made between existing and possible methods in order to determine the feasibility of developing, and thus possibly implementing, a novel separation scheme. A further factor which influenced the selection of solvent R116, was the fact that PECLHEM currently produces R116 onsite at the Pelindaba facilities. Although the toluene process was patented, the toluene separation process designed for this project does not utilise the process design, specifications or operating conditions of (Wiist 1967). In order to have a basis of comparison between the designed toluene and R116 processes, both were designed from the 'ground up' utilising the same logic and methodology i.e. the design of the unit operations, distillation columns and strippers (for the R116 separation process), were designed for both processes according to the same general design procedure and methodology. The design methodology utilised for these unit operations was adapted and modified from the work of (Luyben 2006) which featured both rigorous and heuristic design principles.

As specified by PELCHEM, only the preliminary designs of the separation processes were undertaken. This involved the steady state preliminary design of the key separation units: the distillation columns and the

strippers. No preliminary sizing of equipment, such as heat exchangers or columns was performed, and the flowrates and choice of coolants or refrigerants were also not determined. These factors were neglected since the actual separation of the HFP and HFPO was considered of paramount importance, and as such, emphasis was placed on achieving the actual separation rather than a fully detailed process design. The factors which were excluded in the preliminary design would generally be included in a more detailed design of a separation processes, however such a detailed design was beyond the scope of this project given the preliminary nature of the information provided by PELCHEM as they are still in the process of finalising a reaction scheme to produce HFPO from HFP.

The process design procedure and design methodology utilised in this project are presented in Chapter seven of this dissertation. A detailed design of the toluene separation process is presented in Appendix C. This section presents only the final preliminary design results for the toluene and R116 processes via flowsheet drawings and final column specifications for each unit as well as selected stream results.

The component HFPO is a specialty chemical and as such data for this component was scarce. HFPO was not catalogued in the Aspen Plus pure component databank and had to defined manually. Aspen additionally required Antoine constants for the extended vapour pressure equation and these were determined via data regression of the pure component vapour pressure data for HFP and HFPO.

A reasonable understanding of the VLE between the components of the stream of interest is essential for the analysis and design of separation processes. As such the experimental data measured for this project involving HFP, HFPO, toluene and R116 were regressed in the software Thermopack and imported into Aspen. From the modelling of the experimental data, the most consistent or best performing model set was the PR-WS model set which utilised the MC alpha function and NRTL activity coefficient model. The property method chosen in Aspen to thus simulate the VLE behavior for the separation processes was the 'PRWS' base method, which utilised the Peng-Robinson EOS and Wong-Sandler mixing rules. However, the default PRWS base method in Aspen utilised the UNIFAC activity coefficient model and Boston-Mathias ((Boston and Mathias 1980)) alpha function and as such was modified to mirror the model set used for the regression of the data in Thermopack. The regressed data, in the form of interaction parameters were imported into Aspen. To ascertain the validity of the modified base method and the imported parameters, the binary VLE data for each of the measured HPVLE data sets was re-predicted via the 'Analysis' toolset of Aspen utilising the imported interaction parameters. The data predicted via the modified PRWS Aspen base method matched the data modelled in Thermopack.

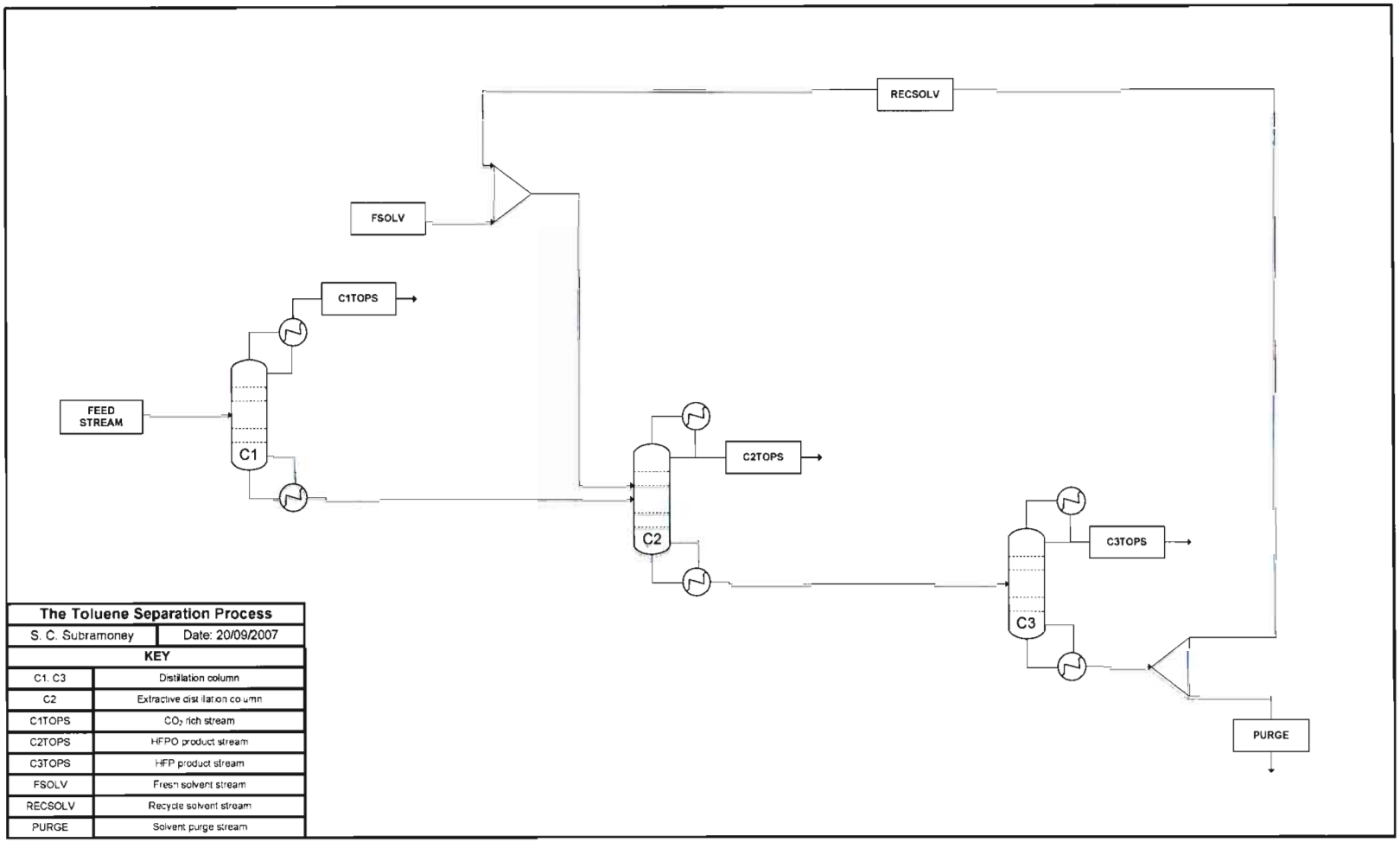

Figure 7.28. The Toluene separation process.

The two processes were designed on the basis of feed stream information provided by PELCHEM. The feed stream at a rate of 5 $kg \cdot hr^{-1}$, contained HFP and HFPO in a 1:2 molar ratio, as well as the impurities CO_2 and toluene. Before the separation of the HFP and HFPO could occur, any impurities from the feed stream were removed so that a cleansed stream could be sent to the extractive distillation column or strippers. Additionally, PELCHEM specified no toluene impurities in the final HFPO product.

For the toluene separation process, only the CO_2 impurity was removed via a distillation operation from the feed stream, as liquid toluene was later added to the stream as the extractive distillation solvent. All of the toluene was later removed after the separation of the HFP and HFPO in a solvent recovery column to produce the Toluene free HFPO product as required by PELCHEM. For the R116 process, all of the CO_2 was removed from the feed stream via a distillation operation and all of the Toluene subsequently removed to produce a pure stream of HFP and HFPO in a 1:2 molar ratio for separation. All of the R116 which was added to the process was removed after separation of the HFP and HFPO via a distillation operation, to produce a purified HFPO product.

7.5.1. The Toluene Process

The completed preliminary design for the toluene process is presented in Figure 7.28. The process contained three columns, with each stream and column designated by the naming convention defined in Section D.2, Appendix D. The process featured the general extractive distillation scheme of an extractive column followed by a solvent recovery column. The feed to the process entered column C1 which removed the CO_2 impurity from the stream. The bottoms product of column C1 which was rich in HFP and HFPO was sent to the extractive distillation column C2 where a liquid toluene stream was added. In column C2 the toluene selectively binds with the HFP which resulted in a distillate stream of high purity HFPO and a bottoms stream of toluene and HFP. This distillate stream rich in HFPO was the final product stream. The bottom stream was sent to the solvent recovery column C3 where the toluene was separated from the HFP. The distillate stream was concentrated in HFP while the bottom stream rich in toluene was sent for solvent recycle to column C2. The toluene process was initially run with the solvent recycle loop open or not operational with the reduced fresh feed of toluene of 11.8814 $kg \cdot hr^{-1}$ as determined by the closing of the recycle loop procedure described in Chapter six and Appendix D. With the initial low feed of toluene and no solvent recycle in the process, low product purities and recoveries were obtained. Once the initial simulation was completed, the recycle loop was closed and with the solvent recycle in place the desired product purities and recoveries were obtained. Physically, this represented running the separation scheme as a continuous process with a solvent recycle loop until the required product purities and recoveries were met, and purging the toluene solvent via the purge stream at the end of the process. The final design specifications for each column and resulting stream information for the toluene separation process with the solvent recycle loop closed or operational, is presented in the following sections. The detailed design of each unit of the separation scheme, including the sensitivity analysis and further stream information, is presented in Section D.2, Appendix D.

7.5.1.1. Column C1

Column C1 was a conventional distillation column employing a partial vapour condenser and a kettle reboiler. The design specifications for column C1, obtained through the design procedure described in Chapter six, is presented in Table 7.27. The purpose of column C1 was to remove all the CO_2 present in the feed stream to the process as a vapour distillate. The feed, distillate and bottoms streams of column C1 are presented in Table 7.28 as C1FEED, C1TOPS and C1BOTTS respectively. The feed stream to C1 was the actual feed stream to the entire process as determined from the feed conditions defined by PECLHEM, and entered the column at a temperature of 298.15 K and 16 atm. The determination of the feed stream temperature and pressure was set to ambient temperature and the operating pressure of the column as in this

stage of the preliminary design, certain factors such as valves and pressure losses along pipes were not taken into account.

C1 contained 26 equilibrium stages (including the reboiler and the condenser) and a distillate rate of 0.6501 $kg \cdot hr^{-1}$ which was equivalent to the total amount of CO_2 in the feed to the column. The molar reflux ratio (RR) was determined by the 'Design/Spec/Vary' (DSV) function of Aspen as 0.8813. The optimum feed stage to the column, with respect to minimizing the reboiler heat input, was determined to be stage 15 which resulted in a reboiler duty of 0.1540 kW. The vapour distillate was removed from the partial condenser, with the liquid bottoms product removed from the final stage, with no intermediate side streams. The condenser duty was determined to be -0.0792 kW with a condenser temperature of 245.83 K, which would allow the use of cooling water, and the reboiler or final stage temperature was 329.66 K.

Specification	Value
N_T	26
Condenser Type	Partial Vapour
Distillate Rate [$kg \cdot hr^{-1}$]	0.6501
Molar Reflux Ratio	0.8813
Feed Stage	15
Solvent Feed Stage	-
Top Product Stage	1
Bottom Product Stage	26
P_{COLUMN} [atm]	15
Condenser Duty [kW]	-0.0792
Condenser Temperature [K]	245.83
Reboiler Duty [kW]	0.1540
Reboiler Temperature [K]	329.66

Table 7.27. Column specifications for column C1 for the Toluene process.

From an analysis of Table 7.28, which presents the stream information for all the streams entering and leaving column C1, 99.99 % of the CO_2 that entered the column via C1FEED, exited the column as a vapour in the distillate stream C1TOPS. The only other component that exited column C1 via the distillate steam was HFPO, with 0.0001 $kg \cdot hr^{-1}$ HFPO present. The bottoms stream contained all the HFP, all the Toluene, 99.99% of the HFPO and 0.0001 % of the CO_2 present in the feed. The stream C1TOPS was discarded while the stream C1BOTTS was sent to column C2.

	C1FEED	C1TOPS	C1BOTTS
Mole Fraction			
HFP	0.2100	0.0000	0.3230
HFPO	0.4200	0.0000	0.6461
Toluene	0.0200	0.0000	0.0308
CO_2	0.3500	1.0000	0.0001
Mass Flow [kg•hr^{-1}]			
HFP	1.3296	0.0000	1.3296
HFPO	2.9425	0.0001	2.9424
Toluene	0.0778	0.0000	0.0778
CO_2	0.6501	0.6500	0.0001
Mass Fraction			
HFP	0.2659	0.0001	0.3057
HFPO	0.5885	0.0001	0.6764
Toluene	0.0156	0.0000	0.0179
CO_2	0.1300	0.9998	0.0000
Total Flow [kg•hr^{-1}]	5.0000	0.6501	4.3499
Temperature [K]	298.15	245.83	329.66
Pressure [atm]	16	15	15
Vapour Fraction	0	1	0
Liquid Fraction	1	0	1

Table 7.28. Stream results for column C1 for the Toluene process.

7.5.1.2. Column C2

Column C2 was the extractive distillation column employing a total condenser and a kettle reboiler. The design specifications for column C2 are presented in Table 7.29. The purpose of column C2 was to add the liquid toluene stream to the mixture to effect the separation of HFP and HFPO. The Toluene selectively binds with the HFP in the mixture and was removed as the bottoms product of the distillation column. HFPO, initially the heavier component in the HFP and HFPO binary mixture, was then removed from the top of the column as the lightest component. The feed stream, solvent feed stream, distillate and bottoms streams of column C2 are presented in Table 7.30 as C2FEED, C2SOLV, C2TOPS and C2BOTTS respectively. The feed stream to C2 was the bottoms stream of column C1 and entered column C2 at the bottoms temperature and pressure of column C1.

C2 had 30 equilibrium stages (including the reboiler) and a distillate rate of 2.8999 kg•hr^{-1} which was set to an amount just under the total amount of HFPO in the feed to the column. The molar reflux ratio was

determined by the DSV function of Aspen as 8.9001. The optimum feed stage to the column, with respect to minimizing the reboiler heat input, was determined to be stage 23 and the optimum solvent feed stage was determined to be stage 5, which resulted in a reboiler duty of 8.1328 kW. The solvent toluene was introduced into column C2 at a high concentration at a feed stage below the condenser but above the primary feed stage. This was to ensure that there were sufficient stages in the column to rectify the non-volatile solvent from the distillate to produce a high purity HFPO stream. The high reboiler duty was required to heat the large amounts of the non-volatile toluene in the distillation column. A lower reboiler duty could have been obtained by lowering the amount of the toluene solvent, however this would have resulted in a lower purity HFPO product. The liquid distillate was removed from the total condenser, with the liquid bottoms product removed from the final stage, with no intermediate side streams. The condenser duty was determined as -0.5905 kW with a condenser operating temperature of 328.68 K, which permitted the use of cooling water in the condenser. The reboiler or final stage temperature was 512.56 K.

Table 7.30 presents the stream information for all the streams entering and leaving column C2. The feed stream C2FEED was the bottoms stream of column C1 which was fed to column C2 at an operating pressure of 16 atm and temperature of 330.90 K. The solvent stream C2SOLV was initially pure toluene at a flowrate of 11.8814 $kg \cdot hr^{-1}$, however with the solvent recycle loop closed, other components such as HFP are introduced into the toluene solvent stream. With the solvent recycle loop closed, the effect was to increase the solvent power of toluene by increasing the hold-up or flowrate of toluene in the column to 59.6974 $kg \cdot hr^{-1}$. The distillate stream of column C2 contained a high purity stream of HFPO of 99.88 % (mole). 98.46 % of the HFPO, or 2.8972 $kg \cdot hr^{-1}$ of HFPO that entered column C2 via the stream C1BOTTS, was recovered in the distillate with the remaining HFPO leaving via the bottoms stream. The distillate stream contained no toluene impurity, as specified by PELCHEM, and contained 0.11 % HFP (mole) and 0.01 % CO_2 (mole). The distillate stream C2TOPS was the final HFPO product stream from the toluene separation process and was sent to storage.

The bottoms stream of column C2, termed C2BOTTS, contained 0.0453 $kg \cdot hr^{-1}$ of HFPO which was not recovered in the distillate stream, as well as all the toluene and 99.80 % of the HFP that entered the feed. The stream C2BOTTS was sent to column C3.

Specification	Value
N_T	30
Condenser Type	Total
Distillate Rate [kg•hr^{-1}]	2.8999
Molar Reflux Ratio	8.9001
Feed Stage	23
Solvent Feed Stage	5
Top Product Stage	1
Bottom Product Stage	30
P_{COLUMN} [atm]	15
Condenser Duty [kW]	-0.5905
Condenser Temperature [K]	328.68
Reboiler Duty [kW]	8.1328
Reboiler Temperature [K]	512.56

Table 7.29. Column specifications for column C2 for the Toluene process.

	C2FEED	C2SOLV	C2TOPS	C2BOTTS
Mole Fraction				
HFP	0.3230	0.0002	0.0011	0.0136
HFPO	0.6461	0.0000	0.9988	0.0004
Toluene	0.0308	0.9998	0.0000	0.9859
CO_2	0.0001	0.0000	0.0001	0.0000
Mass Flow [kg•hr^{-1}]				
HFP	1.3296	0.0204	0.0026	1.3474
HFPO	2.9424	0.0000	2.8972	0.0453
Toluene	0.0778	59.6974	0.0000	59.7750
CO_2	0.0001	0.0000	0.0001	0.0000
Mass Fraction				
HFP	0.3057	0.0003	0.0009	0.0220
HFPO	0.6764	0.0000	0.9990	0.0007
Toluene	0.0179	0.9997	0.0000	0.9772
CO_2	0.0000	0.0000	0.0000	0.0000
Total Flow [kg•hr^{-1}]	4.3499	59.7178	2.8999	61.1677
Temperature [K]	330.90	302.34	328.68	512.56
Pressure [atm]	16	16	15	15
Vapour Fraction	0	0	0	0
Liquid Fraction	1	1	1	1

Table 7.30. Stream results for column C2 for the Toluene process.

7.5.1.3. Column C3

Column C3 was a conventional distillation column which contained a total condenser and a kettle reboiler. The design specifications for column C3 are presented in Table 7.31. The purpose of column C3 was to act as a solvent recovery column to separate the toluene from the HFP to produce the HFP rich product stream. The feed, distillate and bottoms streams of column C3 are presented in Table 7.32 as C3FEED, C3TOPS and C3BOTTS respectively. The feed stream to C3 was the bottoms stream of column C2 which was cooled to a temperature of 300 K and an operating pressure of 16 atm to obtain the Toluene in the liquid phase.

C3 contained 38 equilibrium stages (including the reboiler) and a distillate rate of 1.3772 $kg \cdot hr^{-1}$. The values of the distillate rate were set before the recycle loop was closed, and due to the closing of the recycle loop, these values do not match exactly the amount of toluene and HFP in the feed as HFP is reintroduced to system via the recycled toluene solvent stream. The molar reflux ratio was determined by the DSV function of Aspen as 3.1262. The optimum feed stage to the column, with respect to minimizing the reboiler heat input, was determined to be stage 9 which resulted in a reboiler duty of 7.7657 kW. The liquid distillate was removed from the total condenser, with the liquid bottoms product removed from the final stage, with no intermediate side streams. The condenser duty was determined as -0.1277 kW with a condenser temperature of 327.54 K, which would allow the use of cooling water, and the reboiler or final stage temperature was 515.82 K.

From an analysis of Table 7.32, which presents the stream information for all the stream entering and leaving column C3, 99.99 % of the toluene that entered the column via C3FEED, exited the column as a liquid in the bottoms stream C3BOTTS. The only other component exiting the bottoms stream was 0.0256 $kg \cdot hr^{-1}$ of HFP. The bottoms of stream of column C3 contained primarily toluene and was sent for recycle. For the toluene separation process, the stream was sent to a splitter which split the stream into a recycle stream and a purge stream. Physically, the purge stream represented the point of exit for the bulk of the toluene from the separation process. The stream results for the purge stream are presented in Table 7.33.

The distillate stream from column C3 contained the bulk of the HFP and un-recovered HFPO. This stream was required by PELCHEM for recycle to a reactor for conversion of the HFP into HFPO. The HFP rich stream contained 99.42 % of the HFP that initially entered the toluene separation process at a purity of 96.41 % (mole). The HFP rich stream also contained 2.98 % (mole) of HFPO and 0.61 % (mole) of toluene.

Specification	Value
N_T	38
Condenser Type	Total
Distillate Rate [kg•hr^{-1}]	1.3722
Molar Reflux Ratio	3.1262
Feed Stage	4
Solvent Feed Stage	-
Top Product Stage	1
Bottom Product Stage	18
P_{COLUMN} [atm]	15
Condenser Duty [kW]	-0.1277
Condenser Temperature [K]	327.54
Reboiler Duty [kW]	7.7657
Reboiler Temperature [K]	515.82

Table 7.31. Column specifications for column C3 for the Toluene process.

	C3FEED	C3TOPS	C3BOTTS
Mole Fraction			
HFP	0.0136	0.9641	0.0003
HFPO	0.0004	0.0298	0.0000
Toluene	0.9859	0.0061	0.9997
CO_2	0.0000	0.0000	0.0000
Mass Flow [kg•hr^{-1}]			
HFP	1.3474	1.3219	0.0256
HFPO	0.0453	0.0453	0.0000
Toluene	59.7750	0.0051	59.7699
CO_2	0.0000	0.0000	0.0000
Mass Fraction			
HFP	0.0220	0.9633	0.0004
HFPO	0.0007	0.0330	0.0000
Toluene	0.9772	0.0037	0.9996
CO_2	0.0000	0.0000	0.0000
Total Flow [kg•hr^{-1}]	61.1677	1.3722	59.7955
Temperature [K]	299.37	327.54	515.82
Pressure [atm]	16	15	15
Vapour Fraction	0	0	0
Liquid Fraction	1	1	1

Table 7.32. Stream results for column C3 for the Toluene process.

7.5.1.4. Selected Stream Information

Table 7.33 presents the stream results for the fresh solvent and solvent purge streams for the toluene separation process. The fresh solvent stream contained 11.8814 kg•hr^{-1} of toluene. Before a recycle loop was utilised, a fresh solvent feed rate of approximately 54 kg•hr^{-1} of toluene was required to meet the desired product purities and recoveries of PELCHEM. The fresh solvent feed rate of toluene required for the process was determined by a sensitivity analysis. The application of the recycle loop enabled the required fresh solvent feed rate of toluene to be dramatically decreased to 11.8814 kg•hr^{-1}, which is approximately four and half times less than the original fresh solvent requirements. From the analysis of the purge stream, it was found that the flowrate of toluene exiting the system was 11.9541 kg•hr^{-1} which was greater than the fresh solvent feed rate of 11.8814 kg•hr^{-1}. The additional toluene resulted from the initial amount of toluene that was present in the overall feed stream to the separation process. 0.0778 kg•hr^{-1} of toluene was present in C1FEED and 0.0051 kg•hr^{-1} of toluene exited in the HFP rich product stream of column C3, C3TOPS. This resulted in 0.0727 kg•hr^{-1} of toluene which when added to the 11.8814 kg•hr^{-1} of fresh toluene resulted in a flowrate of 11.9541 kg•hr^{-1} which exited in the purge stream.

	Fresh Solvent	**Purge**
Mole Fraction		
HFP	0.0000	0.0003
HFPO	0.0000	0.0000
Toluene	1.0000	0.9997
CO_2	0.0000	0.0000
Mass Flow [kg•hr^{-1}]		
HFP	0.0000	0.0051
HFPO	0.0000	0.0000
Toluene	11.8814	11.9541
CO_2	0.0000	0.0000
Mass Fraction		
HFP	0.0000	0.0004
HFPO	0.0000	0.0000
Toluene	1.0000	0.9996
CO_2	0.0000	0.0000
Total Flow [kg•hr^{-1}]	11.8814	11.9592
Temperature [K]	298.15	298.28
Pressure [atm]	1	6
Vapour Fraction	0	0
Liquid Fraction	1	1

Table 7.33. Stream results for the fresh solvent and purge streams for the Toluene process.

	Feed Stream	CO_2 Stream	HFPO Product Stream	HFP Product Stream
Mole Fraction				
HFP	0.2100	0.0000	0.0010	0.9641
HFPO	0.4200	0.0000	0.9988	0.0298
Toluene	0.0200	0.0000	0.0000	0.0061
CO_2	0.3500	1.0000	0.0001	0.0000
Mass Flow [kg•hr^{-1}]				
HFP	1.3296	0.0000	0.0026	1.3219
HFPO	2.9425	0.0001	2.8972	0.0453
Toluene	0.0778	0.0000	0.0000	0.0051
CO_2	0.6501	0.6500	0.0002	0.0000
Mass Fraction				
HFP	0.2659	0.0001	0.0009	0.9633
HFPO	0.5885	0.0001	0.9990	0.0330
Toluene	0.0156	0.0000	0.0000	0.0037
CO_2	0.1300	0.9998	0.0000	0.0000
Total Flow [kg•hr^{-1}]	5.0000	0.6501	2.9000	1.3722
Temperature [K]	301.92	245.83	328.68	327.54
Pressure [atm]	16	15	15	15
Vapour Fraction	0	1	0	0
Liquid Fraction	1	0	1	1

Table 7.34. Stream results for the overall feed stream, CO2 stream, HFPO product stream and HFP product stream for the Toluene process.

Table 7.34 presents a summary of selected key streams in the toluene separation process for ease of reference. The overall initial feed stream to the process C1FEED is presented, along with the CO_2 rich stream C1TOPS, the HFPO product stream C2TOPS and the HFP product stream C3TOPS.

The overall product recovery for HFPO was 98.46 % at a product purity of 99.88 % (mole). The only impurities in the HFPO product stream are HFP and CO_2 which were deemed allowable by PELCHEM. The HFPO product purity desired by PECLHEM was 99.9 % and the value obtained from the toluene separation process lies extremely close to the desired specification.

The overall HFP product recovery was 99.42 % at a product purity of 96.41 % (mole) HFP. Impurities in this product stream were toluene and HFPO which were deemed admissible by PELCHEM.

7.5.2. The R116 Process

For the separation process involving the solvent R116, a supercritical extraction process involving supercritical R116 was initially proposed. Initial process design and simulation in Aspen revealed that such a process yielded little or no separation of the HFP and HFPO stream. The *P-x-y* data for the systems R116 + HFP and R116 + HFPO are superimposed and presented in Figures 7.29 to 7.31. The data was obtained through the use of the Analysis toolset in Aspen Plus utilising the regressed interaction parameters from Thermopack and the PRWS base method.

For the 313.15 K isotherm, the system R116 + HFP reached the critical point at 3.13 MPa, while the system R116 + HFPO reached the critical point at 3.32 MPa. At this isotherm there was little appreciable difference between the equilibrium liquid compositions for the two binary systems as the systems approached the critical state. The vapour equilibrium compositions showed a greater difference than the liquid compositions but it was still not significant. The relatively small deviations between the equilibrium vapour and liquid compositions as the system approached the critical state gave an indication that the process of supercritical extraction with supercritical R116 was not feasible at these conditions.

The superimposed *P-x-y* data for the systems at 273.15 K is presented in Figure 7.30. There existed little appreciable difference between the equilibrium vapour and liquid phase compositions for the binary systems at this temperature.

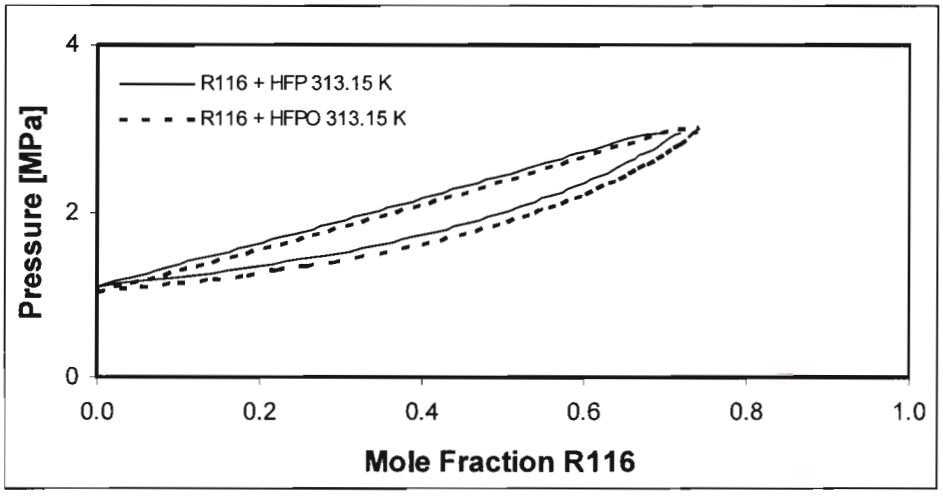

Figure 7.29. P-x-y data for R116 + HFP and R116 + HFPO at 313.15 K.

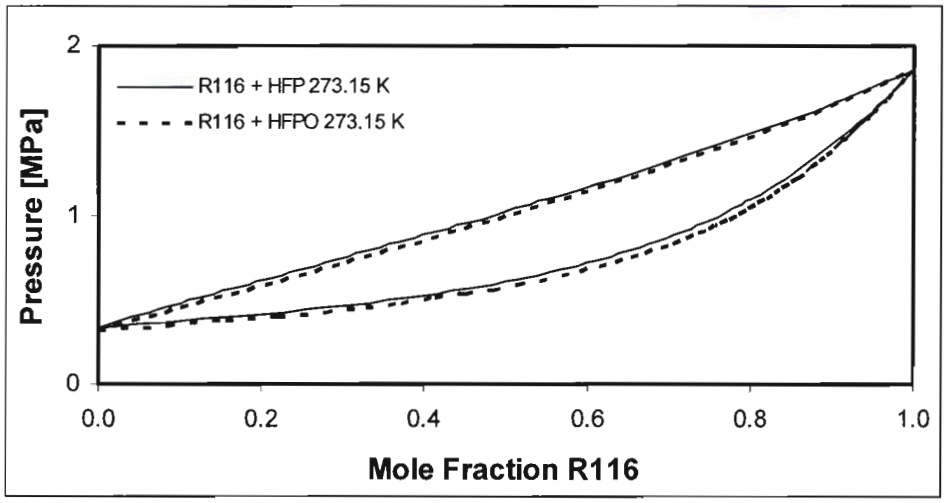

Figure 7.30. P-x-y data for R116 + HFP and R116 + HFPO at 273.15 K.

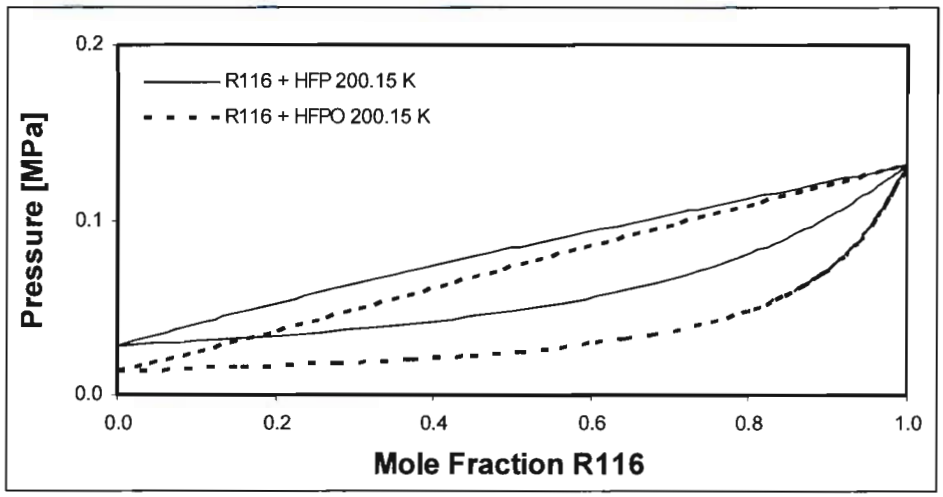

Figure 7.31. P-x-y data for R116 + HFP and R116 + HFPO at 200.15 K.

The superimposed *P-x-y* data for the systems at 200.15 K is presented in Figure 7.31. At this particular isotherm there was a marked difference between the equilibrium liquid phase compositions at low concentrations of R116, while for the vapour phase equilibrium compositions there was a clear distinction between the two binary systems at all compositions of the lighter component R116. This clear distinction between the equilibrium vapour phases for the binary systems indicated that employing a separation process with gaseous R116 at low temperatures of approximately 200.15 K and low pressures of approximately 0.1 MPa or 1 atm would result in greater separation of the HFP and HFPO stream than by

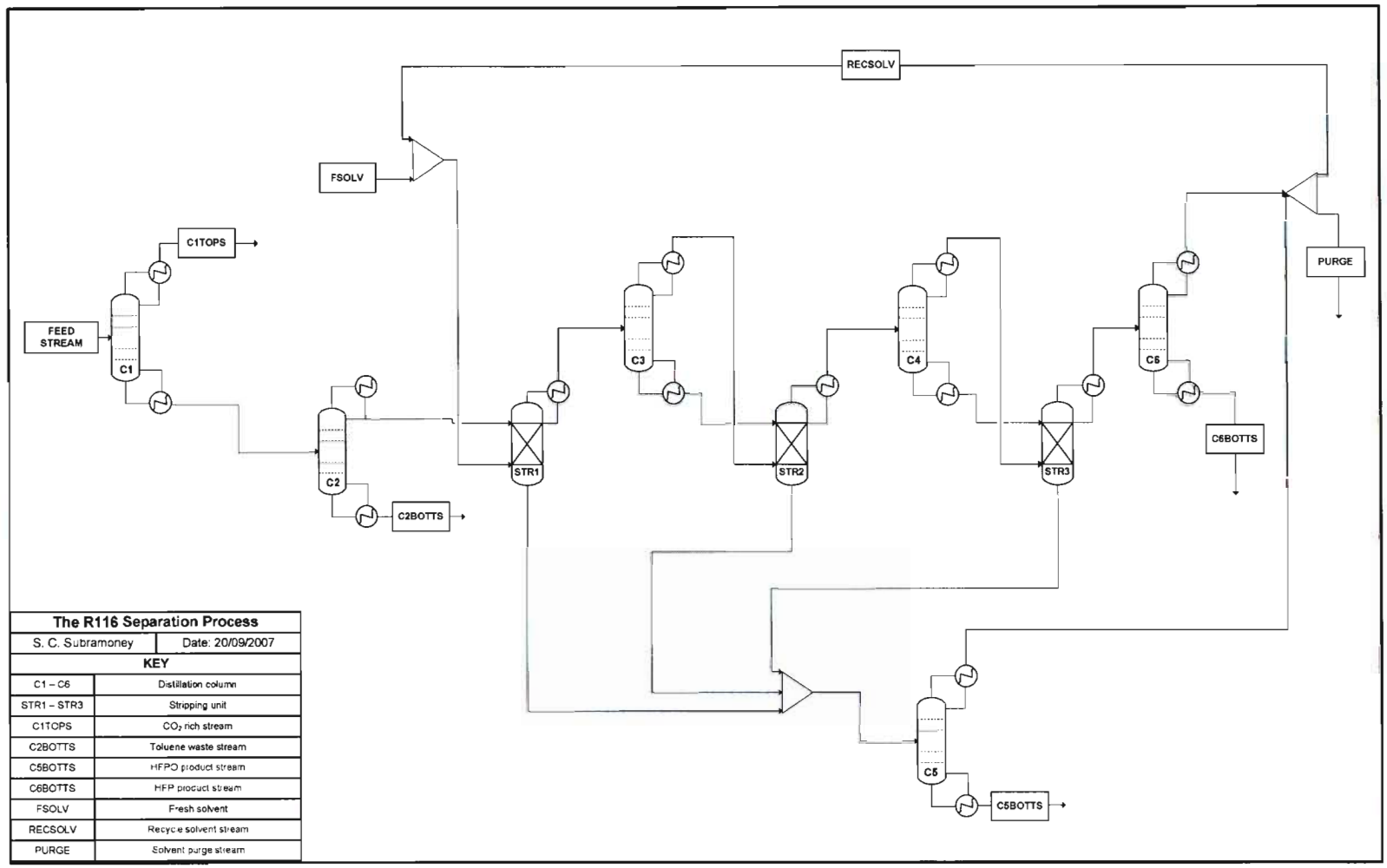

Figure 7.32. The R116 separation process

employing a supercritical extraction process at 313.15 K under high pressures of approximately 3 MPa or 30 atm. Consequently, the process of gas stripping was utilised and the operating pressure of the stripping units was set to 1 atm to ensure significant differentiation between the equilibrium compositions such that separation of the HFP and HFPO was possible.

The completed preliminary design for the R116 process is presented in Figure 7.32. The process contained six distillation columns and three stripping units (strippers), with each stream and column designated by the naming convention previously defined. The proposed separation scheme utilised two columns C1 and C2 to remove the CO_2 and toluene impurities from the initial feed stream, before sending the liquid HFP and HFPO stream to stripper STR1 where it was contacted with gaseous solvent R116. In STR1 the gaseous R116 selectively absorbed a fraction of the HFP resulting in a liquid stream leaving STR1 which was concentrated with HFPO. The gaseous stream containing R116, HFP and some stripped HFPO which exited STR1 was sent to column C3 where the R116 and HFP and HFPO mixture was separated before being re-contacted in a second stripper STR2 to strip away further HFP from the HFP and HFPO liquid mixture. This procedure was repeated in columns C4 and STR3. The three liquid streams of STR1, STR2 and STR3 which were rich in HFPO were mixed and sent to column C6 which produced a bottoms product of high purity HFPO and a distillate product rich in R116. The vapour stream from STR3 which contained the R116 and the stripped HFP was sent to column C5 where a bottom stream of high purity HFP was produced, along with a top distillate stream of high purity R116. The R116 streams from C5 and C6 were mixed and utilised for solvent recycle to STR1. The R116 process was initially run with the solvent recycle loop open or not operational with the reduced fresh feed of R116 of 28.4014 $kg \cdot hr^{-1}$ as determined by the closing of the recycle loop procedure utilised for this project. With the initial reduced feed of R116 and no solvent recycle in the process, low product purities and recoveries were obtained. Once the initial simulation was completed, the recycle loop was closed and with the solvent recycle in place the desired product purities and recoveries were obtained. The final design specifications for each column and the resulting stream information for the R116 separation process with the solvent recycle loop closed or operational, are presented in the following sections.

7.5.2.1. Column C1

Column C1 was identical to the first column of the toluene separation process. C1 was a conventional distillation column employing a partial vapour condenser and a kettle reboiler. The design specifications for column C1, are presented in Table 7.35. The purpose of column C1 was to remove all the CO_2 present in the feed stream to the process as a vapour distillate. The feed, distillate and bottoms streams of column C1 are presented in Table 7.36 as C1FEED, C1TOPS and C1BOTTS respectively.

C1 contained 26 equilibrium stages (including the reboiler and the condenser) and a distillate rate of 0.6501 $kg \cdot hr^{-1}$ which was equivalent to the total amount of CO_2 in the feed to the column. The RR was determined by the DSV function of Aspen as 0.8813. The optimum feed stage to the column, with respect to minimizing the reboiler heat input, was determined to be stage 15 which resulted in a reboiler duty of 0.1540 kW. The vapour distillate was removed from the partial condenser, with the liquid bottoms product removed from the final stage, with no intermediate side streams. The condenser duty was determined as -0.0792 kW with a condenser temperature of 245.83 K, which would allow the use of cooling water, and a reboiler or final stage temperature of 329.66 K.

Specification	Value
N_T	26
Condenser Type	Partial Vapour
Distillate Rate [$kg \cdot hr^{-1}$]	0.6501
Molar Reflux Ratio	0.8813
Feed Stage	15
Solvent Feed Stage	-
Top Product Stage	1
Bottom Product Stage	26
P_{COLUMN} [atm]	15
Condenser Duty [kW]	-0.0792
Condenser Temperature [K]	245.83
Reboiler Duty [kW]	0.1540
Reboiler Temperature [K]	329.66

Table 7.35. Column specifications for column C1 for the R116 process.

From an analysis of Table 7.36, which presents the stream information for all the stream entering and leaving column C1, 99.99 % of the CO_2 that entered the column via C1FEED, exited the column as a vapour in the distillate stream C1TOPS. The only other component that exited the column C1 via the distillate steam was HFPO, with 0.0001 $kg \cdot hr^{-1}$ HFPO present. The bottoms stream contained all the HFP, all the toluene, 99.99% of the HFPO and 0.0001 % of the CO_2 present in the feed. The stream C1TOPS was discarded while the stream C1BOTTS was sent to column C2.

	C1FEED	C1TOPS	C1BOTTS
Mole Fraction			
HFP	0.2100	0.0000	0.3231
HFPO	0.4200	0.0000	0.6461
Toluene	0.0200	0.0000	0.0308
CO_2	0.3500	1.0000	0.0000
R116	0.0000	0.0000	0.0000
Mass Flow [kg•hr^{-1}]			
HFP	1.3296	0.0000	1.3296
HFPO	2.9425	0.0000	2.9425
Toluene	0.0778	0.0000	0.0778
CO_2	0.6501	0.6501	0.0000
R116	0.0000	0.0000	0.0000
Mass Fraction			
HFP	0.2659	0.0000	0.3057
HFPO	0.5885	0.0000	0.6764
Toluene	0.0156	0.0000	0.0179
CO_2	0.1300	1.0000	0.0000
R116	0.0000	0.0000	0.0000
Total Flow [kg•hr^{-1}]	5.0000	0.6501	4.3499
Temperature [K]	301.92	245.83	329.67
Pressure [atm]	16	15	15
Vapour Fraction	0	1	0
Liquid Fraction	1	0	1

Table 7.36. Stream results for column C1 for the R116 process.

7.5.2.2. Column C2

Column C2 was a conventional distillation column employing a total condenser and a kettle reboiler. The design specifications for column C2 are presented in Table 7.37. The purpose of column C2 was to separate the toluene impurity from the feed stream to produce a stream of high purity HFP and HFPO in a 1:2 molar ratio. The feed, distillate and bottoms streams of column C3 are presented in Table 7.38 as C2FEED, C2TOPS and C2BOTTS respectively. The feed stream to C2 was the bottoms stream of column C1.

C2 had 20 equilibrium stages (including the reboiler) and a distillate rate of 4.2740 kg•hr^{-1} which was equivalent to total flow of HFP and HFPO in the feed stream to column C2. The RR was determined by the DSV function of Aspen as 1.5637. The optimum feed stage to the column, with respect to minimizing the reboiler heat input, was determined to be stage 8 which resulted in a reboiler duty of 0.1782 kW due to the small amount of toluene in the stream. The liquid distillate was removed from the total condenser, with the liquid bottoms product removed from the final stage, with no intermediate side streams. The condenser

duty was determined as -0.1793 kW with a condenser temperature of 326.96 K, which would allow the use of cooling water, and a reboiler or final stage temperature of 515.64 K.

From an analysis of Table 7.38, 100 % of the toluene that entered the column via C2FEED, exited the column as a liquid in the bottoms stream C2BOTTS. The only other component exiting the bottoms stream was 0.001 $kg \cdot hr^{-1}$ of HFP which selectively bonded to the toluene.

The distillate stream from column C2 contained all of the HFPO and 99.99 % of the HFP that was present in the feed. The liquid distillate stream contained only HFP and HFPO in a 1:2 molar ratio which was sent to the stripping units for separation.

Specification	Value
N_T	20
Condenser Type	Total
Distillate Rate [$kg \cdot hr^{-1}$]	4.2720
Molar Reflux Ratio	1.5637
Feed Stage	8
Solvent Feed Stage	-
Top Product Stage	1
Bottom Product Stage	20
P_{COLUMN} [atm]	15
Condenser Duty [kW]	-0.1793
Condenser Temperature [K]	326.96
Reboiler Duty [kW]	0.1782
Reboiler Temperature [K]	515.64

Table 7.37. Column specifications for column C2 for the R116 process.

	C2FEED	C2TOPS	C2BOTTS
Mole Fraction			
HFP	0.3231	0.3333	0.0010
HFPO	0.6461	0.6667	0.0000
Toluene	0.0308	0.0000	0.9989
CO_2	0.0000	0.0000	0.0000
R116	0.0000	0.0000	0.0000
Mass Flow [kg•hr^{-1}]			
HFP	1.3296	1.3295	0.0001
HFPO	2.9425	2.9425	0.0000
Toluene	0.0778	0.0000	0.0778
CO_2	0.0000	0.0000	0.0000
R116	0.0000	0.0000	0.0000
Mass Fraction			
HFP	0.3057	0.3112	0.0017
HFPO	0.6764	0.6888	0.0000
Toluene	0.0179	0.0000	0.9983
CO_2	0.0000	0.0000	0.0000
R116	0.0000	0.0000	0.0000
Total Flow [kg•hr^{-1}]	4.3499	4.2720	0.0779
Temperature [K]	330.91	326.96	515.64
Pressure [atm]	16	15	15
Vapour Fraction	0	0	0
Liquid Fraction	1	1	1

Table 7.38. Stream results for column C2 for the R116 process.

7.5.2.3. Stripper STR1

The first stripping unit STR1 was a trayed column which contained a partial vapour condenser to ensure a vapour distillate or exiting vapour stream. The stripping units STR1, STR2 and STR3 were designed according to the design methodology outlined in Chapter six. The specifications for STR1 are presented in Table 7.39. STR1 contained 35 equilibrium stages (including the condenser) and the distillate rate was set to 41.6234 kg•hr^{-1} which was equivalent to the amount of R116 and HFP in the feed stream before the recycle loop was closed. The values of the distillate rate were set before the recycle loop was closed and due to the closing of the recycle loop, these values do not match exactly the amount of R116 and HFP in the feed as HFP is reintroduced to system via the recycled R116 solvent stream. The liquid HFP and HFPO feed stream, STR1F, was introduced at stage one and the gaseous R116 was introduced at stage 35. The vapour distillate left STR1 at stage one, with the liquid stream leaving STR1 at stage 35. The operating pressure of the column was set to 1 atm as discussed in the preceding sections. The condenser duty was observed as -0.5095 kW with an associated condenser temperature of 198.96 K, with a bottoms stage (stage 35) temperature of 210.01 K.

Table 7.40 presents the stream results for unit STR1. STR1F denotes the liquid feed stream entering the unit, SOLV1 denotes the gaseous solvent R116 stream, STR1VAP the exiting vapour stream and STR1LIQ the exiting liquid stream. Initially the solvent stream SOLV1 contained only pure R116, however the results presented show the stream results for the process after the recycle loop was closed, which introduced HFP in the solvent stream from the recycle process. The function of the stripper was to allow the gaseous R116 to contact the liquid stream to selectively strip HFP from the HFP and HFPO liquid feed stream which would result in an exiting liquid stream concentrated in HFPO.

From the analysis of the data presented in Table 7.40 the exiting vapour stream contained 99.85 % of the HFP that entered in the feed stream STR1F, 31.14 % of the HFPO and 97.06 % of the R116. The remaining R116 was absorbed into the liquid phase. The amount of HFPO recovered the liquid phase and the low purity HFP stream in the gaseous phase signified that a single unit stripping operation was not sufficient to meet product specifications. As a result, the exiting vapour stream STR1VAP was sent to a distillation column C3 to produce a gaseous R116 stream and a liquid HFP and HFPO stream which would be re-contacted in a further stripping unit.

The exiting liquid phase which contained 2.0265 $kg \cdot hr^{-1}$ HFPO, or rather 68.86 % of the HFPO in the feed, 1.1924 $kg \cdot hr^{-1}$ of R116 and 0.0031 $kg \cdot hr^{-1}$ of HFP was sent to a distillation column C5 for further purification.

Specification	Value
N_T	35
Condenser Type	Partial Vapour
Distillate Rate [$kg \cdot hr^{-1}$]	41.6234
Liquid Feed Stage	1
Vapour Feed Stage	35
Liquid Product Stage	35
Vapour Product Stage	1
P_{COLUMN} [atm]	1
Condenser Duty [kW]	-0.5094
Condenser Temperature [K]	198.96
Bottom Stage Temperature [K]	210.01

Table 7.39. Column specifications for stripper STR1 for the R116 process.

	STR1F	SOLV1	STR1VAP	STR1LIQ
Mole Fraction				
HFP	0.3333	0.0000	0.0295	0.0010
HFPO	0.6667	0.0000	0.0184	0.5850
Toluene	0.0000	0.0000	0.0000	0.0000
CO_2	0.0000	0.0000	0.0000	0.0000
R116	0.0000	1.0000	0.9521	0.4140
Mass Flow [kg•hr^{-1}]				
HFP	1.3295	0.0012	1.3276	0.0031
HFPO	2.9425	0.0004	0.9164	2.0265
Toluene	0.0000	0.0000	0.0000	0.0000
CO_2	0.0000	0.0000	0.0000	0.0000
R116	0.0000	40.5719	39.3795	1.1924
Mass Fraction				
HFP	0.3112	0.0000	0.0319	0.0010
HFPO	0.6888	0.0000	0.0220	0.6290
Toluene	0.0000	0.0000	0.0000	0.0000
CO_2	0.0000	0.0000	0.0000	0.0000
R116	0.0000	1.0000	0.9461	0.3701
Total Flow [kg•hr^{-1}]	4.2720	40.5734	41.6234	3.2220
Temperature [K]	230.00	273.00	198.96	210.02
Pressure [atm]	2	1	1	1
Vapour Fraction	0	1	1	0
Liquid Fraction	1	0	0	1

Table 7.40. Stream results for stripper STR1 for the R116 process.

7.5.2.4. Column C3

Column C3 was a conventional distillation column which employed a partial vapour condenser and a kettle reboiler. The design specifications for column C3 are presented in Table 7.41. The purpose of column C3 was to separate the exiting vapour stream STR1VAP of stripping unit STR1, into a vapour stream of pure R116 and a liquid stream of HFP and HFPO, such that the vapour and liquid streams could be re-contacted in a further stripping unit. The feed, distillate and bottoms streams of column C3 are presented in Table 7.42 as C3FEED, C3TOPS and C3BOTTS respectively. The feed stream to C3 was the exiting vapour stream STR1VAP of STR1.

C3 had 20 equilibrium stages (including the condenser and reboiler) and a distillate rate of 39.3811kg•hr^{-1} which was initially equivalent to the total flow of R116 in the feed stream to column C3 before the recycle loop was closed. The RR was determined by the DSV function of Aspen as 0.8430. The column operating pressure was set to 1 atm. The optimum feed stage to the column, with respect to minimizing the reboiler heat input, was determined to be stage 12 which resulted in a reboiler duty of 0.9957 kW. The vapour R116

distillate was removed from the partial condenser, with the liquid bottoms product removed from the final stage, with no intermediate side streams. The condenser duty was determined as -1.0704 kW with a condenser temperature of 194.98 K and a final stage temperature of 239.10 K to ensure that the bottoms product was liquid HFP and HFPO.

From an analysis of Table 7.42, 99.96 % of the R116 that entered the column via C3FEED or STR1VAP, exited the column as the vapour distillate stream C3TOPS. The only other component exiting the vapour distillate stream was 0.0164 $kg \cdot hr^{-1}$ of HFP.

The liquid bottoms stream from column C3 contained all of the HFPO, 98.76 % of the HFP and 0.04 % of the R116 that was present in the feed at a pressure of 1 atm and temperature of 239.10 K.

Specification	Value
N_T	20
Condenser Type	Partial Vapour
Distillate Rate [$kg \cdot hr^{-1}$]	39.3811
Molar Reflux Ratio	0.8430
Feed Stage	12
Solvent Feed Stage	-
Top Product Stage	1
Bottom Product Stage	20
P_{COLUMN} [atm]	1
Condenser Duty [kW]	-1.0704
Condenser Temperature [K]	194.98
Reboiler Duty [kW]	0.9957
Reboiler Temperature [K]	239.10

Table 7.41. Column specifications for column C3 for the R116 process.

	C3FEED	C3TOPS	C3BOTTS
Mole Fraction			
HFP	0.0295	0.0004	0.6083
HFPO	0.0184	0.0000	0.3842
Toluene	0.0000	0.0000	0.0000
CO_2	0.0000	0.0000	0.0000
R116	0.9521	0.9996	0.0074
Mass Flow [kg•hr^{-1}]			
HFP	1.3276	0.0164	1.3112
HFPO	0.9164	0.0000	0.9164
Toluene	0.0000	0.0000	0.0000
CO_2	0.0000	0.0000	0.0000
R116	39.3795	39.3647	0.0147
Mass Fraction			
HFP	0.0319	0.0004	0.5848
HFPO	0.0220	0.0000	0.4087
Toluene	0.0000	0.0000	0.0000
CO_2	0.0000	0.0000	0.0000
R116	0.9461	0.9996	0.0066
Total Flow [kg•hr^{-1}]	41.6234	39.3811	2.2423
Temperature [K]	198.96	194.98	239.10
Pressure [atm]	1	1	1
Vapour Fraction	1	1	0
Liquid Fraction	0	0	1

Table 7.42. Stream results for column C3 for the R116 process.

7.5.2.5. Stripper STR2

The second stripping unit STR2 was a trayed column which contained a partial vapour condenser to ensure a vapour distillate. The design specifications for STR2 are presented in Table 7.43. STR2 contained 25 equilibrium stages (including the condenser) and the distillate rate was set to 40.6334 kg•hr^{-1} which was equivalent to the amount of R116 and HFP in the feed stream before the recycle loop was closed. The liquid HFP and HFPO feed stream, C3BOTTS was introduced at stage 1 and the gaseous R116 was introduced at stage 25. The vapour distillate left STR2 at stage 1, with the liquid stream leaving STR2 at stage 25. The operating pressure of the column was set to 1 atm as discussed in the preceding sections. The condenser duty was observed as -0.4926 kW with an associated condenser temperature of 197.13 K, with a bottoms stage, stage 25, temperature of 210.03 K.

Table 7.44 presents the stream results for unit STR2. C3BOTTS denotes the liquid feed stream entering the unit, C3TOPS denotes the gaseous solvent R116 stream, STR2VAP the exiting vapour stream and

STR2LIQ the exiting liquid stream. The function of the stripper was to re-contact the vapour and liquid streams separated in column C3 to allow the gaseous R116 to selectively strip HFP from the HFP and HFPO liquid feed stream which would result in an exiting liquid stream, STR2LIQ, concentrated in HFPO.

From the analysis of the data presented in Table 7.44 the exiting vapour stream contained 99.80 % of the HFP that entered in the feed stream C3TOPS, 32.16 % of the HFPO and 99.10 % of the R116. The remaining R116 was absorbed into the liquid phase. The low recovery of HFPO in the liquid phase and the low purity HFP stream in the gaseous phase signified that the second stripper unit was not sufficient to meet product specifications. As a result, the exiting vapour stream STR2VAP was sent to a distillation column C4 to produce a gaseous R116 and a liquid HFP and HFPO stream which were to be re-contacted in a further stripping unit.

The exiting liquid phase which contained 0.6216 $kg \cdot hr^{-1}$ HFPO, or rather 67.83 % of the HFPO in the feed, 0.3660 $kg \cdot hr^{-1}$ of R116 and 0.0024 $kg \cdot hr^{-1}$ of HFP was sent to a distillation column C5 for further purification.

Specification	Value
N_T	25
Condenser Type	Partial Vapour
Distillate Rate [$kg \cdot hr^{-1}$]	40.6334
Liquid Feed Stage	1
Vapour Feed Stage	26
Liquid Product Stage	26
Vapour Product Stage	1
P_{COLUMN} [atm]	1
Condenser Duty [kW]	-0.4926
Condenser Temperature [K]	197.13
Bottom Stage Temperature [K]	210.03

Table 7.43. Column specifications for stripper STR2 for the R116 process.

	C3TOPS	C3BOTTS	STR2VAP	STR2LIQ
Mole Fraction				
HFP	0.0004	0.6083	0.0301	0.0025
HFPO	0.0000	0.3842	0.0061	0.5840
Toluene	0.0000	0.0000	0.0000	0.0000
CO_2	0.0000	0.0000	0.0000	0.0000
R116	0.9996	0.0074	0.9638	0.4135
Mass Flow [kg•hr^{-1}]				
HFP	0.0164	1.3112	1.3252	0.0024
HFPO	0.0000	0.9164	0.2947	0.6216
Toluene	0.0000	0.0000	0.0000	0.0000
CO_2	0.0000	0.0000	0.0000	0.0000
R116	39.3647	0.0147	39.0135	0.3660
Mass Fraction				
HFP	0.0004	0.5848	0.0326	0.0024
HFPO	0.0000	0.4087	0.0073	0.6279
Toluene	0.0000	0.0000	0.0000	0.0000
CO_2	0.0000	0.0000	0.0000	0.0000
R116	0.9996	0.0066	0.9601	0.3697
Total Flow [kg•hr^{-1}]	39.3811	2.2423	40.6334	0.9900
Temperature [K]	273.00	239.10	197.13	210.04
Pressure [atm]	1	1	1	1
Vapour Fraction	1	0	1	0
Liquid Fraction	0	1	0	1

Table 7.44. Stream results for stripper STR2 for the R116 process.

7.5.2.6. Column C4

Column C4 was a conventional distillation column which employed a partial vapour condenser and a kettle reboiler. The design specifications for column C4 are presented in Table 7.45. The purpose of column C4 was to separate the exiting vapour stream STR2VAP of stripping unit STR2, into a vapour stream of pure R116 and a liquid stream of HFP and HFPO, such that the vapour and liquid streams could be re-contacted in a further stripping unit. The feed, distillate and bottoms streams of column C4 are presented in Table 7.46 as STR2VAP or C4FEED, C4TOPS and C4BOTTS respectively. The feed stream to C4 was the exiting vapour stream STR2VAP of STR2.

C4 had 30 equilibrium stages (including the condenser and reboiler) and a distillate rate of 39.0151 kg•hr^{-1} which was initially equivalent to total flow of R116 in the feed stream to column C4 before the recycle loop was closed. The RR was determined by the DSV function of Aspen as 0.8629. The column operating pressure was set to 1 atm. The optimum feed stage to the column, with respect to minimizing the reboiler heat input, was determined to be stage 20 which resulted in a reboiler duty of 1.0380 kW. The vapour R116

distillate was removed from the partial condenser, with the liquid bottoms product removed from the final stage, with no intermediate side streams. The condenser duty was determined as -1.0863 kW with a condenser temperature of 194.96 K and a final stage temperature of 239.93 K to ensure that the bottoms product was liquid HFP and HFPO.

From an analysis of Table 7.46, 100 % of the R116 that entered the column via C4FEED or STR2VAP, exited the column as the vapour distillate stream C4TOPS. The only other component exiting the vapour distillate stream was 0.0016 $kg \cdot hr^{-1}$ of HFP.

The liquid bottoms stream from column C3 contained all of the HFPO, 99.88 % of the HFP that was present in the feed at a pressure of 1 atm and temperature of 239.93 K.

Specification	Value
N_T	30
Condenser Type	Partial Vapour
Distillate Rate [$kg \cdot hr^{-1}$]	39.0151
Molar Reflux Ratio	0.8629
Feed Stage	20
Solvent Feed Stage	-
Top Product Stage	1
Bottom Product Stage	30
P_{COLUMN} [atm]	1
Condenser Duty [kW]	-1.0863
Condenser Temperature [K]	194.96
Reboiler Duty [kW]	1.0380
Reboiler Temperature [K]	239.93

Table 7.45. Column specifications for column C4 for the R116 process.

	STR2VAP	C4BOTTS	C4TOPS
Mole Fraction			
HFP	0.0301	0.8325	0.0000
HFPO	0.0061	0.1675	0.0000
Toluene	0.0000	0.0000	0.0000
CO_2	0.0000	0.0000	0.0000
R116	0.9638	0.0000	1.0000
Mass Flow [kg•hr^{-1}]			
HFP	1.3252	1.3236	0.0016
HFPO	0.2947	0.2947	0.0000
Toluene	0.0000	0.0000	0.0000
CO_2	0.0000	0.0000	0.0000
R116	39.0135	0.0000	39.0135
Mass Fraction			
HFP	0.0326	0.8179	0.0000
HFPO	0.0073	0.1821	0.0000
Toluene	0.0000	0.0000	0.0000
CO_2	0.0000	0.0000	0.0000
R116	0.9601	0.0000	1.0000
Total Flow [kg•hr^{-1}]	40.6334	1.6183	39.0151
Temperature [K]	197.13	239.93	194.96
Pressure [atm]	1	1	1
Vapour Fraction	1	0	1
Liquid Fraction	0	1	0

Table 7.46. Stream results for column C4 for the R116 process.

7.5.2.7. Stripper STR3

The third stripping unit STR3 was a trayed column which employed a partial vapour condenser to ensure a vapour distillate or exiting vapour stream. The design specifications for STR3 are presented in Table 7.47. STR3 contained 18 equilibrium stages (including the condenser) and the distillate rate was set to 40.3234 kg•hr^{-1} which was equivalent to the amount of R116 and HFP in the feed stream before the recycle loop was closed. The operating pressure of the column was set to one atm as discussed in the preceding sections. The condenser duty was observed as -0.4865 kW with an associated condenser temperature of 196.52 K, with a bottoms stage (stage 18) temperature of 210.01 K.

Table 7.48 presents the stream results for unit STR3. C4BOTTS denotes the liquid feed stream entering the unit, C4TOPS denotes the gaseous solvent R116 stream, STR3VAP the exiting vapour stream and STR3LIQ the exiting liquid stream. The function of the stripper was to re-contact the vapour and liquid streams separated in column C4 to allow the gaseous R116 to selectively strip HFP from the HFP and HFPO liquid feed stream which would result in an exiting liquid stream, STR3LIQ, concentrated in HFPO.

From the analysis of the data presented in Table 7.48 the exiting vapour stream contained 99.96 % of the HFP that entered in the feed stream C4TOPS, 33.89 % of the HFPO and 99.71 % of the R116. The remaining R116 was absorbed into the liquid phase. Only a small amount of HFPO was present in the STR3VAP stream (0.0999 $kg \cdot hr^{-1}$ HFPO) and it was deemed not necessary to employ a fourth stripper to recover the remaining HFPO. The exiting vapour stream STR3VAP was thus sent to the primary solvent recovery column C6.

The exiting liquid phase which contained 0.1948 $kg \cdot hr^{-1}$ HFPO, (66.10 % of the HFPO in the feed), 0.1148 $kg \cdot hr^{-1}$ of R116, and 0.0004 $kg \cdot hr^{-1}$ of HFP was sent to a distillation column C5 for further purification.

Specification	Value
N_T	18
Condenser Type	Partial Vapour
Distillate Rate [$kg \cdot hr^{-1}$]	40.3234
Liquid Feed Stage	1
Vapour Feed Stage	18
Liquid Product Stage	18
Vapour Product Stage	1
P_{COLUMN} [atm]	1
Condenser Duty [kW]	-0.4865
Condenser Temperature [K]	196.52
Bottom Stage Temperature [K]	210.01

Table 7.47. Column specifications for stripper STR3 for the R116 process.

	C4TOPS	C4BOTTS	STR3VAP	STR3LIQ
Mole Fraction				
HFP	0.0000	0.8325	0.0303	0.0015
HFPO	0.0000	0.1675	0.0021	0.5844
Toluene	0.0000	0.0000	0.0000	0.0000
CO_2	0.0000	0.0000	0.0000	0.0000
R116	1.0000	0.0000	0.9676	0.4141
Mass Flow [kg•hr^{-1}]				
HFP	0.0016	1.3236	1.3247	0.0004
HFPO	0.0000	0.2947	0.0999	0.1948
Toluene	0.0000	0.0000	0.0000	0.0000
CO_2	0.0000	0.0000	0.0000	0.0000
R116	39.0135	0.0000	38.8987	0.1148
Mass Fraction				
HFP	0.0000	0.8179	0.0329	0.0014
HFPO	0.0000	0.1821	0.0025	0.6284
Toluene	0.0000	0.0000	0.0000	0.0000
CO_2	0.0000	0.0000	0.0000	0.0000
R116	1.0000	0.0000	0.9647	0.3702
Total Flow [kg•hr^{-1}]	39.0151	1.6183	40.3234	0.3100
Temperature [K]	273.00	239.93	196.52	210.01
Pressure [atm]	1	1	1	1
Vapour Fraction	1	0	1	0
Liquid Fraction	0	1	0	1

Table 7.48. Stream results for stripper STR3 for the R116 process.

7.5.2.8. Column C5

The design specifications for column C5 are presented in Table 7.49. The purpose of column C5 was to combine the exiting HFPO rich liquid streams from the three stripping units, streams STR1LIQ, STR2LIQ and STR3LIQ to produce a vapour distillate of pure R116 and a bottoms liquid product of high purity HFPO. The feed, distillate and bottoms streams of column C5 are presented in Table 7.50 as C5FEED, C5TOPS and C5BOTTS respectively. The feed stream to C5 was obtained by mixing the three HFPO rich product streams before entry into column C5.

C5 had 28 equilibrium stages (including the condenser and reboiler) and a distillate rate of 1.6731 kg•hr^{-1} which was initially equivalent to the total flow of the lighter component R116 in the feed stream to column C5 before the recycle loop was closed. The RR was determined by the DSV function of Aspen as 0.4744. The column operating pressure was set to 1 atm. The optimum feed stage to the column, with respect to minimizing the reboiler heat input, was determined to be stage 8 which resulted in a reboiler duty of 0.0923 kW. The vapour R116 distillate was removed from the partial condenser, with the liquid bottoms product

removed from the final stage, with no intermediate side streams. The condenser duty was determined as -0.0257 kW with a condenser temperature of 195.05 K, and a final stage temperature of 241.54 K to ensure a liquid bottoms product concentrated in HFPO.

From an analysis of Table 7.50, 99.90 % of the R116 that entered the column via C5FEED, exits the column as the vapour distillate stream C5TOPS. Other components exiting the vapour distillate stream are 0.0002 $kg \cdot hr^{-1}$ of HFP and 0.0012 $kg \cdot hr^{-1}$ of HFPO. This stream which consisted primarily of R116 was mixed with the vapour distillate stream of column C6 and used for solvent recycle to stripping unit STR1.

The liquid bottoms stream from column C5 contained 99.96 % HFPO, 96.61 % of the HFP and 0.09 % of the R116 that was present in the feed at a pressure of 1 atm and temperature of 241.54 K. This stream represented the final HFPO rich product stream desired by PELCHEM and was available at a purity of 99.71 % HFPO mole.

Specification	Value
N_T	16
Condenser Type	Partial Vapour
Distillate Rate [$kg \cdot hr^{-1}$]	1.6731
Molar Reflux Ratio	0.4744
Feed Stage	8
Solvent Feed Stage	-
Top Product Stage	1
Bottom Product Stage	16
P_{COLUMN} [atm]	1
Condenser Duty [kW]	-0.0257
Condenser Temperature [K]	195.05
Reboiler Duty [kW]	0.0923
Reboiler Temperature [K]	241.54

Table 7.49. Column specifications for column C5 for the R116 process.

	C5FEED	C5TOPS	C5BOTTS
Mole Fraction			
HFP	0.0014	0.0001	0.0022
HFPO	0.5847	0.0006	0.9971
Toluene	0.0000	0.0000	0.0000
CO_2	0.0000	0.0000	0.0000
R116	0.4139	0.9993	0.0007
Mass Flow [kg•hr^{-1}]			
HFP	0.0059	0.0002	0.0057
HFPO	2.8429	0.0012	2.8417
Toluene	0.0000	0.0000	0.0000
CO_2	0.0000	0.0000	0.0000
R116	1.6732	1.6716	0.0016
Mass Fraction			
HFP	0.0013	0.0001	0.0020
HFPO	0.6287	0.0007	0.9974
Toluene	0.0000	0.0000	0.0000
CO_2	0.0000	0.0000	0.0000
R116	0.3700	0.9991	0.0005
Total Flow [kg•hr^{-1}]	4.5220	1.6731	2.8489
Temperature [K]	210.02	195.05	241.54
Pressure [atm]	1	1	1
Vapour Fraction	0	1	0
Liquid Fraction	1	0	1

Table 7.50. Stream results for column C5 for the R116 process.

7.5.2.9. Column C6

The design specifications for column C6 are presented in Table 7.51. The purpose of column C6 was to recover the gaseous solvent R116 from the STR3VAP vapour stream and produce the HFP rich product stream desired by PELCHEM for recycle for conversion into HFPO. The feed, distillate and bottoms streams of column C6 are presented in Table 7.52 as STR3VAP or C6FEED, C6TOPS and C6BOTTS respectively. The feed stream to C6 was the exiting vapour stream STR3VAP of STR3.

C6 had 24 equilibrium stages (including the condenser and reboiler) and a distillate rate of 38.9004 kg•hr^{-1} which was initially equivalent to total flow of R116 in the feed stream to column C6 before the recycle loop was closed. The molar reflux ratio was determined by the DSV function of Aspen as 0.8359. The column operating pressure was set to 1 atm. The optimum feed stage to the column, with respect to minimizing the reboiler heat input, was determined to be stage 18 which resulted in a reboiler duty of 1.0092 kW. The vapour R116 distillate was removed from the partial condenser, with the liquid bottoms product removed

from the final stage, with no intermediate side streams. The condenser duty was determined as -1.0491 kW with a condenser temperature of 194.96 K, and a final stage temperature of 239.65 K.

From an analysis of Table 7.52, 99.99 % of the R116 that entered the column via C6FEED or STR4VAP, exited the column as the vapour distillate stream C6TOPS. The only other component exiting the vapour distillate stream was 0.0037 $kg \cdot hr^{-1}$ of HFP. This R116 rich stream was mixed with the vapour distillate stream of column C5 and split into a purge stream and a solvent recycle stream.

The liquid bottoms stream from column C6 contained all of the HFPO, 99.73 % of the HFP and 0.005 % of the R116 that was present in the feed at a pressure of 1 atm and temperature of 239.65 K. This stream enriched with HFP at a purity of 93.45 % HFP mole was desired by PELCHEM for recycle for conversion to HFPO.

Specification	Value
N_T	24
Condenser Type	Partial Vapour
Distillate Rate [$kg \cdot hr^{-1}$]	38.9004
Molar Reflux Ratio	0.8359
Feed Stage	18
Solvent Feed Stage	-
Top Product Stage	1
Bottom Product Stage	24
P_{COLUMN} [atm]	1
Condenser Duty [kW]	-1.0491
Condenser Temperature [K]	194.96
Reboiler Duty [kW]	1.0092
Reboiler Temperature [K]	239.65

Table 7.51. Column specifications for column C6 for the R116 process.

	C6FEED	C6TOPS	C6BOTTS
Mole Fraction			
HFP	0.0303	0.0001	0.9345
HFPO	0.0021	0.0000	0.0639
Toluene	0.0000	0.0000	0.0000
CO_2	0.0000	0.0000	0.0000
R116	0.9676	0.9999	0.0016
Mass Flow [kg•hr^{-1}]			
HFP	1.3247	0.0037	1.3211
HFPO	0.0999	0.0000	0.0999
Toluene	0.0000	0.0000	0.0000
CO_2	0.0000	0.0000	0.0000
R116	38.8987	38.8967	0.0021
Mass Fraction			
HFP	0.0329	0.0001	0.9283
HFPO	0.0025	0.0000	0.0702
Toluene	0.0000	0.0000	0.0000
CO_2	0.0000	0.0000	0.0000
R116	0.9647	0.9999	0.0014
Total Flow [kg•hr^{-1}]	40.3234	38.9004	1.4231
Temperature [K]	196.52	194.96	239.65
Pressure [atm]	1	1	1
Vapour Fraction	1	1	0
Liquid Fraction	0	0	1

Table 7.52. Stream results for column C6 for the R116 process.

7.5.2.10. Selected Stream Information

Table 7.53 presents the stream results for the fresh solvent and solvent purge streams for the R116 separation process. The purge stream represents the exit point for the bulk of the solvent in the R116 separation process. The fresh solvent stream contained 28.4014 kg•hr^{-1} of pure R116. Before a recycle loop was utilised, a fresh solvent feed rate of approximately 45 kg•hr^{-1} of R116 was required to meet the desired product purities and recoveries of PELCHEM. The original fresh solvent feed rate of R116 required for the process was determined by a sensitivity analysis. The application of the recycle loop enable the required fresh solvent feed rate of R116 to be dramatically decreased to 28.4014 kg•hr^{-1}, which was approximately one and a half times less than the original fresh solvent requirements. From the analysis of the purge stream, it was evident that the flowrate of R116 exiting the system was 28.3979 kg•hr^{-1} which was less than the fresh solvent feed rate of 28.4014 kg•hr^{-1} by an amount of 0.0037 kg•hr^{-1} of R116. The remaining R116 from the fresh solvent stream exited the R116 separation process in the HFP and HFPO product streams which contained 0.0021 and 0.0016 kg•hr^{-1} of R116 respectively.

	Fresh Solvent	Purge
Mole Fraction		
HFP	0.0000	0.0001
HFPO	0.0000	0.0000
Toluene	0.0000	0.0000
CO_2	0.0000	0.0000
R116	1.0000	0.9999
Mass Flow [kg•hr^{-1}]		
HFP	0.0000	0.0027
HFPO	0.0000	0.0009
Toluene	0.0000	0.0000
CO_2	0.0000	0.0000
R116	28.4014	28.3979
Mass Fraction		
HFP	0.0000	0.0001
HFPO	0.0000	0.0000
Toluene	0.0000	0.0000
CO_2	0.0000	0.0000
R116	1.0000	0.9999
Total Flow [kg•hr^{-1}]	28.4014	28.4014
Temperature [K]	273.00	273.00
Pressure [atm]	1	1
Vapour Fraction	1	1
Liquid Fraction	0	0

Table 7.53. Stream results for the fresh solvent and purge streams for the R116 process.

Table 7.54 presents a summary of selected key streams in the R116 separation process for ease of reference. The toluene rich stream C2BOTTS, the HFPO product stream C5BOTTS and the HFP product stream C6BOTTS are presented. The overall feed stream to the process, C1FEED is of the exact composition and conditions of the feed stream to the toluene separation process. From Table 7.54, all of the toluene that was present in the C1FEED stream, 0.0778 kg•hr^{-1} was removed in column C2.

The overall product recovery for HFPO was 96.57 % at a product purity of 99.71 % (mole). The only impurities in the HFPO product stream were HFP and R116 which were deemed admissible by PELCHEM. The HFPO product purity desired by PECLHEM was 99.9 % and the value obtained from the R116 separation process was close to the desired specification.

The overall HFP product recovery was 99.36 % at a product purity of 93.45 % (mole) HFP. Impurities in this product stream were R116 and HFPO were allowed by PELCHEM. PELCHEM desired an HFP stream of minimum purity 95 % (mole) HFP, unfortunately this specification could not be met with the R116 process without employing a fourth stripping unit. If a fourth stripping unit were employed, it would result

in the addition of a further distillation column C7 to purify the HFP product stream, as a result it was deemed not feasible to add a fourth stripping unit.

	Toluene Stream	HFPO Product Stream	HFP Product Stream
Mole Fraction			
HFP	0.0010	0.0022	0.9345
HFPO	0.0000	0.9971	0.0639
Toluene	0.9989	0.0000	0.0000
CO_2	0.0000	0.0000	0.0000
R116	0.0000	0.0007	0.0016
Mass Flow [kg•hr^{-1}]			
HFP	0.0001	0.0057	1.3211
HFPO	0.0000	2.8417	0.0999
Toluene	0.0778	0.0000	0.0000
CO_2	0.0000	0.0000	0.0000
R116	0.0000	0.0016	0.0021
Mass Fraction			
HFP	0.0017	0.0020	0.9283
HFPO	0.0000	0.9974	0.0702
Toluene	0.9983	0.0000	0.0000
CO_2	0.0000	0.0000	0.0000
R116	0.0000	0.0005	0.0014
Total Flow [kg•hr^{-1}]	0.0779	2.8489	1.4231
Temperature [K]	515.64	241.54	239.65
Pressure [atm]	15	1	1
Vapour Fraction	0	0	0
Liquid Fraction	1	1	1

Table 7.54. Stream results for the overall feed stream, Toluene stream, HFPO product stream and HFP product stream for the R116 process.

7.5.3. Comparison of the Toluene and R116 separation processes

With the preliminary design of two competing processes for the separation of HFP and HFPO undertaken, certain factors were used as a basis of comparison between the processes. These factors included the overall product recoveries and purities of each process, energy usage in terms of total reboiler and condenser duties, the number of individual key unit operations i.e. distillation columns and stripping units, solvent usage before and after employing a recycle loop, solvent availably, environmental considerations and the patent status of each process. Table 7.55 presents the comparison of the two processes numerically where possible.

		Toluene Process	R116 Process
Patent Status			
	Solvent and Process	Yes	No
Unit Operations			
	Distillation Columns	3	6
	Strippers	-	3
Energy			
	Reboilers [kW]	16.05	3.47
	Condensers [kW]	-0.80	-4.98
Product Purities			
	HFPO [mole %]	99.88	99.71
	HFP [mole %]	96.41	93.45
Product Recovery			
	HFPO [%]	98.46	96.57
	HFP [%]	99.42	99.36
Solvent Usage			
	Before Recycle [$kg \cdot hr^{-1}$]	54.0000	45.0000
	After Recycle [$kg \cdot hr^{-1}$]	11.8814	20.4014
Miscellaneous			
	Solvent Flammability	Highly Flammable	Non Flammable
	Solvent ODP	-	0
	Solvent Toxicity	Harmful	Non Toxic
	Solvent Availability	Not Available	Available Onsite

Table 7.55. Comparison between the Toluene and R116 separation processes.

With regards to the patent status of the separation processes and technology, both the solvent and extractive distillation procedure utilising toluene have been previously patented ((Wiist 1967)) for the du Pont Company. A literature review of the various patent databases revealed that the solvent R116 has not yet been patented for the separation of HFP and HFPO. The literature review also revealed that the process of gas stripping for the separation of HFP and HFPO has not been utilised prior to this work. The fact that the solvent toluene and any extractive distillation procedure utilising toluene has been patented makes the use of this technology and process unattractive in a commercial sense as the associated patent royalty fees are a significant prohibitive factor. Conversely, this accentuates the viability of the separation process designed around the gaseous solvent R116 as there are no prohibitive licensing fees to consider.

With only the preliminary design of the separation processes undertaken, it was not possible to perform a reliable costing estimate for each of the processes. However, the number of unit operations employed by each separation process gives a qualitative indication of a portion of the direct costs or fixed capital required for each scheme. In terms of unit operations, the toluene process has a significant advantage over the R116 separation process. For the feed conditions prescribed by PELCHEM, the toluene process utilises, at most, three columns. Two of the columns are conventional distillation columns with the third column an

extractive distillation column. The R116 separation process utilises nine key unit operations viz. six conventional distillation columns and three strippers employing partial condensers. The three columns of the toluene separation process compared to the nine columns of the R116 separation processes indicates that the fixed capital or direct costs required for the R116 separation process is significantly greater than the toluene process for the same initial feed conditions.

The energy usage and thus the bulk of the operating costs for each process could not be quantified in a systematic manner. Due to the preliminary nature of the design, the reliable determination of the heat exchanger surface areas, refrigerant requirements, compression costs, heating costs and cooling costs were beyond the scope of this project. To obtain an approximate indication of the energy requirements for each process, the sum of the reboiler and the condensers duties of each process were evaluated and compared. This comparison can not be considered indicative of the total energy requirements of each individual process as further factors which contribute to the energy costs of a plant could not be taken into account. However, the comparison of the energy requirements of the key unit operations was the only valid basis from which to qualitatively compare the processes. With regards to this comparison, the R116 separation process holds a significant advantage over the toluene process. The total reboiler heat input required for the three columns for the toluene separation process is 16.05 kW as compared to 3.47 kW for the R116 process. This is despite the R116 process containing twice the amount of distillation columns as the toluene separation process. The large energy requirements of the toluene process stems from the fact that toluene is a non-volatile component and as such large amounts of energy are required to heat the solvent, whereas the solvent R116 is volatile and a gas at room temperature. With respect to the condenser energy requirements, the toluene separation process requires 0.80 kW of energy to be removed from the entire process whereas the R116 process requires 4.98 kW of energy to be removed. The significantly higher condenser duties for the R116 processes is a result of each condenser found on nine key unit operations, coupled with the fact that large amounts of energy need to be removed to condense the volatile gaseous key components HFP and HFPO.

PELCHEM desired an HFPO product purity of 99.9 % HFPO (mole) if possible. The toluene process produced the HFPO stream that was closest to the desired product specification of 99.88 % HFPO (mole). The R116 separation process yielded a product stream of 99.71 % HFPO (mole), which was lower than the product specification desired by PELCHEM and lower than that of the toluene separation process, yet still commercially viable when compared to the commercial grade HFPO product presented in Table 1.1. Although PELCHEM did not specify the required product recoveries, these values were evaluated for the individual processes. The toluene process exhibited an overall product recovery of HFPO of 98.46 %, while the R116 process exhibited a slightly lower overall HFPO product recovery of 96.57 %. For the HFP product stream, PECLHEM required an HFP product stream of minimum purity 95 % HFP (mole). The toluene process produced the highest product purity of 96.41 % HFP (mole) while the R116 process was

only able to produce an HFP stream of 93.45 % HFP (mole). In terms of HFP product recovery, both processes produced similar overall HFP recovery values of 99.42 % and 99.36 % for the toluene and R116 separation processes respectively.

A further factor that was used as a basis of comparison for the two individual separation processes was the solvent usage before and after recycle. Solvent usage was an important factor as there are additional considerations that depend on the amount of solvent viz. the financial implications of the solvent, disposal considerations and increased throughput of large solvent volumes leading to higher operating costs. Before the utilization of a solvent recycle loop, the minimum amount of solvent required by the R116 separation process was less than that of the toluene process. The R116 process required 45 $kg \cdot hr^{-1}$ of fresh solvent before recycle whereas the toluene process required 54 $kg \cdot hr^{-1}$ of fresh solvent before recycle. After a solvent recycle loop was utilised, this condition was reversed. The amount of fresh solvent required for the toluene process was 11.8814 $kg \cdot hr^{-1}$ as compared to a fresh solvent flowrate of 20.4014 $kg \cdot hr^{-1}$ as required for the R116 process. The slightly lower product purities obtained for the R116 process resulted from the procedure of attempting to maximise the amount of R116 that was recycled in the R116 separation process. Higher product purities comparable to the toluene separation process can be achieved by the R116 separation process, however this is only at the expense of a higher fresh solvent flow rate of R116 and lower recycled solvent rate. As a result, the HFP and HFPO product streams of the R116 process were deemed acceptable as the reduction in fresh solvent flowrate, and associated economical benefits, compensated for the slightly higher HFP impurities in the HFPO product stream and R116 impurities in the HFP product stream.

As a final basis of comparison between the two developed separation processes, miscellaneous factors such as health, safety considerations, and solvent availability were examined. With respect to the availability of the solvents, PELCHEM originally chose the solvent R116 from the list of ten solvents proposed in August 2006, due to the fact that R116 was produced onsite at the Pelindaba facility in Pretoria. With any separation process involving a solvent, a significant fraction of the operating costs are consumed by the solvent requirements ((Lei et al. 2003)). With R116 available onsite the purchase cost of the solvent is dramatically decreased and additional costs such as transportation, storing, and handling are bypassed, whereas for the toluene process, the liquid solvent would have to be purchased externally, transported to the site and stored. The immediate availability of R116 and the beneficial financial implications which arise from this fact thus gave the R116 separation process a significant advantage over the toluene process. From a safety and environmental viewpoint, the solvent R116 once again has a significant advantage over toluene. R116 is a fluorocarbon with an ODP value of zero which indicates that it is not an ozone depleting substance and is not restricted by the Montreal Protocol. R116 is also an environmentally benign substance as it is non-flammable and non-toxic with no reported LD_{50} oral or dermal values. toluene is a highly flammable liquid which is harmful to organisms. It has an LD_{50} oral value of 636 $mg \cdot kg^{-1}$ and an LD_{50}

dermal value of 12124 $mg \cdot kg^{-1}$ which indicated that special considerations with regards to the handling of accidental spills, releases and disposal any toluene containing streams have to be taken into account.

Although the toluene separation process utilises fewer key unit operations (which is directly related to the required fixed capital costs) and exhibits higher product purities, recoveries and lower solvent usage after recycle, the R116 separation scheme still remains an attractive alternative. This is due to the lower energy usage (which is directly related to operating costs and thus significant in the context of the current energy crisis climate in South Africa), the novel nature of the solvent and developed process, solvent availability and health and safety considerations. Since the toluene solvent and any extractive process utilising toluene as a solvent is patented, exorbitant license fees diminish the viability of the process, whereas with the R116 process, the possibility exists to patent the solvent and associated process as well as to lease out the intellectual property to interested third-parties or companies.

The toluene and R116 separation processes both satisfied the primary aim of the research project: the development of a separation scheme to effect the separation of a stream of HFP and HFPO. The R116 separation process achieved product purities comparable to the toluene separation process and is a novel process requiring no patent or royalty fees. It can be said from the preliminary design that the R116 separation process was comparable with, and surpassed the similarly designed toluene separation process. As such the R116 process can be recommended as a suitable alternative to a separation process involving the patented solvent toluene.

CHAPTER EIGHT

8. CONCLUSIONS

The aim of this project was to propose a separation scheme for a mixture containing the fluorinated hydrocarbons Hexafluoropropylene (HFP) and Hexafluoropropylene oxide (HFPO). A solvent selection procedure was utilised and an initial list of two hundred and seven candidate solvents for the separation of HFP and HFPO compiled. This list was narrowed down on the basis of selectivity values at infinite dilution to a list of thirty solvents. This list of thirty solvents was further shortened on the basis of individual solvent properties to a final list of ten solvents which was presented to PELCHEM in August 2006. PELCHEM chose two solvents for this work, the liquid solvent toluene and the gaseous solvent R116, with the aim of designing an extractive distillation process for the solvent toluene and a supercritical extraction process using supercritical R116.

The lack of published vapour-liquid equilibrium data involving HFP, HFPO and the solvents toluene and R116 necessitated the experimental determination of the HPVLE relationships involving these systems. The experimental measurements were undertaken during a three month period in 2006 at Ecoles des Mines de Paris in Fontainebleau, France at the TEP laboratories. Experimental measurements for the following four binary systems were performed: HFP + toluene, HFPO + toluene, R116 + HFP and R116 + HFPO. The four binary systems were each measured at two isotherms, 273.15 and 313.15 K. In addition to the HPVLE binary data, pure component vapour pressure measurements for the component HFPO were undertaken in the temperature range of 271.90 to 318.20 K. The four sets of binary HPVLE data as well as the pure component HFPO vapour pressure measurements constitute new data as they represent previously unpublished systems and therefore make a positive contribution to the field of HPVLE measurements for the Thermodynamics Research Unit at the University of KwaZulu-Natal.

The measured binary HPVLE data were modelled in the computer software Thermopack using the direct method. Various combinations of popular thermodynamic models were used to correlate the experimental data. These combinations of models involved popular equation of state models, in conjunction with mixing rules to extend the use of the models to mixtures. The models utilised were the Peng-Robinson or Soave-Redlich-Kwong EOS with either the Modified-Huron-Vidal first order or Wong-Sandler mixing rules. For each of the models, the Mathias-Copeman alpha function was used to obtain a better representation of pure component vapour pressures, and the NRTL activity coefficient model employed. Due to a lack of experimental data, binary data for the system HFP + HFPO at 273.15 and 313.15 K was predicted via the Soave-Redlich-Kwong EOS and the PSRK UNIFAC activity coefficient model.

The three model sets were used to correlate the experimental data and the model parameters were optimized using a least squares regression method. On the basis of the modeling results obtained the model set utilising the Peng-Robinson EOS with the Wong-Sandler mixing rules provided the most consistent and accurate description of the measured HPVLE data.

Two processes to effect the separation of a stream of HFP and HFPO were designed and simulated in the Aspen Plus engineering suite. The toluene separation process involved the extractive distillation of a stream of HFP and HFPO through the addition of the liquid solvent toluene, to alter the relative volatility of the mixture to make it amenable to separation. The toluene separation process consisted of three key unit operations and resulted in an HFPO product stream of 99.88 % purity (mole) and an HFP product stream of 96.41 % (mole). The R116 separation process was initially designed to be a supercritical extraction process utilising supercritical R116. Initial process design revealed the process of supercritical extraction was not feasible. The process of gas stripping with the gaseous solvent R116 was thus proposed and the R116 separation process designed. The R116 separation process consisted of nine key unit operations, (three stripping units and six distillation columns), which resulted in an HFPO product stream of 99.71 % HFPO (mole) and an HFP product stream of 93.45 % (mole). Comparison of the two processes were made on the basis of patent issues, the number of key unit operations, basic energy requirements, product purities, product recoveries, solvent usage, solvent availability and safety and environmental considerations.

The toluene and R116 separation processes that were designed satisfied the primary aim of this research project, which was the proposal of a separation scheme to effect the separation of HFP and HFPO. On the basis that the R116 process designed for this project achieved product purities comparable to the toluene process and is a novel process requiring no patent or royalty fees, it can be said that the R116 process was comparable with and surpassed the similarly designed toluene process. As such the R116 separation process can be recommended as a suitable alternative to toluene separation process for the separation of HFP and HFPO. The research work in its entirety was presented to PELCHEM in October 2007. PECLHEM took the decision to initiate, as future work, a more detailed design of the R116 separation process utilising newly measured HPVLE data for the systems in the 200.15 K range, as well as laboratory testing to confirm the efficacy of the R116 process. Pending the outcome of the further work on the R116 process, PELCHEM plans to patent the solvent and the associated process.

CHAPTER NINE

9. RECOMMENDATIONS

1. *Further high pressure vapour-liquid equilibrium measurements:* Further binary HVLE measurements should be undertaken for the specific systems utilised in this project. Binary HPVLE data for the system HFP + HFPO were not measured for this research project, with predicted data utilised in all simulations. Measurements for the system HFP + HFPO are recommended for three isotherms 200.15, 273.15 and 313.15 K. The design of the R116 separation process incorporated data measured at 273.15 K which was extrapolated to 200.15 K. Although the equation of state model and mixing rules utilised allowed for the extrapolation of data over appreciable temperature ranges ((Wong et al. 1992a)), it is recommended that the binary systems R116 + HFP and R116 + HFPO be measured at the 200.15 K isotherm and the experimental data regressed to obtained new model parameters which can be utilised in the Aspen simulation in conjunction with the data regressed for the binary system HFP + HFPO.

2. *Detailed process design for the toluene and R116 processes*: For this research project only a preliminary design for the toluene and R116 separation processes were performed. It is recommended that with more detailed specifications from PELCHEM and NECSA, a detailed process design for both the processes involving the design of heat exchanger units, compression, heating and cooling calculations, equipment sizing and the investigation of process dynamics and control schemes should be undertaken such that a more effective comparison can be made between the two competing processes.

3. *Laboratory scale testing of the R116 process*: Preliminary design of the R116 process was performed on the Aspen Plus simulation engine. It is recommended that subsequent to a more detailed process design, pilot plant work for the R116 separation process should be undertaken to validate the simulation results. With the simulated results and experimental data the process can provisionally be patented.

4. *Regression of the experimental HPVLE data to obtain revised UNIFAC interaction parameters:* It is recommended that the experimental HPVLE data for the binary systems involving HFP, HFPO, toluene and R116 be regressed to obtain revised UNIFAC functional group interaction parameters. These revised functional group interaction parameters can be used to update the existing interaction parameters that were utilised in this project, and in this manner an updated database of parameters can be constructed for use in the Thermodynamics Research Unit.

CHAPTER TEN

10. REFERENCES

Abbott, M. M. (1979). "Cubic Equations of State - Interpretive Review." *Abstracts of Papers of the American Chemical Society*, 182, 24-24.

Abrams, D. S., and Prausnitz, J. M. (1975). "Statistical thermodynamics of liquid mixtures: A new expression for the excess Gibbs energy of partly or completely miscible systems." *AICHE Journal*, 21(1), 116-127.

ACS. (2007). "SciFinder Scholar." American Chemical Society.

Aravindan, V., and Vickraman, P. (2007). "Polyvinylidenefluoride-hexafluoropropylene based nanocomposite polymer electrolytes (NCPE) complexed with $LiPF_3(CF_3CF_2)_3$." *European Polymer Journal*, 43(1), 5121-5127.

AspenTech. (2004). "Engineering Suite Aspen Plus 2004.1." AspenTech.

Atkins, G. M. (1973). "Process for the epoxidation of Hexafluoropropylene - United States Patent 3775439." U. S. Patent, ed., E. I. du Pont de Nemours and Company, 2.

Barton. (2008). "Barton Solvents Inc. Products." <http://www.barsol.com/aspx/Products.aspx> (15 January 2008).

Barwick, V. J. (1997). "Strategies for solvent selection-a literature review." *Trends in Analytical Chemistry*, 16(6), 293-309.

Bastos, J. C., Soares, M. E., and Medina, A. G. (1985). "Selection of Solvents for Extractive Distillation. A Data Bank for Activity Coefficients at Infinite Dilution." *Industrial and Engineering Chemistry Process Design and Development*, 24(1), 420-426.

Bian, J. F., Lujan, W. R., Harper-Nixon, D., Jeon, H. S., and Weinkauf, D. H. (2005). "Effect of hexafluoropropylene oxide plasma polymer particle coatings on the rheological properties of boron nitride/poly(dimethylsiloxane) composites." *Journal of Colloid and Interface Science*, 290(2), 582-591.

BIPM. (2008). "Bureau International des Poids et Mesures - ITS-90 Documents." <http://www.bipm.org/en/publications/its-90.html> (15 January 2008, 2008).

Boston, J. F., and Mathias, P. M. (Year). "Phase equilibria in a third generation process simulator." *2nd International Conference on Phase Equilibria and Fluid Properties in the Chemical Processing Industry*, Berlin.

CARB. (2008). "California Air Resources Board: Consumer product solvent DB." <http://www.arb.ca.gov/db/solvents/class.htm> (15 January 2008).

Chareton, A., Valtz, A., Laugier, S., Richon, D., and Renon, H. (1990). "Bubble pressures and saturated liquid molar volumes of binary and ternary refrigerant mixtures." *Journal of Chemical and Engineering Data*, 35(2), 162-165.

Chen, Z., Feng, Y., Yaosheng, W., and Zhaoli, T. (1989). "Isobaric vapor-liquid equilibria of the binary system of octafluorocyclobutane with dichlorodifluoromethane, chlorodifluoromethane and hexafluoropropylene." *Huagong Xuebao*, 40(1), 113-117.

Chiavone-Filho, O., Amaral Filho, P. G., Silva, D. N., and Terron, L. R. (2001). "Function for a Series of Hydrocarbons to Peng-Robinson and van der Waals Equations of State." *Industrial and Engineering Chemistry Research*, 40(26), 6240-6244.

Cho, J., Denes, F. S., and Timmons, R. B. (2006). "Plasma Processing Approach to Molecular Surface Tailoring of Nanoparticles: Improved Photocatalytic Activity of TiO_2." *Chem. Mater.*, 18(13), 2989-2996.

Coquelet, C., and Baba-Ahmed, A. (2002). "ThermoPack ver 1.10." Ecole des Mines de Paris, Laboratory of Thermodynamics and Phase Equilibria

Coquelet, C., and Baba-Ahmed, A. (2006a). "Thermopack Help (English) - A Client-Server software for experimental data managing and treatment." Ecole des Mines de Paris, Laboratory of Thermodynamics and Phase Equilibria, 33.

Coquelet, C., Chareton, A., Valtz, A., Baba-Ahmed, A., and Richon, D. (2003a). "Vapor-Liquid Equilibrium Data for the Azeotropic Difluoromethane + Propane System at Temperatures from 294.83 to 343.26 K and Pressures up to 5.4 MPa." *Journal of Chemical and Engineering Data*, 48(2), 317-323.

Coquelet, C., Nguyen Hong, D., Chareton, A., Baba-Ahmed, A., and Richon, D. (2003b). "Vapour-liquid equilibrium data for the difluoromethane+1,1,1,2,3,3,3-heptafluoropropane system at temperatures from 283.20 to 343.38 K and pressures up to 4.5 MPa." *International Journal of Refrigeration*, 26(5), 559-565.

Coquelet, C., and Richon, D. (2007). "Need of thermodynamic properties measurements and modelling in the frame of new regulations on refrigerants." *Journal of Zheijiang University Science A*, 8(5), 724-733.

Coquelet, C., Rivollet, F., Jarne, C., Valtz, A., and Richon, D. (2006). "Measurement of physical properties of refrigerant mixtures. Determination of phase diagrams." *Energy Conversion and Management*, 47(20), 3672-3680.

Coquelet, C., Valtz, A., and Richon, D. (2005). "Vapor-liquid equilibrium data for the difluoromethane (R32)-dimethyl ether (RE170) system at temperatures from 283.03 to 363.21 K and pressures up to 5.5 MPa." *Fluid Phase Equilibria*, 232(1-2), 44-49.

Darling, T. R. (1982). "Purification and polymerization of hexafluoropropylene oxide- United States Patent 4356291." U. S. Patent, ed., E. I. du Pont de Nemours and Company, 8.

DDBST. (2007). "Dortmund Data Bank (DDB)." DDBST Software and Separation Technology GmbH.

EFCTC. (2008). "European Fluorocarbons Technical Committee - Fluorocarbons and Sulphur hexafluoride." <http://www.fluorocarbons.org/> (17 January, 2008).

Fontalba, F., Richon, D., and Renon, H. (1984). "Simultaneous Determination of vapour-liquid equilibria and saturated densities up to 45 MPa and 433 K." *Review of Scientific Instruments*, 55(6), 944-951.

Fredenslund, A., Gmehling, J., and Rasmussen, P. (1977). *Vapour-Liquid Equilibria using UNIFAC*, Elsevier, Amsterdam.

Freedonia-Group. (2007). "World Fluorochemicals Forecast for 2011 and 2016 Abstract." <http://www.bharatbook.com/general/WorldFluorochemicalsForecastsfor2011&2016.pdf> (14 January, 2008).

Galivel-Solastiouk, F., Laugier, S., and Richon, D. (1986). "Vapor-liquid equilibrium data for the propane-methanol and propane-methanol-carbon dioxide system." *Fluid Phase Equilibria*, 28(1), 73-85.

Gani, R., and Brignole, E. A. (1983). "Molecular design of solvents for liquid extraction based on UNIFAC." *Fluid Phase Equilibria*, 13(1), 331-340.

Gmehling, J. (1995). "From UNIFAC to Modified UNIFAC to PSRK with the help of DDB." *Fluid Phase Equilibria*, 107(1), 1-29.

Gmehling, J. (1999). "Group Contribution Methods-ideal tools for the synthesis and design of separation processes." *Pure and Applied Chemistry*, 71(6), 939-949.

Gmehling, J. (2001). "Modified Unifac (Dortmund): Reliable Model for the development of Thermal Separation Processes." *Journal of Chemical Engineering of Japan*, 34(1), 43-54.

GNU. (2007). "The GNU General Public Licence-GNU Project-Free Software Foundation (FSF)." <http://www.gnu.org/copyleft/gpl.html> (15 January, 2008).

Guilbot, P., Valtz, A., Legendre, H., and Richon, D. (2000). "Rapid on-line sampler-injector: a reliable tool for HT-HP sampling and on-line GC analysis." *Analysis*, 28(1), 426-431.

Guillevic, J., Richon, D., and Renon, H. (1983). "Vapor-liquid equilibrium measurements up to 558 K and 7 MPa: a new apparatus." *Industrial and Engineering Chemistry Fundamentals*, 22(4), 495-499.

Guillevic, J., Richon, D., and Renon, H. (1985). "Vapor-liquid equilibrium data for the binary system water-ammonia at 403.1, 453.1, and 503.1 K up to 7.0 MPa." *Journal of Chemical and Engineering Data*, 30(3), 332-335.

Heidemann, R. A., and Khalil, A. M. (1980). "The Calculation of critical points." *AICHE Journal*, 26(5), 769-779.

Hirao, A., Sugiyama, K., and Yokoyama, H. (2007). "Precise synthesis and surface structures of architectural per- and semifluorinated polymers with well-defined structures." *Progress in Polymer Science*, 32(12), 1393-1438.

Ho, Q. N., Lee, B. G., Kim, H. G., and lim, J. S. (2004). "Vapor-liquid equilibria for the binary mixture of octafluoropropane + hexafluoropropylene." *Frontiers on Separation Science and Technology, Proceedings of the International Conference on Separation Science and Technology, 4th, Nanning, China, Feb. 18-21, 2004.*, 1(1), 136-141.

Holderbaum, T., and Gmehling, J. (1991). "PSRK: A group contribution equation of state based on UNIFAC." *Fluid Phase Equilibria*, 70(1), 251-265.

Huang, Z., Zhang, Y., Zhao, C., Qin, J., Li, H., Xue, M., and Liu, Y. (2006). "Direct gas-phase epoxidation of hexafluoropropylene with molecular oxygen using Ag catalyst." *Applied Catalysis A: General*, 303(1), 18-22.

Huron, M. J., and Vidal, J. (1979). "New Mixing Rules in Simple Equations of State for Representing Vapour-Liquid Equilibria of Strongly non-ideal Mixtures." *Fluid Phase Equilibria*, 3, 255-271.

Ikeda, M., Miura, M., and Aoshima, A. (1990). "Process for the production of hexafluoropropylene oxide - United States Patent 4902810." U. S. Patent, ed., Asahi Kogaku Kogyo Kabushiki Kaisha, 16.

Jakob, A. (2008). "UNIFAC Consortium." <http://134.106.215.86/UNIFAC/> (15 January 2008).

Klamt, A., and Schuuurmann, G. (1993). "COSMO: a new approach to dielectric screening in solvents with explicit expressions for the screening energy and its gradient." *Journal of the Chemical Society - Perkin Transactions 2*, 1(5), 799-805.

Kojima, K., and Tochigi, K. (1979). *Prediction of vapour-liquid equilibria by ASOG method*, Kodansha-Elsevier, Tokyo, Japan.

Krespan, C. G. (1986). "Fluoroalkyl Azide Chemistry." *Journal of Organic Chemistry*, 51(1), 332-337.

Larsen, B. L., Rasmussen, P., and Fredenslund, A. (1987). "A modified UNIFAC group-contribution model for the prediction of phase equilibria and heats of mixing." *Industrial and Engineering Chemistry Research*, 26, 2274-2286.

Laugier, S., and Richon, D. (1997). "High-Pressure Vapor-Liquid Equilibria of Two Binary Systems: Carbon Dioxide + Cyclohexanol and Carbon Dioxide + Cyclohexanone." *Journal of Chemical and Engineering Data*, 42(1), 155-159.

Laugier, S., Richon, D., and Renon, H. (1994). "Chlorofluorohydrocarbon-alcohol mixtures: bubble pressures and saturated liquid molar volumes (experimental data and modeling)." *Chemical Engineering Science*, 49(13), 2135-2144.

Laugier, S., Richon, D., and Renon, H. (1994a). "Bubble curves and saturated liquid molar volumes for chlorofluorohydrocarbon-hydrocarbon mixtures. Experimental data and modeling." *Journal of Chemical and Engineering Data*, 39(1), 166-171.

Lee, B. I., and Kesler, M. G. (1975). "A Generalized thermodynamic Correlation based on three parameter corresponding states." *AICHE Journal*, 21(1), 510-527.

Legret, D., Richon, D., and Renon, H. (1982). "Vapor-liquid equilibrium of methane-benzene, methane-methylbenzene (toluene), methane-1,3-dimethylbenzene (m-xylene), and methane-1,3,5-trimethylbenzene (mesitylene) at 313.2 K up to the critical point." *Journal of Chemical and Engineering Data*, 27(2), 165-169.

Lei, Z., Li, C., and Chen, B. (2003). "Extractive Distillation: A review." *Separation and Purification Reviews*, 32(2), 121-213.

Li, C., Feng, Y., and Wu, Z. (1996). "Vapour Pressure of Hexafluoropropylene." *Chinese Journal of Chemical Engineering*, 10(1), 64-66.

Luyben, W. L. (2006). *Distillation Design and Control using ASPEN simulation*, John Wiley & Sons, Inc., Hoboken, New Jersey.

Maletskii, V. Y., and Kogan, V. B. (1966). "Liquid-vapor equilibrium in binary systems formed by difluorochloromethane, hexafluoropropylene, and trifluorochloroethylene." *Russian Chemical Reviews*, 42(8), 626-628.

Marquardt, D. W. (1963). "An Algorithm for Least-Squares Estimation of Nonlinear Parameters." *Journal of the Society for Industrial and Applied Mathematics*, 11(2), 431-441.

Mathias, P. M., and Copeman, T. W. (1983). "Extension of the Peng-Robinson Equation of State to Complex Mixtures: Evaluation of Various Forms of the Local Composition Concept." *Fluid Phase Equilibria*, 13(1), 91-108.

Maximov, B. N. (1998). "Commerical fluorinated compounds." Russian Scientific Centre.

Merck. (2008). "Merck Chemicals Ltd. Product List." <http://www.merck.de/servlet/PB/menu/1229120/index.html> (15 January 2008).

Meskel-Lesavre, M., Richon, D., and Renon, H. (1981). "A new variable volume cell for determining vapour liquid equilibria and saturated liquid molar volume by the static method." *Industrial and Engineering Chemistry Fundamentals*, 20, 284-289.

Meskel-Lesavre, M., Richon, D., and Renon, H. (1982). "Bubble pressures and liquid molar volumes of the system chlorotrifluoromethane-1,1,2-trichlorotrifluoroethane." *Journal of Chemical and Engineering Data*, 27(2), 160-165.

Michelsen, M. L. (1990). "A modified HURON-VIDAL mixing rule for cubic equations of state." *Fluid Phase Equilibria*, 60, 213-219.

Michelsen, M. L., and Heidemann, R. A. (1981). "Calculation of critical points from cubic 2 constant equations of state." *AICHE Journal*, 27(3), 521-523.

Mohammadi, A. H., Chapoy, A., Tohidi, B., and Richon, D. (2004). "Measurements and Thermodynamic Modeling of Vapor-Liquid Equilibria in Ethane-Water Systems from 274.26 to 343.08 K." *Industrial and Engineering Chemistry Research*, 43(17), 5418-5424.

Mollerup, J. (1986). "A note on the derivation of mixing rules from excess Gibbs free energy models." *Fluid Phase Equilibria*, 25(1), 323-327.

Muhlbauer, A. L., and Raal, J. D. (1995). "Computation and thermodynamic interpretation of high pressure vapour-liquid equilibrium-a review." *The Chemical Engineering Journal*, 60, 1-29.

Naidoo, P. (2004). "High-Pressure Vapour-Liquid Equilibrium Studies," University of KwaZulu-Natal, Durban.

NCMS. (2008). "National Centre for Manufacturing Sciences Solvents." <http://solvdb.ncms.org/solvdb.htm> (15 January 2008).

Nelson, W. M. (2008). "The separation of HFP and HFPO using R123 and a novel solvent," University of KwaZulu-Natal, Durban.

NIST. (2007). "Propene, hexafluoro-." <http://webbook.nist.gov/cgi/cbook.cgi/116-15-4-2d.mol?Str2File=C116154> (20 September, 2007).

NIST. (2007a). "Oxirane, trifluoro(trifluoromethyl)-." <http://webbook.nist.gov/cgi/cbook.cgi/428-59-1-2d.mol?Str2File=C428591> (20 September, 2007).

NIST. (2007b). "Toluene." <http://webbook.nist.gov/cgi/cbook.cgi/108-88-3-2d.mol?Str2File=C108883> (20 September, 2007).

NIST. (2007c). "Hexafluoroethane." <http://webbook.nist.gov/cgi/cbook.cgi/76-16-4-2d.mol?Str2File=C76164> (20 September, 2007).

O-Ring-Info. (2007a). "O-Ring Info - Nitile/NBR." <http://o-ring.info/en/compounds/nitrile-nbr/#tab-2147> (17 December, 2007).

O-Ring-Info. (2007b). "O-Ring Info - Viton/FKM." <http://o-ring.info/en/compounds/viton-fkm/#tab-2137> (17 December, 2007).

Oda, Y., Uchida, K., and Morikawa, S. (1979). "Method of Purifying Hexafluoropropylene Oxide - Patent 4134796." U. S. Patent, ed., Asahi Glass Company Limited, 5.

Ohsaka, Y., and Tohzuka, T. (1981). "Process for preparing hexafluoropropene oxide - United States Patent 4288376." U. S. Patent, ed., Daikin Kogyo Company Limited, 3.

PELCHEM. (2007). "PELCHEM - Company Profile and Products." <http://www.pelchem.com/index.html> (29 November, 2007).

Peng, D., and Robinson, D. B. (1976). "A new two-constant equation of state." *Industrial and Engineering Chemistry Fundamentals*, 15(1), 59-64.

Perry, R., and Green, D. (1997). *Perry's Chemical Engineers' Handbook*, 7th Edition Ed., McGraw Hill, New York.

ProSim. (2001). "Component Plus 3.0.0.0 Pure Component Database Manager." ProSim SA.

Ramjugernath, D. (2000). "High Pressure Phase Equilibrium Studies," University of Natal, Durban.

Randhol, P., and Engelien, H. (2000). "xlUNIFAC ver. 1." GPL.

Randhol, P., and Engelien, H. (2000a). "xlUNIFAC, a Computer Program for Calculation of Liquid Activity Coeffcients Using the UNIFAC Model." 41.

Redlich, O., and Kwong, J. N. S. (1949). "On Thermodynamics of solutions V: An equation of state. Fugacities of gaseous solutions." *Chemical Reviews*, 44(1), 233-244.

Renon, H., and Prausnitz, J. M. (1968). "Local Composition in Thermodynamic Excess Function for Liquid Mixtures." *AICHE Journal*, 14(1), 135-144.

Richon, D. (1996). "Classification of Experimental Methods of Measuring Equilibrium Between Phases." In: *Elements De Thermodynamique Experimentale*, Ecole Des Mines De Paris, Fontainebleau, 226.

Richon, D., Laugier, S., and Renon, H. (1992). "High-pressure vapor-liquid equilibrium data for binary mixtures containing molecular nitrogen, carbon dioxide, hydrogen sulfide and an aromatic hydrocarbon or propylcyclohexane in the range 313-473 K." *Journal of Chemical and Engineering Data*, 37(2), 264-268.

Richon, D., Laugier, S., and Renon, H. (1992a). "High-pressure vapor-liquid equilibria for binary mixtures containing a light paraffin and an aromatic compound or a naphthene in the range 313-473 K." *Journal of Chemical and Engineering Data*, 36(1), 104-111.

Rivollet, F., Chapoy, A., Coquelet, C., and Richon, D. (2004). "Vapor-liquid equilibrium data for the carbon dioxide (CO2) + difluoromethane (R32) system at temperatures from 283.12 to 343.25 K and pressures up to 7.46 MPa." *Fluid Phase Equilibria*, 218(1), 95-101.

Rohrschneider, L. (1973). "Solvent characterization by gas-liquid partition coefficients of selected solutes." *Analytical Chemistry*, 45(7), 1241-1247.

Sandler, S. I., and Orbey, H. (1998). *Modeling Vapor-Liquid Equilibria: Cubic Equations of State and Their Mixing Rules*, Cambridge University Press, Cambridge.

Seader, J. D., and Henley, E. J. (1998). *Separation Process Principles*, John Wiley & Sons, Inc., Hoboken, New Jersey.

Seader, J. D., Jeffrey, J. S., and Scott, D. B. (1997). "Enhanced Distillation." In: *Perry's Chemical Engineers' Handbook 7th Edition*
McGraw Hill, New York, 79-81.

Shibanuma, T., Tsuchiya, T., Yamada, Y., and Shibata, N. (2005). "Process for producing synthetic resin foam - United States Patent Application 10/493215." U. S. Patent, ed., Settsu-shi, 20.

Sigma-Aldrich. (2008). "Sigma-Aldrich South Africa ", <http://www.sigmaaldrich.com/catalog/search/AdvancedSearchPage> (15 January 2008).

Smith, J. M., Van Ness, H. C., and Abbott, M. M. (2001). *Introduction to Chemical Engineering Thermodynamics*, Sixth Ed., McGraw-Hill Book Company, New York.

Soave, G. (1972). "Equilibrium constants for modified Redlich-Kwong equation of state." *Chemical Engineering Science*, 27(6), 1197-1203.

Stockfleth, R., and Dohrn, R. (1998). "An algorithm for calculating critical points in multicomponent mixtures which can easily be implemented in existing programs to calculate phase equilibria." *Fluid Phase Equilibria*, 145(1), 43-52.

Stolarska, M., Niedzicki, L., Borkowska, R., Zalewska, A., and Wieczorek, W. (2007). "Structure, transport properties and interfacial stability of PVdF/HFP electrolytes containing modified inorganic filler." *Electrochimica Acta*, 53(4), 1512-1517.

Stryjek, R., and Vera, J. H. (1986). "PRSV - an improved Peng-Robinson equation of state with new mixing rules for strongly nonideal mixtures." *Canadian Journal of Chemical Engineering*, 64(2), 334-339.

Sulzbach, R. (1982). "Process for the preparation of pure Hexafluoropropylene Oxide - Patent 4358348." U. S. Patent, ed., Hoechst Aktiengesellschaft, 3.

Ueno, T., Tatematsu, S., Sato, M., and Ehata, K. (1997). "Separation of Hexafluoropropylene Oxide and Hexafluoropropylene by solvent extraction and distillation - Patent 09020765." J. Patent, ed., Asahi Glass Company Limited, 5.

Wilson, G. M. (1964). "Vapour-Liquid Equilibirum. XI. A New Expression for the Excess Free Energy of Mixing." *Journal of the American Chemical Society*, 86(2), 127-130.

Wong, D. S., Orbey, H., and Sandler, S. I. (1992a). "Equation of state mixing rule for nonideal mixtures using available activity coefficient model parameters and that allows extrapolation over large ranges of temperature and pressure." *Industrial and Engineering Chemistry Research*, 31(8), 2033-2039.

Wong, D. S., and Sandler, S. I. (1992a). "A Theoretically Correct Mixing Rule for Cubic Equation of State." *AIChEJ*, 38, 671-680.

Wong, D. S. H., and Sandler, S. I. (1992b). "A theoretically correct mixing rule for cubic equations of state." *AICHE Journal*, 38(5), 671-680.

APPENDIX A

A 1. INITIAL CANDIDATE SOLVENT LIST

No.	Alcohol	T_b [K]
1	Diethylene glycol	518.15
2	Ethanol	351.54
3	Pentafluoropropyl alcohol	353.15
4	Isopropyl alcohol	355.39
5	4-Methyl-2-pentanol	542.21
6	Furfuryl alcohol	444.15
7	Ethylene glycol	470.69
8	1,3-Butanediol	480.65
9	Isooctyl alcohol	461.15
10	Trimethylene glycol	487.55
11	Tetrahydrofurfuryl alcohol	451.15
12	Tetraethylene glycol	600.45
13	2-Octanol	452.95
14	alpha-Terpineol	490.65
15	1-Heptanol	449.15
16	1-Octanol	467.15
17	Triethylene glycol	560.55
18	2-Butanol	372.662
19	Cyclohexanol	434.25
20	1-Hexanol	430.15
21	1-Butanol	390.88
22	1-Pentanol	411.133
23	2-Methylpropanol	381.036
24	Propylene glycol	461.35
25	Methanol	337.7
26	1-Propanol	370.35
	Aromatic Hydrocarbon	**T_b [K]**
27	Benzene	353.24
28	o-Xylene	417.579
29	Toluene	383.78
30	Catechol	518.15
31	Hydroquinone	558.15
32	Xylene	410.15
33	Ethylbenzene	409.343
34	p-Xylene	411.509
35	m-Xylene	412.27
	Chlorinated Hydrocarbon	**T_b [K]**
36	Tetrachloroethylene	394.22
37	Chloromethane	248.95
38	Dichloromethane	312.75
39	1,1,2-Trichloroethylene	359.85
40	Carbon tetrachloride	349.85
41	Trichloromethane	334.33
42	1,1,1-Trichloroethane	347.23

	Ester	T_b [K]
43	Acetic acid, 2-methoxy-1-methylethyl ester	419.15
44	Dipropylene glycol monomethyl ether acetate	473.15
45	Diethylene glycol monobutyl ether acetate	518.15
46	Butyric acid, methyl ester	375.15
47	Lactic acid, butyl ester	460.92
48	Lactic acid, methyl ester	418.15
49	Lactic acid, ethyl ester	427.03
50	Propylene carbonate	514.85
51	Ethyl propionate	372.25
52	Acetic acid, sec-butyl ester	385.49
53	Acetic acid, isopropyl ester	363.15
54	Acetic acid, amyl ester	422.4
55	Diethylene glycol monomethyl ether acetate	482.25
56	Dibutyl oxalate	512.15
57	Ethyl acetate	350.21
58	Methyl propionate	352.85
59	Diethylene glycol monoethyl ether acetate	490.55
60	Butyl acetate	397.15
61	Lactic acid, amyl ester	385.15
62	Ethylene glycol methyl ether acetate	418.15
63	2-Ethoxyethanol acetate	429.25
64	2-Butoxyethanol acetate	465.15
65	gamma-Butyrolactone	477.15
66	Butyric acid, butyl ester	437.15
67	Propyl acetate	374.75
68	Methyl acetate	330.15
69	Dibutyl phthalate	613.15
70	Diethyl oxalate	458.55
	Glycol Ether	**T_b [K]**
71	Diethylene glycol monomethyl ether	466.15
72	Diethylene glycol monoethyl ether	475.15
73	2-(2-n-Butoxyethoxy)ethanol	503.75
74	Diethylene glycol diethyl ether	462.05
75	Ethylene glycol dibutyl ether	476.45
76	Triethylene glycol dimethyl ether	489.15
77	Diethylene glycol dibutyl ether	529.15
78	Ethylene glycol monophenyl ether	518.35
79	Dipropylene glycol monomethyl ether	461.45
80	1-Methoxy-2-propanol	391.15
81	2-Methoxyethanol	397.75
82	2-Ethoxyethanol	408.65
83	Butoxyethanol	443.35
84	Diethylene glycol dimethyl ether	435.15
85	Ethylene glycol monobenzyl ether	538.15
86	1,2-Propanediol, 3-(3-methylbutoxy)-	538.15
87	Ethylene glycol diethyl ether	394.35
88	Propylene glycol monophenyl ether	515.85

	Amine	T_b [K]
89	2-Methylaminoethanol	432.15
90	2-Diethylaminoethanol	434.15
91	Diisopropylamine	356.72
92	N-Methylpyrrolidone	475.15
93	Triethanolamine	608.55
94	Dimethylethanolamine	406.15
95	Dimethylamine	280.04
96	Monoethanolamine	443.95
97	Diethanolamine	541.95
98	Butylamine	350.22
99	Tetraethylene pentamine	606.15
100	Triethylamine	362.15
101	N-Nitrosodimethylamine	427.15
102	Monomethylamine	266.85
103	Monoethylamine	289.75
	Chlorofluorocarbon	**T_b [K]**
104	Dichlorodifluoromethane	243.38
105	1,2-Dichlorotetrafluoroethane	277.25
106	Chloropentafluoroethane	234.04
107	Dichlorofluoromethane	282.05
108	Tetrafluoromethane	145.35
109	1,1,2,2-Tetrachlorodifluoroethane	365.95
110	1,1,2-Trichlorotrifluoroethane	320.783
111	Trifluoromethane	191.15
112	Trichlorofluoromethane	296.78
	Hydrochlorofluorocarbon	**T_b [K]**
113	Chlorodifluoromethane	232.32
114	Trifluoromethane	191.15
115	Dichlorofluoromethane	282.05
	Ether	**T_b [K]**
116	Dipropylene glycol monomethyl ether	461.45
117	1-Methoxy-2-propanol	391.15
118	Butoxyethanol	443.35
119	Trioxane	387.65
120	2-(2-n-Butoxyethoxy)ethanol	503.15
121	Ethylene glycol monophenyl ether	518.35
122	Diethylene glycol dibutyl ether	529.15
123	Diamyl ether	459.95
124	Propylene glycol monophenyl ether	515.85
125	Triethylene glycol dimethyl ether	489.15
126	Tetrahydropyran-2-methanol	460.15
127	Diphenyl ether	531.21
128	Diisopropyl ether	341.66
129	Ethylene glycol diethyl ether	394.35
130	Methyl tert-butyl ether	328.35
131	Methoxybenzene	426.75

132	Ethylene glycol monobenzyl ether	538.15
133	Diethylene glycol dimethyl ether	435.15
134	Dibutyl ether	413.45
135	2-Ethoxyethanol	408.65
136	1,4-Dioxane	374.47
137	2-Methoxyethanol	397.75
138	Diethylene glycol diethyl ether	462.05
139	Ethylene glycol dibutyl ether	476.45
140	n-Hexyl ether	501.15
141	Tetrahydrofuran	339.115
142	Diethylene glycol monomethyl ether	466.15
143	Diethylene glycol monoethyl ether	475.15
144	Diethyl ether	307.581
145	Ethylene oxide	283.85
146	Propylene oxide	307.38
	Ketone	**T_b [K]**
147	Diisobutyl ketone	441.39
148	Methyl isobutyl ketone	390.55
149	3-Methyl-2-butanone	367.15
150	2-Hexanone	400.733
151	2-Pentanone	375.15
152	Diacetone alcohol	441.25
153	Methyl isobutenyl ketone	403.15
154	5-Methyl-3-heptanone	430.15
155	5-Methyl-2-hexanone	418.15
156	2,5-Hexanedione	464.15
157	2-Heptanone	424.25
158	Acetone	329.22
159	2-Butanone	352.75
160	Cyclohexanone	428.8
	Polyhydric Alcohol	**T_b [K]**
161	Propylene glycol	461.35
162	Diethylene glycol	518.15
163	Triethylene glycol	560.55
164	Tetraethylene glycol	600.45
165	Trimethylene glycol	487.55
166	Ethylene glycol	470.69
167	1,3-Butanediol	480.65
	Ethane Series Refrigerants	**T_b [K]**
168	Hexachloroethane	459.95
169	Pentachlorofluoroethane	408.15
170	Tetrachloro-1,2-difluoroethane	366.15
171	1,1,12-Tetrachloro-2,2-difluoroethane	273.15
172	1,1,2-trichlorotrifluoroethane	321.15
173	1,1,1-trichlorotrifluoroethane	321.15
174	1,2 dichlorotetrafluoroethane	276.95
175	1,1 dichlorotetrafluoroethane	276.95

176	Dibromotetrafluoroethane	320.45
177	chloropentafluoroethane	234.15
178	Hexafluoroethane	194.15
179	Pentachloroethane	435.15
180	2,2 dichloro 1,1,1 trifluoroethane	301.15
181	Chlorotetrafluoroethane	262.15
182	Pentafluoroethane	224.15
183	Tetrachloroethane	230.15
184	Chlorotrifluoroethane	280.05
185	1,1,2,2-tetrafluoroethane	246.55
186	Trichloroethane	347.15
187	Dichlorofluoroethane	305.2
188	Chlorodifluoroethane	264.15
189	Trifluoroethane	226.15
190	Difluoroethane	248.15
191	Chloroethane	285.15
	Methane Series Refrigerants	**T_b [K]**
192	Tetrachloromethane	349.15
193	Trichlorofluoromethane	296.95
194	dichlorodifluoromethane	243.35
195	chlorotrifluoromethane	192.15
196	Bromotrifluoromethane	215.15
197	carbon tetrafluoride	145.15
198	Trichloromethane	210.15
199	Dichlorofluoromethane	282.05
200	chlorodifluoromethane	233.15
201	Bromodifluoromethane	215.15
202	trifluoromethane	189.15
203	Dichloromethane	312.95
204	Chlorofluoromethane	263.95
205	Difluoromethane	221.55
206	Chloromethane	249.15
207	Fluoromethane	194.75

Table A.1. The initial candidate solvent list of two hundred and seven solvents

A 2. UNIFAC

UNIFAC ((Fredenslund et al. 1977)) is a group contribution method that combines the solution of groups concept ((Kojima and Tochigi 1979)) and the UNIQUAC ((Abrams and Prausnitz 1975)) model. The UNIQUAC model is used for the calculation of liquid phase activity coefficients and is a generalisation of Guggenheim's quasi-chemical analysis.

The idea of the group contribution method is that a molecule consists of different functional groups and that the thermodynamic properties of a solution can be thus correlated in terms of the functional groups. The primary advantage of this method is that a very large number of mixtures can be described by a relatively small number of functional groups.

A 2.1. Solution of groups method

The basic premise of the method is to utilise existing phase equilibrium data to predict phase equilibria of systems for which no data is currently available.

The solution of groups method entails the following:

1. The assignment of functional groups to a molecule. A group is any convenient structural unit such as: $-CH_3$, $-COCH_2-$ and $-CH_2Cl$ etc. which can be used as 'building blocks' for the representation of the molecules or compounds of interest.

2. The reduction of experimentally obtained phase equilibrium data to obtain parameters characterising interactions between pairs of structural groups in non-electrolyte systems.

3. The use of these interaction parameters to predict activity coefficients for other systems which may not have been studied experimentally, but contain the same functional groups.

The fundamental assumptions made for the solution of groups method are:

1. The logarithm of the activity coefficient is assumed to be the sum of two contributions: a combinatorial part, essentially due to differences in size and shape of the molecules in the mixture, and a residual part, essentially due to energy interactions (essentially the same assumption as the UNIQUAC model).

This can be expressed as (for component i):

$$\ln \gamma_i = \ln \gamma_i^C + \ln \lambda_i^R \qquad \text{(A-1)}$$

A distinction between the residual and combinatorial contributions to the overall activity coefficient has to be made since the liquid phase non-idealities caused by size and shape effects of the molecules are generally different to that due to energy interactions between the molecules.

2. The residual contribution (due to group energy interactions), is assumed to be the sum of the individual contributions of each solute group in the solution less the sum of the individual contributions in the pure component environment.

$$\ln \gamma_i^R = \sum_{all\_groups}^{k} \nu_k^{(i)} \left[\ln \Gamma_k - \ln \Gamma_k^i \right] \qquad \text{(A-2)}$$

where the following definitions apply:

- Γ_k is the residual activity coefficient of group k in a solution.
- k = 1, 2 .... N, where N is the number of different groups in the mixture.
- Γ_k^i is the residual activity coefficient of group k in a reference solution containing only molecules of type i (A pure solution).
- $\nu_k^{(i)}$ is the number of groups of kind k in molecule i.

In equation (A-2), the logarithm of Γ_k^i ($\ln \Gamma_k^i$) is necessary to attain the normalisation that the activity coefficient γ_i becomes unity as $x_i \rightarrow 1$.

3. The individual group contributions in any environment containing groups of kinds 1, 2 .... N are assumed to be only a function of group concentrations and temperature:

$$\Gamma_k, \Gamma_k^i = F(X_1, X_2 .... X_N; T) \qquad \text{(A-3)}$$

where the following definitions apply:

$$X_k = \frac{\sum^{i} \nu_k^i x_i}{\sum^{i}\sum^{j} \nu_j^i x_i} \tag{A-4}$$

i = 1, 2 .... M (Number of components).

j = 1, 2 .... N (Number of different groups in mixture).

X_k = group fraction.

A 2.2. The UNIQUAC model

In the UNIQUAC model ((Abrams and Prausnitz 1975)), the expression for the activity coefficient is divided into two terms:

(1) The combinatorial contribution: This accounts for differences that arise due to differences in the size and shape of the molecules.

(2) The residual contribution: This accounts for energy interactions between the functional groups that make up the molecule.

This can be expressed as (for component k):

$$\ln \gamma_k = \ln \gamma_k^C + \ln \lambda_k^R \tag{A-5}$$

The combinatorial contribution, $\ln \gamma_k^C$, is given by:

$$\ln \gamma_k^C = \ln \frac{\Phi_k}{x_k} + \frac{z}{2} q_k \ln \frac{\Theta_k}{\Phi_k} + l_k - \frac{\Phi_k}{x_k} \sum^{j} x_j l_j \tag{A-6}$$

where the following definitions apply:

$$l_k = \frac{z}{2}(r_k - q_k) - (r_k - 1) \tag{A-7}$$

$$\Theta_k = \frac{q_k x_k}{\sum^{j} q_j x_j} \tag{A-8}$$

$$\Phi_k = \frac{r_k x_k}{\sum^{j} r_j x_j} \tag{A-9}$$

In equation (A-7), z = 10, Θ_k represents the volume fraction of component k and Φ_k represents the surface area fraction of component k. The letter 'j' denotes the counter variable running from component 1 to M components, i.e. j = 1, 2 .... M.

Pure component properties R_k and Q_k are, respectively, a measure of molecular van der Waals volumes and molecular surface areas and are obtained from literature sources.

The residual contribution, $\ln \gamma_k^R$, is given by (for M components):

$$\ln \gamma_k^R = q_k \left[1 - \ln\left(\sum_j^j \Theta_j \tau_{jk} \right) - \sum_j^j \left(\frac{\Theta_j \tau_{kj}}{\sum_i^i \Theta_i \tau_{ij}} \right) \right] \qquad \text{(A-10)}$$

where the following definitions apply:

$$\tau_{ji} = e^{-\left[\frac{u_{ji} - u_{ii}}{RT}\right]} \qquad \text{(A-11)}$$

- i and j = 1, 2 .... M.
- $u_{ji} = u_{ij}$ and $\tau_{ji} \neq \tau_{ij}$.

A 2.3. The UNIFAC model

Combining the UNIQUAC model with the solution of groups model leads to the UNIFAC method. In the UNIFAC method:

1. The combinatorial contribution to the activity coefficient is calculated using Staverman's potential in exactly the same manner as that described by the UNIQUAC model. The calculation includes the well defined (in literature) group volume and area constant parameters R_k and Q_k, respectively.

2. The group residual activity coefficients are represented by the residual part of the UNIQUAC equation, where the group fraction X_k represents an independent concentration variable.

3. R_k and Q_k represent the group sizes and surface areas and are obtained from atomic and molecular structure data i.e. the van der Waals group volumes and surface areas V_k and A_k.

$$R_k = \frac{V_k}{15.17} \tag{A-12}$$

$$Q_k = \frac{A_k}{\left(2.5\times10^9\right)} \tag{A-13}$$

Thus combining the UNQUAC model and the solution of groups concept, the defining equations for the UNIFAC model are:

Combinatorial activity coefficient for component i:

$$\ln\gamma_i^C = \ln\frac{\Phi_i}{x_i} + \frac{z}{2}q_i\ln\frac{\Theta_i}{\Phi_i} + l_i - \frac{\Phi_i}{x_i}\sum^{j} x_j l_j \tag{A-14}$$

where the following definitions apply:

$$l_i = \frac{z}{2}(r_i - q_i) - (r_i - 1) \tag{A-15}$$

$$\Theta_i = \frac{q_i x_i}{\sum^{j} q_j x_j} \tag{A-16}$$

$$\Phi_i = \frac{r_i x_i}{\sum^{j} r_j x_j} \tag{A-17}$$

Θ_i is defined as the molecular surface area fraction and Φ_i the molecular volume fraction, with the parameters r_i and q_i being pure component properties. The parameter z is the lattice coordination number which depends on how the molecules are packed. It may have a value of between 6 and 12, however for liquid at ordinary conditions, it is found empirically that z is approximately 10.

The Van der Waals volume is given by:

$$r_i = \sum^{k} \nu_k^i R_k \tag{A-18}$$

The Van der Waals surface area is give by:

$$q_i = \sum^{k} v_k^i Q_k \tag{A-19}$$

Residual activity coefficient for group k:

$$\ln \Gamma_k = Qk\left[1 - \ln\left(\sum^{m} \Theta_m \Psi_{mk}\right) - \sum^{m}\left(\frac{\Theta_m \Psi_{km}}{\sum^{n} \Theta_n \Psi_{nm}}\right)\right] \tag{A-20}$$

The group surface area fraction Θ_m is given by:

$$\Theta_m = \frac{Q_m X_m}{\sum^{n} Q_n X_n} \tag{A-21}$$

The group fraction X_m is given by:

$$X_m = \frac{\sum^{j} v_m^j x_j}{\sum^{j}\sum^{n} v_n^j x_j} \tag{A-22}$$

- m =1, 2 .... N (All groups).
- n = 1, 2 .... N (All groups).
- j = 1, 2 .... M

The parameter Ψ_{nm} is given by:

$$\Psi_{nm} = \exp\left(\frac{-a_{nm}}{T}\right) \tag{A-23}$$

The variable a_{nm} is the group interaction parameter, which is a measure of the difference in energy interactions between a group *n* and a group *m* and between two groups *m*. Note that $a_{nm} \neq a_{mn}$ and that the group interaction parameters are assumed independent of temperature.

A 3. XLUNIFAC

The evaluation of the selectivity values at infinite dilution for each of the one hundred and eighty solvents on the candidate solvent list was undertaken in the computer software xlUNIFAC ((Randhol and Engelien 2000)). This section describes the xlUNIFAC software and the use of each individual worksheet for the calculation of activity coefficients, and hence selectivity, at infinite dilution. xlUNIFAC has the ability to calculate the activity coefficients of mixtures containing up to fifteen components, and can be used to calculate five different mixtures of fifteen components simultaneously. However, there were some limitations with the use of the program which resulted from the limitations of the UNIFAC model:

1. Temperature range for calculation was restricted from 273.15 to 423.15 K
2. Pressure was restricted to less than 0.5 MPa
3. Components could not contain more than 10 functional groups.

The software is an Excel workbook with embedded visual basic functions. The workbook is divided into several worksheets, as outlined in the Table A.2. For the actual calculation of the liquid phase activity coefficients, the components, their mole fractions and the temperature were defined and input in the 'Calculation' worksheet. All components, HFP, HFPO and each solvent were pre-defined in the 'Define Component' worksheet and were thus available for selection in the 'Calculation' worksheet. With the components specified, the mole fractions of the solvent and HFP and HFPO were input, along with the temperature of the calculations, at either 273.15 or 323.15 K. The calculations were initiated via the 'F9' key and the results presented as either $\ln \gamma_i$ or γ_i in the tables at the bottom of the 'Calculation' worksheet. A screenshot of the 'Calculation' worksheet is presented in Figure A.1.

Worksheet Name	Purpose
xlUNIFAC	Welcomes the user and shows copyright notice with a link to the license
Calculation	Where the values are entered and the activity coefficients calculated
Define Component	Where the components are defined
Table R_k, Q_k	Contains the tables of Rk and Qk parameters
Table Interaction	Contains the tables for the group interaction parameters a_{nm} and a_{mn}
Calc Combinatorial Part	Where the combinatorial part of the activity coefficients are calculated
Calc Residual Part	Where the residual part of the activity coefficients are calculated
License	Contains the programme license
Table Combo-box	A hidden worksheet used internally by the programme

Table A.2. The different worksheets located in the xlUNIFAC workbook ((Randhol and Engelien 2000a)).

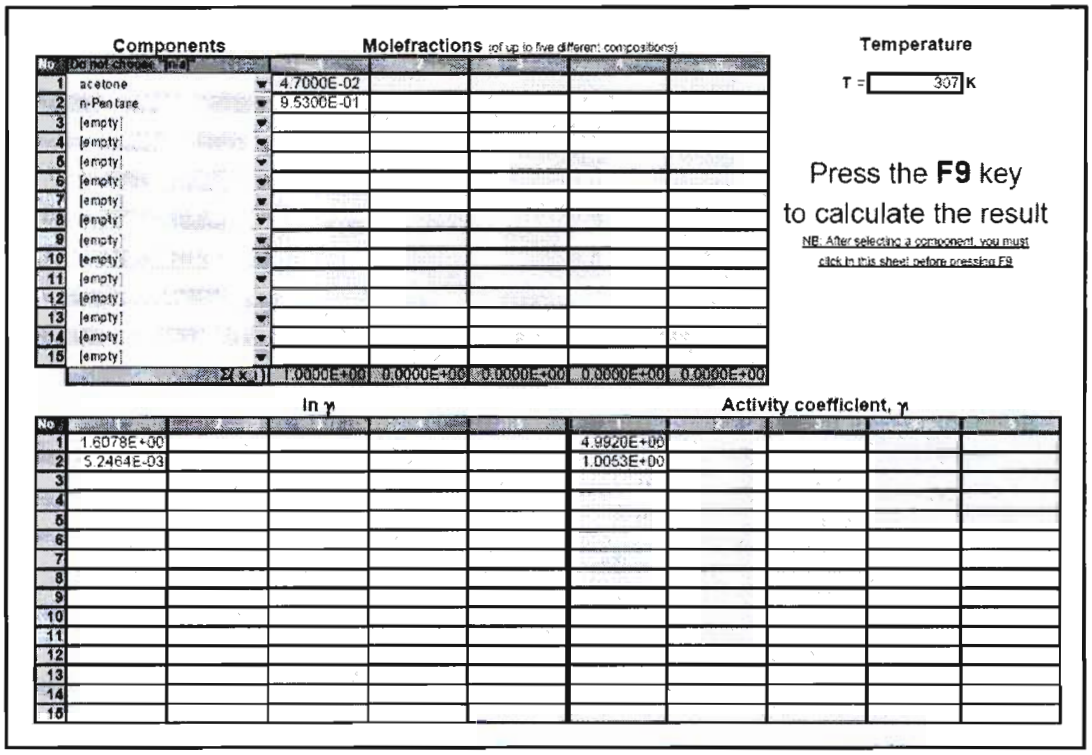

Figure A.1. Screenshot of the 'Calculation' worksheet of the xlUNIFAC computer software.

For the addition of a new component to the program, for example the solvent acetone, the 'Define Component' worksheet was used. A section of the worksheet is illustrated in Figure A.2.

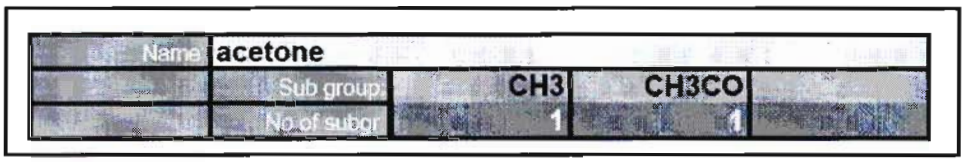

Figure A.2. Definition or fragmentation for component acetone on the 'Define Component' worksheet.

The name of the component was first entered in the first available 'Name' field, and the functional groups defined in the rows below. A list of the names of the various sub-groups can be found in the worksheet 'Table R_k, Q_k', a section of which is presented in Figure A.3. The name of the sub-group was then entered and the number of sub-groups entered directly below it. For the component acetone, the fragmentation contains a single CH_3 group and a single CH_3CO group. In the definition of the compound benzene, the

sub-group name would be ACH and there would six ACH sub-groups in the molecule. The subgroups were defined from left to right without skipping any cells and after definition of a new component, the program was saved and the 'F9' button pressed to add the new component into the component list.

Main group	Subgroup	Group name	R_k	Q_k
1	1	CH3	0.9011	0.848
1	2	CH2	0.6744	0.540
1	3	CH	0.4469	0.228
1	4	C	0.2195	0.000
2	5	CH2=CH	1.3454	1.176
2	6	CH=CH	1.1167	0.867
2	7	CH2=C	1.1173	0.988
2	8	CH=C	0.8886	0.676
2	9	C=C	0.6605	0.485
3	10	ACH	0.5313	0.400
3	11	AC	0.3652	0.120

Figure A.3. A section of the "Table R_k, Q_k" worksheet of the xlUNIFAC software.

The binary interaction parameters, which represented data regressed from multiple sets of binary vapour liquid equilibria, are found on the 'Table Interaction' worksheet., a section of which is presented in Figure A.4.

The binary interaction parameters are presented in matrix form in the xlUNIFAC software, which facilitates easy modification to allow for the updating and expansion of binary interaction parameters. The parameters are denoted by a_{nm} and a_{mn} where $a_{nm} \neq a_{mn}$.

	n	1	2	3	4	5
m	Name	CH2	C=C	ACH	ACCH2	OH
1	CH2		86.02	61.13	76.5	986.5
2	C=C	-35.36		38.81	74.15	524.1
3	ACH	-11.12	3.446		167	636.1
4	ACCH2	-69.7	-113.6	-146.8		803.2
5	OH	156.4	457	89.6	25.82	

Figure A.4. A section of the 'Table Interaction' worksheet of the xlUNIFAC software.

A 4. SOLVENT LIST WITH SELECTIVITY VALUES

Alcohols	
223.15 K	**β∞**
Diethylene glycol	0.77
Ethanol	0.75
Pentafluoropropyl alcohol	0.72
Isopropyl alcohol	0.77
4-Methyl-2-pentanol	0.79
Furfuryl alcohol	1.14
Ethylene glycol	0.65
1,3-Butanediol	0.71
2-Octanol	0.79
1-Heptanol	0.79
1-Octanol	0.79
2-Butanol	0.78
1-Hexanol	0.79
1-Butanol	0.78
2-Methylpropanol	0.78
Propylene glycol	0.69
Methanol	0.71
1-Propanol	0.77
Isooctyl alcohol	0.77
Trimethylene glycol	0.73
Tetraethylene glycol	0.72
Triethylene glycol	0.78
273.15 K	**β∞**
Diethylene glycol	0.74
Ethanol	0.80
Pentafluoropropyl alcohol	0.70
Isopropyl alcohol	0.83
4-Methyl-2-pentanol	0.86
Furfuryl alcohol	1.16
Ethylene glycol	0.63
1,3-Butanediol	0.64
2-Octanol	0.87
1-Heptanol	0.86
1-Octanol	0.87
2-Butanol	0.85
1-Hexanol	0.86
1-Butanol	0.85
2-Methylpropanol	0.85
Propylene glycol	0.77
Methanol	0.75
1-Propanol	0.83
Isooctyl alcohol	0.84
Trimethylene glycol	0.78

Aromatic Hydrocarbon	
223.15 K	**β∞**
Benzene	1.41
o-Xylene	1.17
Toluene	1.36
Catechol	4.72
Hydroquinone	4.65
Ethylbenzene	1.17
273.15 K	**β∞**
Benzene	1.40
o-Xylene	1.11
Toluene	1.35
Catechol	3.71
Hydroquinone	4.65
Ethylbenzene	1.14

Chlorofluorocarbon	
223.15 K	**β∞**
Dichlorodifluoromethane	1.18
1,2-Dichlorotetrafluoroethane	1.04
Chloropentafluoroethane	0.72
1,1,2,2-Tetrachlorodifluoroethane	1.13
1,1,2-Trichlorotrifluoroethane	1.09
Trichlorofluoromethane	1.23
Chlorotrifluoromethane	1.06
273.15 K	**β∞**
Dichlorodifluoromethane	1.18
1,2-Dichlorotetrafluoroethane	1.04
Chloropentafluoroethane	0.71
1,1,2,2-Tetrachlorodifluoroethane	1.13
1,1,2-Trichlorotrifluoroethane	1.09
Trichlorofluoromethane	1.23
Chlorotrifluoromethane	1.06

Hydrochlorofluorocarbon	
223.15 K	**β∞**
Chlorodifluoromethane	1.42
Trifluoromethane	0.52
Dichlorofluoromethane	1.46
273.15 K	**β∞**
Chlorodifluoromethane	1.42
Trifluoromethane	0.52
Dichlorofluoromethane	1.51

Ester	
223.15 K	**β∞**
Dibutyl oxalate	0.81
Ethyl acetate	0.95
Methyl propionate	0.88
Butyl acetate	0.84
2-Ethoxyethanol acetate	0.90
Propyl acetate	0.89
Methyl acetate	1.02
Dipropylene glycol monomethyl ether acetate	0.82
Diethylene glycol monobutyl ether acetate	0.78
Butyric acid, methyl ester	0.89
Ethylene glycol methyl ether acetate	0.79
2-Butoxyethanol acetate	0.92
Diethyl oxalate	0.96
273.15 K	**β∞**
Dibutyl oxalate	0.83
Ethyl acetate	0.96
Methyl propionate	0.90
Butyl acetate	0.86
2-Ethoxyethanol acetate	0.92
Propyl acetate	0.90
Methyl acetate	1.02
Dipropylene glycol monomethyl ether acetate	0.84
Diethylene glycol monobutyl ether acetate	0.79
Butyric acid, methyl ester	0.91
Ethylene glycol methyl ether acetate	0.81
2-Butoxyethanol acetate	0.94
Diethyl oxalate	0.97
Ether	
223.15 K	**β∞**
1-Methoxy-2-propanol	0.69
Butoxyethanol	0.65
2-(2-n-Butoxyethoxy)ethanol	0.64
Diethylene glycol dibutyl ether	0.67
Diamyl ether	0.54
Diisopropyl ether	0.62
Ethylene glycol diethyl ether	0.58
2-Propanol, 1,3-bis(3-methylbutoxy)-	0.66
1,2-Propanediol, 3-methoxy-	0.56
2-Propanol, 1,3-dimethoxy-	0.76
Diethylene glycol dimethyl ether	0.86
3-Ethoxy-1-propanol	0.65
Triethylene glycol diethyl ether	0.68
2-Methoxyethanol	0.64
Propylene glycol monophenyl ether	0.58

Triethylene glycol dimethyl ether	0.61
Tetrahydropyran-2-methanol	0.61
Methyl tert-butyl ether	0.60
1,2-Propanediol, 3-butoxy-	0.74
1,3-Butylene glycol methyl ether	0.68
Diethylene glycol monomethyl ether	0.61
273.15 K	**β∞**
1-Methoxy-2-propanol	0.75
Butoxyethanol	0.72
2-(2-n-Butoxyethoxy)ethanol	0.71
Diethylene glycol dibutyl ether	0.71
Diamyl ether	0.59
Diisopropyl ether	0.67
Ethylene glycol diethyl ether	0.59
2-Propanol, 1,3-bis(3-methylbutoxy)-	0.73
1,2-Propanediol, 3-methoxy-	0.62
2-Propanol, 1,3-dimethoxy-	0.82
Diethylene glycol dimethyl ether	0.89
Dibutyl ether	0.62
2-Ethoxyethanol	0.71
3-Ethoxy-1-propanol	0.72
Triethylene glycol diethyl ether	0.72
2-Methoxyethanol	0.71
Propylene glycol monophenyl ether	0.63
Triethylene glycol dimethyl ether	0.67
Tetrahydropyran-2-methanol	0.68
Methyl tert-butyl ether	0.64
1,2-Propanediol, 3-butoxy-	0.80
1,3-Butylene glycol methyl ether	0.74
Diethylene glycol monomethyl ether	0.65

Glycol Ether	
223.15 K	**β∞**
Diethylene glycol monoethyl ether	0.71
2-(2-n-Butoxyethoxy)ethanol	0.70
Diethylene glycol diethyl ether	0.70
Ethylene glycol dibutyl ether	0.64
Diethylene glycol dibutyl ether	0.67
Triethylene glycol diethyl ether	0.75
1-Methoxy-2-propanol	0.58
2-Methoxyethanol	0.68
2-Ethoxyethanol	0.65
3-Ethoxy-1-propanol	0.65
Diethylene glycol dimethyl ether	0.86
1,2-Propanediol, 3-methoxy-	0.56
2-Propanol, 1,3-dimethoxy-	0.76
2-Propanol, 1,3-bis(3-methylbutoxy)-	0.66

273.15 K	β∞
Diethylene glycol monoethyl ether	0.74
2-(2-n-Butoxyethoxy)ethanol	0.74
Diethylene glycol diethyl ether	0.75
Ethylene glycol dibutyl ether	0.69
Diethylene glycol dibutyl ether	0.72
Triethylene glycol diethyl ether	0.80
1-Methoxy-2-propanol	0.84
2-Methoxyethanol	0.69
2-Ethoxyethanol	0.67
Diethylene glycol dimethyl ether	0.89
1,2-Propanediol, 3-methoxy-	0.56
2-Propanol, 1,3-dimethoxy-	0.78
2-Propanol, 1,3-bis(3-methylbutoxy)-	0.73

Ketone

223.15 K	β∞
Diisobutyl ketone	0.66
3-Methyl-2-butanone	0.87
2-Hexanone	0.93
2-Pentanone	0.98
Diacetone alcohol	1.03
5-Methyl-2-hexanone	0.81
2,5-Hexanedione	1.08
2-Heptanone	0.88
Acetone	1.12
2-Butanone	1.04

273.15 K	β∞
Diisobutyl ketone	0.68
3-Methyl-2-butanone	0.87
2-Hexanone	0.94
2-Pentanone	0.98
Diacetone alcohol	1.04
5-Methyl-2-hexanone	0.82
2,5-Hexanedione	1.07
2-Heptanone	0.90
Acetone	1.12
2-Butanone	1.04

Polyhydric Alcohol

223.15 K	β∞
Propylene glycol	0.74
Diethylene glycol	0.67
Ethylene glycol	0.55
1,3-Butanediol	0.58

273.15 K	β∞
Propylene glycol	0.81
Diethylene glycol	0.72
Ethylene glycol	0.59
1,3-Butanediol	0.62

Refrigerants

223.15 K	β∞
Hexachloroethane	2.38
Pentachlorofluoroethane	1.67
Tetrachloro-1,2-difluoroethane	1.13
1,1,12-Tetrachloro-2,2-difluoroethane	1.66
1,1,2-trichlorotrifluoroethane	1.09
1,1,1-trichlorotrifluoroethane	1.46
1,2 dichlorotetrafluoroethane	1.04
1,1 dichlorotetrafluoroethane	0.81
Dibromotetrafluoroethane	1.06
chloropentafluoroethane	0.72
Hexafluoroethane	1.35
Pentachloroethane	2.10
Tetrachlorofluoroethane	1.21
Trichlorodifluoroethane	1.18
2,2 dichloro 1,1,1 trifluoroethane	1.40
Chlorotetrafluoroethane	0.79
Tetrachloroethane	1.30
Trichlorofluoroethane	1.28
Dichlorodifluoroethane	1.18
1,2Dibromo-1,1-difluoroethane	1.10
Chlorotrifluoroethane	0.85
Trichloroethane	1.69
Dichlorofluoroethane	1.45
Chlorodifluoroethane	0.92
Trifluoroethane	0.51
Chloroethane	1.10

273.15 K	β∞
Hexachloroethane	2.30
Pentachlorofluoroethane	1.63
Tetrachloro-1,2-difluoroethane	1.13
1,1,12-Tetrachloro-2,2-difluoroethane	1.65
1,1,2-trichlorotrifluoroethane	1.09
1,1,1-trichlorotrifluoroethane	1.46
1,2 dichlorotetrafluoroethane	1.04
1,1 dichlorotetrafluoroethane	0.80
Dibromotetrafluoroethane	1.06
chloropentafluoroethane	0.71
Hexafluoroethane	1.30
Pentachloroethane	2.01

Tetrachlorofluoroethane	1.21
Trichlorodifluoroethane	1.18
2,2 dichloro 1,1,1 trifluoroethane	1.42
Chlorotetrafluoroethane	0.78
Tetrachloroethane	1.30
Trichlorofluoroethane	1.22
Dichlorodifluoroethane	1.19
1,2Dibromo-1,1-difluoroethane	1.11
Chlorotrifluoroethane	0.85
Trichloroethane	1.66
Dichlorofluoroethane	1.46
Chlorodifluoroethane	0.94
Trifluoroethane	0.52
Chloroethane	1.12
223.15 K	**β∞**
Tetrachloromethane	0.74
Trichlorofluoromethane	1.23
dichlorodifluoromethane	1.18
Bromochlorodifluoromethane	1.18
Dibromodifluoromethane	1.19
chlorotrifluoromethane	1.06
Bromotrifluoromethane	0.68
Trichloromethane	2.74
Dichlorofluoromethane	1.32
chlorodifluoromethane	1.42
Dichloromethane	1.36
273.15 K	**β∞**
Tetrachloromethane	0.81
Trichlorofluoromethane	1.21
dichlorodifluoromethane	1.29
Bromochlorodifluoromethane	1.19
Dibromodifluoromethane	1.19
chlorotrifluoromethane	1.06
Bromotrifluoromethane	0.68
Trichloromethane	2.59
Dichlorofluoromethane	1.38
chlorodifluoromethane	1.38
Dichloromethane	1.32

Amines	
273.15 K	**β∞**
Diisopropylamine	0.81
Dimethylethanolamine	0.85
Dimethylamine	0.88
Butylamine	0.70
Triethylamine	0.83
Monoethylamine	0.80

323.15 K	β^{∞}
Diisopropylamine	0.83
Dimethylethanolamine	0.86
Dimethylamine	0.89
Butylamine	0.84
Triethylamine	0.88
Monoethylamine	0.90

Table A.3. The list of one hundred and eighty solvents with selectivity at infinite dilution values.

APPENDIX B

B 1. CALIBRATION DATA

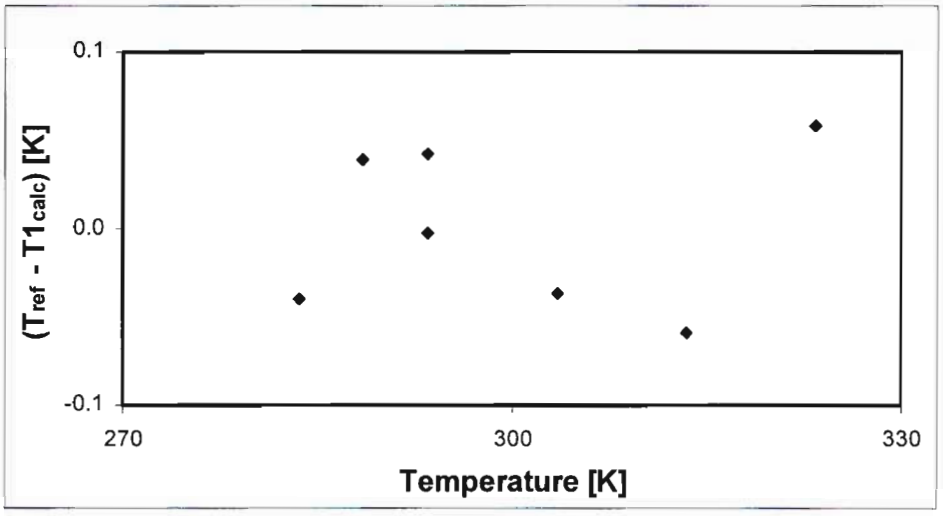

Figure B.1. Error comparison between the reference temperature and the calculated temperature obtained from calibration of probe T1 for the static synthetic apparatus via a first order regression. Resulting temperature uncertainty is ± 0.06 K.

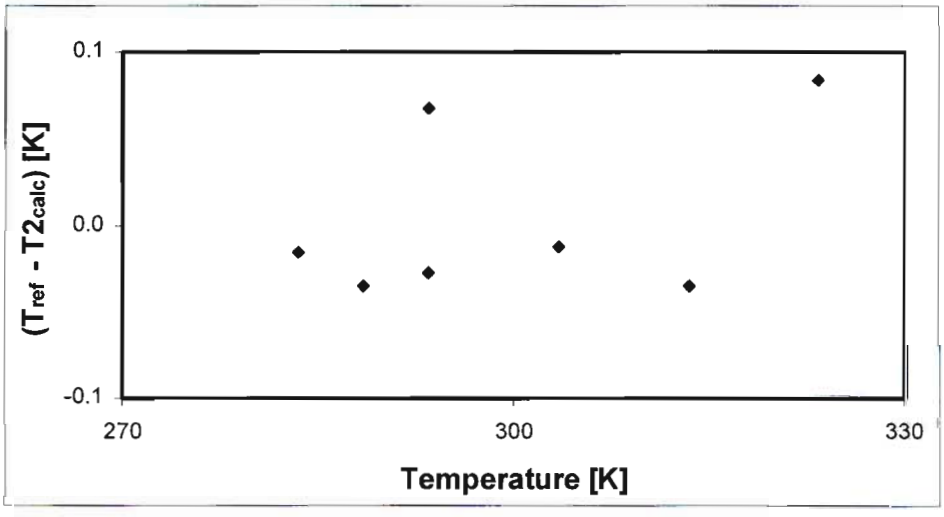

Figure B.2. Error comparison between the reference temperature and the calculated temperature obtained from calibration of probe T2 for the static synthetic apparatus via a first order regression. Resulting temperature uncertainty is ± 0.08 K.

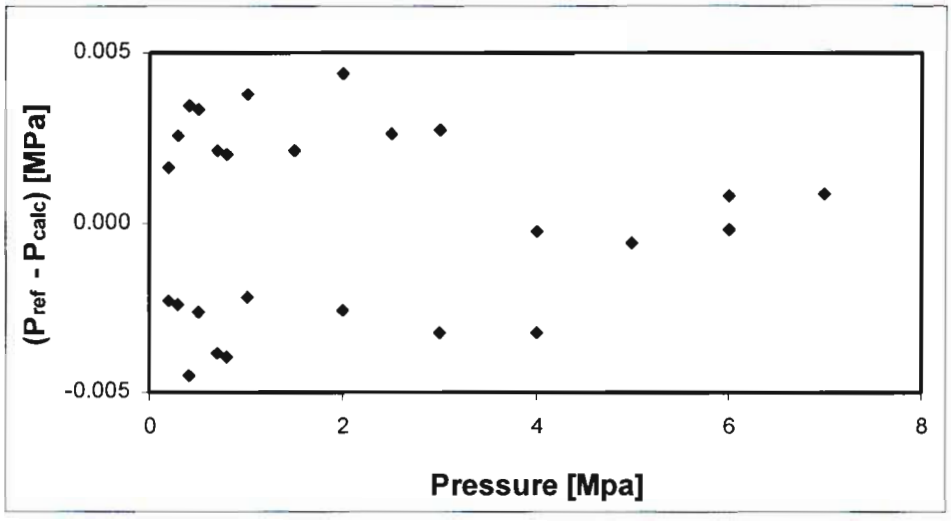

Figure B.3. Error comparison between the reference pressure and the calculated pressure obtained from calibration of the pressure transducer at 273.15 K for the static synthetic apparatus via a second order regression. Resulting pressure uncertainty is ± 0.005 MPa.

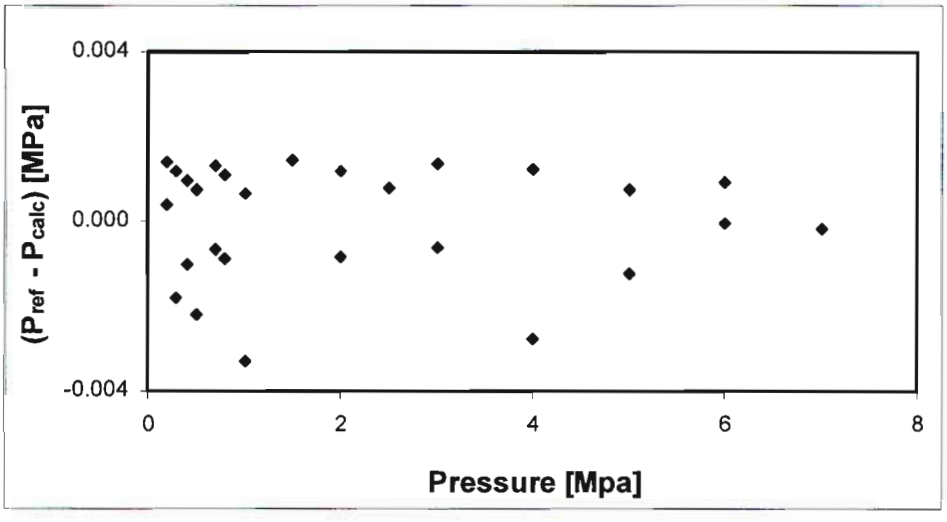

Figure B.4. Error comparison between the reference pressure and the calculated pressure obtained from calibration of the pressure transducer at 313.15 K for the static synthetic apparatus via a second order regression. Resulting pressure uncertainty is ± 0.004 MPa.

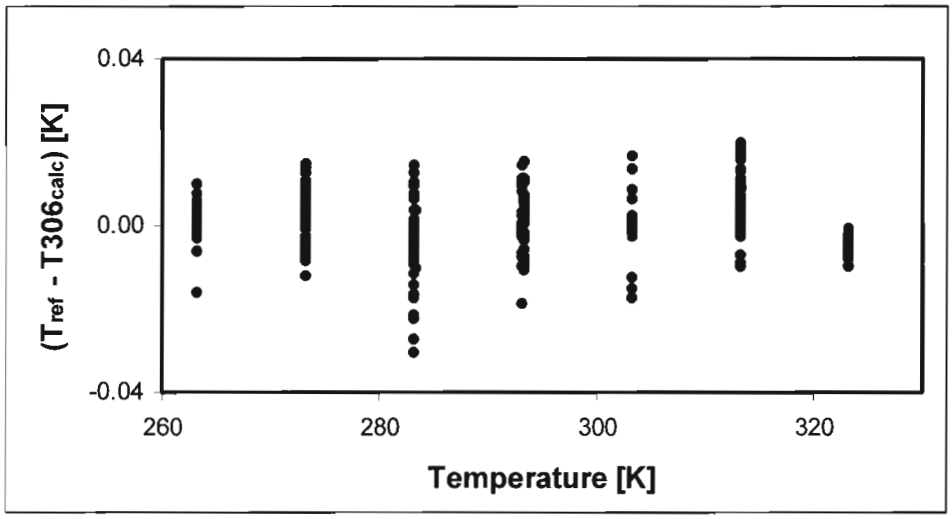

Figure B.5. Error comparison between the reference temperature and the calculated temperature obtained from calibration of temperature probe T306 for the static analytic apparatus via a second order regression. Resulting temperature uncertainty is ± 0.04 K.

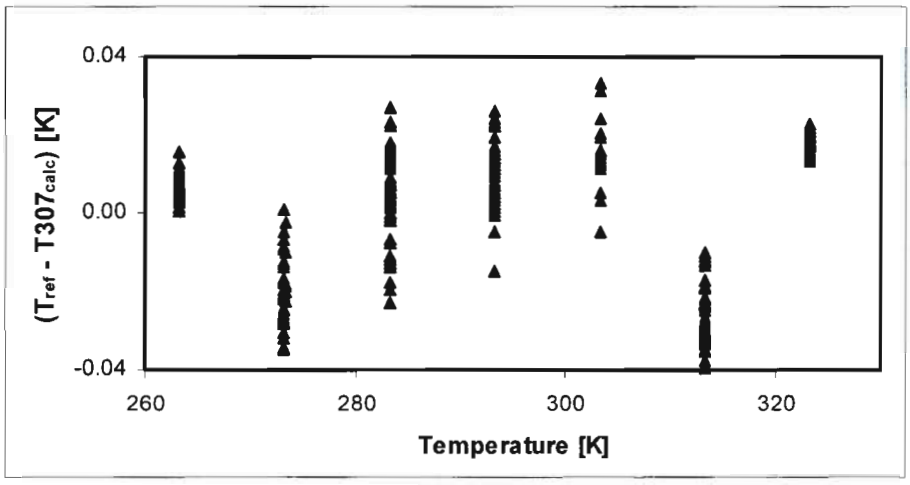

Figure B.6. Error comparison between the reference temperature and the calculated temperature obtained from calibration of temperature probe T307 for the static analytic apparatus via a second order regression. Resulting temperature uncertainty is ± 0.04 K.

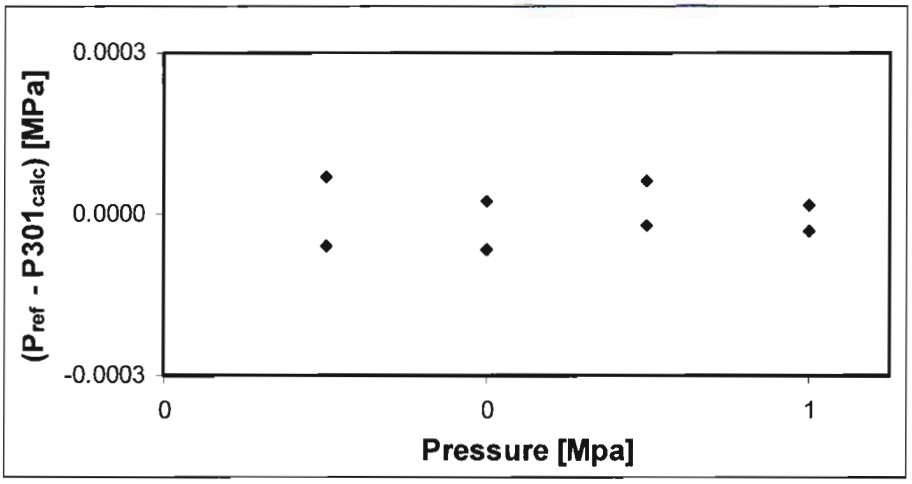

Figure B.7. Error comparison between the reference pressure and the calculated pressure obtained from calibration of pressure transducer P301 for the static analytic apparatus via a second order regression. Resulting pressure uncertainty is ± 0.0003 MPa.

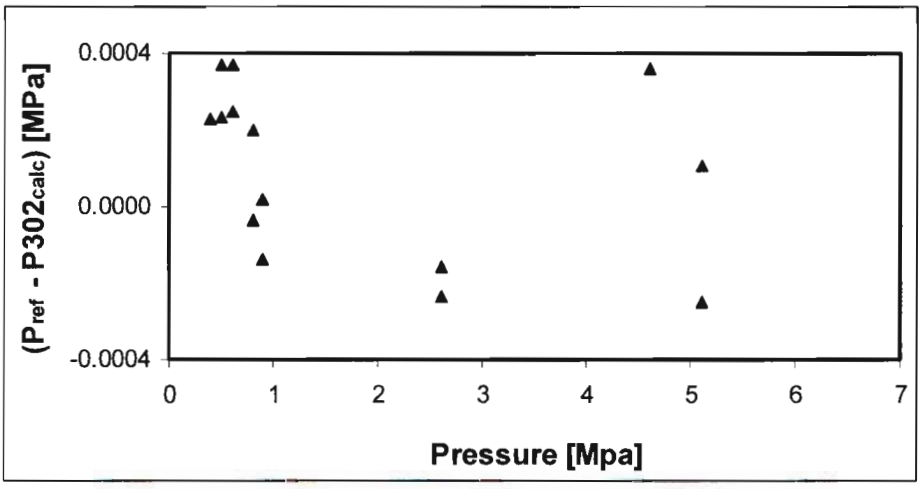

Figure B.8. Error comparison between the reference pressure and the calculated pressure obtained from calibration of pressure transducer P302 for the static analytic apparatus via a second order regression. Resulting pressure uncertainty is ± 0.0004 MPa.

B 2. HFP VAPOUR PRESSURE DATA

Temperature [K]	Pressure [MPa]
256.45	0.1833
260.60	0.2117
263.75	0.2430
265.49	0.2588
266.78	0.2714
273.32	0.3414
277.93	0.4021
279.89	0.4296
282.92	0.4737
286.10	0.5247
288.05	0.5562
290.29	0.6023
293.23	0.6661

Table B.1. Pure component vapour pressure data for HFP in the temperature range 256.45 to 293.23 K from the work of (Li et al. 1996).

Temperature [K]	Pressure [MPa]
272.30	0.3271
279.60	0.4207
299.30	0.7633
302.20	0.8257
317.60	1.2321
312.30	1.0773

Table B.2. Pure component vapour pressure data for HFP for the temperature range 272.30 to 312.30 K from the work of (Nelson 2008).

B 3. EXPERIMENTAL P-V DATA FOR THE STATIC SYNTHETIC APPARATUS

B 3.1. HFP + Toluene: 273.15 K isotherm

The full recorded pressure versus volume data for each loading of the equilibrium cell for the system HFP + Toluene at 273.15 K are presented in Tables B.3 through B.6. This data is also presented graphically from Figures B.9 to B.12.

Pressure [MPa]	Volume [x10^{-5} m^3]
0.711	3.6414
0.581	3.6408
0.484	3.6405
0.386	3.6403
0.285	3.6400
0.233	3.6399
0.115	3.6396
0.091	3.6396
0.089	3.6382
0.087	3.6247
0.085	3.5642
0.081	3.4855

Table B.3. Measured P-V data for HFP + Toluene at 273.15 K and mole fraction HFP 0.0854.

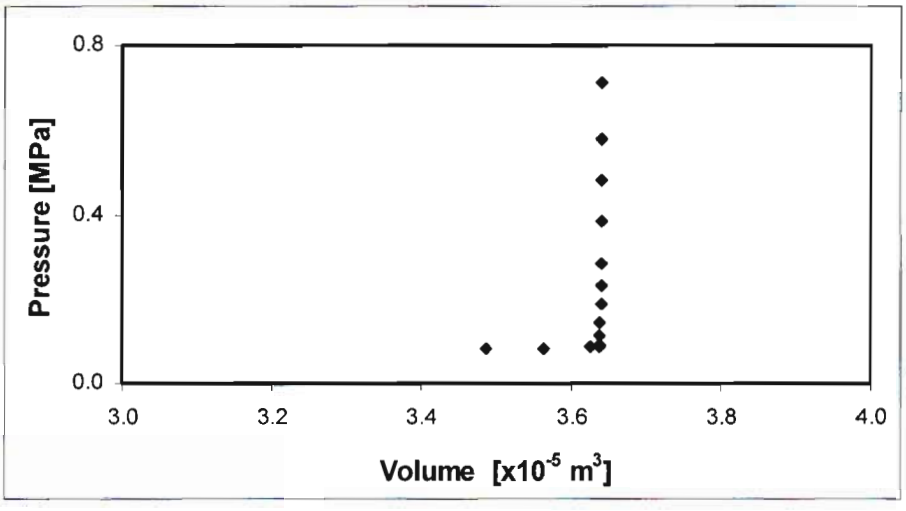

Figure B.9. Measured P-V data for HFP + Toluene at 273.15 K and mole fraction HFP 0.0854.

Pressure [MPa]	Volume [x10^{-5} m^3]
6.928	3.3011
1.434	3.2885
0.930	3.2866
0.561	3.2853
0.421	3.2844
0.324	3.2841
0.246	3.2836
0.168	3.2391
0.167	3.2080
0.167	3.1651
0.167	3.1323
0.166	3.0211

Table B.4. Measured P-V data for HFP + Toluene at 273.15 K and mole fraction HFP 0.2050.

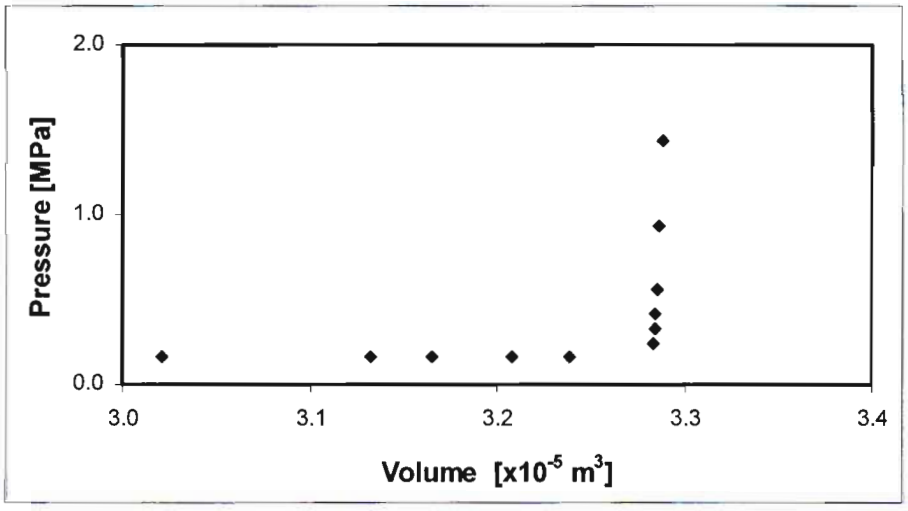

Figure B.10. Measured P-V data for HFP + Toluene at 273.15 K and mole fraction HFP 0.2050.

Pressure [MPa]	Volume [x10^{-5} m^3]
6.031	2.7141
1.146	2.6937
0.880	2.6915
0.691	2.6905
0.594	2.6899
0.494	2.6891
0.425	2.6888
0.392	2.6885
0.326	2.6881
0.286	2.6879
0.232	2.6876
0.202	2.6870
0.182	2.6695
0.181	2.4933
0.181	2.3470

Table B.5. Measured P-V data for HFP + Toluene at 273.15 K and mole fraction HFP 0.3909.

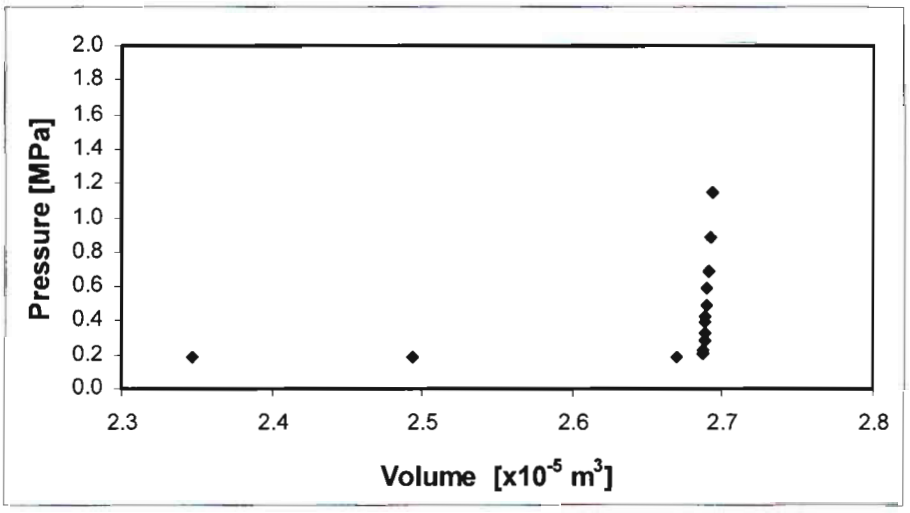

Figure B.11. Measured P-V data for HFP + Toluene at 273.15 K and mole fraction HFP 0.3909.

Pressure [MPa]	Volume [x10^{-5} m^3]
0.908	3.0133
0.576	3.0111
0.530	3.0106
0.476	3.0102
0.383	3.0094
0.331	3.0089
0.279	3.0085
0.226	3.0080
0.184	3.0076
0.182	2.9900
0.180	2.8838

Table B.6. Measured P-V data for HFP + Toluene at 273.15 K and mole fraction HFP 0.7040.

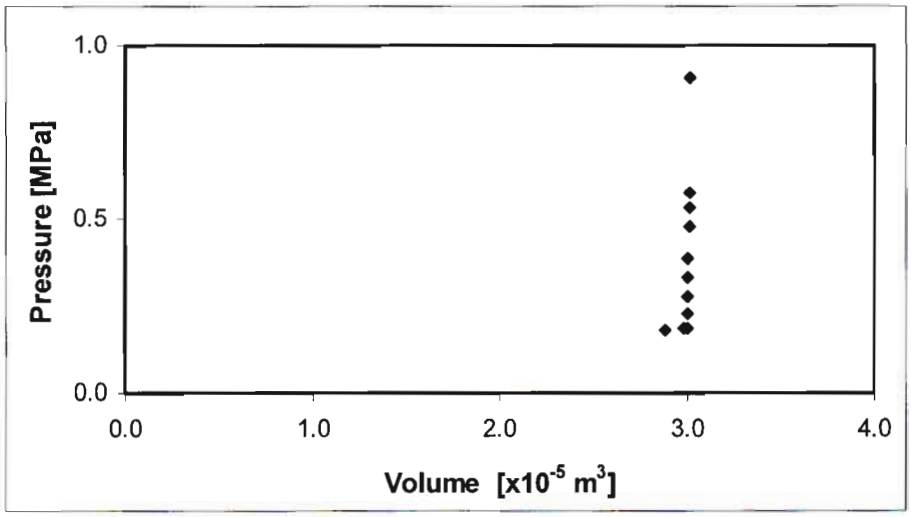

Figure B.12. Measured P-V data for HFP + Toluene at 273.15 K and mole fraction HFP 0.7040.

B 3.2. HFP + Toluene: 313.15 K isotherm

The full recorded pressure versus volume data for each loading of the equilibrium cell for the system HFP + Toluene at 313.15 K are presented in Tables B.7 through B.10. This data is also presented graphically from Figures B.13 to B.16.

Pressure [MPa]	Volume [$x10^{-5}$ m^3]
7.467	3.5392
1.180	3.5207
0.811	3.5187
0.715	3.5183
0.655	3.5180
0.561	3.5177
0.466	3.5174
0.368	3.5169
0.351	3.5154
0.300	3.3888
0.293	3.2049
0.264	2.8615
0.232	2.4169
0.229	2.1296

Table B.7. Measured P-V data for HFP + Toluene at 313.15 K and mole fraction HFP 0.0854.

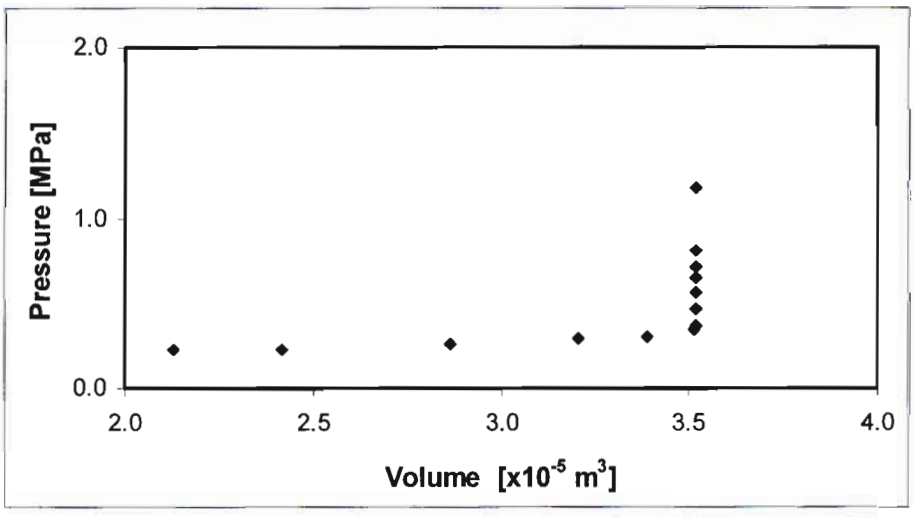

Figure B.13. Measured P-V data for HFP + Toluene at 313.15 K and mole fraction HFP 0.0854.

Pressure [MPa]	Volume [x10^{-5} m^3]
1.183	3.1326
0.975	3.1309
0.870	3.1303
0.760	3.1296
0.663	3.1291
0.689	3.1284
0.653	3.1212
0.619	3.1153
0.621	3.0829
0.620	3.0607
0.609	2.9185

Table B.8. Measured P-V data for HFP + Toluene at 313.15 K and mole fraction HFP 0.2050.

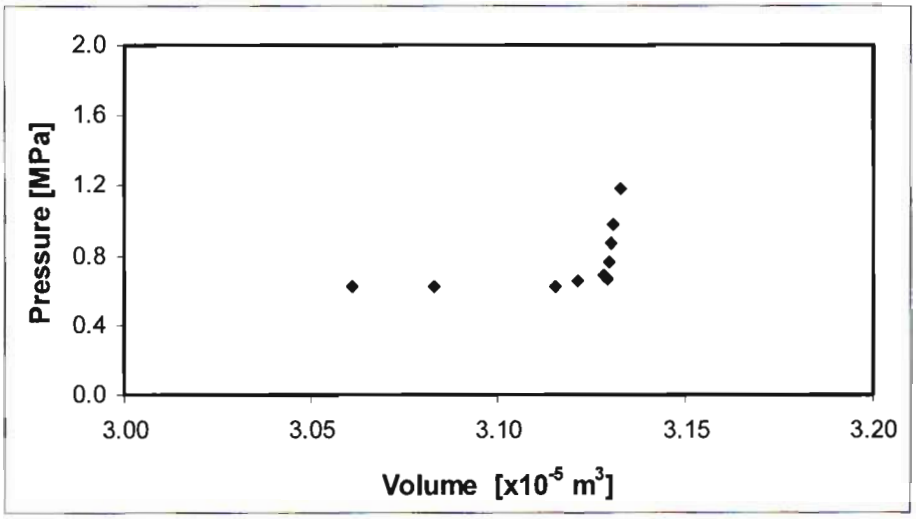

Figure B.14. Measured P-V data for HFP + Toluene at 313.15 K and mole fraction HFP 0.2050.

Pressure [MPa]	Volume [x10^{-5} m^3]
6.502	2.4979
2.169	2.4690
1.651	2.4634
1.279	2.4595
1.126	2.4575
1.007	2.4561
0.913	2.4550
0.864	2.4543
0.805	2.4537
0.747	2.4520
0.746	2.4209
0.744	2.1370

Table B.9. Measured P-V data for HFP + Toluene at 313.15 K and mole fraction HFP 0.3909.

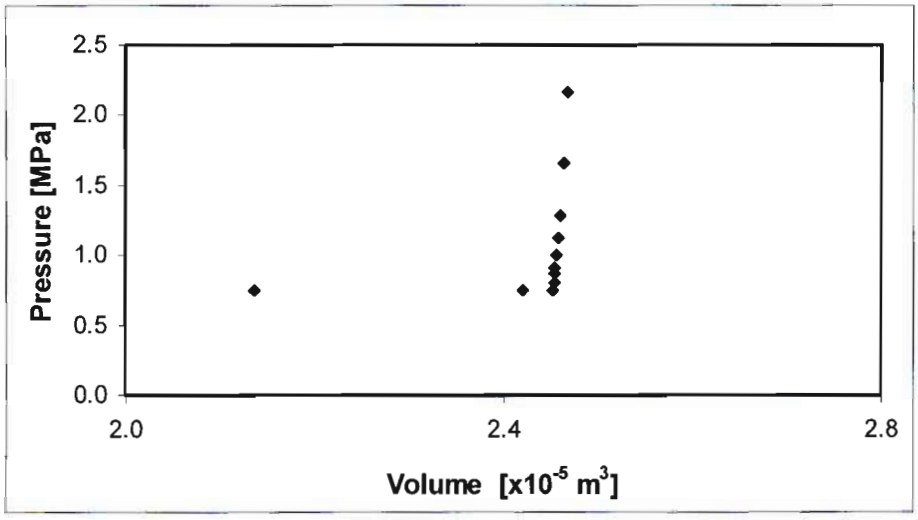

Figure B.15. Measured P-V data for HFP + Toluene at 313.15 K and mole fraction HFP 0.3909.

Pressure [MPa]	Volume [x10^{-5} m^3]
2.990	2.7296
1.949	2.7181
1.537	2.7123
1.155	2.7063
1.040	2.7042
0.973	2.7025
0.929	2.7015
0.871	2.7004
0.800	2.6990
0.783	2.6402
0.779	2.4939

Table B.10. Measured P-V data for HFP + Toluene at 313.15 K and mole fraction HFP 0.7040.

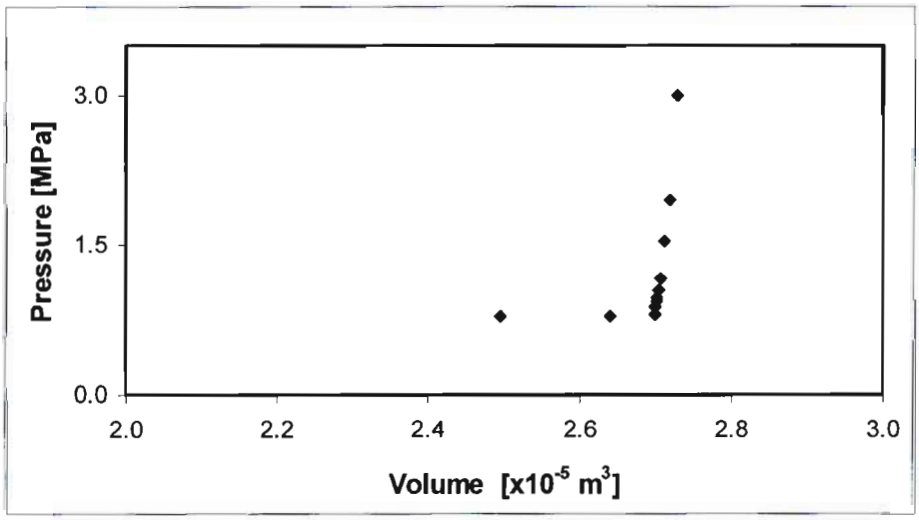

Figure B.16. Measured P-V data for HFP + Toluene at 313.15 K and mole fraction HFP 0.7040.

B 3.3. HFPO + Toluene: 273.15 K isotherm

The full recorded pressure versus volume data for each loading of the equilibrium cell for the system HFPO + Toluene at 273.15 K are presented in Tables B.11 through B.14. This data is also presented graphically from Figures B.17 to B.20.

Pressure [MPa]	Volume [$x10^{-5}$ m^3]
2.124	3.5300
1.195	3.5262
0.581	3.5239
0.483	3.5234
0.376	3.5228
0.334	3.5228
0.288	3.5226
0.236	3.5225
0.196	3.5222
0.191	3.5054
0.190	3.4914
0.188	3.4222

Table B.11. Measured P-V data for HFPO + Toluene at 273.15 K and mole fraction HFPO 0.1765.

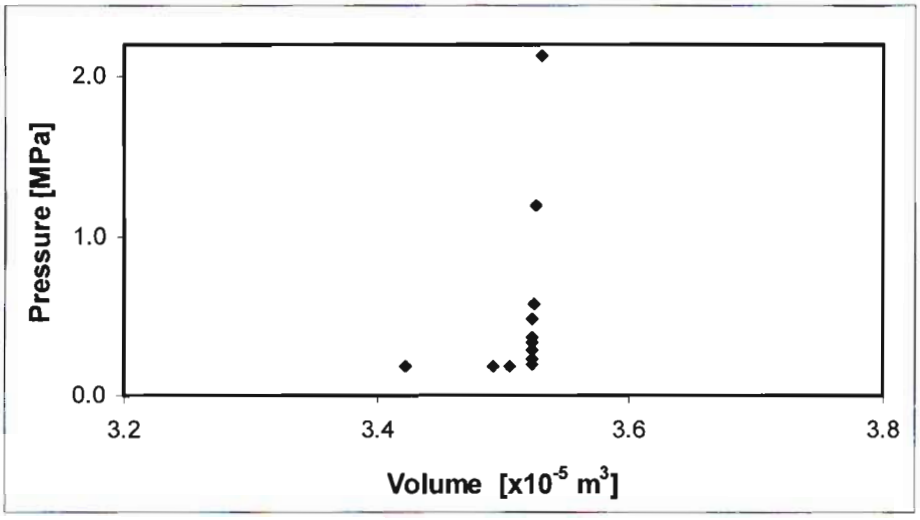

Figure B.17. Measured P-V data for HFPO + Toluene at 273.15 K and mole fraction HFPO 0.1765.

Pressure [MPa]	Volume [x10^{-5} m^3]
2.250	3.0316
1.544	3.0290
1.040	3.0262
0.638	3.0238
0.514	3.0229
0.478	3.0227
0.434	3.0224
0.389	3.0221
0.339	3.0219
0.286	3.0215
0.233	3.0212
0.197	3.0207
0.197	2.9945
0.194	2.9230

Table B.12. Measured P-V data for HFPO + Toluene at 273.15 K and mole fraction HFPO 0.2771.

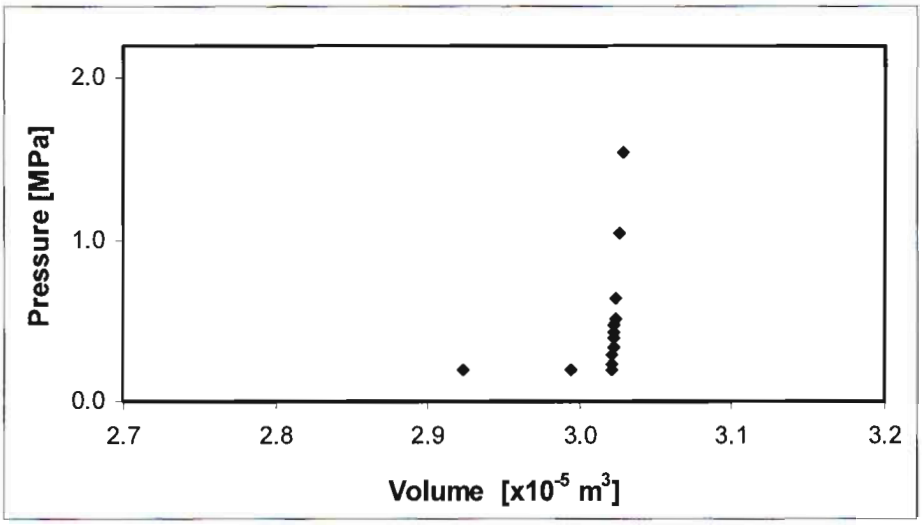

Figure B.18. Measured P-V data for HFPO + Toluene at 273.15 K and mole fraction HFPO 0.2771.

Pressure [MPa]	Volume [x10^{-5} m^3]
1.804	3.2572
1.361	3.2553
1.033	3.2533
0.621	3.2507
0.562	3.2501
0.497	3.2495
0.443	3.2492
0.391	3.2487
0.339	3.2482
0.296	3.2477
0.248	3.2467
0.199	3.2365
0.197	3.2074
0.194	3.1812

Table B.13. Measured P-V data for HFPO + Toluene at 273.15 K and mole fraction HFPO 0.3722.

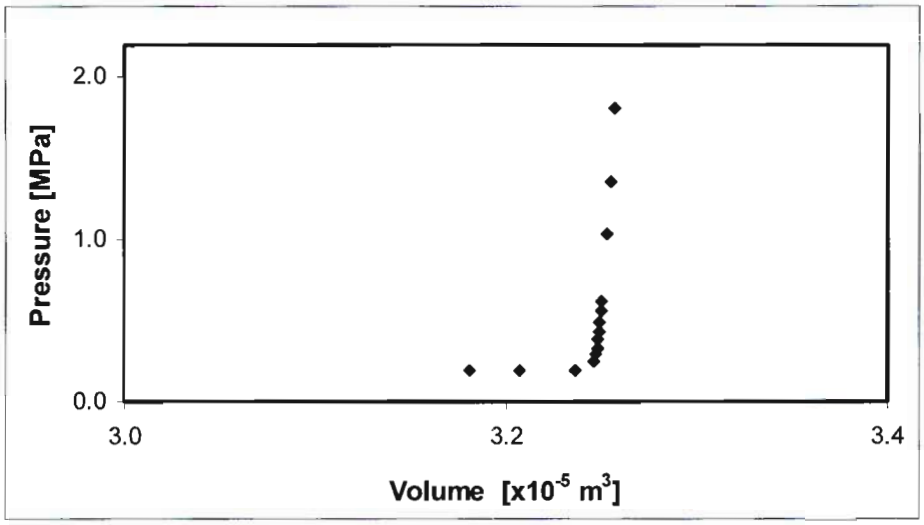

Figure B.19. Measured P-V data for HFPO + Toluene at 273.15 K and mole fraction HFPO 0.3722.

Pressure [MPa]	Volume [x10^{-5} m^3]
2.367	2.7941
1.500	2.7866
1.074	2.7818
0.685	2.7771
0.561	2.7753
0.494	2.7742
0.395	2.7731
0.339	2.7723
0.287	2.7717
0.244	2.7708
0.200	2.7434
0.200	2.7007
0.198	2.6367

Table B.14. Measured P-V data for HFPO + Toluene at 273.15 K and mole fraction HFPO 0.7306.

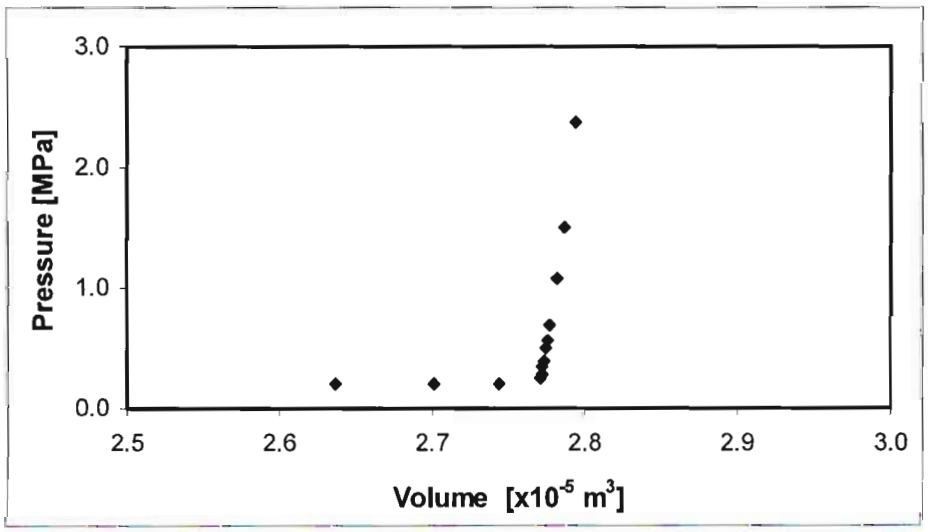

Figure B.20. Measured P-V data for HFPO + Toluene at 273.15 K and mole fraction HFPO 0.7306.

B 3.4. HFPO + Toluene: 313.15 K isotherm

The full recorded pressure versus volume data for each loading of the equilibrium cell for the system HFPO + Toluene at 313.15 K are presented in Tables B.15 through B.19. This data is also presented graphically from Figures B.21 to B.25.

Pressure [MPa]	Volume [$x10^{-5}$ m^3]
1.855	3.4376
1.480	3.4360
1.207	3.4349
1.003	3.4337
0.949	3.4336
0.917	3.4333
0.859	3.4330
0.822	3.4328
0.792	3.3520
0.784	3.2086
0.777	2.9194

Table B.15. Measured P-V data for HFPO + Toluene at 313.15 K and mole fraction HFPO 0.1615.

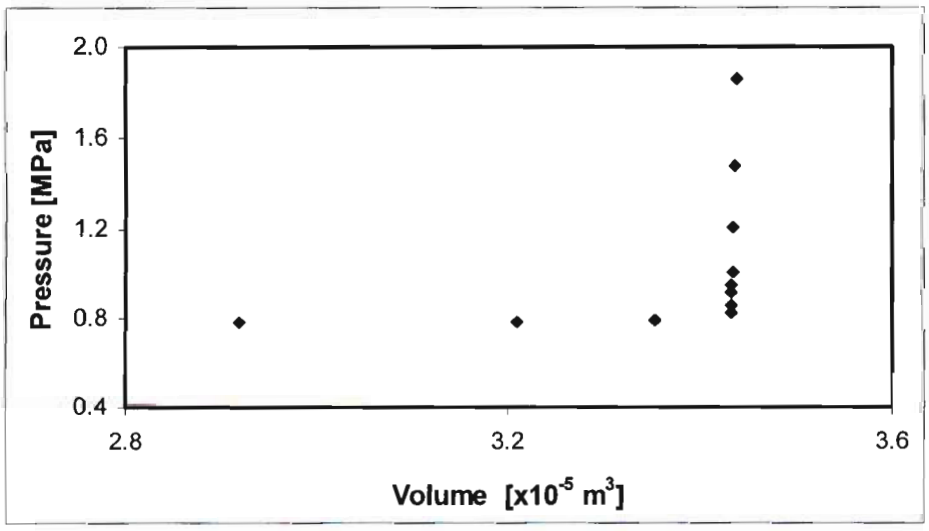

Figure B.21. Measured P-V data for HFPO + Toluene at 313.15 K and mole fraction HFPO 0.1615.

Pressure [MPa]	Volume [x10^{-5} m^3]
2.326	3.3780
1.712	3.3741
1.252	3.3714
1.057	3.3700
1.016	3.3698
0.926	3.3692
0.866	3.3689
0.819	3.3685
0.815	3.3672
0.815	3.3507
0.805	3.2049

Table B.16. Measured P-V data for HFPO + Toluene at 313.15 K and mole fraction HFPO 0.1765.

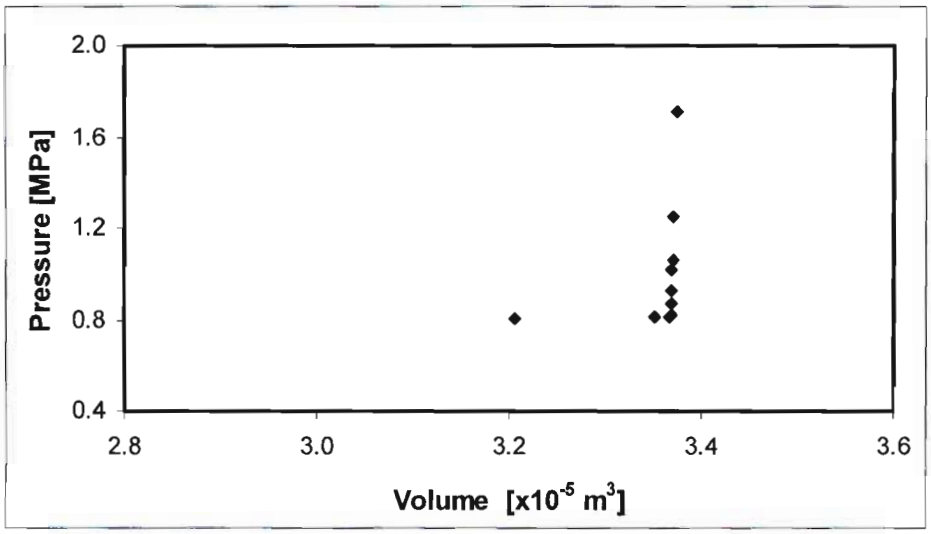

Figure B.22. Measured P-V data for HFPO + Toluene at 313.15 K and mole fraction HFPO 0.1765.

Pressure [MPa]	Volume [x10^{-5} m^3]
2.303	2.8149
1.604	2.8077
1.279	2.8040
1.064	2.8018
0.966	2.8008
0.917	2.8001
0.874	2.7996
0.841	2.7991
0.816	2.7977
0.813	2.7762
0.813	2.6393

Table B.17. Measured P-V data for HFPO + Toluene at 313.15 K and mole fraction HFPO 0.2771.

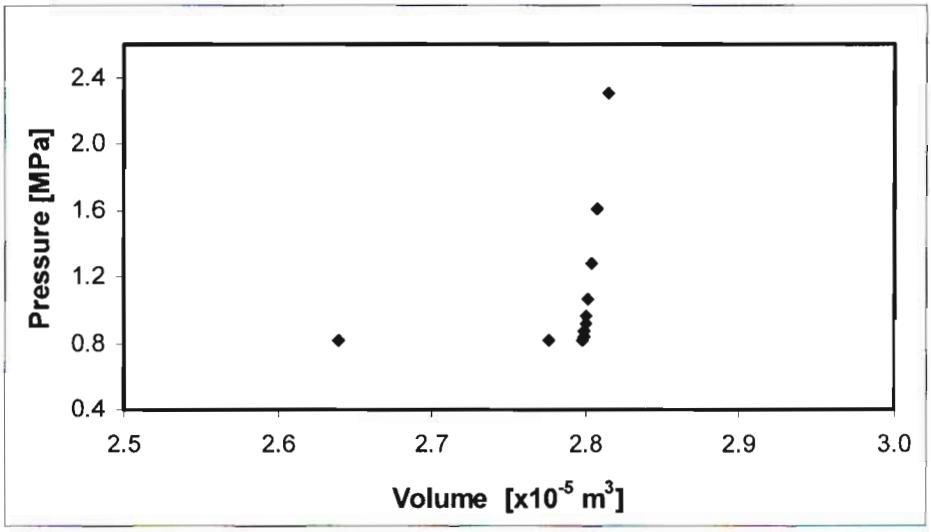

Figure B.23. Measured P-V data for HFPO + Toluene at 313.15 K and mole fraction HFPO 0.2771.

Pressure [MPa]	Volume [x10-5 m3]
1.959	3.0240
1.536	3.0198
1.305	3.0168
1.064	3.0138
1.025	3.0131
0.974	3.0124
0.934	3.0117
0.876	3.0109
0.829	3.0099
0.828	2.9928
0.822	2.8391

Table B.18. Measured P-V data for HFPO + Toluene at 313.15 K and mole fraction HFPO 0.3722.

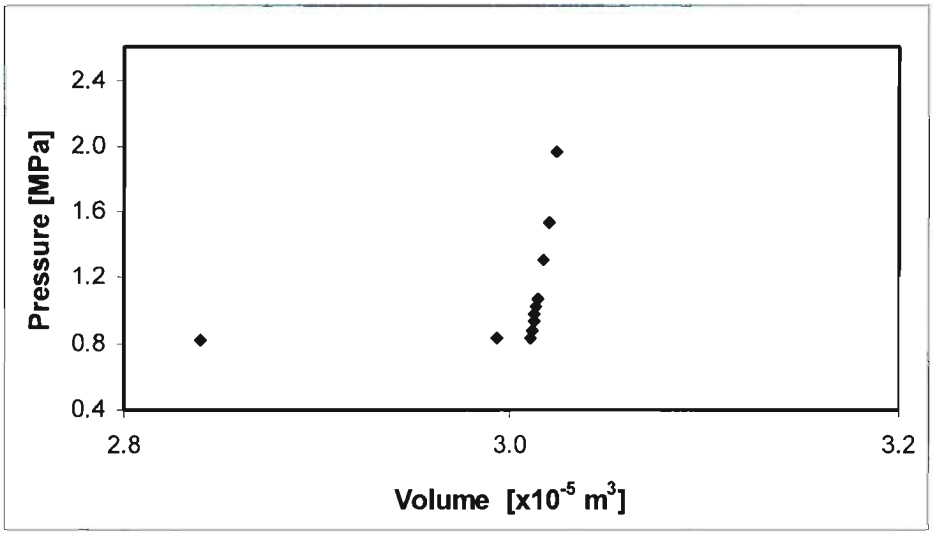

Figure B.24. Measured P-V data for HFPO + Toluene at 313.15 K and mole fraction HFPO 0.3722.

Pressure [MPa]	Volume [x10-5 m3]
2.068	2.4125
1.574	2.4027
1.251	2.3949
1.052	2.3899
0.980	2.3881
0.915	2.3866
0.874	2.3856
0.831	2.3848
0.802	2.3519
0.801	2.2863

Table B.19. Measured P-V data for HFPO + Toluene at 313.15 K and mole fraction HFPO 0.7306.

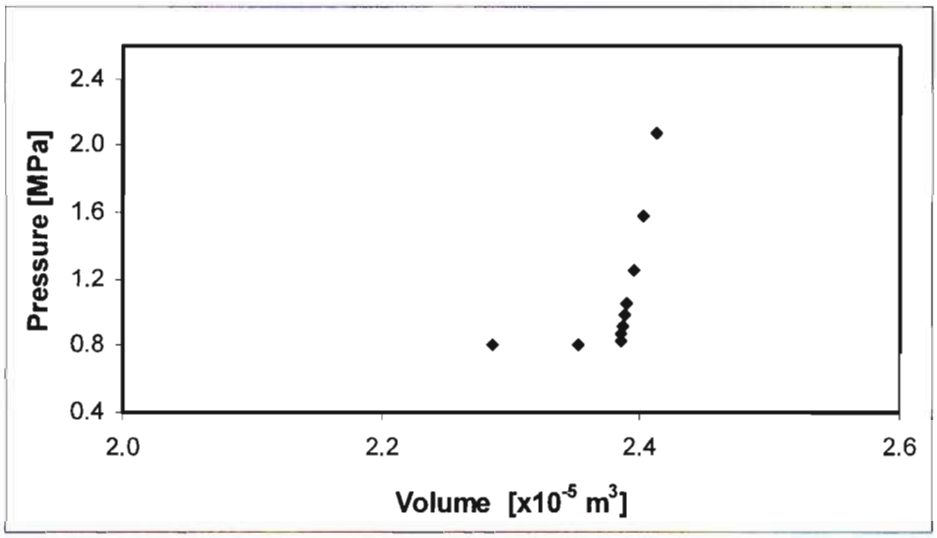

Figure B.25. Measured P-V data for HFPO + Toluene at 313.15 K and mole fraction HFPO 0.7306.

B 4. EXPERIMENTAL P-X-Y DATA FOR THE STATIC ANALYTIC APPARATUS

B 4.1. R116 + HFP: 273.15 K isotherm

The measured P-x-y data for the system R116 + HFP at 273.15 K are presented in Table B.20. For a single data point, four samples each of the equilibrium vapour and liquid phases were obtained to determine measurement accuracy and reproducibility. The standard deviation of the measurements as well as the average values for liquid and vapour mole fractions are presented.

Pressure [Mpa]	Liquid Composition X_{R116}	Standard Deviation σX_{R116}	Liquid Composition $X_{R116AVG}$	Vapour Composition Y_{R116}	Standard Deviation σY_{R116}	Vapour Composition $Y_{R116AVG}$
0.5057	0.1154	0.0008	0.1154	0.3705	0.0006	0.3714
	0.1166			0.3718		
	0.1152			0.3716		
	0.1146			0.3716		
0.6935	0.2492	0.2463	0.0029	0.5774	0.0012	0.5790
	0.2434			0.5789		
	0.2464			0.5794		
	0.2423			0.5804		
1.0133	0.4631	0.0030	0.4612	0.7551	0.0010	0.7564
	0.4602			0.7562		
	0.4641			0.7571		
	0.4574			0.7574		
1.1863	0.5897	0.0010	0.5884	0.8239	0.0003	0.8243
	0.5885			0.8245		
	0.5870			0.8242		
	0.5881			0.8245		
1.4180	0.7460	0.0004	0.7457	0.8923	0.0011	0.8939
	0.7452			0.8941		
	0.7456			0.8945		
	0.7459			0.8946		
1.5402	0.8223	0.0003	0.8218	0.9243	0.0007	0.9253
	0.8217			0.9253		
	0.8216			0.9255		
	0.8216			0.9261		

Table B.20. Measured P-x-y data for the system R116 + HFP at 273.15 K.

B 4.2. R116 + HFP: 313.15 K isotherm

The measured P-x-y data for the system R116 + HFP at 313.15 K are presented in Table B.21. For a single data point, four samples each of the equilibrium vapour and liquid phases were obtained to determine measurement accuracy and reproducibility. The standard deviation of the measurements as well as the average values for liquid and vapour mole fractions are presented. The system reached the supercritical state for pressures greater than 3.6 MPa.

Pressure [Mpa]	Liquid Composition X_{R116}	Standard Deviation σX_{R116}	Liquid Composition $X_{R116AVG}$	Vapour Composition Y_{R116}	Standard Deviation σY_{R116}	Vapour Composition $Y_{R116AVG}$
1.6760	0.1456	0.0003	0.1454	0.2522	0.0253	0.2537
	0.1451			0.2500		
	0.1452			0.2549		
	0.1457			0.2578		
2.0493	0.2649	0.0006	0.2652	0.4241	0.0020	0.4262
	0.2646			0.4250		
	0.2655			0.4279		
	0.2656			0.4278		
2.6021	0.4363	0.0003	0.4367	0.5690	0.0016	0.5667
	0.4366			0.5657		
	0.4369			0.5658		
	0.4370			0.5662		
2.9621	0.5424	0.0002	0.5425	0.6496	0.0005	0.6490
	0.5422			0.6491		
	0.5427			0.6491		
	0.5427			0.6484		
3.2983	0.6438	0.0003	0.6437	0.6863	0.0003	0.6864
	0.6433			0.6860		
	0.6440			0.6866		
	0.6439			0.6865		

Table B.21. Measured P-x-y data for the system R116 + HFP at 313.15 K.

B 4.3. R116 + HFPO: 273.15 K isotherm

The measured P-x-y data for the system R116 + HFPO at 273.15 K are presented in Table B.22. For a single data point, four samples each of the equilibrium vapour and liquid phases were obtained to determine measurement accuracy and reproducibility. The standard deviation of the measurements as well as the average values for liquid and vapour mole fractions are presented.

Pressure [Mpa]	Liquid Composition X_{R116}	tandard Deviation σX_{R116}	Liquid Composition $X_{R116AVG}$	Vapour Composition Y_{R116}	Standard Deviation σY_{R116}	Vapour Composition $Y_{R116AVG}$
0.5314	0.1580	0.0020	0.1562	0.4491	0.0042	0.4516
	0.1553			0.4491		
	0.1577			0.4505		
	0.1538			0.4579		
0.7725	0.3273	0.0020	0.3267	0.6595	0.0004	0.6600
	0.3270			0.6604		
	0.3239			0.6602		
	0.3285			0.6601		
1.0371	0.5118	0.0015	0.5111	0.7875	0.0003	0.7878
	0.5103			0.7882		
	0.5094			0.7878		
	0.5129			0.7876		
1.1772	0.6035	0.0005	0.6036	0.8360	0.0010	0.8365
	0.6043			0.8378		
	0.6032			0.8355		
	0.6034			0.8368		
1.4015	0.7438	0.0011	0.7422	0.8992	0.0006	0.8987
	0.7415			0.8993		
	0.7419			0.8984		
	0.7416			0.8982		
1.6293	0.8774	0.0009	0.8768	0.9519	0.0012	0.9526
	0.8756			0.9519		
	0.8775			0.9544		
	0.8765			0.9521		

Table B.22. Measured P-x-y data for the system R116 + HFPO at 273.15 K.

B 4.4. R116 + HFPO: 313.15 K isotherm

The measured P-x-y data for the system R116 + HFPO at 313.15 K are presented in Table B.23. For a single data point, four samples each of the equilibrium vapour and liquid phases were obtained to determine measurement accuracy and reproducibility. The standard deviation of the measurements as well as the average values for liquid and vapour mole fractions are presented. The system reached the supercritical state for pressures greater than 3.3 MPa. Sampling of the equilibrium vapour phase for the equilibrium pressure of 3.3986 MPa was not possible as the system had reached the supercritical state and only a single liquid phase was present.

Pressure [Mpa]	Liquid Composition X_{R116}	Standard Deviation σX_{R116}	Liquid Composition $X_{R116AVG}$	Vapour Composition Y_{R116}	Standard Deviation σY_{R116}	Vapour Composition $Y_{R116AVG}$
1.6560	0.1654	0.0005	0.1654	0.2458	0.0036	0.2421
	0.1660			0.2388		
	0.1653			0.2392		
	0.1649			0.2446		
1.9984	0.2691	0.0001	0.2690	0.4445	0.0005	0.4452
	0.2689			0.4455		
	0.2690			0.4453		
	0.2692			0.4454		
2.5419	0.4326	0.0011	0.4312	0.5867	0.0006	0.5859
	0.4306			0.5857		
	0.4301			0.5856		
	0.4316			0.5855		
3.0224	0.5695	0.0001	0.5696	0.6577	0.0003	0.6580
	0.5697			0.6582		
	0.5695			0.6583		
	0.5696			0.6577		
3.3986	0.6652	0.0006	0.6645	-	-	-
	0.6648			-		
	0.6644			-		
	0.6637			-		

Table B.23. Measured P-x-y data for the system R116 + HFPO at 313.15 K.

APPENDIX C

C 1. THERMOPACK

The data regression and modelling of the HPVLE data measured for this research project were undertaken in the computer software Thermopack, version 1.10, ((Coquelet and Baba-Ahmed 2002)), which was developed at the TEP laboratory specifically for HPVLE systems. The Thermopack software, which was used under permission by the authors, is a proprietary software set capable of the following:

1. Fitting of pure component parameters to pure component vapour pressure data
2. Fitting binary interaction parameters to binary and multicomponent phase equilibrium
3. Calculating phase equilibrium for unlimited number of components (Bubble and dew points, T-P flash and P-T envelope)
4. Calculation of the critical point and critical line
5. Calculation and output of thermodynamics properties:-
    a. Pure components: compressibility factor, density, enthalpy, entropy
    b. Mixtures: Activity coefficients, Excess Gibbs energy, enthalpy and entropy
6. Graphical output of pure-component and mixture properties for all the calculated properties
7. A graphical tool which allows easy comparison of literature data (isobaric data, isothermal data, various zoom, etc...) for data selection.
8. Interface between the graphical tool module and the computational engine to directly transfer selected data.

For the calculation of pure component properties, Thermopack contained the following models:

1. Peng-Robinson EOS
2. Soave-Redlich-Kwong EOS
3. Lee-Kesler EOS ((Lee and Kesler 1975))
4. Mathias-Copeman alpha function
5. Soave one parameter alpha function ((Soave 1972))
6. Stryjek-Vera alpha function ((Stryjek and Vera 1986)).

For the calculation of multicomponent mixture properties, Thermopack contained several popular model combinations which are presented in Table C.1:

Equations of State	Mixing Rules	T dependence
Soave – Redlich - Kwong	Van der Waals	aij
Peng – Robinson	Huron - Vidal	aij + bij*T
Patel – Teja	Wong - Sandler	aij + bij*T + cij * T^2
	MHV1	
	MHV2 (SRK)	
	PSRK (SRK)	
Alpha functions	**Excess function**	**Algorithm**
Soave one parameter	NRTL (68)	Simplex
Mathias – Copeman	Modified NRTL	Marquardt
Stryjek - Vera	Uniquac	
	Unifac	
	Modified Unifac (Dortmund)	
	PSRK Unifac	

Table C.1. A summary of the thermodynamic model combinations available in the Thermopack software for multicomponent modelling ((Coquelet and Baba-Ahmed 2006a)).

The software was installed on a Hewlett-Packard AMD Turion laptop computer with a 1600 MHz x2 processor and 1024 MB of RAM, with the input files prepared on Microsoft Excel 2002 and imported into Thermopack. Intellectual property protection of the software was through the granting of a confidential username and password from the software authors.

C 1.1. Pure component data regression

The 'Pure Component' selection screen of the software is presented in Figure C.1. In this screen the components of the system were selected from the internal database of Thermopack via a search function. The software allowed the modification of all available pure component properties which included the molecular weight, boiling point, critical constants, UNIFAC R and Q parameters, MC parameters for the PR or SRK EOS as well as accentric factor ω and critical compressibility Z_C.

For the data regression of pure component experimental data, for example vapour pressures, the procedure is illustrated for the fitting of the PR-MC parameters for component HFPO. The 'Problem Definition' screen for the fitting of pure component data is presented in Figure C.2. Once the components were defined in the 'Pure Component' sheet of Thermopack, they are then available for selection throughout the programme. The component HFPO was selected as indicated in Figure C.2 and the pure component data to be regressed was first prepared in Excel (in terms of SI units and arrangement of data into separate columns) and pasted in the workspace on the 'Problem Definition' area. In the 'Models' selection sheet, as presented in Figure C.3, the appropriate thermodynamic models are chosen for the regression from a drop

down list of available models, for this particular application the PR EOS with the MC alpha function was chosen. Figure C.6 presents the 'Run' worksheet of the programme. The 'Clear Results' button performs the function of clearing the software memory of any previous calculations and re-initialisation. The 'Adjust Pure' button initiated the calculation with the results presented in text format in the workspace directly below the buttons. The information presented in the results workspace includes the thermodynamic models used, the MC1, MC2 and MC3 parameters, the value of the objective function and the experimental and calculated property values. The 'Save to File' button on the 'Run' worksheet saved all of the data presented in the results workspace to a text document of the hard drive which could later be imported into Excel for manipulation.

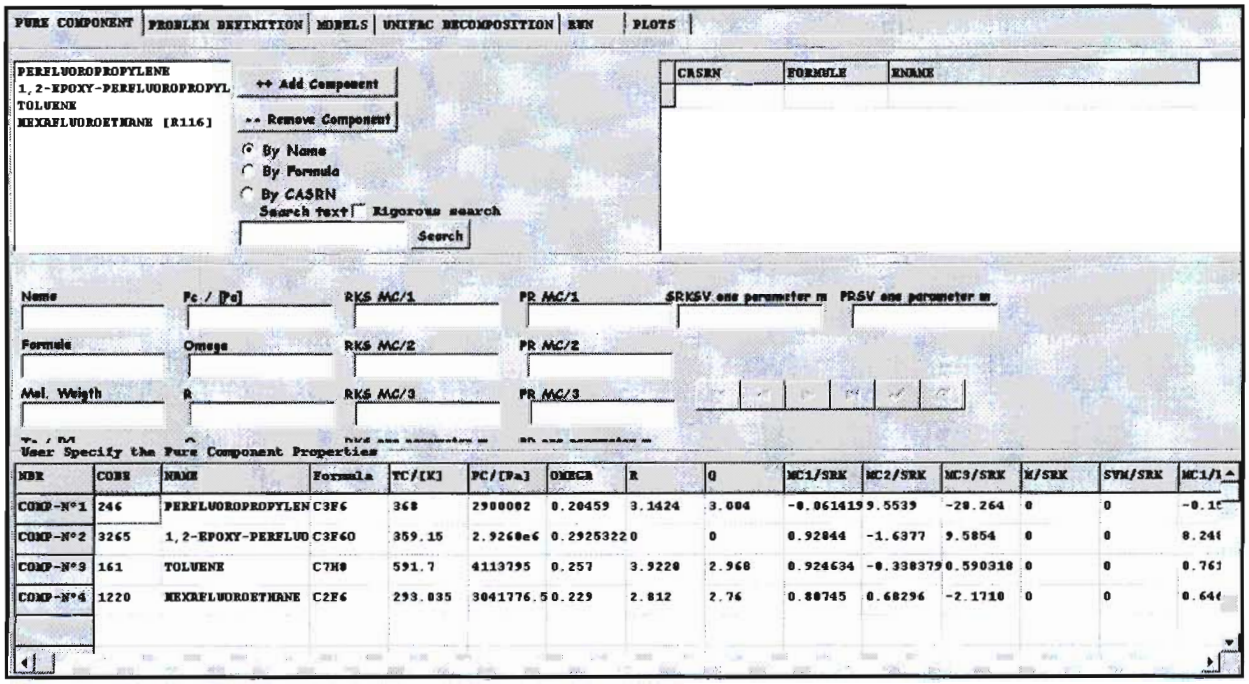

Figure C.3. The Thermopack 'Pure Component' selection screen.

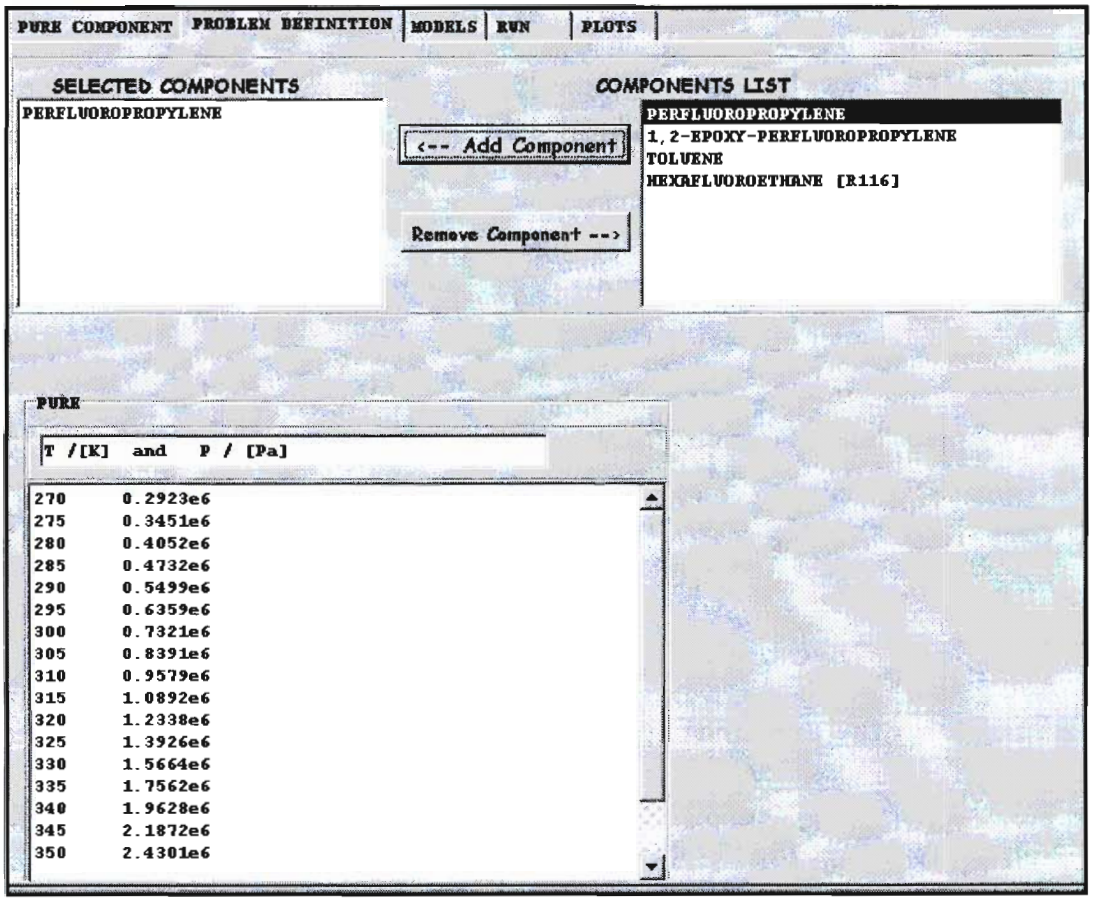

Figure C.4. The Thermopack 'Problem Definition' screen for a pure component data regression.

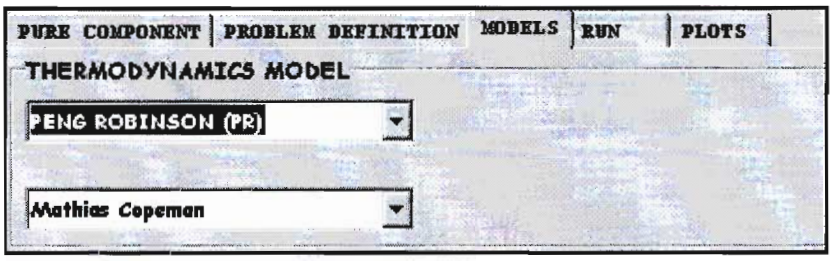

Figure C.5. The Thermopack 'Models' worksheet for a pure component data regression.

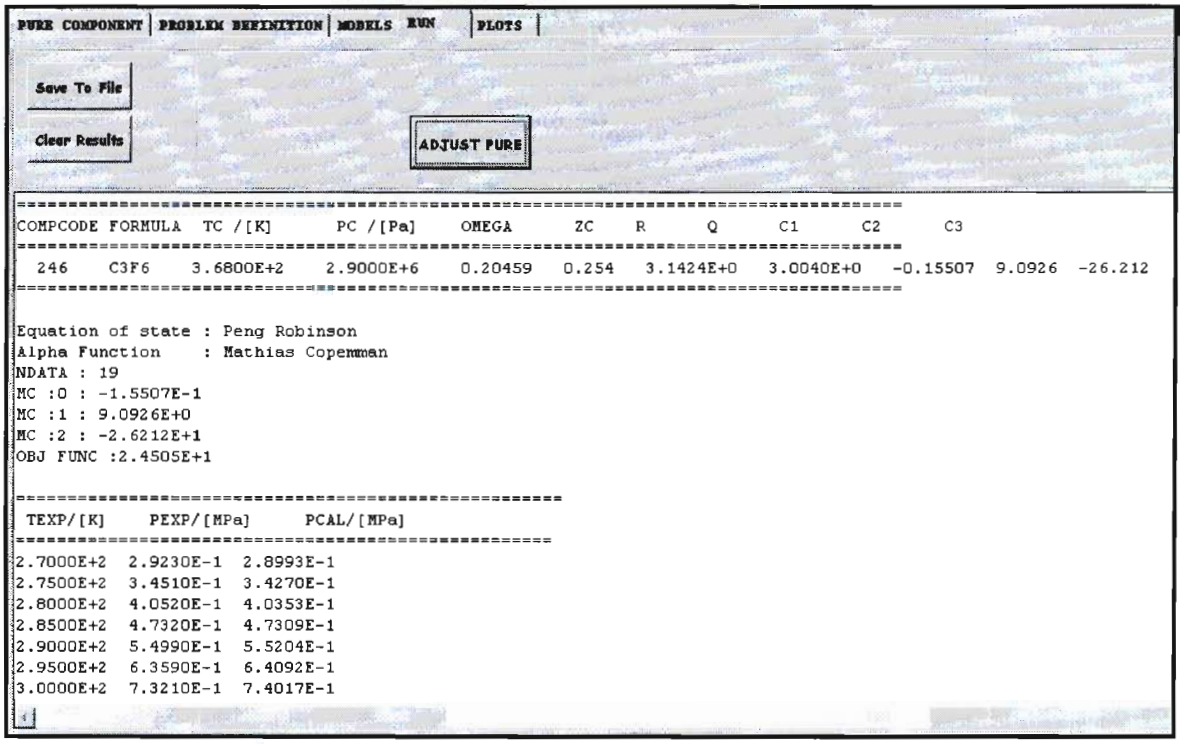

Figure C.6. The Thermopack 'Run' worksheet for a pure component.

C 1.2. Multicomponent data regression

For the data regression for binary mixtures, the components are once defined in the 'Pure Component' worksheet in Figure C.1. Figure C.7 presents the 'Problem Definition' screen for a multicomponent (binary) data regression for the system R116 + HFP. The two components of the binary system were selected from the available components list and the data which was prepared in Excel pasted into the workspace. The input data for a multicomponent regression contained columns for the experimental values of temperature, pressure, vapour and liquid mole fractions, gamma (liquid activity coefficients), code (an internal command of the Thermopack software, set to zero for all calculations) and F_{obj}, the objective function, with an objective function of four corresponding to the flash adjustment of equation (6-46).

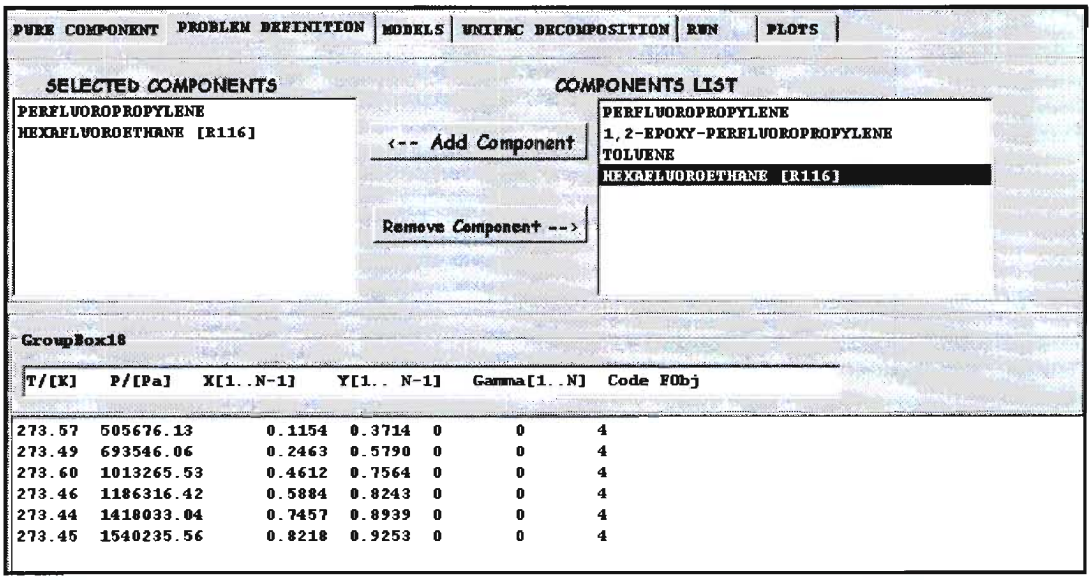

Figure C.7. The Thermopack 'Problem Definition' screen for a multicomponent data regression.

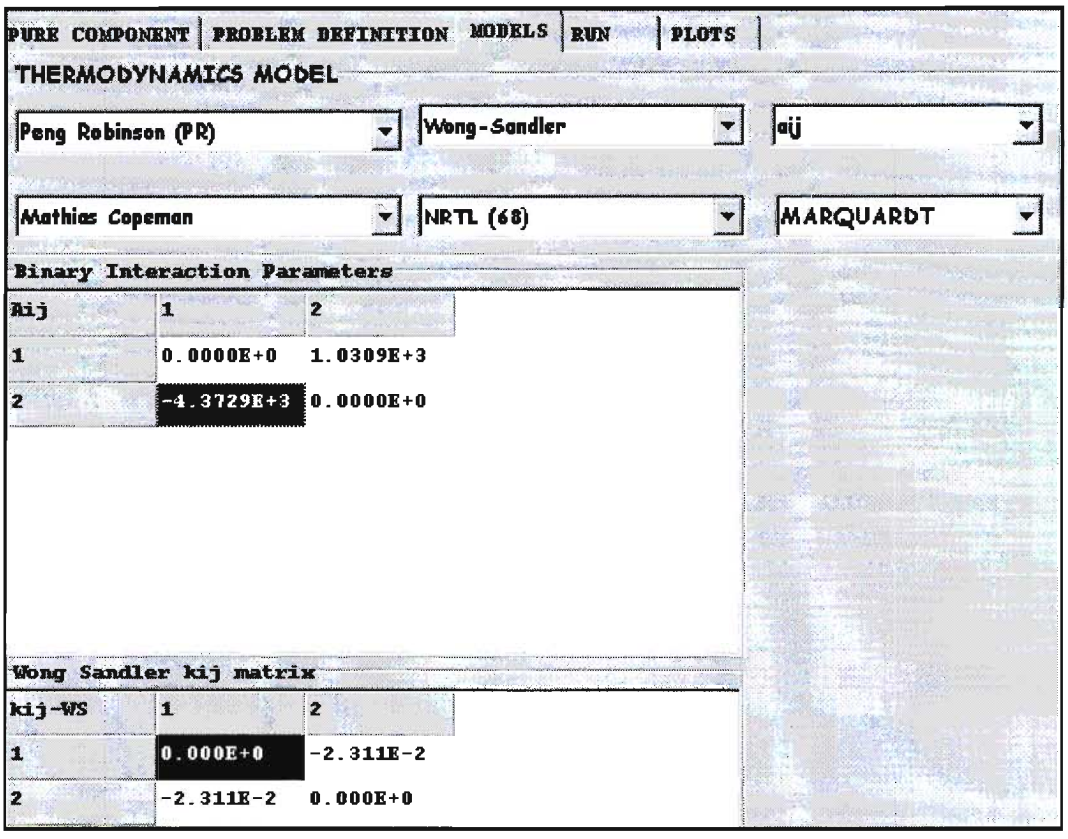

Figure C.8. The Thermopack 'Models' worksheet for a multicomponent data regression.

The 'Models' worksheet for a multicomponent data regression is presented in Figure C.8. The required models were selected from the available models from the drop down menu, for this particular system, R116 + HFP, the models used were the PR EOS with the MC alpha function, WS mixing rules and the NRTL activity coefficient model. The binary interaction parameters were set to be temperature independent and estimates of initial values were entered into the provided workspace. The algorithm for the regression could also be selected form a drop down menu, for this research project the Marquardt algorithm ((Marquardt 1963)) was used for all calculations.

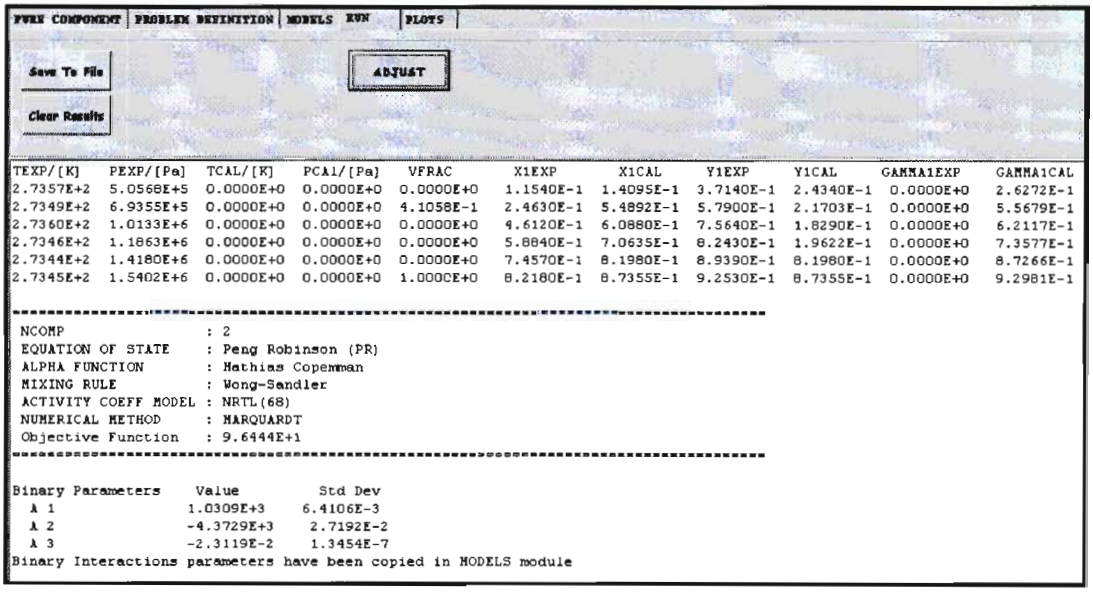

Figure C.9. The Thermopack 'Run' worksheet for a multicomponent regression.

Figure C.9 presents the 'Run' worksheet for a multicomponent regression. The 'Clear Results' button was depressed to reinitialise the software, while the 'Adjust' button initiated the calculation with the results presented in text format in the workspace directly below the buttons. The information presented in the results workspace includes the thermodynamic models used, the NRTL binary interaction parameters, the WS k_{ij} parameter, the value of the objective function and the experimental and calculated property values, which included predictions of the activity coefficient values for the system. The 'Save to File' button on the 'Run' worksheet saved all of the data presented in the results workspace to a text document of the hard drive which could later be imported into Excel for manipulation. The pure component vapour pressure data regression for HFPO was performed in the manner described above with PR and SRK EOS and MC alpha function, while the binary HPVLE data was regressed in the manner described using the four possible model combinations for all four binary systems at two isotherms.

APPENDIX D

D 1. ASPEN

The Aspen Engineering Suite ((AspenTech 2004)) was utilised for the design and simulation of the Toluene and R116 separation processes presented in this dissertation. Before the simulations were undertaken, the key components of the system had to be defined, and an appropriate property method defined.

D 1.1. Component Definition

The first step of the preliminary design process lay in the specification of the components HFP, HFPO, Toluene and R116 in the simulation package. Aspen Plus stores physical property parameters for a large number of components in several internal databanks. A component for use in the simulation was selected by searching the Aspen databank using either the name, molecular formula or CAS registry number with the components HFP, Toluene and R116 available in the Aspen Plus pure component databanks. The component HFPO did not exist in any of the Aspen pure component databanks and had be specified manually. The specification for the component HFPO involved the input of the pure component parameters as listed in Table D.1, along with the molecular structure of HFPO:

T_b [K]	T_f [K]	M.W. [g•mol^{-1}]	S.G.	ω	T_c [K]	P_c [Pa]	V_c [cm^3•mol^{-1}]	Z_c
248.75	147.70	166.02	1.30	0.2925	359.15	2926000	0.3290	0.2360

Table D.1. Pure component properties for HFPO required for the ASPEN pure component definition.

The molecular structure of HFPO was entered into Aspen via the use of '*.mol' file which contained information on a components molecular structure. The two dimensional molecular structure file was obtained from the NIST website ((NIST 2007a)). The pure component data that was required for the definition of HFPO is presented in Table D.1 and included the normal boiling point, freezing point, molecular weight, specific gravity, accentric factor and critical properties.

The next step in the pure component definition was the input of further pure component properties. For vapour pressure calculations without the use of an equation of state (EOS), Aspen utilized the extended Antoine vapour pressure equation and thus required extended Antoine vapour pressure coefficients, denoted by the internal referral term 'PLXANT' in Aspen. The PLXANT coefficients were available for the components Toluene and R116 but were not available for HFP and HFPO. As such, the parameters were regressed from pure component vapour pressure data for HFP and HFPO utilising the built in Aspen data regression function. The pure component vapour pressure data for HFPO measured for this research project was used for the regression of the HFPO PLXANT parameters, while the pure component vapour

pressure data measured by (Nelson 2008) was used to obtain the HFP PLXANT parameters. The regressed parameters used in the simulations are presented in Table D.2:

Component	PLXANT 1 [Pa]	PLXANT 2 [Pa]
HFP	70.3258	-4500.4466
HFPO	70.7595	-4492.3579

Table D.2. Regressed extended Antoine (PLXANT) coefficients for HFP and HFPO.

D 1.2. Property Method

An important step in the process simulation was the selection of the correct base method or physical property method. A property method in Aspen is a collection of methods and models used to compute the following thermodynamic and transport properties:

1. Fugacity coefficient
2. K-values
3. Entropy
4. Gibbs free energy
5. Volume
6. Viscosity
7. Thermal conductivity
8. Diffusion coefficient
9. Surface tension.

Available property methods in Aspen included 'Ideal property methods', 'Equation of state property methods', 'Activity coefficient property methods' and 'Property methods for special systems'. The correct choice of property method was critical to ensure the correct representation and calculation of the various thermodynamic and transport properties for the system.

For the regression of the measured binary HPVLE data, as detailed in Chapter six, an equation of state property method (with three possible model combinations) via the software Thermopack was utilized. Of the three possible model combinations, the PR EOS with the WS mixing was the best performing model set.

The equation of state property method in Aspen was chosen to match the data regression done in ThermoPack with the PR EOS and WS mixing rules, involving the MC alpha function and NRTL activity

coefficient model. The base method chosen in Aspen was termed 'PRWS' which utilized the PR EOS and WS mixing rules. However the default PRWS base method in Aspen had to be modified as it utilized the Boston-Mathias ((Boston and Mathias 1980)) alpha function in the EOS as well as the UNIFAC ((Fredenslund et al. 1977)) activity coefficient model for the calculation of activity coefficients. Via the use of the property method selection tool the default base method PRWS was modified to incorporate the MC alpha function, and the activity coefficient model was modified from the UNIFAC method to the NRTL model.

D 1.3. Importing Data into Aspen

The thermodynamic model parameters which were regressed via Thermopack were imported into Aspen.

System	T [K]	$\tau_{1,2}$ [J•mol^{-1}]	$\tau_{2,1}$ [J•mol^{-1}]	$k_{1,2}$
HFP + HFPO	273.15	-1163.70	1035.60	0.0911
	313.15	-1225.30	1056.20	0.0877
HFP + Toluene	273.15	5850.00	4150.00	-0.7720
	313.15	7224.00	2961.10	-0.2561
HFPO + Toluene	273.15	5299.60	5924.00	-0.5087
	313.15	3656.50	5013.30	0.0644
R116 + HFP	273.15	1451.90	-548.42	-0.0027
	313.15	-2295.30	3509.20	0.1444
R116 + HFPO	273.15	3179.60	-1721.90	-0.0377
	313.15	6631.60	-3000.30	0.0677

Table D.3. A summary of the regressed thermodynamic model parameters which were imported into Aspen for the modified PRWS property set.

A summary of the parameters imported into Aspen is presented in Table D.3. These parameters could only be utilized in conjunction with the modified PRWS base method. The parameters for the binary system HFP + HFPO at 273.15 and 313.15 K were regressed from the data predicted via the PSRK UNIFAC method ((Holderbaum and Gmehling 1991)). The parameters for the remaining systems involving R116, Toluene, HFP and HFPO were regressed from the experimentally measured HPVLE data. The MC parameters for the PR EOS were imported into Aspen and utilized in conjunction with the modified PRWS base method to allow a better representation of vapour pressures.

As a check of the validity of the modified base method and the imported interaction parameters, use was made of the 'Analysis' toolset of Aspen which allowed the prediction of pure component and binary mixture properties for a chosen property method assuming the interaction parameters are available. The pure component vapour pressures for HFPO in the experimental temperature range were predicted as well

as each of the five binary systems listed in Table D.3 at each of the two isotherms, resulting in a total of ten predicted binary data sets. The data predicted by the Aspen Analysis toolset matched exactly the measured HPVLE data the binary systems, as well as the pure component vapour pressure data for HFPO, which confirmed that the property method for our system, as well as the data, was chosen and imported correctly.

D 2. The Toluene Separation Process

The design of the Toluene process, utilising the methodology presented in the preceding paragraphs, is detailed for each unit operation in the following sections.

For the process design procedure the following naming convention is used:

1. Distillation column names were denoted by the prefix 'C' with the number of the column on the flowsheet indicated after the 'C'. For example, the CO_2 removal column was the first column on the flowsheet and was denoted as 'C1'
2. The distillate stream of any column was named by attaching the suffix 'TOPS' to the name of the column as defined in (1). For example, the distillate stream for C1 was designated 'C1TOPS'
3. The bottoms product stream of any column was named by attaching the suffix 'BOTTS' to the name of the column as defined in (1). For example, the bottoms stream for C1 was designated 'C1BOTTS'.
4. The feed stream to any column was named by adding the suffix 'FEED' to the name of the column as defined in (1). For example, the feed stream for C1 was designated 'C1FEED'.

The feed composition for the stream entering the Toluene and R116 separation processes was specified by PELCHEM and is presented in Table D.4:

	Mole Fraction
HFP	0.21
HFPO	0.42
CO_2	0.35
Toluene	0.02

Table D.4. Feed composition for the HFP and HFPO feed stream to be separated.

D 2.1. Column C1

The purpose of column C1 was to remove the CO_2 from the feed stream containing the HFP and HFPO mixture. A schematic of column C1 is presented in Figure D.1.

The feed conditions listed in Table D.4 at a flowrate of 5 $kg \cdot hr^{-1}$ were used as the input for the process. For both the Toluene and R116 separation processes, the impurities in the feed stream, termed 'C1FEED', were removed to produce a stream consisting primarily of HFP and HFPO. The C1FEED stream contained 35 % (mole) of CO_2 which was sent to column C1 to be removed via distillation. For the design of the Toluene separation process, the 2 % (mole) of Toluene in the C1FEED stream was not removed as more Toluene in the form of the solvent was added to the system at a later point. The RadFrac model was chosen for C1 and the initial specifications for the column and the C1FEED stream are presented in Table D.5:

C1	
Stages	20
Distillate rate [$kg \cdot hr^{-1}$]	0.65
Molar RR	5
Column P [atm]	15
C1FEED	
Flowrate [$kg \cdot hr^{-1}$]	5
T [K]	298.15
P [atm]	21
N_F	10

Table D.5. Initial operating and feed stream conditions for distillation column C1 for the Toluene separation process.

The initial estimated values for the molar RR, column pressure, N_T and N_F values were specified according to the procedure outlined in the design methodology. Since CO_2 was removed at the top of the distillation column as the light key component, the distillate rate for column C1 was set to 0.65 $kg \cdot hr^{-1}$, which represented the total amount of CO_2 in the 5 $kg \cdot hr^{-1}$ feed. A partial condenser was chosen for column C1 to remove the CO_2 as a vapour distillate. The operating pressure of the column was set to 15 atm as the vapour pressure of CO_2 at 325.15 K is 114 atm and setting the pressure of the column at 114 atm was impractical. The schematic of column C1 is presented in Figure D.1.

With the input specifications for the CO_2 removal column completed, the Aspen simulation was run and selected stream results are presented in Table D.6. It is evident from the table that even with the default conditions, the majority of the CO_2 (99.78 %) that was in the feed left the column through the distillate stream in a vapour mixture (vapour fraction = 1). From the analysis of the mole fractions of the C1TOPS

stream, little HFP and HFPO exit, with all the Toluene leaving via the bottoms product as Toluene is a non volatile liquid.

Following the general design methodology for the design of a distillation column, the next step was to perform a sensitivity analysis by varying the number of the stages and monitoring the recovery and purity of CO2 in C1TOPS stream. The results of the sensitivity analysis are presented graphically in Figure D.2.

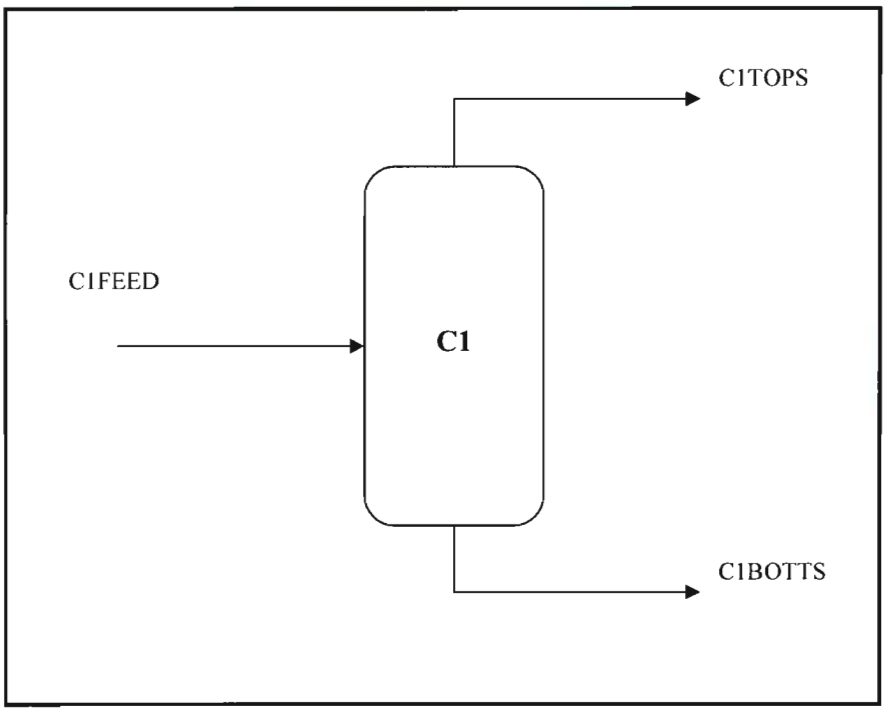

Figure D.1. The schematic of column C1 for the Toluene separation process.

	C1BOTTS	C1FEED	C1TOPS
Mole Fraction			
HFP	0.3227	0.2100	0.0002
HFPO	0.6454	0.4200	0.0004
Toluene	0.0307	0.0200	0.0000
CO_2	0.0011	0.3500	0.9994
Mass Flow [kg•hr^{-1}]			
HFP	1.3292	1.3296	0.0005
HFPO	2.9416	2.9425	0.0009
Toluene	0.0778	0.0778	0.0000
CO_2	0.0014	0.6501	0.6487
Mass Fraction			
HFP	0.3056	0.2659	0.0007
HFPO	0.6762	0.5885	0.0014
Toluene	0.0179	0.0156	0.0000
CO_2	0.0003	0.1300	0.9979
Total Flow [kg•hr^{-1}]	4.3499	5.0000	0.6501
Temperature [K]	329.46	301.92	245.89
Pressure [atm]	15	16	15
Vapour Fraction	0	0	1
Liquid Fraction	1	1	0

Table D.6. The stream results for the initial run for the CO_2 removal column.

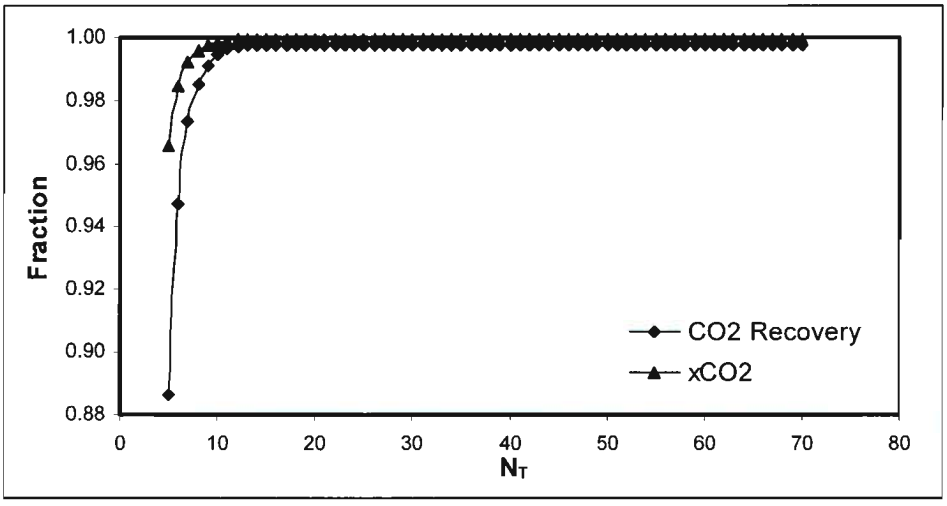

Figure D.2. Sensitivity analysis of N_T for column C1 for the Toluene separation process.

The number of stages, N_T, was varied, keeping the feed stage N_F constant and the effect on the recovery and the purity of CO_2 in the distillate monitored. The purity of the CO_2 was defined as the amount of CO_2

leaving in the distillate divided by the amount of CO_2 entering the feed, while the purity of CO_2 was defined as the mole fraction, X_{CO2}, in the distillate. From Figure D.2, N_T had a dramatic effect on the recovery and purity of CO_2 from approximately 5 to 12 stages, which resulted in a maximum purity of CO_2 of 99.94 % (mole) and a maximum recovery (for the initial conditions) of 99.78 %. The revised estimate of N_T obtained from the sensitivity analysis was N_T = 14 and this value was used for the further design of column C1.

The following step of the design procedure was to utilize the DSV function to determine the optimum value of the molar RR while holding the impurity of CO_2 in the bottoms stream constant. The impurity of CO_2 in bottoms stream, i.e. the maximum amount of CO_2 that was allowed to leave in the bottom stream, was set to a mole fraction of 0.0002 CO_2. The DSV vary function, utilizing the specified controlled and manipulated variables, resulted in a molar RR of 4.3857 which was used for further process design. The process simulation was run with the new values of N_T and molar RR and the results presented in Table D.7.

	C1BOTTS	**C1FEED**	**C1TOPS**
Mole Fraction			
HFP	0.3229	0.2100	0.0001
HFPO	0.6459	0.4200	0.0001
Toluene	0.0308	0.0200	0.0000
CO_2	0.0004	0.3500	0.9998
Mass Flow [kg•hr^{-1}]			
HFP	1.3295	1.3296	0.0002
HFPO	2.9422	2.9425	0.0003
Toluene	0.0778	0.0778	0.0000
CO_2	0.0005	0.6501	0.6496
Mass Fraction			
HFP	0.3056	0.2659	0.0003
HFPO	0.6764	0.5885	0.0005
Toluene	0.0179	0.0156	0.0000
CO_2	0.0001	0.1300	0.9992
Total Flow [kg•hr^{-1}]	4.3499	5.0000	0.6501
Temperature [K]	329.59	301.92	245.86
Pressure [atm]	15	16	15
Vapour Fraction	0	0	1
Liquid Fraction	1	1	0

Table D.7. Stream results for column C1 for the Toluene separation process.

Table D.7 presents the stream results for the Aspen simulation utilising revised column parameters. From a quick comparison with Table D.6, the amount of HFP and HFPO leaving the top stream as waste with the

CO_2 gas stream has been decreased, with the amount of CO_2 leaving in the top increased from 0.6487 to 0.6496 kg•hr^{-1}, with the heavy, non-volatile component Toluene concentrated in the bottom stream.

The determination of the optimum location of the feed stage to minimise reboiler heat input was undertaken via the use of the DSV function. The DSV function was used to hold the impurity of CO_2 in the bottoms stream constant at 0.002 mole fraction, via manipulation of the molar RR. The location of the feed stage, N_F, was manually adjusted and at each different feed stage location, the reboiler heat duty (kW) analysed. The results of the optimum feed tray determination are presented in Figure D.3. From the analysis, the minimum reboiler heat input of 0.5549 kW occurred at a feed stage location of 8. With the optimum feed tray location of 8 for a total number of stages of 14, the ratio of N_F/N_T was 0.5714. Keeping the value of N_F/N_T constant, the total number of stages, and thus feed stage, were varied while holding the impurity of CO_2 in the bottoms stream constant at 0.0002 via the DSV function. The objective was to find N_{MIN}, i.e. the minimum number of stages for the column which corresponded to an infinite reflux ratio. From the variation of the RR with N_T presented graphically in Figure D.4, the RR became increasingly large as N_T approached 12.

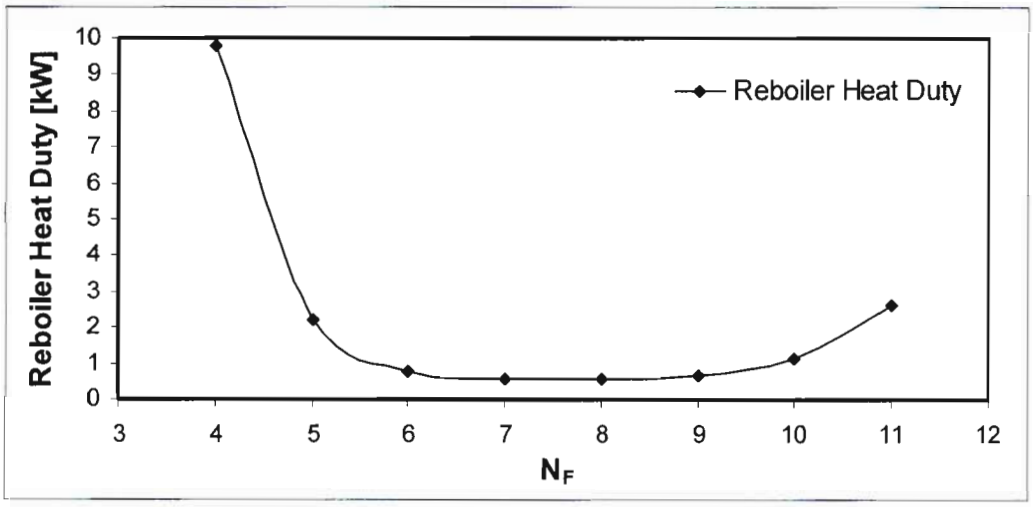

Figure D.3. Determination of the optimum feed tray location with respect to reboiler heat input for column C1 for the Toluene separation process.

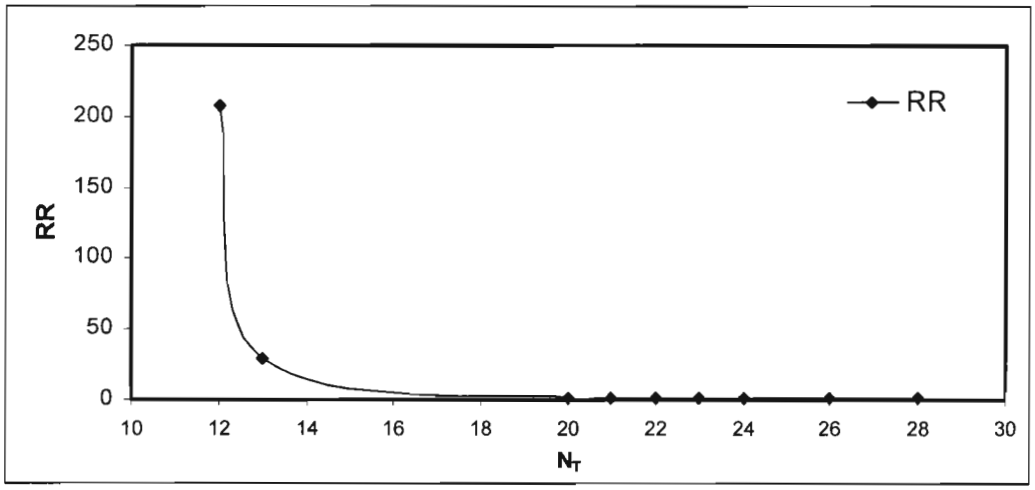

Figure D.4. Determination of N_{MIN} by the variation of RR and N_T for column C1 for the Toluene separation process.

Using the heuristic method of setting the total number of stages of a distillation column to twice that of the minimum value, the revised estimate of N_T was calculated to be 26 stages, with the two extra stages accounting for the condenser, which is considered an equilibrium stage if a partial condenser is utilized, and the reboiler.

Using the revised estimate of N_T, N_F was determined from the N_F/N_T ratio and the Aspen simulation performed to yield the stream results presented in Table D.8. From the table, 99.99 % of the CO_2 was removed from the C1FEED stream, which allowed the C1BOTTS stream to contain only 0.0001 kg•hr^{-1} of CO_2 from the initial amount of 0.6501 kg•hr^{-1} that was present in the feed. No HFP and 0.0001 kg•hr^{-1} of HFPO were lost to the top stream which was sent for disposal, while the bottom stream C1BOTTS, which consisted primarily of HFP, HFPO and some of the original Toluene in the feed stream, was sent to the extractive distillation column for separation.

	C1BOTTS	C1FEED	C1TOPS
Mole Fraction			
HFP	0.3230	0.2100	0.0000
HFPO	0.6461	0.4200	0.0000
Toluene	0.0308	0.0200	0.0000
CO_2	0.0001	0.3500	1.0000
Mass Flow [kg•hr^{-1}]			
HFP	1.3296	1.3296	0.0000
HFPO	2.9424	2.9425	0.0001
Toluene	0.0778	0.0778	0.0000
CO_2	0.0001	0.6501	0.6500
Mass Fraction			
HFP	0.3057	0.2659	0.0001
HFPO	0.6764	0.5885	0.0001
Toluene	0.0179	0.0156	0.0000
CO_2	0.0000	0.1300	0.9998
Total Flow [kg•hr^{-1}]	4.3499	5.0000	0.6501
Temperature [K]	329.66	301.92	245.83
Pressure [atm]	15	16	15
Vapour Fraction	0	0	1
Liquid Fraction	1	1	0

Table D.8. Final stream results for column C1 for the Toluene separation process.

D 2.2. Column C2

The purpose of column C2 was the addition of the solvent Toluene to selectively remove the HFP from the bottoms stream, resulting in a distillate stream of pure HFPO.

Column C2 was the extractive distillation column where the actual separation of HFP and HFPO occurred through the addition of the solvent Toluene. The feed to column C2, termed 'C2FEED' was the bottom stream from column C1, i.e. C1BOTTS, and the stream conditions are presented in Table D.8. The schematic for column C2 indicating the feed streams C2FEED, the solvent feed stream C2SOLV, as well as the output streams, C2TOPS and C2BOTTS is presented in Figure D.5:

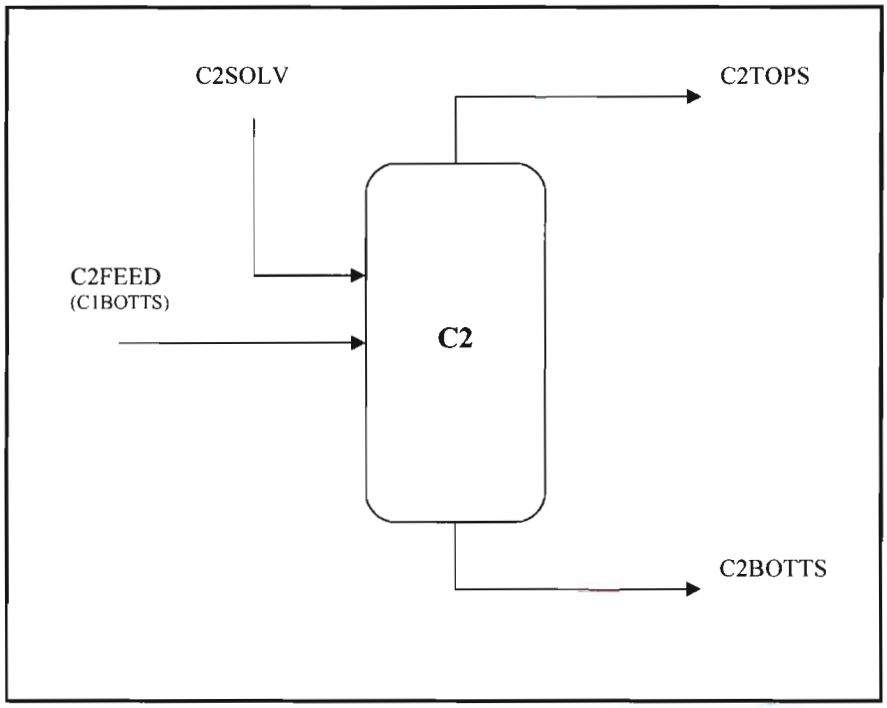

Figure D.5. The schematic of column C2 for the Toluene separation process

For the design of the extractive distillation column, the column was initially designed in the manner of a general distillation column with no solvent feed stream present. When the initial design was completed, the solvent feed stream containing Toluene was added to the process.

C2	
Stages	24
Feed stage	11
Distillate rate [kg•hr^{-1}]	2.942
Molar RR	6.7821
Column P [atm]	15

Table D.9. Initial operating conditions for distillation column C2 for the Toluene separation process with no solvent stream present.

	C2FEED	C2TOPS	C2BOTTS
Mole Fraction			
HFP	0.3230	0.3670	0.2338
HFPO	0.6461	0.6328	0.6730
Toluene	0.0308	0.0000	0.0932
CO_2	0.0001	0.0001	0.0000
Mass Flow [kg•hr^{-1}]			
HFP	1.3296	1.0119	0.3177
HFPO	2.9424	1.9305	1.0120
Toluene	0.0778	0.0000	0.0778
CO_2	0.0001	0.0001	0.0000
Mass Fraction			
HFP	0.3057	0.3439	0.2258
HFPO	0.6764	0.6561	0.7190
Toluene	0.0179	0.0000	0.0553
CO_2	0.0000	0.0000	0.0000
Total Flow [kg•hr^{-1}]	4.3499	2.9424	1.4075
Temperature [K]	330.90	326.83	336.98
Pressure [atm]	16	15	15
Vapour Fraction	0	0	0
Liquid Fraction	1	1	1

Table D.10. Initial stream results for column C2 for the Toluene separation process with no solvent stream present.

The data presented in Table D.9 lists the initial column specifications for the distillation column with no solvent feed stream present. The column specifications were estimated as for column C1. In column C2, the Toluene was added to selectively bond with the HFP (initially the most volatile component) to alter the relative volatility of the mixture such that HFP could be removed from the bottoms stream C2BOTTS, which would allow a purified stream of HFPO to be removed from the distillate. The distillate rate for column C2 was initially set to be the total amount of HFPO in the C2FEED stream, i.e. 2.942 kg•hr^{-1}, with N_F, N_T and the molar RR determined as described in the general design methodology. The vapour pressure

of the new light key component HFPO at 325.15 K was approximately 13 atm, with the column operating pressure set to 15 atm to maintain a reflux drum temperature of 325.15 K. The stream results from the simulation which were run without the addition of the solvent stream are presented in Table D.10. From the results without the use of the solvent, the original Toluene 'impurity' that was present in the primary feed stream C1FEED, was concentrated in the column bottoms as it was the heaviest component, while the majority of the HFP that was present in the feed mixture left via the distillate stream. Without the use of a solvent it was evident that there was no real separation of the HFP and HFPO mixture, as the action of the multistage contacting via the distillation column caused the mixture of HFP and HFPO to only split in almost equal compositions between the tops and bottoms streams.

The solvent stream, consisting of pure Toluene in a 1:1 mole ratio to HFPO was added to the column in the stream C2SOLV at feed stage 2, above the column feed stage of 11. The results of this addition are presented via the stream results in Table D.11:

	C2FEED	**C2SOLV**	**C2TOPS**	**C2BOTTS**
Mole Fraction				
HFP	0.3230	0.0000	0.2324	0.1717
HFPO	0.6461	0.0000	0.7501	0.1494
Toluene	0.0308	1.0000	0.0174	0.6790
CO_2	0.0001	0.0000	0.0001	0.0000
Mass Flow [kg•hr^{-1}]				
HFP	1.3296	0.0000	0.6372	0.6924
HFPO	2.9424	0.0000	2.2759	0.6665
Toluene	0.0778	1.6332	0.0292	1.6818
CO_2	0.0001	0.0000	0.0001	0.0000
Mass Fraction				
HFP	0.3057	0.0000	0.2166	0.2277
HFPO	0.6764	0.0000	0.7735	0.2192
Toluene	0.0179	1.0000	0.0099	0.5531
CO_2	0.0000	0.0000	0.0000	0.0000
Total Flow [kg•hr^{-1}]	4.3499	1.6332	2.9424	3.0407
Temperature [K]	330.90	301.90	328.73	403.40
Pressure [atm]	16	16	15	15
Vapour Fraction	0	0	0	0
Liquid Fraction	1	1	1	1

Table D.11. Initial stream results for column C2 for the Toluene separation process with un-optimized solvent stream present.

From the presented data, the action of adding Toluene in a 1:1 mole ratio with HFPO, was to dramatically alter the relative volatility of the mixture to concentrate HFP in the bottoms product i.e. amount of HFP that

left in the bottoms stream increased from a value of 0.3177 to 0.6924 kg•hr^{-1}. The amount of HFPO that left in the distillate increased from 1.9305 to 2.2759 kg•hr^{-1}, with the majority of the solvent Toluene concentrated in the bottoms stream.

A sensitivity analysis was performed on the variation of the solvent flow rate. The variables that were monitored for the analysis were the mole fraction of HFPO in the distillate which gave an indication of the product purity, and the recovery of HFPO, defined as the number of moles of HFPO leaving in the distillate divided by the number of moles of HFPO entering in the feed.

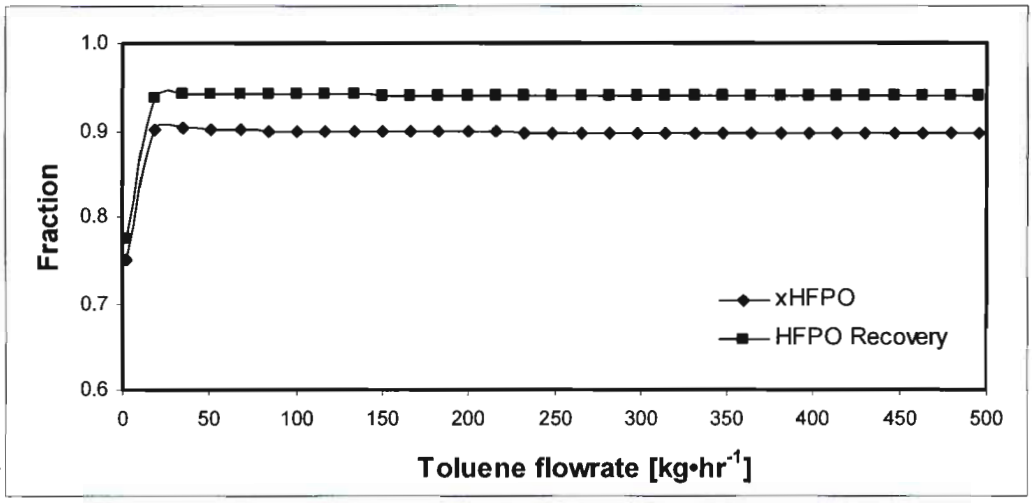

Figure D.6. Sensitivity analysis of toluene flowrate for column C2 for the Toluene separation process to determine the effect on HFPO product purity and recovery.

The results for the sensitivity analysis on solvent flowrate are presented graphically in Figure D.6. The solvent flowrate was varied and all other variables kept constant. The effect on the purity and recovery of the HFPO product in the distillate stream was thus determined. As the solvent flowrate increased from 1.6322 to 54 kg•hr^{-1}, the fractional values of the HFPO purity and recovery increased from 0.7501 and 0.7735 to maximum values of 0.9029 and 0.9380 respectively. The sensitivity analysis revealed that no further increase in Toluene solvent flowrate increased the purity or recovery values by a significant amount. A solvent flowrate of 53.0727 kg•hr^{-1} was thus utilised for further design of the separation process.

The location of the solvent feed stage, N_{SF}, was determined through the manual adjustment of the N_{SF} while keeping all other variables constant while the effect on the HFPO product purity and recovery was monitored. The N_{SF} value which gave the highest values of HFPO recovery and product purity was feed stage 4. To determine final estimates of the total number of stages, the ratio of N_F/N_T, which was calculated

for the case when no solvent stream was present, was utilised along with the ratio of N_{SF}/N_T to manually determine which configuration of N_{SF}, N_F and N_T, gave the highest HFPO product purity and least Toluene impurity in the distillate.

N_T	N_{SF}	N_F	RR	Reboiler Duty [kW]	Condenser Duty [kW]	X_{HFPO} [mole]	$X_{Toluene}$ [mole]
40	7	31	34.0475	8.8000	-1.5833	0.9998	0.0000
35	6	27	22.2364	8.0980	-1.3813	0.9997	0.0000
30	5	23	8.9916	7.3114	-0.5947	0.9992	0.0000
29	5	22	5.1408	7.0825	-0.3658	0.9989	0.0001
28	5	21	2.4880	6.9249	-0.2085	0.9987	0.0001
26	4	20	2.7539	6.9464	-0.2338	0.9949	0.0015
25	4	19	3.7043	7.0045	-0.2893	0.9758	0.0015
20	3	15	7.9406	7.3262	-0.6201	0.9758	0.0161
15	3	12	6.7769	7.2455	-0.5482	0.9606	0.0160
10	2	8	0.1677	6.7569	-0.1016	0.8717	0.0951

Table D.12. A summary of the manual sensitivity analysis to obtain the optimum value of N_{SF}, N_F and N_T for column C2 for the Toluene separation process.

A summary of the manual sensitivity analysis is presented in Table D.12. The mole fractions listed in the table refer to the amount of that particular substance in the distillate. The Toluene impurity in the distillate was an important measured variable as PELCHEM specified no Toluene solvent impurities in the final HFPO product. The reboiler and condenser duties were analysed and can be seen to be not overtly sensitive to the number of stages in the column. The factor which most influenced the reboiler and condenser duties was the solvent flowrate, as large amounts of Toluene required large amounts of energy for the reboiler in the column. The purity of the required HFPO product was given preference over the minimization of reboiler duty, and as such, the previous sensitivity analysis was performed to determine the optimum solvent flowrate which gave the best HFPO product purity and not the solvent flowrate which minimized reboiler heat input. With the calculated ratios of N_F/N_T and N_{SF}/N_T, the total number of stages was varied. It was found that 30 stages gave the best configuration in terms of HFPO product purity and Toluene impurity in the distillate. 30 stages corresponded to a feed stage of 23 and a solvent feed stage of 5, which resulted in a molar RR of 8.9916 and an HFPO product purity of 0.9992 (mole fraction), with no Toluene impurities in the product distillate. The remaining distillate was composed of unseparated HFP.

With the revised column parameters, feed stage locations for the solvent and feed and optimum solvent flow rate determined, the simulation was run and the stream results presented in Table D.13. The solvent flowrate of fresh Toluene was determined to be 53.0729 $kg \cdot hr^{-1}$, with the column operating at a molar RR of 8.9916. The final HFPO product purity was 0.999 (mole fraction) with the only impurities being HFP

and CO_2 which were deemed admissible by PELCHEM. The recovery of HFPO from the feed stream was 98.5 %.

	C2FEED	C2SOLV	C2TOPS	C2BOTTS
Mole Fraction				
HFP	0.3230	0.0000	0.0008	0.0151
HFPO	0.6461	0.0000	0.9990	0.0005
Toluene	0.0308	1.0000	0.0000	0.9844
CO_2	0.0001	0.0000	0.0002	0.0000
Mass Flow [kg•hr^{-1}]				
HFP	1.3296	0.0000	0.0021	1.3275
HFPO	2.9424	0.0000	2.8977	0.0447
Toluene	0.0778	53.0729	0.0000	53.1506
CO_2	0.0001	0.0000	0.0001	0.0000
Mass Fraction				
HFP	0.3057	0.0000	0.0007	0.0243
HFPO	0.6764	0.0000	0.9992	0.0008
Toluene	0.0179	1.0000	0.0000	0.9748
CO_2	0.0000	0.0000	0.0000	0.0000
Total Flow [kg•hr^{-1}]	4.3499	53.0729	2.9000	54.5229
Temperature [K]	330.90	301.90	328.68	512.21
Pressure [atm]	16	16	15	15
Vapour Fraction	0	0	0	0
Liquid Fraction	1	1	1	1

Table D.13. Final stream results for column C2 for the Toluene separation process.

D 2.3. Column C3

The purpose of column C3 was to separate the solvent Toluene from the HFP and un-recovered HFPO for recycle purposes.

The schematic for column C2 is presented in Figure D.7. The feed to the column was the bottoms stream of column C2, i.e. C2BOTTS, for which the compositions are presented in Table D.13.

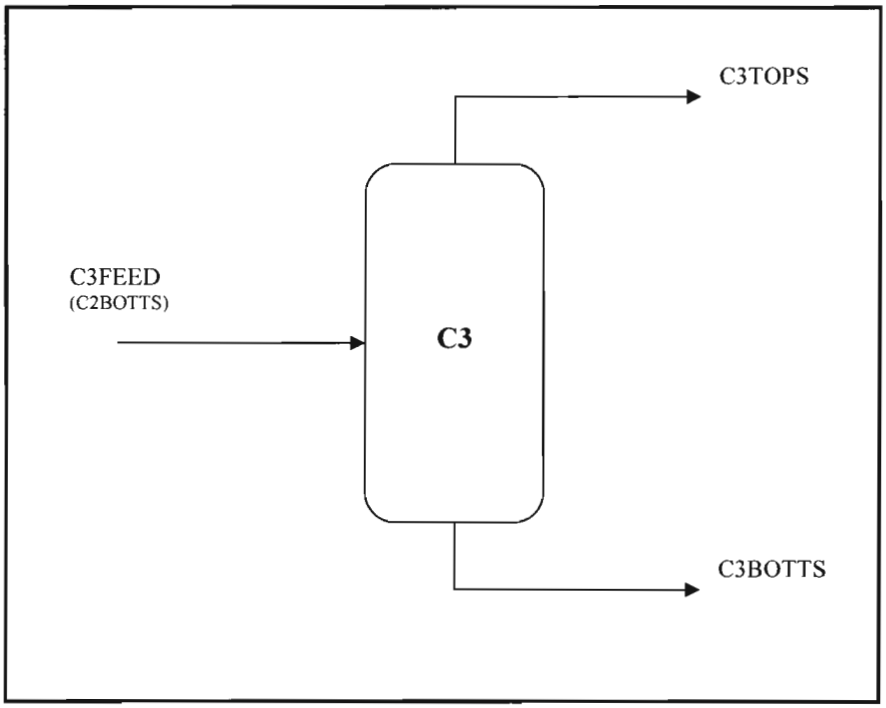

Figure D.7. The schematic of column C3 for the Toluene separation process.

C3	
Stages	10
Feed stage	5
Distillate rate [kg•hr^{-1}]	1.3722
Molar RR	5
Column P [atm]	15

Table D.14. Initial operating conditions for distillation column C3 for the Toluene separation process.

The initial column conditions for C3 are presented in Table D.14. The number of stages, column pressure, feed stage and reflux ratio were estimated as before. The distillate rate was set to the sum of the flowrates of HFP and HFPO in the feed stream, C3FEED, as the purpose of this column was to produce a pure stream of Toluene from the bottoms and to recover the HFP and HFPO via the distillate stream.

	C3FEED	C3TOPS	C3BOTTS
Mole Fraction			
HFP	0.0151	0.7716	0.0021
HFPO	0.0005	0.0272	0.0000
Toluene	0.9844	0.2011	0.9979
CO_2	0.0000	0.0000	0.0000
Mass Flow [kg•hr^{-1}]			
HFP	1.3275	1.1443	0.1832
HFPO	0.0447	0.0447	0.0000
Toluene	53.1506	0.1832	52.9674
CO_2	0.0000	0.0000	0.0000
Mass Fraction			
HFP	0.0243	0.8339	0.0034
HFPO	0.0008	0.0326	0.0000
Toluene	0.9748	0.1335	0.9966
CO_2	0.0000	0.0000	0.0000
Total Flow [kg•hr^{-1}]	54.5229	1.3722	53.1506
Temperature [K]	299.37	357.94	515.42
Pressure [atm]	16	15	15
Vapour Fraction	0	0	0
Liquid Fraction	1	1	1

Table D.15. Initial stream results for column C3 for the Toluene separation process.

The data presented in Table D.15 shows the stream results for the initial simulation with the un-optimized or estimated column parameters. The analysis of the data showed that 99.65 % of the Toluene was concentrated in the bottoms stream C3BOTTS, however, 13.80 % of the HFP in the feed stream was also lost to the bottoms stream. PELCHEM desired an HFP stream of minimum purity 95 % (mole). A sensitivity analysis on N_T was performed to determine the effect of Toluene recovery in the bottom stream and HFP product purity in the tops stream. The results of the sensitivity analysis are presented graphically in Figure D.8. From the graph, the Toluene recovery was generally high (> 97 %) for most values of N_T. However, the HFP product purity measured by the mole fraction of HFP in the top stream, C3TOPS, increased to approximately 96 % (mole) as the number of stages increased from 5 stages to 20 stages. The number of equilibrium stages chosen for further design of column C3 was 17.

The determination of the optimum feed tray location was undertaken and the optimum feed stage was found to be stage 4. To determine the revised estimate of the N_T value, the ratio N_F/N_T was used to find N_{MIN}. The results are presented graphically in Figure D.9, where the HFP product purity was held constant at a value of 96 % (mole) via the DSV function and the total number of stages varied until the molar RR became exceedingly large. Utilizing this method, N_{MIN} corresponded to a value of 18. According to the common engineering heuristic the revised estimate of N_T thus became 38 stages.

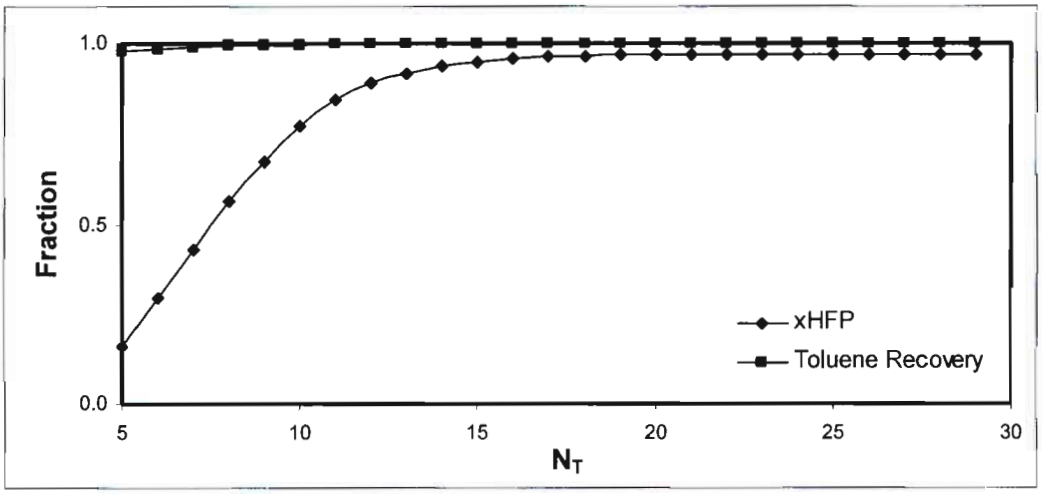

Figure D.8. Sensitivity analysis of N_T for column C3 for the Toluene separation process to determine the effect on HFPO product purity and Toluene recovery.

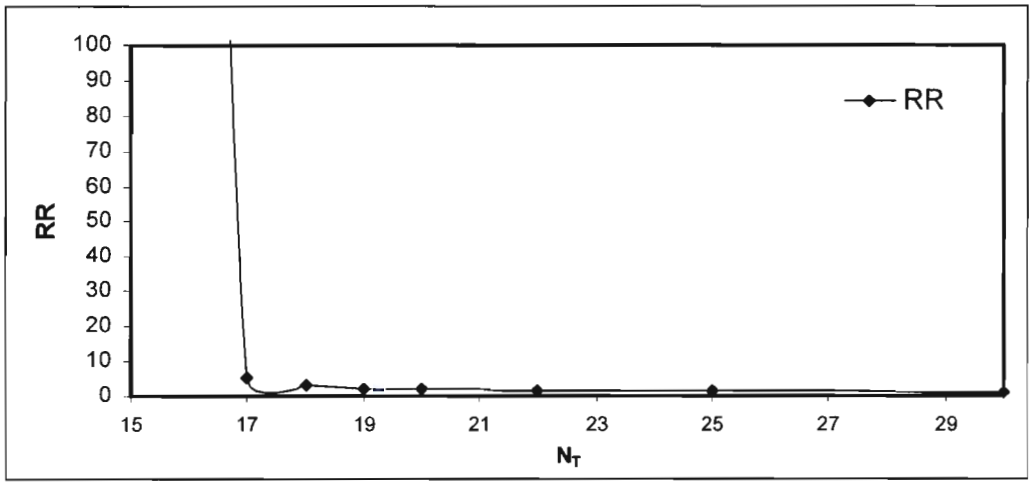

Figure D.9. Determination of N_{MIN} by the variation of RR and N_T for column C3 for the Toluene separation process.

Utilizing the newly determined parameters, the Aspen simulation for column C3 was performed and the results presented in Table D.16. From the analysis of the data, the purity of HFP in the distillate stream was 96 % (mole) with the purity of the Toluene in the bottoms stream 99.99 % (mole). The bottoms stream of almost pure Toluene was sent to a splitter for recycle to column C2, the extractive distillation column.

	C3FEED	**C3TOPS**	**C3BOTTS**
Mole Fraction			
HFP	0.0151	0.9600	0.0001
HFPO	0.0005	0.0294	0.0000
Toluene	0.9844	0.0106	0.9999
CO_2	0.0000	0.0000	0.0000
Mass Flow [kg•hr^{-1}]			
HFP	1.3275	1.3186	0.0089
HFPO	0.0447	0.0447	0.0000
Toluene	53.1506	0.0089	53.1417
CO_2	0.0000	0.0000	0.0000
Mass Fraction			
HFP	0.0243	0.9609	0.0002
HFPO	0.0008	0.0326	0.0000
Toluene	0.9748	0.0065	0.9998
CO_2	0.0000	0.0000	0.0000
Total Flow [kg•hr^{-1}]	54.5229	1.3722	53.1506
Temperature [K]	299.37	327.96	515.86
Pressure [atm]	16	15	15
Vapour Fraction	0	0	0
Liquid Fraction	1	1	1

Table D.16. Final stream results for column C3 for the Toluene separation process.

D 2.4. Closing the Recycle Loop

The Toluene recovered from the bottoms stream of column C3 was partially recycled to column C2, the extractive distillation column. To set up the flowsheet for recycle, the procedure outlined in Chapter six was utilized. A schematic of the recycle process is presented in Figure D.10. The 'dotted' block represents the Toluene separation process which consisted of columns C1, C2 and C3. The recovered solvent from column C3 was sent to a stream splitter, denoted by the letter 'S' in the diagram. The splitter split the stream into a recycle stream and a purge stream depending on the split fraction, where a split fraction value of one corresponded to the full flowrate of the recovered solvent stream going to the purge stream.

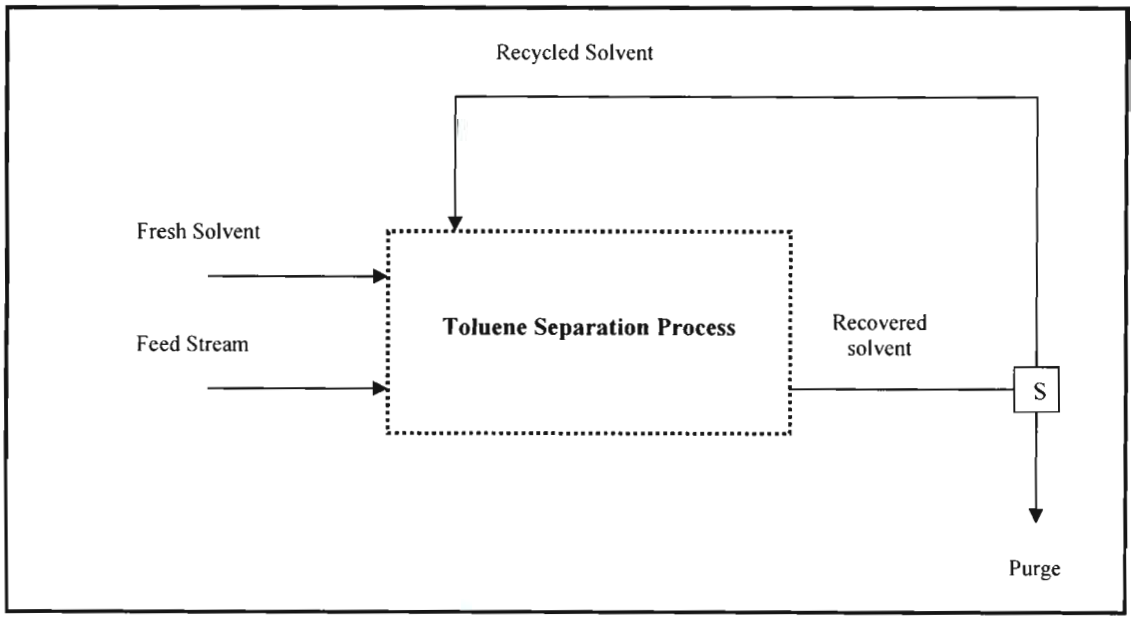

Figure D.10. A schematic of the recycle loop for the Toluene separation process.

To close the recycle loop, small amounts of recovered solvent were recycled to the Toluene process with initially no change in the fresh solvent feed rate. The HFP and HFPO product purities were monitored and if they were found to be within specification, the fresh solvent flowrate was decreased gradually in a step wise manner in small increments of Toluene solvent flowrate until the amount of fresh solvent decreased equated to the amount of solvent that was being recycled. This procedure is illustrated numerically in Table D.17. At each increment of the recycle solvent rate, and each decrease of the fresh solvent flowrate, the product purities for HFP and HFPO were constantly monitored. This procedure of gradually decreasing the split fraction to allow more solvent to be recycled, and gradually decreasing the fresh solvent flow rate, was continued until the product specifications for HFP and HFPO could not be fulfilled.

Purge [kg•hr^{-1}]	Recycle [kg•hr^{-1}]	Split Ratio	Decrease Fresh Solvent [kg•hr^{-1}]	New Fresh Solvent [kg•hr^{-1}]	x_{HFPO} [mole]	x_{HFP} [mole]
47.8355	5.3151	0.9	0.0000	53.0729	0.9991	0.9601
-	-	-	5.3151	47.7579	0.9990	0.9604
41.1917	17.6536	0.7	0.0000	41.1141	0.9991	0.9611
-	-	-	5.6947	35.4193	0.9989	0.9614
29.4859	29.4859	0.5	0.0000	29.4083	0.9988	0.9619
-	-	-	5.8212	23.5871	0.9987	0.9624
17.6535	41.1915	0.3	0.0000	17.5758	0.9989	0.9634
-	-	-	5.6944	11.8814	0.9988	0.9631
11.9591	47.8364	0.2	0.0000	11.8814	0.9988	0.9641
-	-	-	6.6449	5.2366	0.9957	0.9605

Table D.17. A summary of the procedure for the closing of the recycle loop for the Toluene separation process.

The fresh Toluene feed at a rate of 53.0729 kg•hr^{-1} was gradually decreased as the recycled solvent rate was increased, as indicated in Table D.17. With the implementation of the recycle loop, the original fresh solvent feed rate of Toluene was decreased by a significant amount with a new fresh solvent rate of 11.8814 kg•hr^{-1} required to maintain an HFP product purity of 96.41 % (mole) and an HFPO product purity of 99.88 % mole. If the split ratio was decreased any lower than 0.3 and the fresh solvent feed rate decreased, then the product purities of HFP and HFPO decreased and were not within specifications. These product purities were the final overall product purities for the Toluene separation process.